# Engineering of decellularised porcine bladder patches

Ashley James Ward MEng

Submitted in accordance with the requirements for the degree of

Doctor of Philosophy

University of Leeds

School of Mechanical Engineering

February, 2017

The candidate confirms that the work submitted is his own and that appropriate credit has been given where reference has been made to the work of others.

# Acknowledgements

I foremostly express my deepest thanks to my supervisor, Eileen Ingham. Her unfaltering kindness and support never failed to spur me on, even in times of darkness. Without her patience and guidance this work would not have been possible, and I would not have come to where I am today. I would also like to thank my other supervisors: Jenny Southgate, who always encouraged me to be better and never gave up on me; Helen Berry, for her constant support and industrial guidance; John Fisher for his engineering insights; and Jen Edwards for being a continual source of practical help.

Many thanks also to all the members of Lab 7.63 for making it an enjoyable place to work, particularly Fiona Walker for her helpfulness and cheerfulness, and Dan Thomas for his infinite sources of wisdom and kindness. Thanks also to the people whom I have had the joy of working alongside in Office 6.63. You are too numerous to name, but in your own way, each of you made my time there a better one.

My time at Leeds would also never have been what it was without each and every one of my friends. You helped me take a step back when I needed to the most, and I owe a lot of my happiness over the past five years to you. From the first pint to the last laugh and everything in between, thanks to Steve, Em, Jen, Chrislee, K-dog, Linda, Anna and Ned. A special thanks to Steve/Em/Jen/Chrislee for lending me a place in your house so frequently; for supporting me with a broken hip and a thesis to write, I owe you all the beer in the world. I must also shout out to every member of the Leeds Uni A Cappella Society I have had the pleasure of working alongside. I have never been involved with such a close group of friends that has worked towards something with such unified focus and dedication. So many special times were had with so many of you, which I'm sure I will treasure for years to come.

Lastly and far from leastly, I would like to thank my family. Mum and Dad, your bedrock of love and support is more than I could ever wish for, and I could not have done this without you. Thanks for putting me up and putting up with me over the last several months, despite me constantly emptying the peanut butter jar and eating all the bananas.

# Abstract

For patients with end-stage bladder disease for which other treatment options have failed, the patient is treated surgically with either urinary diversion or bladder augmentation. Enterocystoplasty is the most common of these options, and it involves augmenting the bladder using a section of the patient's own intestine. However, there are several problems associated with the use of intestine for augmenting the bladder, and therefore an alternative augmentation material may be of benefit to patients. Numerous approaches have been used to develop tissue-engineered scaffolds capable of successfully augmenting bladders. Some of these approaches have involved the use of acellular tissue-derived materials, whereby the tissues are decellularised in order to remove immunogenic material and therefore prevent an immune reaction when transplanted allogeneically or xenogeneically. Decellularisation protocols typically involve a variety of chemical and physical processes which remove cells and other immunogenic material from the tissues.

A protocol was previously developed to decellularise full-thickness porcine bladders. This material may have utility in bladder augmentation. The process involved distending the bladders with, and placing them in, a series of solutions. It was demonstrated that distending the whole organs was a necessary step in the decellularisation process. It was thought that this procedure applied biaxial strain to the wall of the tissue and reduced its thickness sufficiently for the solutions to penetrate the entire wall of the tissue. However, the method of distending whole bladders was not compatible with a scalable manufacturing process, and therefore the biomaterial was not able to be developed further. The overall aim of this project was to develop a novel method of manipulating bladder tissue which would enable bladder tissue to be decellularised in a way which would be compatible with a commercial manufacturing process.

The original bladder decellularisation process used 500 ml of solutions to distend bladders. Preliminary experiments demonstrated that this volume was not always adequate to decellularise larger bladders. Filling experiments were performed to find relationships between bladder size and bladder capacity. A relationship between

bladder capacity and bladder width × length was found to have a high correlation. Bladders were decellularised when filled to capacities calculated using the relationship. No signs of cellular material were observed in histological sections of these bladders, and DNA quantification indicated a removal of more than 99 % of the DNA relative to native tissue.

In order to determine the state of mechanical deformation of bladders during decellularisation, markers were placed on the surface of twelve bladders which were immersed in isotonic solution and slowly filled. Images taken of the bladders and markers during filling were used to calculate the strain of the tissues during the tests. The previously found relationships for bladder capacity were used to calculate the capacity of these bladders. The stress, strain and thickness of the bladders were calculated at the point the bladders were filled to their respective capacities. These strains were invariant with bladder capacity, and were equal to 2.0 and 1.4 in the circumferential and longitudinal directions respectively. Applying these strains to three bladders during decellularisation appeared to result in a complete removal of cellular material.

It was thought that applying the required strains to bladder tissue deformed in a flat sheet configuration would be compatible with a manufacturing process. In order to apply biaxial strain to this highly compliant material, it was recognised that it would be appropriate to deform it using discrete points, placed along the edges of the tissue. The stretching of flat sheets of bladder using this method was modelled using finite element modelling to find an optimal stretching regime. The models demonstrated that deforming the tissue using five discrete points along each edge of the material would be adequate to ensure that the required strains would be applied to the tissue for decellularisation to occur.

So that flat sheets of bladder could be decellularised, a piece of equipment was designed to hold pieces of bladder in the state of deformation which was previously modelled. The equipment took the form of a 3D-printed frame. A procedure was developed to stretch bladder tissue onto the frame. To test the hypothesis that bladder tissue could be decellularised in a flat sheet configuration, six bladders were stretched onto the frames and subject to the decellularisation process. Histological sections taken from decellularised bladder samples demonstrated a complete removal of cellular material, and a DNA extraction and quantification assay demonstrated that 99 % of the DNA had been removed relative to the native controls.

Bladders decellularised using the original process were transported in transport medium and processed within 4 h of bladder collection. A manufacturing process would require the tissue to be stored before processing. It was also recog-

nised that it may not be necessary to transport bladders—which are destined for decellularisation—in transport medium, which was developed in order to maintain viable urothelial cells. To test the effects of freezing and transportation without transport medium, bladders were collected from the abattoir, transported without transport medium and subject to either one (six bladders) or two (six bladders) freeze-thaw cycles. Twelve fresh bladders were transported with transport medium. Bladders were immersed in solution and mechanically tested by distension, and their stress–strain curves calculated. There was no statistical difference between the toe region modulus and the transition stress of fresh, once-frozen and twice frozen bladders. There was a small but significant increase in the linear region modulus and transition stress of fresh bladders compared to the once- and twice-frozen bladders. No significant differences were found between once-frozen and twice-frozen bladders. To determine the effect of this revised transportation regime on bladder decellularisation, six bladders were transported without transport medium, subject to two freeze-thaw cycles and subject to the decellularisation process. Samples taken from these bladders for histological analysis and DNA quantification exhibited a complete removal of cellular material.

In conclusion, this study demonstrated that applying suitable strains to flat sheets of bladder tissue was a viable method of deforming bladder tissue in order for it to be decellularised. Freezing the tissue up to two times before decellularisation resulted in some small but significant changes to the mechanical properties of the tissue, but did not affect the efficacy of the decellularisation process. It therefore may now be feasible to commercially produce decellularised full-thickness porcine bladder tissue.

# Contents

# List of Figures

# List of Tables

# List of Abbreviations

| | |
|---|---|
| BSA | Bovine serum albumin |
| DMEM | Dulbecco's minimal essential medium |
| DMSO | Dimethyl sulfoxide |
| DPBS | Dulbecco's phosphate buffered saline |
| DSC | Differential scanning calorimetry |
| ECM | Extracellular matrix |
| EDTA | Ethylene-diamine tetra-acetic acid |
| FBS | Foetal bovine serum |
| FEM | Finite element modelling |
| GAG | Glycosaminoglycan |
| GMEM | Glasgow's minimal essential medium |
| HBSS | Hanks' balanced salt solution |
| HCl | Hydrochloric acid |
| H&E | Haematoxylin and eosin |
| NaCl | Sodium chloride |
| NaOH | Sodium hydroxide |
| NBF | Neutral buffered formalin |
| PAA | Peracetic acid |
| PBS | Phosphate buffered saline |
| PGA | Polyglycolic acid |
| PLGA | Poly(lactic-co-glycolic acid) |
| PLLA | Poly(L-lactide) |
| PU | Poly(etherurethane) |
| SDS | Sodium dodecyl sulphate |
| SIS | Small intestine submucosa |
| SLS | Selective laser sintering |
| TPB | Tryptone phosphate broth |
| Tris | Trizma® Base |
| UE strain | Uniaxial equivalent strain |

# Chapter 1

# Introduction

## 1.1 General Introduction

The bladder is an organ of the lower urinary system whose job is to store urine, and then release it when required. Although seemingly simple, its improper function can have a dramatic effect on the lives of the people it affects. There are a variety of acquired and congenital disorders that result in bladder dysfunction, and which require augmentation of the bladder when other medical options have failed (Tanagho & McAninch, 2004). The current standard surgical procedure of bladder augmentation enterocystoplasty involves enlarging the bladder using a section of intestine. The use of intestine as a bladder wall replacement causes many problems, such as an increased bladder infection risk, metabolic abnormalities and bladder perforation (Flood *et al.*, 1995; Biers *et al.*, 2012). Therefore an alternative tissue-engineered regenerative bladder patch material would be of benefit to patients (Gilbert, 2012). This review will look at the physiology of the bladder and the clinical need for alternative surgical interventions, and will then investigate the previous methods that have been explored in the literature to produce tissue-engineered materials that have been developed for use as a bladder augmentation implant.

## 1.2 Human urinary bladder

### 1.2.1 Anatomy and physiology

The urinary bladder is situated in the anterior half of the pelvis and is bounded anteriorly and laterally by the pelvic skeleton (Scott *et al.*, 1982). The superior surface of the bladder lies adjacent to the peritoneal lining, and the base is supported

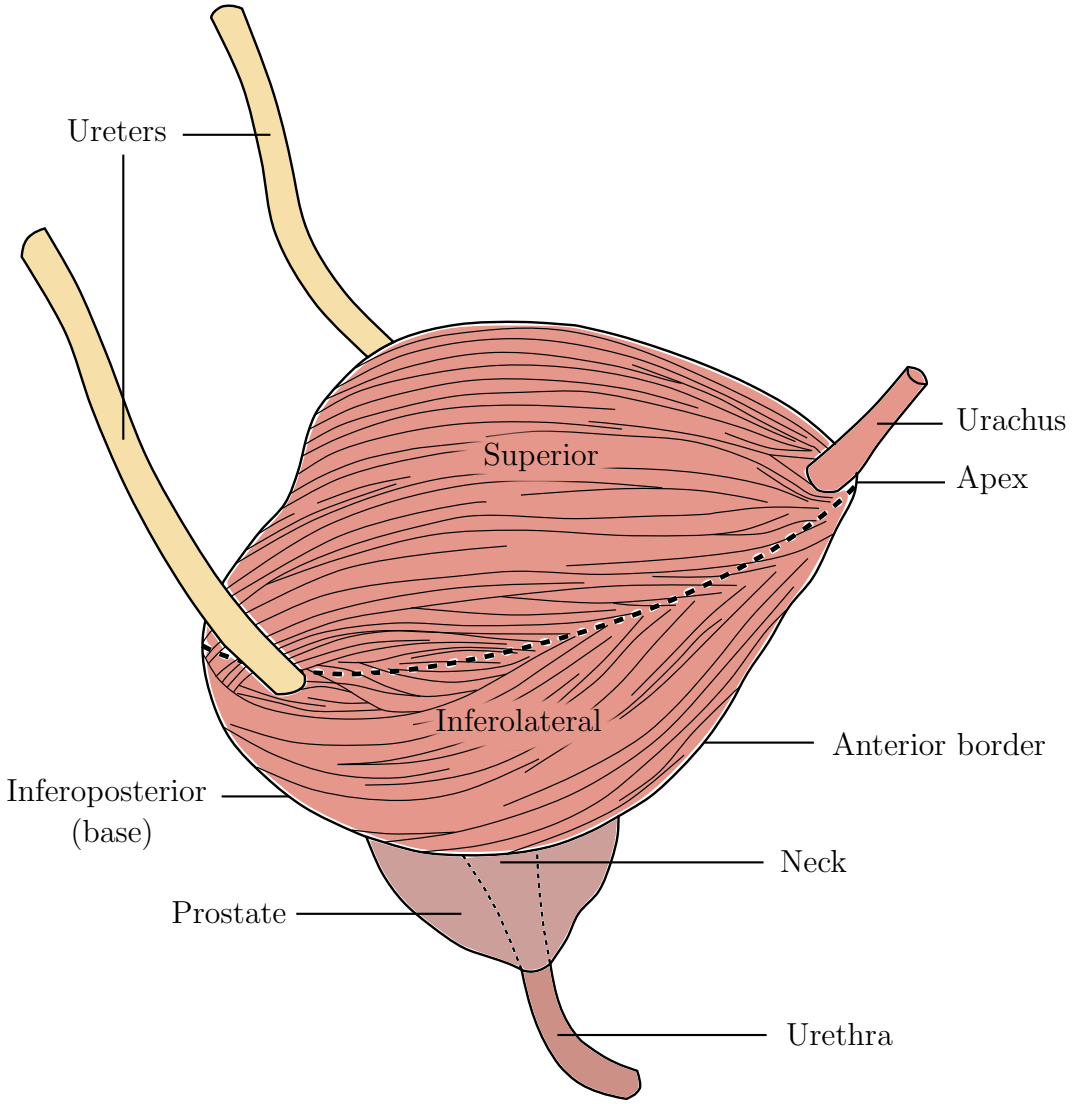


**Figure 1.1: A macroscopic schematic of the human urinary bladder.**

by the pelvic floor Stoker, 2009. The bladder is enveloped by thin connective tissue (Lapides & Nesbit, 1976). The macroscopic structure of the bladder is shown in Figure 1.1. The bladder has four surfaces: the superior surface, the inferoposterior surface (the base), and two infero-lateral surfaces (the lateral walls) (Scott *et al.*, 1982). The urachus (the median umbilical ligament) connects the anterior tip of the bladder to the umbilicus. The point at which the urachus meets the bladder is known as the apex, and the junction of the urethra and the bladder is known as the neck (Skandalakis & Colborn, 2004).

Two ureters transport urine into the bladder from the kidneys via peristalsis (Skandalakis & Colborn, 2004). The ureters enter the bladder wall at an oblique angle, with a geometry which acts as a natural valve (Bullock *et al.*, 1994). A single urethra allows urine to pass out of the bladder. The urethra begins at the bladder neck, and is continuous with the bladder (Mundy *et al.*, 2004). Urine flow out of the bladder is controlled by muscle in the urethral wall (Tanagho & McAninch, 2004). Inside the

bladder, a triangular region is marked out between the two ureteral orifices and the urethral opening (Tanagho & McAninch, 2004). This region—called the trigone—is not as extensible as the rest of the bladder tissue, and remains in place as the bladder distends and voids (Lapides & Nesbit, 1976).

The function of the bladder is to collect and store urine from the kidneys until it is released at a suitable and convenient time. During filling, the bladder distends and expands up out of the pelvis and towards the abdomen (Bullock *et al.*, 1994). Several nerve paths sense and control bladder and urethra function (Bullock *et al.*, 1994). Somatic and autonomic nervous control of the bladder and urethra allow for voluntary control over the release of urine, and are necessary for normal micturition (Tanagho & McAninch, 2004).

### 1.2.2 Bladder wall structure

The bladder wall comprises of four main layers: the outer serous layer, the muscular layer, the lamina propria and the inner epithelium. The serous layer, or adventitia, is a covering of the bladder with either peritoneum or fibrous stroma. The muscular layer is known as the detrusor muscle, and is made from whorls and spirals of smooth muscle. The lamina propria consists of connective tissue and cells responsible for maintaining the extracellular matrix (ECM). The inner epithelium is a thick coat of several layers of transitional epithelium, called the urothelium (Skandalakis & Colborn, 2004). This structure is shown in Figure 1.2. The bladder wall remains structurally similar throughout the majority of the bladder, except that the trigone and neck regions, where the detrusor muscle is composed of a more structured arrangement of two or three distinct longitudinal and circumferentially aligned muscle fibre layers (Skandalakis & Colborn, 2004). The majority of muscle fibres on the external surface of the bladder wall tend to run in a longitudinal direction (Lapides & Nesbit, 1976).

The urothelium is made up of a transitional epithelium of urothelial cells. It is made impermeable to many fluids and solutes due to the tight junctions between these urothelial cells, but certain substances can still pass through this boundary. It has been suggested that there are some cells in the subepithelium that act as touch and chemical receptors, as well as cells in the epithelium that are sensitive to hydrostatic pressure (Mundy *et al.*, 2004). During filling and voiding, the morphology of the urothelial cells changes so that they are columnar when the bladder is collapsed but stretched out and flattened when the bladder is distended (Tanagho & McAninch, 2004). Urothelial cells are able to survive in a close proximity to urine due to the glycosaminoglycans (mainly chondroitin sulphate and heparan sulphate) which

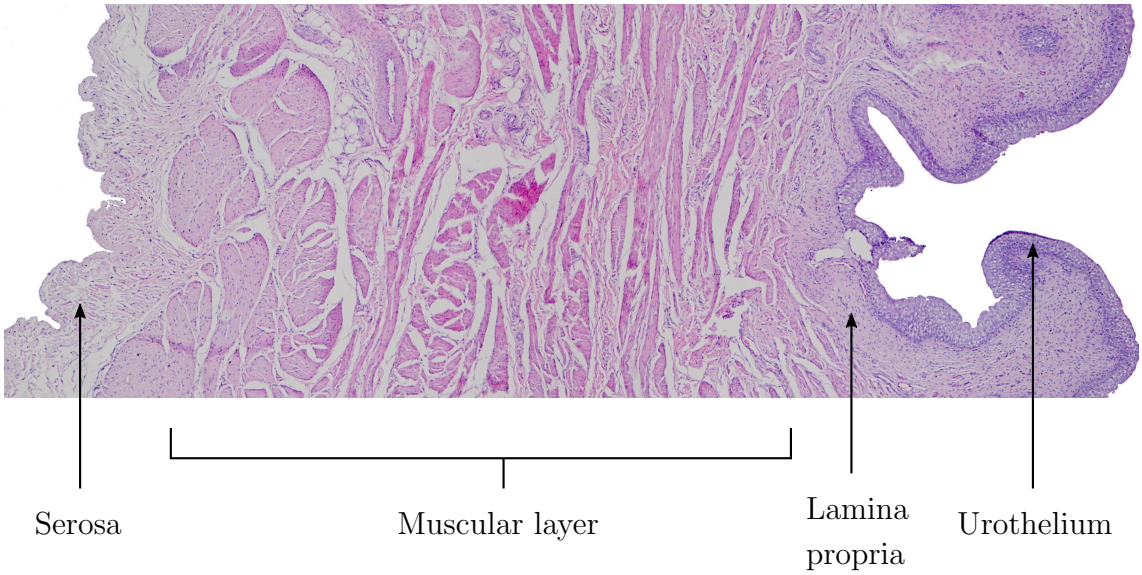


**Figure 1.2: Structure of the bladder wall.** A histological section of urinary bladder stained with haematoxylin and eosin.

cover the cells. This takes the form of a charged gel-like barrier to urine. Enzymes regulate the periodic shedding of urothelial cells in order to maintain the urothelium (Aitken & Bägli, 2009).

The lamina propria is a layer of connective and elastic tissues, mostly composed of densely packed and randomly oriented collagen fibres. This means therefore that it contributes significantly to the mechanical properties of bladder tissue. It also contains a large proportion of ECM and is populated by myofibroblasts. The presence of nerve fibres, blood vessels and lymphatic tissue mean that other cell types, including cells of the immune system, also exist here (Aitken & Bägli, 2009).

The detrusor muscle layer makes up the majority of the thickness of the bladder wall and consists primarily of large smooth muscle bundles, with some connective tissue, and is heavily populated with the smooth muscle cells that make up the muscle fibres (Mundy *et al.*, 2004). It has been suggested that the muscle fiber bundles slide past one another to re-organise their orientation as the bladder distends, until there comes a point where the bundles finally align parallel to the bladder surface, and can then bear mechanical tension and elongate. This mode of expansion means that the detrusor only begins to bear stress in the bladder wall as the bladder nears full capacity (Chang *et al.*, 1998).

### 1.2.3 Extracellular matrix

Bladder ECM is a structural scaffold that provides mechanical support to the tissue and signals to cells. It contains proteins, proteoglycans and glycosaminoglycans

(GAGs). It is actively involved in the growth, differentiation, nutrition, repair and homeostasis of embedded cells through constant dynamic conversation, mediated by ECM receptors (Mundy *et al.*, 2004; Aitken & Bägli, 2009).

The majority of the fibrillar protein content of the bladder is composed of collagen I and collagen III. These fibrillar proteins exist mainly in the lamina propria and the connective tissue surrounding the smooth muscle cells). The fibres give the bladder tensile strength, structure, and the ability to be highly compliant. Compliance is provided by the intricate coiling of these proteins. Collagen III provides the majority of this compliance, which exists as loosely coiled bundles in the lamina propria. The network of collagen III fibres has been shown to change in morphology significantly as the bladder changes in size: undistended, the fibres are highly bundled, but as the bladder fills the fibres form distinct coils which finally elongate when the bladder is fully distended (Chang *et al.*, 1998). Collagen IV has a structure which has been likened to a sheet, and it is this reticular structure which forms a membrane that covers the connective tissue of smooth muscle fibres as well as the lamina propria, preventing cells from migrating to and from muscle fibres and the urothelium (Aitken & Bägli, 2009). A large number of other collagens (IX, X, XII, XIV, XVI) are known to be present and form cross-bridges between other collagens, but exist in relatively low abundance. Of these, collagen XII has been reported to play an increased role in cross-linking other collagens, thus stiffening the bladder and reducing compliance during bladder injury (Aitken & Bägli, 2009).

Elastin in the bladder wall assists in contracting the bladder to its original non-distended shape after voiding has occurred. Elastin molecules have a hydrophobic and random-coil structure that are cross-linked via other proteins to form a highly recoiling elastic fibre. Elastin highly contributes to bladder compliance, and is remodelled at a very slow rate (Aitken & Bägli, 2009).

Cells continually remodel the extra-cellular matrix of the bladder in a process called dynamic reciprocacy. Integrin ECM receptors on cells allow outside-in cellular signalling that either informs the cell to maintain homeostasis, or change cellular function to change the rate of matrix remodelling or proliferation (Aitken & Bägli, 2009). For examples, bladder overstretching has been linked to various changes of gene expression of bladder cells which leads to the synthesis and subsequent deposition of collagens I, III and XII. These changes are considered to be among the possible mechanisms that later lead to bladder fibrosis, and therefore a decrease in compliance (Capolicchio *et al.*, 2001).

### 1.2.4 Mechanics

The normal capacity of the human bladder is typically in the range 300–500 ml (Skandalakis & Colborn, 2004). Bladder pressure for a normal subject is typically 6 $cmH_2O$ (Wahl *et al.*, 2004), however the maximum safe pressure for the human bladder is 40 $cmH_2O$ (Clayton *et al.*, 2010). Compliance is a measure of the amount by which a material deforms when subject to a force, and is the inverse of stiffness.

Although compliance is typically measured in terms of the length of extension per force applied, it is more appropriate to measure bladder compliance in terms of its volume and pressure. Therefore bladder compliance $C$, is defined as the change in bladder volume, $\Delta V$, divided by the change in detrusor pressure, $\Delta p_{det}$ (Equation 1.1). This measure of compliance is commonly used clinically to assess bladder performance, and is typically given in units of ml/$cmH_2O$ (Abrams *et al.*, 2002; Wyndaele *et al.*, 2011). Bladder compliance is 90 ml/$cmH_2O$ for a healthy adult male, however due to the variation of compliance with patient age, sex and size it has been suggested that this traditional method of calculating compliance is not clinically useful and that a dimensionless quantity may be more appropriate (Wahl *et al.*, 2004).

$$C = \frac{\Delta V}{\Delta p_{det}} \tag{1.1}$$

The bladder is a tissue with relatively large compliance, as it demonstrates very little rise in pressure over a very large change in volume over filling (Scott *et al.*, 1982). It is this compliance that allows the bladder to store large volumes of urine at low pressures. Disease can cause the bladder wall to become stiff (non-compliant), resulting in an abnormally large increase in pressure over bladder filling (Mundy *et al.*, 2004).

## 1.3 The clinical problem

There are many causes of bladder dysfunction, including a variety of neurological problems, congenital disorders or physical damage. Some more common causes include spina bifida, multiple sclerosis, spinal cord injury, age-related degeneration and bladder cancer (Aitken & Bägli, 2009). These can ultimately lead to poor lower urinary tract function, resulting in urinary tract infections, incontinence, reduced bladder capacity and increased intravesical pressure. Increased bladder pressure can

lead to vesicoureteral reflux, thus increasing the pressure in the ureters and kidneys, leading to kidney damage and renal failure. These problems are typically treated using medication, or other treatment options such as botulinum-A toxin injection (Reynard *et al.*, 2009; Aitken & Bägli, 2009).

Patients for whom these less invasive interventions have failed are typically treated surgically with either urinary diversion or augmentation cystoplasty (Greenwell *et al.*, 2001). The most common of these is augmentation enterocystoplasty: bladder augmentation using a section of the patient's own small intestine (Biers *et al.*, 2012). It is performed in order to increase bladder capacity and compliance, reduce intravesical pressure, prevent ureter reflux, reduce the risk of kidney damage and help improve urinary continence (Clayton *et al.*, 2010; Sharma *et al.*, 2013). It has been demonstrated to be a viable procedure to enhance the function of the bladder (Novick *et al.*, 1978). However, the use of a tissue with a mucous-secreting and absorptive epithelium to enlarge the bladder is known to cause several deleterious side effects, such as metabolic disturbances, urinary tract infections, stone formation, incontinence and risk of malignancy (Khoury *et al.*, 1992; Gough, 2001).

The number of patients in the UK who were treated with enterocystoplasty was 155 in 2000. This has been steadily declining, and in 2010 the number of operations had dropped to 91 (Biers *et al.*, 2012). This was likely due to the emergence of other interventions such as botulinum-A toxin injection. Even with the success of these alternative treatment options, there is still is a clinical need for patients who remain unresponsive to these. Therefore, there exists a clinical need for a bladder augmentation material which is able to increase bladder capacity and reduce bladder pressure, but which does not carry with it the complications observed with the use of small intestine.

## 1.4 Transplantation approaches to bladder augmentation

There have been several attempts to augment the bladder using novel methods of transplantation. There are three main types of transplants: 1) autografts, which employ the use of tissue from the host; 2) allografts, which use of tissue from a donor of the same species; and 3) xenografts, whereby tissue is transplanted between species (Knight & Ingham, 2006).

### 1.4.1 Autotransplantation

Autografts employ the use of tissue which is transplanted from one site in the body to a different site in the same individual. The body does not elicit an immune response against this tissue because the immune system recognises it as part of the individuals body (Knight & Ingham, 2006). The existing gold standard of bladder augmentation—enterocystoplasty—is an example of autotransplantation. Several approaches have been taken to devise new methods of augmenting the bladder using autotransplantation.

In order to augment the bladder without the use of bowel, a procedure was developed which used omentum, a highly vascular large sheet of connective tissue which is present in the abdominal cavity. In a sheep model which involved ten lambs, Dewan *et al.*, (1994) removed the detrusor of the bladders, leaving behind the underlying mucosa. The omentum was then sutured onto the bladder to cover the exposed mucosa. The control group consisted of seven lambs. Cystograms revealed that most of the augmented bladders were small and irregular in shape after 10 days, but these symptoms appeared to recover after 3 weeks. Urodynamic studies performed on the animals *in vivo* demonstrated that after 6 months the autoaugmented bladders had reduced in volume and compliance relative to the control group. Renal function of the animals was demonstrated to remain unaffected by the surgery when assessed using intravenous urograms 3 weeks after surgery. Some animals were sacrificed for histological analysis. Histological sections showed great variations of fibrosis and inflammation between bladders. The level of inflammation and fibrosis in some of the bladders was reported as being severe. These findings demonstrated that covering the exposed bladder muscosa with omentum was not sufficient for bladder capacity to be increased, even though all tissues appeared to be viable, likely due to the highly vascular nature of the omentum. The varied outcomes observed between the bladders examined histologically suggests that this procedure is may result in the worsening of any bladder condition it may be treating.

A similar study tried to combine the principles developed with omentocystoplasty with the current gold standard of enterocystoplasty whereby the detrusor muscle was dissected from the bladders of 16 patients, and replaced with de-epithelialised colon in a process named seromuscular colocystoplasty (Gonzalez *et al.*, 1995). Two hourglass deformities were able to be surgically corrected after surgery, and two patients who failed to augment went on to undergo enterocystoplasty. Urodynamic studies revealed there was a mean 2.4-fold increase in bladder capacity (excluding the patients for whom there was no observed improvement) and a mean 1.9-fold decrease in end-filling pressures. Cystograms indicated that the colonic transplant

did not show any signs of peristaltic activity, and continence among patients was generally improved. However, biopsies taken of the bladders postoperatively demonstrated that the epithelium inside the organs were often a mixture of both colonic mucosa and bladder urothelium. Despite the promising urodynamic results, the biopsies therefore demonstrated that the problem of maintaining the urothelium of the bladder was not able to be addressed by this surgical technique. It is therefore possible that many of the problems with enterocystoplasty which are caused by the presence of intestinal epithelium will also be prevalent in patients treated with seromuscular colocystoplasty.

Stenzl *et al.*, (2000) performed a study to determine whether skeletal muscle could be used as a functional detrusor muscle graft, so that patients with acontractile bladders could be restored to proper function. The latissimus dorsi (LD) muscle was dissected from the back of 14 dogs, and then either used to replace the detrusor muscle over 50 % of the bladder (mucosa-sparing partial cystectomy), or replace the full-thickness bladder wall over 50 % of the bladder (partial cystectomy). The detrusor muscle replacement procedure (latissimus dorsi detrusor myoplasty, LDDM) showed signs of muscle regeneration and innervation—aided by a step in the procedure to re-attach the nerve of the muscle to a pre-existing nerve—and enabled normal bladder function. The full-thickness partial cystectomy, however, led to death in all subjects, indicating that skeletal muscle is not suited to contact with urine, as it lacks an epithelium. Following the success of the mucosa-sparing partial cystectomy, LDDM was performed in 11 human patients. There were some minor complications including bladder stones in two patients, however eight patients were able to spontaneously void, two others did not require catheterisation as frequently, and one showed no improvement postoperatively. This was an admirable innovation, however it did not address the situation where bladder augmentation is required. The approach could potentially be combined with another material to act as a urine barrier for the muscle. In addition to this, the use of the the latissimus dorsi muscle constituted a significant donor site morbidity.

### 1.4.2 Allotransplantation and xenotransplantation

Allografts use tissue donated from a donor which is of the same species as the recipient. The two individuals are consequently genetically different and therefore the recipient recognises the donor tissue as ‘non-self’. This would result in the tissue being rejected from the host by either acute or chronic rejection, depending how close a genetic match the donor is to the receiver. However, allotransplantation is made clinically viable through the use of immunosuppressive drugs (Knight & Ingham,

2006). The side-effects of immunosuppression, combined with the lack of available donor tissue demonstrates that allotransplantation represents a sub-optimal solution for bladder augmentation (Nerem, 1995).

Xenotransplantation involves transplanting tissue between different species. The tissue is therefore of a very different genome to the host, and so in this case the recipient body also recognises the donor tissue as 'non-self'. In this situation, the tissue body would be quickly rejected from the tissue body through a hyperacute rejection mechanism. Additionally, there is a sugar residue called gal$\alpha$1-3gal ($\alpha$-gal) which is present on the surface of all cells of all mammalian species, with the exception of humans and some primates. This sugar is similar in shape to a sugar epitope which is present on bacteria which live in the human gut, and due to exposure to this sugar humans therefore have large numbers of antibodies against this sugar. Therefore, the transplantation of mammalian tissue into humans quickly triggers a severe immune reaction caused by the presence of $\alpha$-gal expressed on the surface of the mammalian cells (Knight & Ingham, 2006). The use of xenografts is therefore not clinically viable.

## 1.5 Tissue engineering approaches to bladder augmentation

### 1.5.1 Principles of tissue engineering

Due to the problems which are associated with traditional transplantation techniques, a tissue engineering approach to augmenting the urinary bladder may provide an improved outcome for patients compared to enterocystoplasty. Tissue engineering is the pursuit of understanding the structure and function of tissues, and the development of biological substitutes with the capability to restore, maintain or improve tissue or organ function (Nerem, 1995). From this definition, three main strategies of tissue engineering have emerged in order to try and restore tissue function (Langer & Vacanti, 1993):

1. Cells are implanted that are specifically selected to provide a particular function.
2. Scaffolds are implanted that encourage the development and regeneration of a tissue.
3. A combination of the above (a cell-seeded scaffold).

Engineered scaffolds, both seeded and unseeded with cells, have been shown to

induce tissue regeneration in many types of applications and tissues (Langer & Vacanti, 1993), so there is potential for the development of commercially-available tissue engineered grafts for widespread clinical use. Tissue engineering offers the prospect of better solutions to current procedures, in the way of cheaper, more widely available, more effective and earlier interventions of morbidities, to provide a more substantial improvement to the quality of life of patients.

Cells provide the functional element of any tissue or tissue-engineered construct. This desired function may be any *in vivo* cellular function, and is typically the function of the tissue that is being replaced. This function may be temporary or permanent, depending on the desired result of the implant. Cells should not cause an immune response in the host, either by ensuring that they are immunocapable or by keeping them isolated from the immune system of the host by a permeable barrier (Langer & Vacanti, 1993). Immunosuppressive drugs could be used, but this would forgo one of the fundamental advantages of tissue engineering. The types of cells that can be used depends on their difficulty to isolate and the conditions under which they grow, including which growth factors they require. This step would be very difficult for a cell that has not been cultured before, as devising a method of isolation, identifying and supplying growth factors, and controlling differentiation is a very challenging task without even considering immunological rejection. Immunocompatibility is improved if cells are sourced from other humans, and ideal if the patient's own cells can be used, but this may not always be feasible. Cells could be genetically manipulated to provide the desired cellular function. This could involve manipulating cells to prevent rejection, or to alter the behaviour of a cell so that it synthesizes a desired protein (Nerem, 1995). Due to these numerous difficulties in preparing suitable cells, the use of cells in tissue engineering remains a highly problematic and complex task.

Scaffolds should be able to support the growth of cells, be biocompatible, and have suitable mechanical properties. Such a scaffold should be a viable ECM for cells to exist in and should also be easy to handle for use in surgery (Nakanishi *et al.*, 2003). *In vivo* cells exist in a complex biochemical and biomechanical environment, and it is this combination of signals from chemicals and the mechanical environment that drives tissue-specific cellular functions. A tissue-engineered scaffold must therefore be able to provide these signals (either directly or when implanted) to enable and support the desired cellular functions, whilst also not causing an inflammatory or fibrotic response, i.e. be biocompatible (Nerem, 1995). This means that scaffolds must provide a suitable biomechanical structure in order to suitably integrate with the host and provide a mechanical function, whilst also providing a suitable biochemical environment in order to signal to cells in a manner to produce the desired cellular

functions. Therefore, implanted materials will vary depending on their *in vivo* application (Nerem, 1995). These biomaterials may be made from natural materials such as collagen, or synthetic polymers such as polylactic acid (PLA), polyglycolic acid (PGA), or hydrogels. Polymers can be nondegradable, or biodegradable for cells to replace the scaffold with their own secreted ECM (Nerem, 1995; Chen *et al.*, 2001). Biodegradable materials would rely on the cells remodelling the implant and would not provide any problems regarding long-term biocompatibility (Langer & Vacanti, 1993). Due to the need of cells to receive nutrients, vascularisation of any cell-supporting biomaterial is highly desired due to the difficulty of nutrients to diffuse over a large distance (Nerem, 1995). Encapsulation refers to the implantation of a biomaterial that separates the cells inside it from the immune system of the host by a semi-permeable membrane (Nerem, 1995).

Synthetic polymers have the advantage of being able to be precisely manufactured to control their properties (degradation time, hydrophobicity, etc.), however they do not always support cells as well as natural materials, and the morphology and hydrophobicity of biodegradable polymer scaffolds can hinder cell seeding and growth (Langer & Vacanti, 1993; Chen *et al.*, 2000). They should be highly porous, have a large surface to volume ratio, and be able to be made in many different geometries. Materials that have been used include PGA, PLA, poly(L-lactic acid) (PLLA) and poly(DL-lactic-co-glycolic acid) (PLGA), and they are prepared using a variety of techniques and parameters which have resulted in different structures, mechanical properties and degradation times (Chen *et al.*, 2001).

The use of certain cell-signalling molecules (tissue-inducing factors, growth factors, angiogenesis stimulators) to stimulate cellular growth has been shown to aid tissue regeneration when combined with synthetic scaffolds (Langer & Vacanti, 1993). This is unsurprising, as these factors are naturally present *in vivo* and regulate tissue homeostasis. The surface of synthetic biomaterials may also be coated with adhesion peptides in order to enhance cell attachment (Nerem, 1995). A biomaterial containing biologically active molecules, could also be used to purely stimulate nearby cells by secreting these molecules, rather than existing as a scaffold (Nerem, 1995).

Natural materials are typically made by extracting natural materials from tissues (e.g. collagen), and processing them in order to produce a scaffold made using the extracted material (Magnan *et al.*, 2006). They may contain cell-signalling amino acid sequences that aid cell attachment and function, however there is usually significant variability between samples (Langer & Vacanti, 1993). These materials are more hydrophilic and support cell growth better than synthetic materials (Chen *et al.*, 2001). Natural materials also include the use of decellularised tissues, which

are typically intended for allogeneic or xenogeneic transplantation. Decellularised tissues are produced by subjecting tissues to a combination of chemical, physical and enzymatic treatments in order to remove cells and other immunogenic material from the tissues (Gilbert *et al.*, 2006), but leaving behind the ECM of the original tissue. It is thought that that these protocols would produce materials which would not be rejected by the body, but which still retain the same histoarchitecture and extracellular molecules of the original matrix, which promote constructive remodelling of the tissue (Gilbert, 2012).

Some of the problems of synthetic scaffolds can be overcome by combining a synthetic graft with natural materials. Hybrid scaffolds combine synthetic polymers with naturally derived materials, whereby the natural material can provide a good cell-seeding substrate, and the synthetic one can provide mechanical strength (Nakanishi *et al.*, 2003). These too can be made using a variety of techniques to produce various types of hybrid graft (Chen *et al.*, 2001). Indeed, several of these composites have been produced for use with tissue engineering applications (Chen *et al.*, 2000).

Although implanting cell-seeded scaffolds could improve recovery times by effectively implanting a fully-functional tissue, there are numerous ethical and safety issues associated with this, notwithstanding the even greater concern of immune system rejection. However, an unseeded scaffold would have many benefits in clinical use, as it circumvents the problems of cell sourcing, manipulation and seeding (Langer & Vacanti, 1993). This option would reduce time, work and cost of each implant, with a potential for off-the-shelf availability.

A tissue-engineered bladder must be capable of containing urine at a low pressure, while facilitating the construction of a functional bladder wall including functioning urothelium, blood vessels and smooth muscle, and not be immunogenic. Such a graft could potentially be a better alternative to enterocystoplasty, and may also have applications in reconstruction of other tissues in the urinary system, such as the ureters or urethra (Magnan *et al.*, 2006). Several approaches in the literature have been taken to engineer bladder tissue. These will be looked at below.

### 1.5.2 Synthetic matrices

Synthetic bladder augmentation materials have typically taken two different forms: replacement of a bladder with an artificial bladder made of a nonresorbable material, or augmentation using a resorbable material which is able to integrate with the bladder wall and eventually be completely degraded and subsequently replaced by the ECM of the patient. Rohrmann *et al.*, 1996 investigated the use of a nonre-

sorbable silicon rubber prosthesis as a bladder replacement device. Two artificial bladders were implanted into each of five sheep, one leading from each kidney and then joining before exit via the urethra. Valves were present in the prosthesis to prevent reflux of urine towards the kidneys, and voiding was achieved by manually compressing the artificial bladders through the skin. Urine leakage was prevented at the kidneys using a dacron patch glued to the kidneys, and a seal was made with the urethral tube by gluing a dacron patch to the tube and suturing that to the urethra. Urinary leakage occurred in three animals, which were consequently sacrificed. Leakages in two of the animals was caused by a defect in the wall of the artificial bladder, and the remaining leakage was the result of a disconnection of a pipe leading to the urethra. The remaining two animals presented as normal until being scarified at 18 and 19 months due to limited funding. All ultrasounds were normal throughout the experiment, however histological analysis revealed signs of a foreign body reaction in the renal pelvis, ureters and urethra. Although this solution may be more convenient for a patient than a urostomy, the foreign body response indicated a lack of prosthesis biocompatibility, and the pipe disconnection and defects in the artificial bladder wall demonstrated that designs of this type are susceptible to mechanical failure, particularly because the prosthesis is not able to be repaired by the body over time.

Polyglycolic acid (PGA), poly(L-lactide) (PLLA) and poly(lactic-co-glycolic acid) (PLGA) are all polymers which are able to be degraded by the body and have been investigated as potential materials for use in tissue engineering.Regarding the treatment of children requiring surgical repair of congenital abnormalities, research has been conducted in an animal model in which cells were harvested from a foetus in vivo so that they could be expanded and used neonatally (Fauza *et al.*, 1998). A bladder exstrophy defect was created in lamb foetuses *in utero*, and a sample taken of the full-thickness bladder. Urothelial and detrusor muscle cells from these samples were independently expanded for 50–55 days in vitro. After performing tests to analyse cell phenotype, they were seeded onto PGA scaffolds (unwoven fiber mesh sheets of PGA polymer) and incubated for between 4 and 7 days for urothelial cells, and between 7 and 10 days for detrusor muscle cells. After birth, this engineered tissue was used for bladder augmentation during the repair of the bladder defect, and in a control group the defect was repaired with no augmentation. The animals that received augmentation demonstrated a greater bladder capacity and compliance than the control group. However, despite the engineered tissue resembled the appearance of natural bladder tissue, it did not mimic it exactly and the compliance curve for the engineered bladder was not the typical shape of a normal bladder filling to capacity. Although the bladder augmentation seemed to enhance bladder function,

the performance of it was difficult to evaluate without also including animals that did not undergo any surgery as a negative control group. In addition, a non-seeded scaffold was not used for comparison. This approach could only be used clinically as a personalised medical procedure in a limited number of patients due to the high cost associated with producing the cell-seeded patch material.

A similar method was adopted in another study, the difference being that the PGA fibre matrix was coated with PLLA 50:50 (Oberpenning *et al.*, 1999). Bladder biopsies were taken from beagle dogs (n = 14, age unspecified), and used to culture urothelial and smooth muscle cells which were then seeded onto the scaffolds. It took a mean of 32 days to extract cells from biopsies, expand them *in vitro*, and culture them on the seeded scaffold. The resulting spherical cellular scaffold was used in an allogeneic trigone-sparing bladder replacement. A control group ($n = 2$) underwent trigone-sparing cystectomy without bladder augmentation. Animals were studied 11 months post-operatively. Animals that received the cell-seeded scaffold ($n = 6$) achieved a mean bladder capacity of 95 % postoperatively, whereas animals that received scaffolds not seeded with cells ($n = 6$) achieved a mean bladder capacity of 46 %. Bladder compliance also was greater for cell-seeded scaffolds than for unseeded scaffolds (reduced postoperatively by a mean of 10 % and 42 %, respectively). Bladders replaced with acellular scaffolds were subject to graft shrinkage, scar tissue formation and partial collapse of the original spherical architecture, and a bladder stone was found in one bladder. Microscopically these bladders showed signs of angiogenesis and fibrosis at the bladder-scaffold interface, and connective tissue formed where the polymer had degraded. Bladders replaced with the cell-seeded scaffolds appeared continuous with the pre-existing host tissue after 3 months. The polymer completely resorbed, and the tissue demonstrated angiogenesis, muscle fibre alignment, a tri-layered structure and neural tissue ingrowth. Both types of graft supported an intact urothelium, but in general the acellular scaffold resulted in fibrotic neo-bladders with low compliance, whereas the cell-seeded scaffolds appeared to function as normal bladder tissue. However, this procedure would involve culturing the patient's own bladder cells before seeding them onto a scaffold and then finally performing the bladder augmentation surgery. This type of procedure would be extremely expensive, so would only be suitable for a very small number of patients. Additionally, it has been seen that urothelial cells extracted and cultured from abnormal bladders have a reduced capacity for proliferation and differentiation *in vitro* (Subramaniam *et al.*, 2011). It is therefore likely that a procedure of this type would have a less positive result if performed on patients with diseased bladders.

Synthetic matrices have the benefit of being designed from the ground up, which

means that their structural, mechanical, chemical and biochemical properties can be changed to suit the required application (LamVanBa *et al.*, 2015). For example, Pattison *et al.*, 2007 synthesised PLGA scaffolds using different ratios of the monomers lactic acid and glycolid acid (50:50, 75:25 and 85:15 wt.-%). Poly(etherurethane) (PU) scaffolds (grades SG100A, 93A and 80A) were also made. Porous scaffolds were made using a solvent casting and salt leaching process. Some scaffolds were further modified to create polymeric scaffolds with nano-dimensional surface features using either NaOH (for PLGA) or $HNO_3$ (for PU). The suitability of the materials to replace bladder tissue was assessed my means of cell proliferation and adhesion studies and preliminary animal studies using rats. Scaffolds of either PLGA or PU patch were used to augment the bladder of a total of 20 animals using different combinations of the aforementioned scaffold attributes. Scanning electron microscopy revealed that the untreated samples had surface feature dimensions of 20 µm or greater, whereas the treated samples had surface features with dimensions less than 100 nm. This resulted in in increase in both the average pore diameter (two-fold increase), percentage porosity (mean increase of 30 %) and surface area (four- and two-fold increase respectively) for treated PLGA (50:50) and PU samples. In the cell adhesion and proliferation studies, cells grew and attached in the greatest number on the treated PLGA (50:50) scaffold. Approximately four-fold fewer cells grew and attached to both the untreated PLGA (50:50) and treated PU samples, and approximately half fewer cells again grew and attached to the untreated PU scaffold. Initial animal studies demonstrated that treated and untreated 50:50 PLGA was not mechanically strong enough for implantation due to bladder leakage. PU (100A) was considered to be too strong and was not tested. Subsequently, treated 75:25 PLGA was implanted into four animals, treated 85:15 PLGA into one animal, and both 80A and 93A PU (treated) were implanted into a total of eight animals. It was noted that the 85:15 PLGA was very brittle, and that all the PLGA samples was degraded at the final nine-month time point without any sign of bladder stones. Of the eight animals implanted with PU, one died prematurely. Of the seven remaining, two had a patch which was located outside the bladder, whereas the patches of the remaining five were located inside the bladder. The PLGA patches were therefore more readily absorbed by the hosts than the PU patches. This study demonstrated that many different facets of synthetic scaffolds can be manipulated, however without any clear data regarding the *in vivo* graft performance (such as histology or cystometry), it was difficult to assess the success of the implantations.

Atala *et al.*, (2006) attempted to engineer human bladder tissue by seeding autologous cells onto collagen matrices. A small bladder biopsy was obtained from the dome of 7 patients' bladders and explant techniques were used to culture smooth

muscle and urothelial cells for approximately 6 weeks. Scaffold size was tailored to the requirements of each individual patient. Two matrices were used: decellularised homologous bladder submucosa for four patients, and a PGA-collagen composite for three more. All scaffolds were sterilised by UV light then ethylene oxide. Approximately $700 \times 10^6$ of each cell type were seeded onto each bladder. Smooth muscle cells were seeded onto the outside, incubated for 48 h, urothelial cells seeded onto the inside, and incubated for 72–96 h. Bladders were surgically attached to pre-existing bladders using sutures and fibrin glue. Four patients (one with bladder submucosa, three with collagen scaffold) had their bladders covered with omentum. Postoperatively, the mean capacity of bladders increased by 29 % and the mean compliance increased by 118 %. PGA-collagen composite scaffolds and scaffolds wrapped in omentum were significantly more successful than decellularised bladder submucosa and bladders not wrapped in omentum. The omentum wrap is highly vascular, and most likely helped promote vascularisation during the healing process. Histologically, the tissue engineered bladders were very similar to native bladder tissue, and the follow-up post-operative findings showed that bladders did continue to function up to 61 months later. There will have been no aspect of these procedures that did not cost large mounts: custom-made scaffolds, many weeks of cell and organ culture, and numerous post-operative tests. The procedure seemed to have improved the quality of life of the seven people that took part, but it would not be possible on a larger scale. Also, all the patients were young (4–19 y), so the rate of healing and regeneration may be not be adequate for the process to be used in older patients. Although this study appeared successful, the authors reported that more studies would be needed before this procedure is more widely used. However, a similar study is yet to be seen.

Silks are used in nature as materials for constructing spider webs and cocoons. They are both degradable and have good mechanical properties properties (e.g. high tensile strength). For these reasons, they have been used clinically in the form of sutures. However, silk fibroin has also been used as a material for tissue engineering. Mauney *et al.*, 2011 compared the *in vivo* performance of a silk-based biomaterial with small intestine submucosa (SIS) and PGA matrices in a mouse bladder augmentation model. Silk tubes were spun using a gel spinning technique whereby silk fibroin solutions were harvested from silkworm cocoons and spun onto a rotating tube at constant rotational and axial speeds using a needle. The tube was then treated with methanol to transform the amorphous liquid silk into $\beta$-form silk fibroin. Silk tubes were opened into sheets and surgically implanted into 17 mice. Bladder augmentation was also performed on 9 mice using PGA matrices and 7 mice using SIS scaffolds. Histological analysis showed that the silk scaffolds supported ECM

deposition, formation of a multi-layered epithelium and presence of smooth muscle bundles, both of which were comparable to the tissues of the non-surgical control mice. SIS scaffolds exhibited dense connective tissue with an epithelium comparable to the silk augmented bladders and a highly organized layer of smooth muscle. PGA scaffolds were thinner and less mature than the other engineered tissues, with thinner epithelial layers, bundles of less organised smooth muscle and evidence of fibrosis. Histological analysis also revealed signs of inflammation at all the sites of implantation, with these being severe chronic in the PGA group, mild chronic in the SIS group and minimally acute in the silk scaffold group. This suggests that silk has a superior biocompatibility compared to PGA, and is better suited to this application. Cystometric analysis of the tissue-engineered bladders demonstrated that the voiding volumes, capacities and compliance of silk scaffolds were greater than those of the SIS and PGA matrices as well as the control bladders. However, all augmented bladders demonstrated a voiding frequency much lower than the control group, suggesting that normal bladder function had not been replicated. These findings indicated that silk may be a viable bladder augmentation material, however this small animal model does not guarantee equal success in larger animals. One study was found which used silk in a large animal model of augmentation cystoplasty. (Tu *et al.*, 2013) implanted acellular bi-layer silk scaffolds into 10 juvenile swine, with 3 control animals. Histological examination revealed in-growth of the surrounding tissue into the implanted scaffolds, with a structure which resembled that of native bladder. As with the small animal model previously discussed, some regions of the silk scaffolds elicited a minimal acute inflammatory response. Cystograms revealed a large variation in bladder capacity and compliance, likely due to the young age of the animals, however a marked increase in bladder capacity and compliance of the test animals was evident from the data. The findings indicated that the implanted silk scaffolds were a potent bladder augmentation material, however more data—particularly long-term data on older animals which have a lesser capacity for regeneration—is required.

Studies performed using synthetic scaffolds suggested that the current technology surrounding polymer-based and silk scaffolds is not advanced enough in order to provide a viable alternative for bladder augmentation. Silk scaffold technology it yet to prove itself in larger animal models, and although there have been concerns regarding the biocompatibility of silk, these have since been explained by the presence of sericins, which typically form a coat around silk fibres. Methods have been developed to completely isolate silk from these proteins, and the biocompatibility of isolated silk has since been demonstrated (Meinel *et al.*, 2005). Tissue-engineered scaffolds synthesised using polymers such as PLGA are able to be modified in order

to produce a material with specific physical properties, including attributes such as cell adhesion, degradation rate (Pattison *et al.*, 2007) and structure (Pattison *et al.*, 2005). However, polymers fail to mimic the *in vivo* environment and do not contain any of the cell-signalling factors which are present in tissue, such as cell-adhesion ligands and growth factors, which are though to be required for the regeneration of functional tissue (Atala, 2011). Furthermore, evidence has indicated that the the breakdown of PGA in the body elicits an immune response, (Ceonzo *et al.*, 2006) which suggests that PGA-based materials may not be biocompatible.

### 1.5.3 Processed natural tissue

Magnan *et al.*, (2006) reported that acellular biomaterials did not always lead to a good outcome, and autologous cell-seeded scaffolds were limited by slow vascularisation, leading to necrosis and fibrosis. Subsequently, they isolated urothelial cells, smooth muscle cells and endothelial cells from a porcine bladder biopsy, and verified the cell types by immunofluorescent staining. Fibroblasts were also reported to be present with the smooth muscle cells. Collagen sponges were made from bovine collagens I and III. Endothelial and smooth muscle cells were seeded in equal densities on the sponges for 10 days, then urothelial cells were seeded onto the surface and cultured for 7 days. Following this, the resulting engineered bladder appeared to resemble native bladder tissue, with a multi-layered epithelium similar in thickness to native bladder supported by a basal membrane, capillary-like tubes spaced throughout the region beneath the urothelium, and some presence of smooth muscle cells in the region beneath the urothelium. One of the main goals of the study was to attempt to induce the formation of blood vessels in the structure so that potentially the graft could integrate with the host and receive a blood supply soon after implantation. The authors stated that cells in the middle of a matrix thicker than 3 mm will be at risk of dying without an adequate vascular supply (which can take up to 15 days to form), leading to fibrosis and contraction. Thinner grafts are unlikely to have the adequate mechanical strength for a bladder wall replacement. The formation of pseudo-capillaries has shown that this may be possible. This well-documented study also thoroughly described a method for endothelial cell isolation from the bladder, which was reported to be necessary to seed endothelial cells along with the urothelial, smooth muscle and fibroblast cells for pseudo-tissue formation. However, although the study reported that a minimum thickness of graft would be required for suitable mechanical properties, no mechanical properties were tested or discussed in detail in the paper, so the mechanical suitability of this engineered tissue for implantation is unknown. Also, while a urothelium was present it did not

quite mimic the fluctuating surface morphology of native urothelium, suggesting that it may not have been as compliant as native bladder. The statically cultured bladder also did not seem to have a smooth muscle structure that resembled that of native bladder.

### 1.5.4 Hybrid natural–synthetic matrices

An *in vitro* study was conducted to compare the tissue engineering potential of hybrid scaffolds of PLGA/collagen sponge and PLGA/collagen gel (Nakanishi *et al.*, 2003). Urothelial cells and smooth muscle cells were extracted from porcine bladders and cultured. For the PLGA/collagen sponge scaffold, a Vicryl knitted mesh was made of PLGA, which was then immersed in a bovine collagen solution, frozen and freeze-dried to form the collagen sponge. This was cross-linked with glutaraldehyde vapour and freeze-dried once more. Urothelial and smooth muscle cells were cultured independently onto the scaffold. The PLGA/collagen gel scaffold was prepared by first making a PLGA knitted mesh. An acid-soluble collagen solution was mixed with minimum essential medium (MEM), reconstruction buffer, and the cultured cells. This was poured onto the PLGA mesh, and both incubated to allow gel formation. The urothelial cells showed urothelial phenotype, and the muscle cells showed characteristics of smooth muscle cells. On the PLGA/collagen sponge scaffold the urothelial cells grew well and formed a layer of stratified urothelium, 3-4 cells thick (verified by confocal microscopy), and were kept alive for 3-4 weeks. Smooth muscle cells did not proliferate on this scaffold. On the PLGA/collagen sponge scaffold, urothelial cells were cultured but did not spread over the surface, remaining in clusters. Smooth muscle cells grew well and could be cultured for 2 weeks. A structure was made to mimic the bladder wall by combining the urothelial layer from the PLGA/collagen mesh scaffold and the smooth muscle layer from the PLGA/collagen gel scaffold. The study claimed that the two cell-seeded scaffolds produced were useful biomaterials for tissue engineering. Although the PLGA/collagen mesh urothelium produced seemed to be similar to that seen *in vivo*, and the PLGA/collagen gel supported smooth muscle cells well, it was not reported whether the combined construct was viable to produce. The problem it seems with these materials was that neither could support both cell types well, and although it showed some potential, a combined construct of the two materials after cell seeding would be hightly labour-intensive, and possibly not viable to offer clinically.

### 1.5.5 Acellular matrices

#### 1.5.5.1 Pericardium

Novick *et al.*, (1978) realised that a biodegradable graft may be more successful than previous attempts to substitute the bladder using natural and synthetic materials, and used bovine pericardium as a starting material, which had previously been shown to be resorbed by the body when implanted subcutaneously. Patches were prepared by mechanically removing fatty tissue, washing in ethanol, incubating in acetic anhydride and rinsing in sterile saline. This process significantly altered the appearance of the scaffold material. To implant the material, a 50 % partial cystectomy was performed in 10 adult female dogs with healthy bladders and the pericardial graft was used to replace the excised portion of the bladder. This was also performed in 4 dogs with artificially induced fibrotic bladders. A control group of 6 dogs received a partial cystectomy with no enlargement graft. Postoperatively, the control group showed a drop to 45 % of bladder capacity, which recovered to 70 % a year after surgery. The dogs with healthy bladders had normal bladder function and showed almost no change in bladder capacity at any time point up to a year postoperatively. After induced bladder fibrosis (to simulate a chronic contracted bladder state) the dogs had 25 % bladder capacity, but following augmentation and recovery the capacity returned to 90 % capacity 6 months postoperatively. Most grafts integrated well into the bladder wall and showed little sign of residual graft at the end of the study. After 14 weeks the graft was typically completely reabsorbed. However, during the healing process some bladders showed signs of contraction, inflammation and fibrosis. Furthermore, some dogs showed signs of fibrotic and scar tissue, calcium deposition, and other problems. Although these outcomes were dismissed as problems by the authors, no grafts were left in animals beyond a year, and some only 6 months, and therefore the longer-term effects of the grafts are largely unknown.

#### 1.5.5.2 Small intestine submucosa

The use of small intestine submucosa (SIS) as a tissue autograft was first described by Matsumoto *et al.*, (1966a), where it was mechanically isolated from jejunum and used to replace a large vein. Subsequent studies using this method (Matsumoto *et al.*, 1966b; Egusa, 1968; Lawler *et al.*, 1971) also demonstrated that the material was a strong, thin membrane that was able to be sutured to other tissues of the body. It integrated with other tissues with varying success when used as either an autograft or allograft, and showed signs of regeneration in some circumstances.

This method of producing SIS was later refined by Badylak *et al.*, (1989) to form large vascular autologous grafts. It was developed to improve upon the moderate success rates of the synthetic grafts used at that time. SIS was produced by removing a segment of the proximal jejunum of dogs, which was then wrapped in surgical sponges soaked in physiologic saline. Following this, the tunica serosa and tunica muscularis were mechanically removed using a scalpel blade and moistened gauze, the intestine segment was everted, and the tunica mucosa removed using the same method. The remaining tube was everted to its original orientation, rinsed with saline, and placed in 10 % neomycin sulphate solution for approximately 20 min before use. SIS produced in this manner was very flexible and strong due to its high collagen content, contained a relatively small number of cells, had a good capillary supply and had a thickness of approximately 0.1 mm.

Following that, numerous studies used the material as a graft for many different tissues such as blood vessels (Badylak *et al.*, 1989; Lantz *et al.*, 1990), musculoskeletal repair (Badylak *et al.*, 1995) and abdominal wall repair (Prevel *et al.*, 1995). These demonstrated some infiltration of the graft by inflammatory cells, capillary formation, formation of collagen fibres and new tissue around the grafts, infiltration of some native cells, signs of host integration and cellular remodelling, and biodegrading of the graft. Some of these studies also sterilised the SIS graft using peracetic acid before use, and all showed promise that a SIS graft may be clinically useful in some circumstances.

To assess the morphology of SIS used as a bladder augmentation material, nine dogs underwent a full-thickness partial cystectomy and augmentation using SIS (Badylak *et al.*, 1998). Dogs were sacrificed at 4, 8 and 12 weeks after surgery. Samples of the bladder and SIS were analysed using histology. After 4 weeks, the biomaterial showed significant cell in-growth and an intact urothelium at the bladder lumen. After 8 weeks, smooth muscle cell bundles and good vasularisation could be seen, with an absence of inflammatory cells. At 12 weeks the tissue very closely resembled native bladder tissue, and there was no evidence whatsoever of the SIS graft. This indicated that the SIS has completely degraded, and left behind bladder tissue closely resembling native tissue. This demonstrated that SIS may be a good biomaterial to use for human cystoplasty. However, the method of producing SIS involves a lot of careful mechanical handling, and the only chemical treatment is a peracetic acid step. This means that while cells may be dead, cellular and other immunogenic material may still be present in the SIS, including $\alpha$-Gal, which is known to cause transplant rejection in humans (Daly *et al.*, 2009).

The integration of cell-seeded SIS in athymic nude mice has also been investigated (Zhang *et al.*, 2004). Their lack of T-cells allows the acceptance of xenogeneic tis-

sues without rejection. Bladder smooth muscle cells and urothelial cells were isolated from human bladders and expanded *in vitro*. These cells were subsequently seeded onto the graft, smooth-muscle first to produce a layered co-culture, and incubated for 14 days *in vitro*. This graft was cut into $1\,\mathrm{cm}^2 \times 1\,\mathrm{cm}^2$ pieces, folded over and sutured so that cultured cells faced each other, and implanted subcutaneously into a flank. Control unseeded SIS grafts were implanted similarly into the contralateral flank. During *in vitro* co-culture cells grew in a layered structure; the urothelial cells forming a layer above the smooth muscle cells, which themselves showed signs of infiltrating the SIS matrix. At each time point in the study, the non-cell seeded controls showed signs of graft shrinkage, whereas the cell-seeded grafts appeared to be stable. Neovascularisation was apparent on the surface of both types of implant. Tissue regeneration occurred in all cell-seeded grafts. Generally over the time points, the number of cells supported by the SIS grew to the point where a layered urothelium and initial smooth muscle bundle formation was observed at 12 weeks. Small blood vessel formation was also observed. Control scaffolds did not demonstrate any bladder-specific cell growth. Only fibroblasts were seen by the grafts, in addition to some small blood vessel penetration. The study showed that SIS has the potential to be used as a bladder augmentation graft, and that it can support primary human bladder cells *in vivo*. However, the use of athymic mice and the subcutaneous position of implantation of the scaffold does not test how the graft would perform functionally as a bladder, or if it would provoke an immune response.

Although there have been some promising advances using SIS material, Zheng *et al.*, 2005 recognised that the use of SIS for tendon repair resulted in swelling and pain local to the implantation site, and consequently conducted an assessment of the material to ascertain its biological constituents. Histological analysis of SIS material demonstrated an abundance of porcine cells in the matrix, and nested PCR analysis for the detection of porcine DNA using the pig immunoreceptor gene DAP12 exhibited the presence of the DAP122 immunoreceptor gene. When SIS was implanted subcutaneously in 10 BALB/c mice there was an infiltration of the matrix by fibroblasts and a small number of macrophages, lymphocytes and eosinophils were seen proximal to the implant. Additionally, the repair of a rotator cuff defect in a total of 20 New Zealand White rabbits resulted in the infiltration of lymphocytes in and around the SIS material, whereas the autologous tendon control group demonstrated a relatively reparative host response. These findings demonstrated that the SIS material contained porcine DNA, and that cellular material in the matrix was present in sufficient quantities to elicit an immune response when implanted xenogeneically. Therefore, SIS appears not to be a viable material for use in human tissue repair.

#### 1.5.5.3 Bladder accellular matrix graft

The bladder acellular matrix graft (BAMG) is a graft based on a full-thickness bladder that has been treated to produce a scaffold for bladder augmentation (Probst *et al.*, 1997). To produce the graft, the bladder was: harvested; the mucosa mechanically removed; placed in a PBS and sodium azide solution to partially lyse the cells; washed in PBS; placed in a NaCl and DNase solution; placed in a sodium deoxycholate and sodium azide solution to wash out membrane lipids; washed in PBS and stored in neomycin sulphate. Probst *et al.*, (1997) prepared these scaffolds from rat tissue, and implanted them into 34 rats. Of these, 11 died prematurely due to urinary extravasation caused by bladder stones or blood clots. The remaining 23 were sacrificed for analysis at different stages in the study. It took 2 weeks for a multi-layered epithelium to appear on the grafts, and a total of 4 weeks for this to appear similar to the host tissue. Also at 4 weeks small blood vessels were visible inside and outside of the grafts and nerves were noticeable in the graft. These continued to increase in size and number as time progressed. The bladder integrated with the host macro- and microscopically after fewer than 8 weeks from implantation, and the observed angiogenesis and infiltration of urothelial and smooth muscle cells into the graft suggested that it was re-forming functional bladder tissue. After 16 weeks host muscle cells had infiltrated the implant and formed new muscle fibres. However, the high prevalence of bladder stones (9 of the 23) and the problems they caused indicated that this graft was not ideal. Although the graft did not contract but successfully increased the volume of the bladder, no cystometry data was reported to demonstrate how functional the bladders were, and the inclusion of sodium azide to prepare the graft would hinder approval for clinical use.

More recently the BAMG has been tested for its suitability to support oral keratinocytes and dermal fibroblasts when used as a urethral repair material *in vivo* for male rabbits (Li *et al.*, 2013). Autologous cells were used and expanded *in vitro* in order to reduce donor site morbidity. These scaffolds were then used to repair a mucosal defect in the urethras of male rabbits (n = 3). In the grafts seeded with both oral keratinocytes and fibroblasts (with siRNA inhibited TGF-$\beta$1 expression and reduced collagen I secretion), tissue inflammation was minimal and a complete stratified epithelial layer formed. In the group receiving scaffold seeded with only keratinocytes (n = 3), a stratified epithelial layer also formed. In the control group with no cells seeded to scaffolds(n = 3), fibrosis and stricturing occurred and a complete cellular layer was not generated. The study showed that the seeded cells significantly improved the efficacy of the BAMG as a urethral patch, but this patch was only applied to a very small area. Also, this study was only conducted for 6

months, and it was not mentioned whether the exposure to urine of these cells may become a problem in the longer term.

#### 1.5.5.4 Bladder acellular matrix allograft

Bladder acellular matrix allograft (BAMA) is another approach to produce an acellular bladder-derived material. Brown *et al.*, (2002) investigated the use of this material as a bladder augmentation material. The material was derived from whole (full-thickness) porcine bladders which were placed in a series of solutions, including a hypotonic tris buffer; Triton X-100 solution (1 %); DNase and RNase solution; sodium dodecyl sulphate (SDS) solution and finally ethanol sterilisation. The BAMA was then used as a bladder augmentation material in ten pigs, which were sacrificed in stages at 14, 18 and 22 weeks. Freshly prepared BAMA and implanted BAMA were assessed both histologically and by tensile testing. Although there appeared to be scarring in the centre of the grafts, their gross appearance was similar to that of native tissue, with minimal inflammation. However, graft sizes shrunk by 48 %, and mechanical tests demonstrated that the grafts also got weaker and stiffer over time. Histological sections of the grafts demonstrated that the urothelium, smooth muscle and blood vessels had shown signs of growing into the periphery of the grafts, but in the centre of the grafts there were mostly signs of collagen and glycosaminoglycan (GAG) deposition. The findings suggested that there was a significant amount of fibrous material laid down in the centre of the grafts, which would explain the stiffness which was observed when samples were tested mechanically. Therefore the grafts did not appear to have been able to successfully regenerate bladder tissue, demonstrated by a deterioration rather than an improvement of the grafts over time. Consequently, this material would not be suitable for bladder augmentation. The authors also reported that the decellularisation process had to be performed several times for the tissue to become acellular, and that no GAGs were present in the grafts before implantation. The process had therefore failed to preserve the ECM of the tissue. These findings suggest that the decellularisation method was not suitable for the material, which may have been a result of the thick nature of the bladder material, which the solutions may have been unable to penetrate fully during a single cycle of the process.

#### 1.5.5.5 Full-thickness porcine acellular bladder matrix (PABM)

A process was developed by Bolland *et al.*, 2007 to produce an porcine acellular bladder matrix (PABM) derived from intact full-thickness porcine bladders. It was based on a process initially developed by Booth *et al.*, 2002 to decellularise

porcine cardiac valves. In order to develop an alternative to mechanical cardiac valve prostheses, Booth *et al.*, 2002 investigated several different methods of removing immunogenic material from the tissue. The process initially involved placing porcine aortic heart valves into hypotonic Tris buffer for 14 h to cause cell lysis. The tissue was then treated with different concentrations of either Triton X-100, SDS, sodium deoxycholate, MEGA 10, TnBP, CHAPS or Tween 20 for up to 72 h. This was followed by washing in isotonic Tris-buffered saline. Protease inhibitors (aprotinin and EDTA) were added to all solutions in order to minimise degradation of the matrix by host proteases. The samples were assesses for evidence of decellularisation histologically. Only sodium deoxycholate and SDS were reported to adequately decellularise the tissue, and it was found that a hypotonic buffer was necessary for these reagents to perform as desired. Incubation times greater than 24 h were not required for these chemicals to produce acellular tissue. In order to minimise disruption of the ECM by the detergents, titrations of deoxycholate and SDS were performed to find the minimum concentrations at which the tissues were decellularised. Sodium deoxycholate and SDS were still effective at concentrations of 0.5 % (w/v) and 0.1 % (w/v) respectively for the decellularisation of whole aortic valve roots. For the matrix to be of use for tissue engineering, tissue immunogenicity needed to be minimised whilst also maintaining the structural components and biomechanical properties of the matrix. Complete cell removal was demonstrated whilst the overall tissue histoarchitecture was preserved, including retention of collagen I, elastin and GAGs. Sodium deoxycholate and SDS are both detergents, and therefore were effective at solubilising the phospholipid bilayer of cell membranes, resulting in complete cell lysis. Washing steps were used to remove residual SDS, which is thought to have a cytotoxic effect on cells (Rieder *et al.*, 2004). Electron microscopy revealed that collagen fibre integrity was maintained. Samples tested using uniaxial tensile mechanical exhibited a typical stress–strain curve for soft tissue, an increase in tissue extensibility, but no significant change in ultimate tensile stress (Korossis *et al.*, 2002).

The decellularisation process for intact porcine aortic roots was later developed by Wilcox *et al.*, 2005. Aortic valves were isolated, washed in phosphate buffered saline (PBS), and valve leaflets excised from them. As performed previously, leaflets were incubated in hypotonic Tris buffer followed by a 0.1 % (w/v) hypotonic SDS solution, then washed using PBS. Samples then went on to be incubated in DNase/RNase solution for 3 h, and finally washed with PBS. Whole aortic roots were decellularised using further modifications to the protocol. Following isolation, the root walls were thinned by mechanical dissection to a thickness of 1.5–2 mm, washed using PBS; incubated in hypotonic Tris buffer; washed with PBS; treated with trypsin (1.25 %,

w/v); washed with PBS; incubated in 0.1 % (w/v) hypotonic SDS solution for 24 h; washed with PBS; incubated in DNase/RNase solution for 4 h and finally washed with PBS. EDTA and aprotinin were used to inhibit tissue autolysis throughout all steps for both valve leaflets and aortic roots. These extra steps (mechanical thinning and enzymatic digestion using trypsin) were required to achieve an acellular matrix due to the increased thickness of the aortic root compared to the leaflets. Trypsin treatment leads to loosening of interfibrillar spaces (Bader *et al.*, 1998), and therefore allowed cellular components to be more easily washed from the tissue. DNase and RNase was used to break down nucleic acids in the tissues in order for them to be more easily removed from the tissue. This step was taken because the presence of residual cellular material in decellularised matrices, such as DNA and other organelles, are thought to be cytotoxic to cells and have been seen to cause adverse and inflammatory host responses (Zheng *et al.*, 2005; Feil *et al.*, 2006; Crapo *et al.*, 2011). Likely due to the use of a nuclease digestion step, haematoxylin and eosin (H&E)- and Hoechst-stained histological sections of valve leaflets and aortic roots did not indicate the presence of any cells, cellular remains or residual DNA, and cell-seeding studies demonstrated that the decellularised tissue had and no cytotoxic effects on cells. Following decellularisation, whole aortic roots demonstrated a significant reduction in tissue stiffness in the toe region of the stress–strain curve, but no significant difference in ultimate tensile strength. Preservation of leaflet kinematics indicated that the decellularisation process did not cause changes to the ECM which would prevent functional use (Korossis *et al.*, 2005).

The full-thickness porcine bladder decellularisation process developed by (Bolland *et al.*, 2007) involved transporting bladders in transport medium to preserve the tissue in readiness for processing, followed by washing in PBS. The process then followed the same sequence of decellularisation solutions which were used on valve leaflets, including incubation in hypotonic Tris buffer for 24 h at 4 °C; incubation in hypotonic 1 % (w/v) SDS solution for 24 h at ambient temperature; washing with PBS and incubation in DNase/RNase solution for 24 h at 37 °C. The resulting biomaterials were sterilised using 0.1 % peracetic acid solution and aseptically washed in sterile PBS. Analysis of H&E-stained histological sections showed that the process resulted in a complete removal of visual cellular components, and biochemical characterisation demonstrated a significant decrease in DNA content and a retention of ECM components including hydroxyproline and glycosaminoglycans. Bladder tissue in its relaxed state was reported to be too thick (4–5 mm) for solutions to effectively penetrate the tissue and facilitate decellularisation. The process consequently utilised the compliant nature of the tissue by filling each organ with solution in order to stretch the tissue, reduce its thickness, and allow the solutions

to diffuse into the tissue in sufficient concentrations to produce acellular matrices. It is evident from the study that the procedure of distending the organs at each stage of the decellularisation process resulted in a significant increase in labour intensity compared to the protocol on which it was based ((Booth *et al.*, 2002; Wilcox *et al.*, 2005)). Alternatively, the protocol could have been adapted to use an alternative chemical process, for example using trypsin, as was used when decellularising whole aortic roots (Wilcox *et al.*, 2005). However, this may have resulted in additional disruption to the extracellular matrix. Penetration of solutions into the tissue could also have been increased by increasing the time, temperature or concentrations of the solutions which were used to decellularised the tissue. It was reported in the original study by Booth *et al.*, 2002 that a minimal concentration of SDS was sought in order to minimise damage to the matrix whilst still ensuring complete decellularisation. This was likely due to the evidence that exposure of biological tissue to SDS has been demonstrated to affect collagen structure (Cartmell & Dunn, 2000). The reasons for the chosen duration and temperature of each incubation were not given in the study, however prolonged exposure to SDS was also likely to have resulted in increased alteration to the tissue ECM. The temperatures of some stages may have been able to be increased, provided there was no risk of denaturing any ECM constituents. For example, collagen thermal denaturation has been seen to begin at approximately 60 °C (Venkatasubramanian *et al.*, 2010). However, the nuclease digestion step would not have been able to be performed at temperatures higher than 37 °C due to the active temperature range of the enzymes. Therefore, the temperatures, lengths and solution concentrations of some stages of the protocol could have been increased, however it is likely that doing so would have increased the trauma which would have been caused to components of the ECM during the process, and therefore mechanically stretching the tissue was likely to have been the best method of ensuring decellularisation whilst minimising damage to the tissue.

### 1.5.6 Commercial products

Tengion, Inc. is a company that develops regenerative medicine solutions, and helps push products to market. It publicly acknowledges that many of it's main regenerative medicine technologies were initially developed by Dr. Anthony Atala, director of the Wake Forest Institute for Regenerative Medicine. The ethos at Tengion is to use biopsies from patients in order to seed cells onto scaffolds so they can be implanted into the patient. Despite the success of the paper published in 2006 (Atala *et al.*, 2006), the Neo-Bladder Augment$^{TM}$ product is "not in active development". Of the clinical trials involving the Tengion Neo-Bladder Augment available

on `http://clinicaltrials.gov`, one has been cancelled, and of the other two: 17/18 participants suffered adverse effects and 10/18 suffered serious adverse effects.

## 1.6 Other applications

Several studies have mentioned or shown that materials intended for bladder augmentation cystoplasty also have potential for use as a repair material in other areas of the body, especially the lower urinary system Magnan *et al.*, (2006) and Li *et al.*, (2013). Therefore, a successful bladder patch material may prove successful in repairing urethral defects, and congenital abnormalities such as hypospadias, epispadias and bladder exstrophy.

## 1.7 Rationale for study

Several studies have shown that a fairly successful tissue engineered bladder can be implanted into the host using previously expanded autologous bladder cells (Fauza *et al.*, 1998; Li *et al.*, 2013). However, similar studies using a scaffold alone have typically resulted in a graft that is not as successful as its cell-seeded counterpart, and typically results in graft failure or subject death (Oberpenning *et al.*, 1999; Stenzl *et al.*, 2000). However, because of the huge cost involved in providing customised cell-seeded scaffolds for patients, it would be unfeasible for a product such as that to be widely used clinically.

Numerous studies have demonstrated the benefits of using natural tissue as an implant material, because natural tissue already contain many proteins and growth factors that promote regeneration and host integration (Langer & Vacanti, 1993; Gilbert *et al.*, 2006). Their natural tissue architecture is well suited to cellular integration, meaning that they have to potential to be an ideal graft material, provided that they possess the desired structural and biochemical properties and are not immunogenic.

Currently no naturally-derived material exists on the clinical market that is able to be used as a graft to promote lower urinary tract repair and regeneration. Such a material would be of great benefit to patients requiring bladder augmentation or urethral repair. A bladder patch material which would be of relevant clinical use would need to be: at least 8 cm × 8 cm in size (information gathered from surgeons); bladder-derived in order for the tissue histoarchitecture to match that of native tis-

sue; acellular to prevent rejection by the host and able to be sterilised and packaged as an off-the-shelf material in order for it to be economically viable.

Previously, an acellular porcine bladder biomaterial was developed using a proprietary process, which has potential for development as a patch for use during bladder augmentation and other surgeries of the lower urinary tract (Bolland *et al.*, 2007; Wezel *et al.*, 2011). However, the procedure that was developed to produce the acellular porcine bladder biomaterial involved inflating the intact porcine bladder and using large volumes of solutions to distend bladders with and place bladders in, which is an approach which is not compatible with commercial manufacture. If a the process of decellularising the porcine bladder could be adapted to avoid this awkward step, the acellular porcine bladder biomaterial would have clinical market potential. Additionally, the previous decellularisation method collected, transported, and begin processing porcine bladders within a few hours. This would not be compatible with a manufacturing process which may have to deal with large batch numbers and long transportation times, and therefore a revised transportation and storage protocol would also be required.

## 1.8 Aims and objectives

### Aims

The main aim of this project was to develop a bioprocess for the decellularisation of porcine bladder which would be compatible with a scalable commercial manufacturing process.

### Objectives

- To find a relationship between porcine bladder size and capacity such that porcine bladders filled with this volume during the decellularisation process would be successfully decellularised.
- To determine the mechanical deformation state of bladders during decellularisation (when filled using the previously found relationship), and confirm that application of this state to bladders during decellularisation would result in tissue which was acellular.
- To model the deformation of flat sheets of bladder material in order to find the optimal mode of stretching the tissue for decellularisation.
- To design and test a piece of equipment which would adequately stretch bladders in the way which was previously modelled and allow bladders to be sub-

jected to the decellularisation process whilst in their deformed state.

# Chapter 2

# Materials and Methods

## 2.1 General Materials

A list of chemicals, reagents and their sources is shown in Appendix A.1. A list of equipment and their sources is shown in Appendix A.2. Water referred to as deionised water was the water produced by either a Purelab Option Water Purification System or a Triplered SG Series Compact water purifier. A list of glassware, plasticware and their sources is shown in Appendix A.3. A list of consumables and their sources is shown in Appendix A.4

### 2.1.1 Dissection Kit

A dissection kit was used for all dissection and tissue handling. It comprised of standard forceps, rat tooth forceps, fine curved forceps, straight scissors, curved scissors, and a scalpel handle (no. 4). Sterile and non-sterile scalpel blades (no. 22) were used. To clean, the dissection kit was soaked in 1 % (w/v) Virkon disinfectant for 20 min, washed with hot water and air dried. The dissection kit was sterilised by dry heat as required.

### 2.1.2 Solutions

All solutions were stored in either Duran bottles, plastic Sterilin pots or universal containers unless specified otherwise.

### 2.1.3 General use solutions

**Sodium hydroxide solution, 6 M**

NaOH pellets, 120 g, were dissolved into deionised water and the solution made up to 500 ml. The solution was stored at room temperature.

**Hydrochloric acid, 6 M**

HCl (6 M), 500 ml, was aliquoted from the stock solution. The solution was stored at room temperature.

**Phosphate buffered saline (PBS)**

Ten Oxoid Dulbecco's PBS tablets were dissolved into deionised water and the solution made up to 1 L. The solution was autoclaved and stored for up to 1 month at room temperature.

**Ethanol, 70 % (v/v)**

Ethanol, 700 ml, was made up to 1 L using deionised water.

**Alcohol (90 % v/v)**

Methylated spirits, 1350 ml, was made up to 1.5 L using deionised water.

## 2.2 General Methods

### 2.2.1 Software

The following software was used.

**ImageJ 1.48** Used for image analysis (National Institutes of Health, Maryland, USA, `imagej.nih.gov/ij`).

**Matlab R2011b** Used for data processing and for plotting graphs

| | |
|---|---|
| | (Mathworks, Massachusetts, United States). |
| **Inkscape 0.91** | Used for drawing diagrams (`inkscape.org`). |
| **Zeiss ZEN** | Microscope control and image capture (Carl Zeiss AG, Oberkochen, Germany). |
| **SolidWorks** | Used to create 3D models of designs (Dassault Systèmes, Vélizy-Villacoublay, France). |

### 2.2.2 Use of Class II safety cabinets

Class II safety cabinets were cleaned with 1 % (w/v) Virkon disinfectant followed by 70 % (v/v) ethanol before and after use. All items entering safety cabinets were sprayed with 70 % (v/v) ethanol.

### 2.2.3 Cleaning of glassware and plasticware

Glassware and plasticware was rinsed using tap water immediately after use. Items were washed in a Lancer 810 LX laboratory glassware washer using tap water, LancerClean detergent, acetic acid (diluted to 20 % (v/v) from glacial using tap water) and deionised water. The washing program was as follows: prewash with tap water (1 min); wash with tap water (60 °C, 4 min); wash with detergent (30 s); rinse with tap water; rinse with 20 % (v/v) acetic acid (2 min); rinse with 20 % (v/v) acetic acid (30 s); rinse with tap water; rinse with deionised water (50 °C, 1 min).

### 2.2.4 Sterilisation

#### 2.2.4.1 Dry heat sterilisation

Items were sterilised by dry heat by placing in a hot air oven at 190 °C for 4 h.

#### 2.2.4.2 Autoclaving

Solutions were sterilised by autoclaving at 121 °C and 15 psi for 20 min.

Autoclavable plasticware and other equipment that required sterilisation was wrapped in either an autoclave bag or a sterilisation pouch and sealed with a heat sealer. These were then autoclaved at 121 °C and 15 psi for 20 min.

#### 2.2.4.3 Filter sterilisation

Filter sterilisation was performed aseptically in a class II safety cabinet. The solution was drawn into a syringe, a syringe filter (pore size 0.2 µm) placed on the end of the syringe, and the solution filtered into a sterile container.

### 2.2.5 Preparation of solutions

All solutions were made in duran bottles unless otherwise specified. Liquid volumes were measured using a measuring cylinder.

Chemicals were weighed using a Precision Balance GR-200 (accurate to 0.1 µg). A magnetic stirrer and flea were used to stir solutions to aid dissolution. When required, solutions were placed on a hotplate set to 60 °C.

### 2.2.6 Solution aliquoting

Solutions were aliquoted using an electric pipette filler with graded transfer pipettes (Sarstedt serological pipettes), or Gilson PIPETMAN® adjustable pipettes with STARLAB TipOne® Pipette Tips.

Sterile aliquoting was performed aseptically in a class II safety cabinet using a Starlab ErgoOne® FAST Pipette Controller with graded transfer pipettes, or adjustable pipettes. Non-sterile solutions were aliquoted on a laboratory bench using either an Accumax pipette controller, or adjustable pipettes.

Aprotinin was aliquoted aseptically in a class II safety cabinet using a syringe and needle to draw out the solution through the rubber lid of the solution container.

### 2.2.7 Adjustment of pH

A JenWay 3510 pH meter was used to measure the pH of solutions. The pH meter was calibrated before use using buffer solutions of pH 4, 7 and 10. When not in use, the pH probe was kept in a storage buffer. All pH measurements were taken using temperature compensation. The pH of solutions was adjusted by adding either 6 M HCl or 6 M NaOH drop-wise whilst stirring.

### 2.2.8 Microscopy

Bright-field microscopy was performed using an Oylmpus BX51 or a Zeiss AX10 microscope. Fluorescent microscopy was performed with the addition of a Zeiss HXP 100 metal halide fluorescence light source and fluorescent filter. Images were captured using ZEN microscope software running on a desktop computer.

Samples in tissue culture flasks and 6-well plates were observed using an inverted Olympus CK40 microscope. Images of these were captured using an Olympus IX71 inverted microscope with an Olympus U-CMAD3 digital camera attachment, and Cell$^{B}$ software running on a desktop computer.

### 2.2.9 Sterility testing

#### 2.2.9.1 Streaking onto agar plates

All work was performed close to a Bunsen burner flame. An inoculating loop was heated in the Bunsen burner until red hot. The loop was left to cool. The cap was removed from the sample bottle, and the neck of the bottle was flamed. The loop was placed in the sample, and the cap was replaced on the bottle. The inoculating loop was streaked onto an agar plate. Each sample was streaked onto a plate of nutrient agar, fresh blood agar and Sabouraud dextrose. Plates were placed in a 37 °C incubator. After 48 h, plates were inspected for signs of microbial growth.

#### 2.2.9.2 Nutrient broth

Work was performed in a class II safety cabinet. Square samples of tissue, 1 cm × 1 cm, were added to 10 ml nutrient broth and placed in a 37 °C incubator for 48 h. Nutrient broth samples were inspected for signs of microbial growth.

## 2.3 Cell culture

### 2.3.1 Materials

#### 2.3.1.1 Culture Media

The following culture media were made up aseptically. All media were warmed to 37 °C in a water bath before use.

#### Tryptone phosphate broth solution, 10 % (v/v)

Tryptone phosphate broth (TPB), 7.38 g, was dissolved into 250 ml deionised water. This was filter sterilised into 10 ml or 20 ml aliquots and stored at −20 °C for up to 6 months.

#### 3T3 and L929 cell line culture medium

Glasgow's minimal essential medium (GMEM) was used with 10 % (v/v) TPB solution, 5 % (v/v) foetal bovine serum (FBS), 100 U · $ml^{-1}$ penicillin, 100 U · $ml^{-1}$ streptomycin and 2 mM L-glutamine. The solution was mixed by inverting and stored at 4 °C for up to 4 weeks.

#### BHK cell line culture medium

Dulbecco's minimal essential medium (DMEM) was used with 10 % (v/v) FBS, 100 U · $ml^{-1}$ penicillin, 100 U · $ml^{-1}$ streptomycin and 2 mM L-glutamine. The solution was mixed by inverting and stored at 4 °C for up to 4 weeks.

### 2.3.2 Cell line manipulation

#### 2.3.2.1 Cell culture environment

Cells were cultured by placing in humidified incubators at 37 °C in an atmosphere of 5 % (v/v) $CO_2$ in air. All cell line manipulation was performed in a class II safety cabinet.

#### 2.3.2.2 Resurrecting cells

To resurrect cells, vials were removed from liquid nitrogen storage and placed in a 37 °C water bath. Once thawed, cell suspensions were transferred into a universal container, and 10 ml warm cell culture medium was added dropwise. The cell suspension was centrifuged at 150 *g* for 10 min. The supernatant was discarded, and the cell pellet was resuspended in 1 ml cell culture medium. Cells were counted and diluted as required, and placed into a fresh T75 tissue culture flask.

#### 2.3.2.3 Cell maintenance

Cell culture medium was replaced every 2–3 days. Cell culture medium was removed from the flasks, and fresh culture medium was added. Cells were observed using an Olympus CK40 inverted microscope with phase contrast. Cells were passaged if they were >80 % confluent.

#### 2.3.2.4 Passaging of cells

Culture medium was carefully removed from the flasks. Flasks were washed with 10 ml Dulbecco's phosphate buffered saline (DPBS) (without $Ca^{2+}/Mg^{2+}$). Trypsin-ethylene-diamine tetra-acetic acid (EDTA) solution (Hanks' balanced salt solution (HBSS) with phenol red, with $0.5\,g \cdot l^{-1}$ porcine trypsin and $0.2\,g \cdot l^{-1}$ EDTA) was added to each flask (1.5 ml for T75, 3 ml for T175), and flasks were rocked to ensure the entire surface was covered by the trypsin-EDTA solution. Flasks were incubated at 37 °C in 5 % (v/v) $CO_2$ in air for 5 min. Flasks were firmly tapped to dislodge cells. Fresh culture medium (10 ml for T75, 25 ml for T175) was added to the flasks, and the suspensions were removed and placed into universal containers. The cell suspensions were centrifuged at 150 $g$ for 10 min. The supernatants were discarded and the cell pellets were re-suspended in 1 ml cell culture medium. Cells were counted and diluted as required, and placed into fresh tissue culture flasks.

#### 2.3.2.5 Cryopreservation of cells

Cell pellets were obtained as described in Section 2.3.2.4. Cell pellets were re-suspended in 1 ml cell culture medium containing 10 % (w/v) dimethyl sulfoxide (DMSO). The suspension was aliquoted into cryovials. Cryovials were placed into a Mr Frosty containing isopropanol, and stored at −80 °C overnight. Cryovials were then placed into a liquid nitrogen Dewar.

#### 2.3.2.6 Cell counting

A trypan blue dye exclusion assay was used to estimate the number of viable cells in a suspension. A 1 ml suspension of cells was obtained as described in Section 2.3.2.4. A 20 µl aliquot of this was added to 20 µl Trypan blue. The mixture was loaded onto a haemocytometer, and viewed using an Olympus CK40 inverted microscope with phase contrast. The number of viable cells in a 1 $mm^2$ area was counted. Viable cells are able to exclude trypan blue, whereas non-viable cells are stained dark blue. If the number of viable cells was less than 30, the process was repeated with a higher

density of cells. If the number was greater than 300, then an area of $0.2\,\mathrm{mm}^2$ was counted. The cell density was then calculated using Equation 2.1 below.

$$\text{Cell density } (\text{cells} \cdot \text{mm}^{-3}) = \frac{\text{Cell count} \times \text{Dilution factor} \times 10^4}{\text{Area counted } (\text{mm}^2)} \tag{2.1}$$

## 2.4 Porcine bladder procurement

### 2.4.1 Materials

#### Transport medium (0.01 M HEPES, 20 KIU · ml$^{-1}$ Aprotinin)

Aprotinin (1 ml, 10 000 KIU · ml$^{-1}$) and HEPES (5 ml, 1 M) were aseptically added to 500 ml HBSS with $Ca^{2+}$/$Mg^{2+}$, $NaHCO_3$, and phenol red. This was aseptically aliquoted into five sterile 250 ml Sterilin pots (100 ml per pot) and stored for up to 3 months at 4 °C.

### 2.4.2 Sourcing

Porcine bladders were supplied by Alec Traves Ltd Abattoir (Escrick, York) within 15 min of slaughter. Pigs were aged between 20 and 26 weeks, and were a mix of male and female.

A greater number of bladders were collected than required (50 % extra) to account for some bladders being unsuitable for research purposes.

### 2.4.3 Transportation

#### 2.4.3.1 Transportation in transport medium

At the abattoir, bladders were supplied in a sealed plastic bag. In turn, bladders were removed from the plastic bag, inspected, and discarded if signs of damage were observed due to the retrieval process. Suitable bladders were each filled via the urethra with 50 ml transport medium using a 50 ml syringe, and placed in a 250 ml Sterilin pot containing a further 50 ml transport medium. Bladder necks were not actively sealed; the bladder neck tissue was contracted enough for bladders to retain the delivered transport medium. Bladders were transported to the laboratory by road.

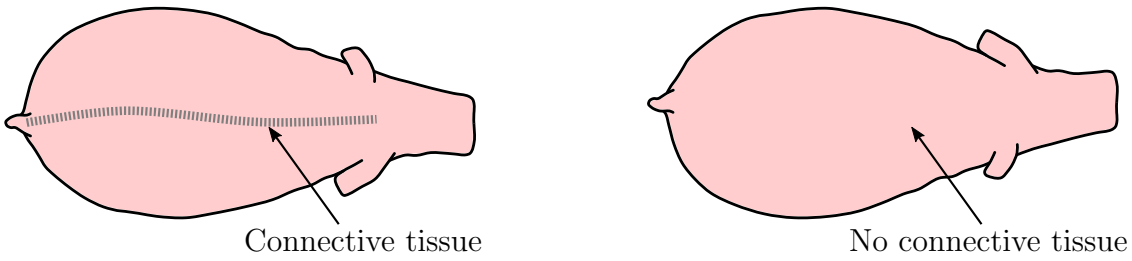


**(a)** The ventral surface **(b)** The dorsal surface

**Figure 2.1: Differences between the dorsal and ventral surfaces of porcine bladders.** When laid flat so the ureters are symmetrical, the appearance of a seam along the midline indicates the ventral surface (a), and the absence of this line indicates the dorsal surface (b).

#### 2.4.3.2 Transportation without transport medium

At the abattoir, bladders were supplied in a sealed plastic bag. Bladders were immediately transported to the laboratory by road.

### 2.4.4 Bladder orientation

To orientate bladders such that their dorsal surfaces were facing upwards, bladders were first laid flat. Bladders were then rotated about their longitudinal (neck-apex) midline until the ureters were symmetrical, on either edge of the bladder.In this position, either the dorsal surface was facing upwards and the ventral surface downwards, or *vice versa*.

The ventral surface of the bladder has a longitudinal band which runs down its midline—a mark which remains from where connective tissue had connected to the bladder before it was cleaned during dissection. If such a band was seen, bladders were turned over so that the dorsal surface was then facing upwards. Bladders with no such band visible had the dorsal surface facing upwards. This is shown in Figure 2.1.

### 2.4.5 Rinsing in wash buffer

To rinse bladders internally and externally, each bladder was placed into a large petri dish. A syringe was used to administer 50 ml wash buffer to the lumen of the bladder. Forceps were used to pick up the bladder by the urachus. The bladder was held over a liquid waste disposal container, and a second pair of forceps was used to eject the wash buffer from the bladder. This was done by placing these forceps

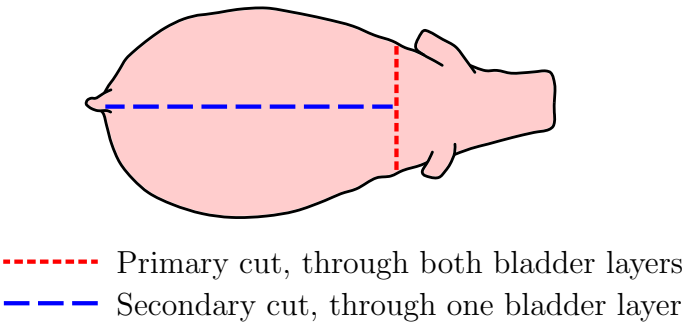


**Figure 2.2: Diagram to illustrate how the bladders were dissected flat using two cuts.** Following the primary cut the bladder neck was able to be discarded. After the secondary cut, the tissue was able to opened out into a single-layered sheet.

across the width of the bladder near the apex, squeezing them, and drawing them down towards the neck; an action comparable to squeezing out toothpaste from a tube. This action was repeated until all the wash buffer had been ejected. Bladders were rinsed externally by pouring approximately 5 ml wash buffer onto them.

### 2.4.6 Dissection

#### 2.4.6.1 Basic dissection

Bladders were placed on a dissection board and inspected for suitability of use. Bladders were discarded if they showed signs of damage from retrieval, such as cuts or slashes. Using a dissection kit, excess fatty and connective tissue was removed; the urethra was cut to 3 cm in length and the ureters were cut to 0.5–1 cm in length.

Aseptic dissection was performed in a sterile 200 mm petri dish inside a class II safety cabinet.

#### 2.4.6.2 Dissecting flat using 2 cuts

Bladders were dissected flat by cutting off and discarding the neck and ureters, and cutting the bladder wall longitudinally from neck to apex, as shown in Figure 2.2. Bladders could then be laid flat as a single-layered sheet.

#### 2.4.6.3 Dissecting flat using 3 cuts

An improved method of dissecting bladders flat was performed using three cuts. The neck was cut off just below the ureters and discarded. The apex was also cut off and

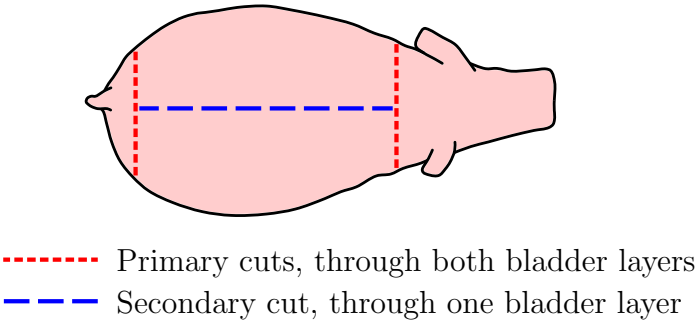


**Figure 2.3: Diagram to illustrate how bladders were dissected flat using three cuts.** Following the primary cuts, the bladder neck and apex are able to be discarded. After the secondary cut, the tissue was able to opened out into a single-layered sheet.

discarded. The second of these two cuts was made so that it was the same length as the first cut. A further cut was then made longitudinally through one bladder layer from neck to apex, as shown in Figure 2.3. Bladders could then be laid flat as a single-layered sheet.

This method of cutting the bladder allowed the material to lay flat with greater ease, in a more rectangular shape. This was particularly important when dissecting fresh (as opposed to decellularised) bladder.

### 2.4.7 Preparatory measurements

Before use, the volume, length and width of each bladder was recorded as described below.

#### 2.4.7.1 Tissue Volume

To determine the volume of the tissue of a bladder, a 250 ml measuring cylinder was filled with $100 \pm 10$ ml transport medium and this initial volume ($v_{\text{initial}}$) was recorded. Excess fluid was gently excluded from the bladder using a scalpel handle. The bladder was then placed in the measuring cylinder, ensuring that the bladder was fully submerged in transport medium. The new volume ($v_{\text{final}}$) was recorded. The bladder tissue volume ($v_{\text{tissue}}$) was equal to the difference between these values, shown in Equation 2.2

$$v_{\text{tissue}} = v_{\text{final}} - v_{\text{initial}} \tag{2.2}$$

#### 2.4.7.2 Tissue Mass

Before weighing, the bladder to be weighed was placed in a 150 ml Sterilin pot, and then was removed from the pot. This was carried out in order to wet the pot, to reduce the moisture transfer that would occur between the bladder and the pot during the actual weighing procedure.

The 150 ml Sterilin pot was then sealed and weighed, and its mass ($m_{\text{pot}}$) recorded to the nearest 0.1 g. The bladder was then placed in the pot, the pot sealed, and this was weighed again and its mass ($m_{\text{total}}$) recorded to the nearest 0.1 g. The bladder tissue mass ($m_{\text{tissue}}$) was determined by taking the difference of these values, shown in Equation 2.3

$$m_{\text{tissue}} = m_{\text{final}} - m_{\text{pot}} \tag{2.3}$$

#### 2.4.7.3 Length and Width

To determine the length and width of bladders, they were laid flat and excess fluid gently excluded from them using a scalpel handle.

**Width**

The bladder width was measured at the widest part of the bladder in the transverse direction, as shown in Figure 2.4, to the nearest 1 mm.

**Length, elliptical**

The bladder elliptical length was determined by estimating (by eye) the length of the ellipse that would lie on the perimeter of the bladder, in the region between the apex and the ureters. This was recorded to the nearest 1 mm. A schematic of this distance is shown in Figure 2.4. This was referred to as the elliptical method for measuring bladder length.

**Length, apex-to-ureter**

The bladder length—from apex to the midpoint of the ureters—was recorded to the nearest 1 mm, as shown in Figure 2.5. This was referred to as the ureter-to-apex method for measuring bladder length, and was the usual method for recording bladder length.

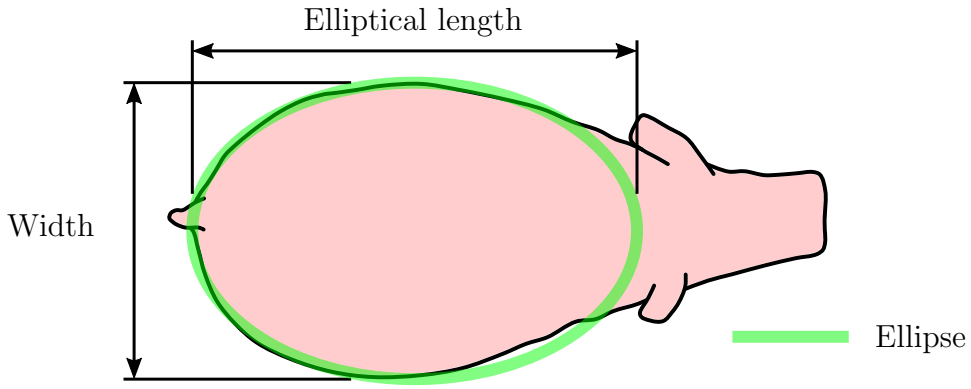


**Figure 2.4: The method used to measure the elliptical length of bladders.** This length was equal to the length of an imagined ellipse lying on the perimeter of each bladder. Bladder width is also shown.

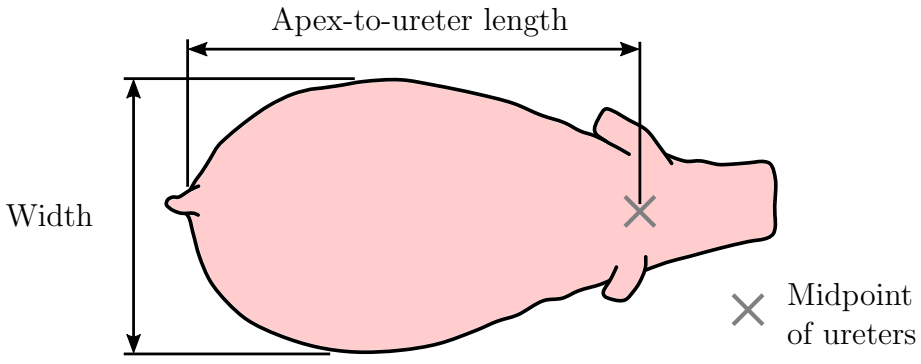


**Figure 2.5: The method used to measure the apex-to-ureter length of bladders.** This length is equal to the longitudinal distance between the midpoint of the ureters and the bottom of each bladder. Width is also shown.

#### Pig gender

The gender of the pig from which the bladder was removed was determined by inspecting the connecting tissues:

**Male** Bladders from male pigs sometimes had seminal vesicles still attached to the bladder neck, and a urethra which was firmer, stiffer, and more muscular than bladder tissue.

**Female** Bladders from female pigs had a urethra which had a similar compliance to that of bladder tissue.

**Unknown** The sex of the pig could not be determined if the urethra had been removed.

## 2.5 Porcine bladder decellularisation

### 2.5.1 Materials

#### 2.5.1.1 Stock Solutions

The following stock solutions were made for the decellularisation process.

#### EDTA solution (10 % (w/v))

Ethylene-diamine tetra-acetic acid (EDTA), 100 g, was dissolved into 900 ml deionised water on a hotplate. The volume was made up to 1 L with deionised water. The solution was autoclaved. This was stored for up to 1 month at room temperature.

#### SDS solution (10 % (w/v))

Sodium dodecyl sulphate (SDS), 10 g, was dissolved into 90 ml deionised water. The volume was made up to 100 ml with deionised water. This solution was filter sterilised into sterile universals (10 ml per universal). These were stored for up to 6 months at room temperature.

**$MgCl_2$ solution (1 M)**

Magnesium chloride hexahydrate ($MgCl_2(H_2O)_6$), 203.3 g, was dissolved into 700 ml deionised water. The volume was made up to 1 L with deionised water. The solution was autoclaved. This was stored for up to 1 month at room temperature.

**Tris solution (2 M, pH 7.5)**

Trizma® Base (Tris), 242.4 g, was dissolved into 600 ml deionised water on a hotplate. The pH was adjusted to 7.5 by adding 6 M HCl dropwise at room temperature. The volume was made up to 1 L with deionised water. The solution was autoclaved. This was stored for up to 1 month at room temperature.

**Tris solution (2 M, pH 8.0)**

Trizma® Base (Tris), 242.4 g, was dissolved into 600 ml deionised water on a hotplate. The pH was adjusted to 8.0 by adding 6 M HCl dropwise at room temperature. The volume was made up to 1 L with deionised water. The solution was autoclaved. This was stored for up to 1 month at room temperature.

#### 2.5.1.2 Working Solutions

The following solutions were made for use in the decellularisation process.

**Wash buffer with EDTA (0.1 % (w/v) EDTA; 10 KIU $\cdot$ $ml^{-1}$ Aprotinin)**

Oxoid Dulbecco's PBS tablets (10) and 10 ml EDTA solution were added to 989 ml deionised water. The solution was autoclaved. This was stored for up to 1 month at room temperature. Immediately before use, 1 ml Aprotinin (10 000 KIU $\cdot$ $ml^{-1}$) was added aseptically.

**Wash buffer without EDTA (10 KIU $\cdot$ $ml^{-1}$ Aprotinin)**

Oxoid Dulbecco's PBS tablets (10) were added to 999 ml deionised water. The solution was autoclaved. This was stored for up to 1 month at room temperature. Immediately before use, 1 ml Aprotinin (10 000 KIU $\cdot$ $ml^{-1}$) was added aseptically.

**Hypotonic buffer (10 mM Tris; 0.1 % (w/v) EDTA; 10 KIU · $ml^{-1}$ Aprotinin)**

Tris solution (pH 8), 5 ml, and 10 ml EDTA solution (10 % w/v) were added aseptically to 984 ml deionised water. The solution was autoclaved. This was stored for up to 1 month at room temperature. Immediately before use, 1 ml Aprotinin (10 000 KIU · $ml^{-1}$) was added aseptically.

**SDS buffer (10 mM Tris; 0.1 % (w/v) EDTA; 0.1 % (w/v) SDS; 10 KIU · $ml^{-1}$ Aprotinin)**

Tris solution (pH 8) 5 ml and 10 ml EDTA solution (10 %, w/v) were added aseptically to 974 ml deionised water. The solution was autoclaved. This was stored for up to 1 month at room temperature. Immediately before use, 10 ml SDS solution (10 %, w/v) and 1 ml Aprotinin (10 000 KIU · $ml^{-1}$) were added aseptically.

**Nuclease solution (50 mM Tris; 10 mM $MgCl_2$; 1 U · $ml^{-1}$ RNase; 50 U · $ml^{-1}$ DNase)**

Tris solution (pH 7.5), 25 ml, and 10 ml $MgCl_2$ solution (1 M) were added aseptically to 965 ml deionised water. The solution was autoclaved. This was stored for up to 1 month at room temperature. Immediately before use, 50 mg bovine serum albumin (BSA) was dissolved aseptically in a 10 ml aliquot of the previously made solution. This BSA solution, 10 ml RNase A (100 U · $ml^{-1}$), and 5 ml DNase I (10 000 U · $ml^{-1}$) were filter sterilised into the nuclease solution.

**Benzonase solution (50 mM Tris; 10 mM $MgCl_2$; 1 U · $L^{-1}$ Benzonase)**

Tris solution (pH 7.5), 25 ml, and 10 ml $MgCl_2$ solution (1 M) were added aseptically to 950 ml deionised water. The solution was autoclaved. This was stored for up to 1 month at room temperature. Immediately before use, 4 µl Benzonase (250 U · $\mu l^{-1}$) was added aseptically.

**Hypertonic buffer (1.5 M NaCl; 50 mM Tris)**

Sodium chloride (NaCl), 87.66 g, and 6.057 g Tris were dissolved in 800 ml deionised water. The pH was adjusted to 7.5. The volume was made up to 1 L using deionised

water. The solution was autoclaved. This was stored for up to 1 month at room temperature.

#### Peracetic acid (PAA) solution (0.1 %, v/v)

Ten Oxoid Dulbecco's PBS tablets and 2.8 ml PAA (36–40 %, v/v) were added to 800 ml deionised water in a fume cupboard. The pH was adjusted to 7.2. The volume was made up to 1 L using deionised water. This was used within 1 hour of preparation.

### 2.5.2 Original method

This method was based on the procedure developed by Bolland *et al.*, (2007). All steps were performed aseptically in a class II safety cabinet. All equipment was sterilised by autoclave before use.

For each step of the process, bladders were held from the neck with forceps and filled with 500 ml of decellularisation solution using either a 50 ml syringe (day 1), or a measuring cylinder and a long-neck funnel (subsequent days). When filling, the forceps holding the neck were used to prevent leakage from the urethras where necessary. This was done by rotating the forceps, which wrapped the urethra around them and blocked the flow of solution. Bladders were then closed at the neck using plastic forceps, ensuring no air was trapped inside. Bladders were placed in a 1 L wide-neck jar containing 500 ml of the same solution, and the lid screwed on and secured with Parafilm. The jar was then placed either in a 4 °C cold room, a 37 °C incubator, or at room temperature. Where necessary, the jar was placed on a Grant PSU 10i shaker at 140 rpm or an IKA KS130 shaker at 160 rpm. For the nuclease step both types of shaker were set to 80 rpm. The process is summarised in Table 2.1

The solutions used were as follows: hypotonic buffer, SDS buffer, wash buffer without EDTA, nuclease solution, wash buffer with EDTA, hypertonic buffer, wash buffer with EDTA, peracetic acid solution, PBS × 4. At the end of each step, bladders were emptied by removing the plastic forceps which were closed around the neck. Using forceps to grip the apex, bladders were removed from the container which caused the solution to drain from the bladders.

After peracetic acid treatment the bladders were dissected into single-layered sheets (Sections 2.4.6.2 and 2.4.6.3) and placed into 150 ml Sterilin pots. The pots were filled with PBS until 125 ml full (including the volume of the bladder) and placed

| Day | Solution | Temperature | Shaker speed | Duration |
|---|---|---|---|---|
| 1 | Hypotonic buffer | 4 °C | None | 22–26 h |
| 2 | SDS buffer | Room | 140–160 rpm | 22–26 h |
| 3 | Wash buffer w/o EDTA | 37 °C | 140–160 rpm | 22–26 h |
| 4 | Nuclease solution* | 37 °C | 80 rpm | 22–26 h |
| 5 | Wash buffer with EDTA | 37 °C | None | 60–74 h |
| 7 | Wash buffer with EDTA | 37 °C | 140–160 rpm | 22–26 h |
| 8 i | Peracetic acid solution | Room | 140–160 rpm | 3.0–3.5 h |
| 8 ii | PBS* | Room | 140–160 rpm | 50–70 min |
| 8 iii | PBS* | Room | 140–160 rpm | 50–70 min |
| 8 iv | PBS* | Room | 140–160 rpm | 50–70 min |
| 8 v | PBS* | Room | 140–160 rpm | 22–26 h |
| 9 | PBS* | 4 °C | None | Storage |

*Bladders were placed into fresh containers.

**Table 2.1: Schedule for the original porcine bladder decellularisation process.**

on a Grant PSU 10i shaker at 140 rpm or an IKA KS130 shaker at 160 rpm at room temperature. This was carried out three times for a duration of 50–70 min each, and a fourth time for a duration of 22–26 h. Bladders were placed into fresh Sterilin pots, filled with fresh PBS for each of these washes. At the end of the process bladders were transferred into fresh 150 ml Sterilin pots containing PBS at 4 °C and stored for up to three months.

### 2.5.3 Modified bladder decellularisation methods

In this thesis the original bladder decellularisation method was performed with various modifications in order to develop the method into one more compatible with a scalable manufacturing process. A summary of these decellularisation processes, and the differences made from the original process, is shown in Table 2.2. The changes to the process are detailed in their respective chapters.

| | Process | Bladder condition | Nucleic acid removal | Volume of solutions | Stretching method |
|---|---|---|---|---|---|
| Chapter 3 | Original process | Fresh | DNase/RNase | 1 L | Distended with 500 ml decellularisation solution. |
| | Calculated volume filling, initial | Fresh | Benzonase | 2 L | Distended with volumes calculated using the initial formula for bladder capacity. |
| | Calculated volume filling, revised | Frozen | Benzonase | 2 L | Distended with volumes calculated using the revised formula for bladder capacity. |
| Chapter 4 | Controlled strain, suspended | Fresh | Benzonase | 2 L | Distended whilst suspended with volumes sufficient to apply strains to the tissue of at least 2.0 and 1.4*. |
| | Controlled strain, immersed | Fresh | Benzonase | 2 L | Distended whilst immersed in solution with volumes sufficient to apply strains to the tissue of at least 2.0 and 1.4*. |
| Chapter 6 | Flat-bed method | Fresh | Benzonase | 2 L | Stretched onto a frame as a flat sheet. Strains of 2.0 and 1.4 were applied*. |
| | Flat-bed method | Frozen | Benzonase | 2 L | Stretched onto a frame as a flat sheet. Strains of 2.0 and 1.4 were applied*. |

*in the circumferential and longitudinal directions respectively

**Table 2.2: A summary of the decellularisation processes used in this thesis.** Variations made to the original process are summarised. The table shows whether bladders were decellularised from fresh or from frozen; whether nuclease solution (DNse and RNase) or benzonase solution was used to digest nucleic acids, and the volume of solution per bladder used at each stage of the process. Fresh bladders were transported in transport medium and frozen bladders were transported without transport medium. The method used to stretch the bladder tissue is also briefly described.

## 2.6 Tissue Characterisation

### 2.6.1 Histology

Tissue sections were stained with haematoxylin and eosin (H&E) in order to visualise cells and tissue histoarchitecture. H&E stains cell nuclei violet, the cytoplasm of cells red, and collagen pink.

#### 2.6.1.1 Solutions

**Neutral buffered formalin (NBF) (10 % v/v)**

NBF (10 % v/v), 20 ml, was aliquoted into 20 ml universals from the stock solution in a fume hood.

**DAPI dye buffer (10 mM Tris; 1 mM EDTA; 1 mM NaCl)**

Tris, 1.211 g; 0.372 g EDTA and 0.058 g NaCl were dissolved into 1000 ml deionised water. The solution was autoclaved and aseptically aliquoted into 200 ml volumes. This was stored for up to 6 months at room temperature. The pH was adjusted to 7.4 immediately before use.

**DAPI dye stock solution ($1\,\mathrm{mg \cdot ml^{-1}}$)**

Nuclease-free water, 10 ml, was added to 10 mg DAPI. This was wrapped in foil and stored for up to 6 months at −25 °C.

**DAPI dye working solution ($0.1\,\mathrm{\mu g \cdot ml^{-1}}$)**

DAPI dye solution, 20 µl, was added to a dark bottle containing 200 ml DAPI dye buffer. This was mixed by inverting. The pH was adjusted to 7.4. The solution was used immediately.

#### 2.6.1.2 Sample processing

Square samples, 1 $\mathrm{cm^2}$, were cut from fresh and decellularised bladder using a scalpel. Samples were placed into 20 ml universals containing 20 ml NBF. Samples were fixed

for 48 h in NBF then transferred into histology cassettes.

A tissue processor was used to prepare fixed samples for paraffin was embedding. Cassettes were cycled through solutions which contained decreasing concentrations of water in order to dehydrate the tissue. Samples were placed in the tissue processor, which successively immersed samples in NBF (10 % v/v) for 1 h; 70 % (v/v) ethanol for 1 h; 90 % (v/v) methylated spirits for 1 h; 100 % methylated spirits for $3 \times 1$ h; xylene for $3 \times 1$ h and molten paraffin wax for $3 \times 1$ h. At the end of processing, cassettes were left in molten paraffin wax until the samples were embedded.

#### 2.6.1.3 Paraffin wax embedding

Tissue cassettes were removed from the molten wax, and the tissue samples removed from the cassettes. Samples were placed into moulds so that they stood vertically, touching the bottom of the moulds along one edge of each sample. This was carried out to ensure that the bladder tissue would be sectioned perpendicularly to the surface of the bladder wall so that sections would be a cross-section of the entire bladder wall. Samples were attached to the moulds by placing the bottom of moulds on an ice pack to solidify the wax interface between sample and mould. Each mould was filled with molten wax and the cassette placed on top. These were left at room temperature until the wax had solidified.

Wax blocks were removed from moulds by turning the moulds upside down and knocking them firmly on a lab bench until the blocks fell from the moulds. To allow the microtome to properly grip wax blocks during sectioning, excess wax was scraped from the cassettes.

#### 2.6.1.4 Sectioning

Blocks were cooled to −18 °C prior to sectioning to improve block cutting. Wax blocks were sectioned using a Leica RM2255 microtome with the cutting thickness set to 4 µm and blade angle set to 2.5°. Sections were floated onto the surface of a water bath (set to 40 °C) and transferred onto microscope slides. Superfrost™ slides were used for samples to be stained with H&E, and Superfrost™ Plus slides were used for samples to be stained with DAPI. Two sections were placed on each slide. Sections were left to air dry overnight.

#### 2.6.1.5 De-waxing and Re-hydration

Once dry, slides were loaded into a slide holder. All solutions were contained in glass troughs. Sections were dewaxed using two xylene washes (10 min each) and rehydrated using three 100 % methylated spirits washes (for 3 min, 2 min and 2 min), a 70 % (v/v) ethanol wash (2 min) and by being placed in running tap water for 3 min.

#### 2.6.1.6 Staining and Mounting

**Haematoxylin and eosin (H&E)**

H&E staining was used to identify the cellular distribution across sections of the bladder wall in both native and decellularised tissue. The stain allowed visualisation of cell nuclei, cytoplasm and connective tissues. Haematoxylin stains cell nuclei a dark blue, whereas eosin stains cell cytoplasm and connective tissue fibres different intensities of pink and red. After dewaxing and rehydration, sections were immersed in haematoxylin for 1 min, rinsed in running tap water until the water ran clear, immersed in Scott's tap water for 3 min, rinsed in running tap water for 3 min and immersed in eosin for 3 min.

Once stained, sections were dehydrated by immersion in a 70 % (v/v) ethanol wash (5 s), three 100 % methylated spirits washes (for 1 min, 2 min and 3 min), and two xylene washes (10 min each).

Sections were mounted by placing a drop of DPX mountant on each section followed by a coverslip. Bubbles were pressed from under coverslips using forceps. Slides were left to dry overnight inside a fume hood. Sections were viewed using bright-field microscopy.

**DAPI**

DAPI (4',6-diamidino-2-phenylindole dihydrochloride) was used to visualise DNA in stained sections. It intercalates with double-stranded DNA, and emits light with an emission maximum of 460 nm when excited with ultraviolet light (maximum absorption is at 358 nm). Cell nuclei can therefore easily be identified as blue dots when stained using DAPI and visualised using fluorescent microscopy.

Once tissue sections had been dewaxed and rehydrated, work was performed in the dark. Sections were immersed in 200 ml DAPI dye working solution for 10 min,

followed by $3 \times 10$ min PBS washes.

Sections were left to air dry in the dark for approximately 30 min. Sections were mounted by placing a drop of Dako fluorescence mounting medium on each section, followed by a coverslip. Slides were left to air-dry in the dark until the mounting medium had set. Sections were viewed using fluorescent microscopy with a DAPI filter.

### 2.6.2 DNA extraction and quantification assay

#### 2.6.2.1 Sample preparation and freeze-drying

In order to quantify their DNA content, fresh and decellularised bladder tissue samples were freeze dried in bijous. The bijous were weighed before samples were placed inside them. Bijous were weighed sequentially and their masses recorded. This was repeated until three sequential readings were acquired for each bijou which had a range of no more than 0.5 mg.

Samples from decellularised bladder were cut aseptically using a scalpel and transferred into bijous. Native bladder samples were cut out on a dissection board. Samples were macerated on a dissection board and placed into the previously weighed bijous. Tissue was added or removed from each bijou until the (wet) mass of the tissue inside it was $250 \pm 10$ mg for decellularised bladder, or $25 \pm 5$ mg for native bladder.

Bijous were opened and placed in a freeze-drier ($-50$ °C, 150 mbar). Samples were periodically weighed as described above, leaving at least 24 h between readings. Samples were removed from the freeze-drier once three sequential readings were acquired with a range of no more than 0.5 mg.

#### 2.6.2.2 DNA extraction using the DNeasy kit

The DNeasy kit is designed to isolate the total DNA from xenogeneic and allogeneic tissues. The DNeasy membrane is a silica-based membrane which DNA adsorbs to in the presence of high concentrations of chaotropic salt. Samples are initially lysed using proteinase K, then buffering conditions of samples are adjusted to promote the specific adsorption of DNA to the silica-based membranes. During centrifugation, DNA is selectively bound to the membranes and the contaminants pass through. The remaining contaminants and enzyme inhibitors are removed in two wash steps, allowing the DNA to be eluted from the membranes in water or buffer.

The DNeasy kit contained the following: Buffer ATL, Buffer AL, Buffer AW1, Buffer AW2, Buffer AE, proteinase K, DNeasy Mini spin columns and 2 ml collection tubes. Buffers ATL and AL were warmed to 56 °C before use to dissolve precipitates. Buffers AW1 and AW2 were diluted with ethanol (100 % v/v) as indicated by the manufacturer to obtain working solutions.

#### 2.6.2.3 DNA isolation

After freeze-drying, 360 µl Buffer ATL and 40 µl proteinase K was added to tissue samples. Samples were vortexed in an Eppendorf thermomixer overnight at 56 °C to ensure complete tissue lysis. Each sample was vortexed for 15 s before the addition of 400 µl Buffer AL, vortexed again for 15 s before the addition of 400 µl ethanol (100 % v/v), then vortexed for a further 15 s. Approximately half of each sample (620 µl) was transferred into DNeasy Mini spin columns, which were placed into 2 ml collection tubes, centrifuged at 6000 $g$ for 1 min at 18 °C. The flow-through and collection tubes were discarded, and the process repeated for the remainder of each sample. The DNeasy Mini spin columns were placed into new 2 ml collection tubes, and 500 µl Buffer AW1 was added to each column before being centrifuged at 6000 $g$ for 1 min at 18 °C. The flow-through and collection tubes were discarded. The DNeasy Mini spin columns were placed into new 2 ml collection tubes, and 500 µl Buffer AW2 was added to each column before being centrifuged at 16 100 $g$ for 5 min at 18 °C. The flow-through and collection tubes were discarded. To fully elute the DNA from the membrane, DNeasy Mini spin columns were placed into 1.5 ml micro-centrifuge tubes; 200 µl Buffer AE was pipetted directly onto membranes; spin columns were incubated for 1 min at room temperature and centrifuged for 1 min at 6000 $g$. The elution with Buffer AE was repeated using a further 200 µl. Spin columns were discarded after the final rinse.

#### 2.6.2.4 DNA quantification

A NanoDrop ND-1000 spectrophotometer was calibrated using 2 µl nuclease-free water. Buffer AE, 2 µl, was then loaded onto the spectrophotometer to record a blank reading. To determine the concentration of DNA (dsDNA, ssDNA and ssRNA) in samples, 2 µl of each sample was loaded onto the spectrophotometer and the absorbance measured at 260 nm. Readings were taken of each sample to until three conforming readings were recorded. The mean of these readings was calculated, and the DNA concentration of each sample was normalised for DNA solution volume and initial dry tissue mass to determine the mass of DNA per tissue dry weight mass.

### 2.6.3 Cytotoxicity testing

It has been reported that residual SDS in the tissue is cytotoxic to cells, and would result in a reduction in tissue biocompatibility (Rieder *et al.*, 2004). Residual PAA, used to sterilise the tissue at the end of the process, would also affect cell growth. In order to assess that these chemicals have been sufficiently washed from tissues so as not to affect cells, *in vitro* biocompatibility tests were performed.

#### 2.6.3.1 Contact cytotoxicity assay

A contact cytotoxicity assay was used to assess the effect of the decellularised bladder tissue on the growth of mouse fibroblast (L929) and baby hamster kidney (BHK) cells. This was assessed by observing cell viability and morphology in the regions surrounding the tissue.

**Sodium hydroxide (NaOH) solution (0.1 % w/v)**

NaOH, 0.2 g, was added to 200 ml deionised water. The solution was autoclaved and stored at room temperature for up to 3 months.

**Rat tail collagen**

Tails were removed from rats that had been sacrificed by a scheduled procedure for unrelated purposes, and stored at −20 °C. Tails were placed into large petri dishes containing methanol (five tails per petri dish). A scalpel was used to make several slices along the length of each tail, and the skin was peeled off. The four visible tendons were sliced, peeled off, and placed in a petri dish containing glacial acetic acid (17.4 mM). The tendons were macerated and placed into glacial acetic acid, 50 ml per tail, to solubilise the collagen. This mixture was incubated at 4 °C for 48 h with magnetic stirring.

A high-speed refrigerated centrifuge (Sorvall Evolution RC) was used to spin down the solution at 30 000 $g$ at 4 °C for 1 h. The supernatant was transferred to a fresh sterile bottle and the pellet discarded. The solution was neutralised with NaOH solution (0.1 M) using litmus paper, stirred for 2 h at 4 °C, and centrifuged at 20 000 $g$ at 4 °C for 30 min. The supernatant was discarded and the pellet carefully resuspended in glacial acetic acid, 15 ml per tail, and stored at 4 °C.

**Procedure**

Samples of bladder tissue were dissected into 5 mm × 5 mm squares and temporarily stored in DPBS (without $Ca^{2+}/Mg^{2+}$). Rat tail collagen, 15 µl, was pipetted into the centre of the wells of a 6-well plate, and 7.5 µl NaOH solution (0.1 % w/v) was immediately added to it. Tissue samples were placed on top of the neutralised collagen gel, and left for 15 min to set. Drops of cyanoacrylate contact adhesive were placed into seperate wells for positive controls. Collagen gel alone was used for negative controls. Cell-only controls were also included.

Wells were washed three times for 10 min with DPBS (without $Ca^{2+}/Mg^{2+}$). BHK and L929 cells were passaged and counted (see Sections 2.3.2.4 and 2.3.2.6), and resuspended to densities of 250 000 cells $\cdot$ ml$^{-1}$ in their respective culture media. Cell suspension, 2 ml, was added to each well. Samples and controls were tested in triplicate for each cell type. Plates were incubated for 48 h at 37 °C in 5% (v/v) $CO_2$ in air.

Culture medim was aspirated from wells. DPBS (with $Ca^{2+}/Mg^{2+}$), 2 ml, was added to and aspirated from each well. NBF, 10 ml, was added to each well in order to fix the cells. NBF was aspirated after incubating for 10 min. A Pasteur pipette was used to add three drops of Giemsa stain per well. Wells were incubated for 5 min then rinsed with tap water until clear. Plates were left to air dry and observed using an Olympus IX71 Inverted Microscope with bright field illumination.

## 2.6.4 Differential scanning calorimetry

Differential scanning calorimetry (DSC) is a thermal analysis experimental technique used to find changes in the heat capacity of a material over a temperature range. The procedure involves heating a sample over a temperature range and recording and the heat flux required to raise the temperature of the sample. Materials with constant heat capacities have a flat response becuase the heat flux is invariant with temperature. There are peaks in the heat flux for a materials which undergo changes of phase, or any other changes of state, during the test.

### 2.6.4.1 Rationale

DSC was used to find the denaturation temperature of the collagen in tissue samples. Collagen constitutes the majority of the structural proteins in bladder tissue (Aitken & Bägli, 2009). A single collagen molecule is called tropocollagen, and is a triple helix of three polypeptide chains. These polypeptides are held together by interchain

hydrogen bonding. Collagen fibril segments are made of a staggered array of several tropocollagen molecules. The staggering in these segments allow them to join end-to-end to result in a collagen fibril. Hydrogen bonding between tropocollagen molecules mediates this collagen fibril structure. When tissue is heated, a point at which the hydrogen bonds start to break and the tropocollagen molecules change from a helical structure into a random coil arrangement is known as the collagen denaturation temperature (Bigi *et al.*, 1987).

As well as hydrogen bonds, there are naturally occurring covalent crosslinks between collagen molecules in normal tissue.The degree of crosslinking varies with the type of tissue and age of the organism (Ricard-Blum & Ville, 1989). Crosslinking of collagen in *ex vivo* tissue can be caused using physical and chemical processes. Atypical levels of collagen crosslinking in tissues are associated with abnormal tissue function (Skrzyński *et al.*, 2010). A change in the level of crosslinking may affect the mechanical performance of a bladder patch when used *in vivo*. Any change in the degree of crosslinking within the collagen structure results in a change in the collagen denaturation temperature of the tissue (Sionkowska & Kamińska, 1999). DSC was used to find the denaturation temperature of normal and decellularised bladder tissue to assess if there was a difference in the degree of crosslinking, and therefore the physical properties, of these two types of tissue.

#### 2.6.4.2 Method

Samples were placed in bijous containing PBS, couriered overnight on dry ice over 24 h, and stored at 4 °C for up to 1 week before testing. Testing was performed by staff at the Department of Materials Science at the University of Cambridge as follows: samples were loaded into a TA Instruments Q2000 differential scanning calorimeter, the temperature of each sample was increased from 15 °C to 105 °C at a rate of 4 °C/ min and the heat flow to the sample was recorded at a rate of 10 Hz.

The collagen denaturation temperature was found by analysing the graph of heat flow against temperature for each sample. The heat flow was normalised against the mass of each tissue sample and plotted against temperature. If a peak in the heat flow was observed, the transition temperature was taken as the temperature at the peak maximum. This transition temperature was taken as the collagen denaturation temperature. An example of this data is shown in Figure 2.6.

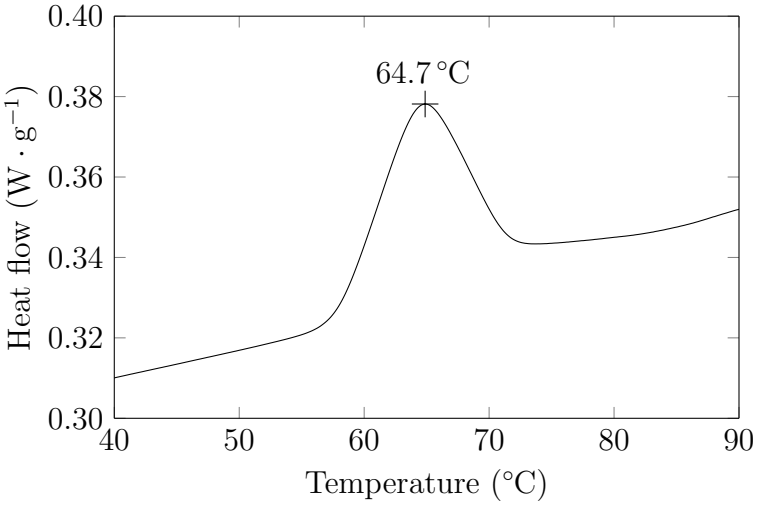


**Figure 2.6: A DSC curve of heat flow against temperature for bladder tissue.** The peak in the curve represents the temperature range over which the collagen denatured. The collagen denaturation temperature was taken as the temperature at the maximum heat flow, shown as a + on the graph.

## 2.7 Suspended bladder distension

### 2.7.1 Rationale

The suspended bladder distension experiment was a mechanical test designed to determine the capacity of bladders. It was designed to replicate the method by which bladders were filled during the original decellularisation process. When filled for decellularisation, bladders were held at the neck using forceps which allowed them to hang freely. The suspended distension experiment was designed to secure bladders at the neck and fill them with PBS until the level of PBS was equal with the height of the neck of each bladder. Bladder capacity was defined as the volume of liquid bladders were filled with to reach this point of filling.

### 2.7.2 Equipment setup

A bench vice was attached to a lower laboratory shelf, and retort stand on an upper shelf. A clamp was placed on the retort stand 100 cm above the vice. A 150 cm ruler was placed in the vice so that the ruler hung 30 cm below the vice. The ruler was also secured at the clamp. A pipe fitting (male) was also placed in the vice, and a funnel secured at the clamp. Transparent rubber tubing was placed between the funnel and pipe fitting, alongside the ruler. This arrangement is shown in Figure 2.7.

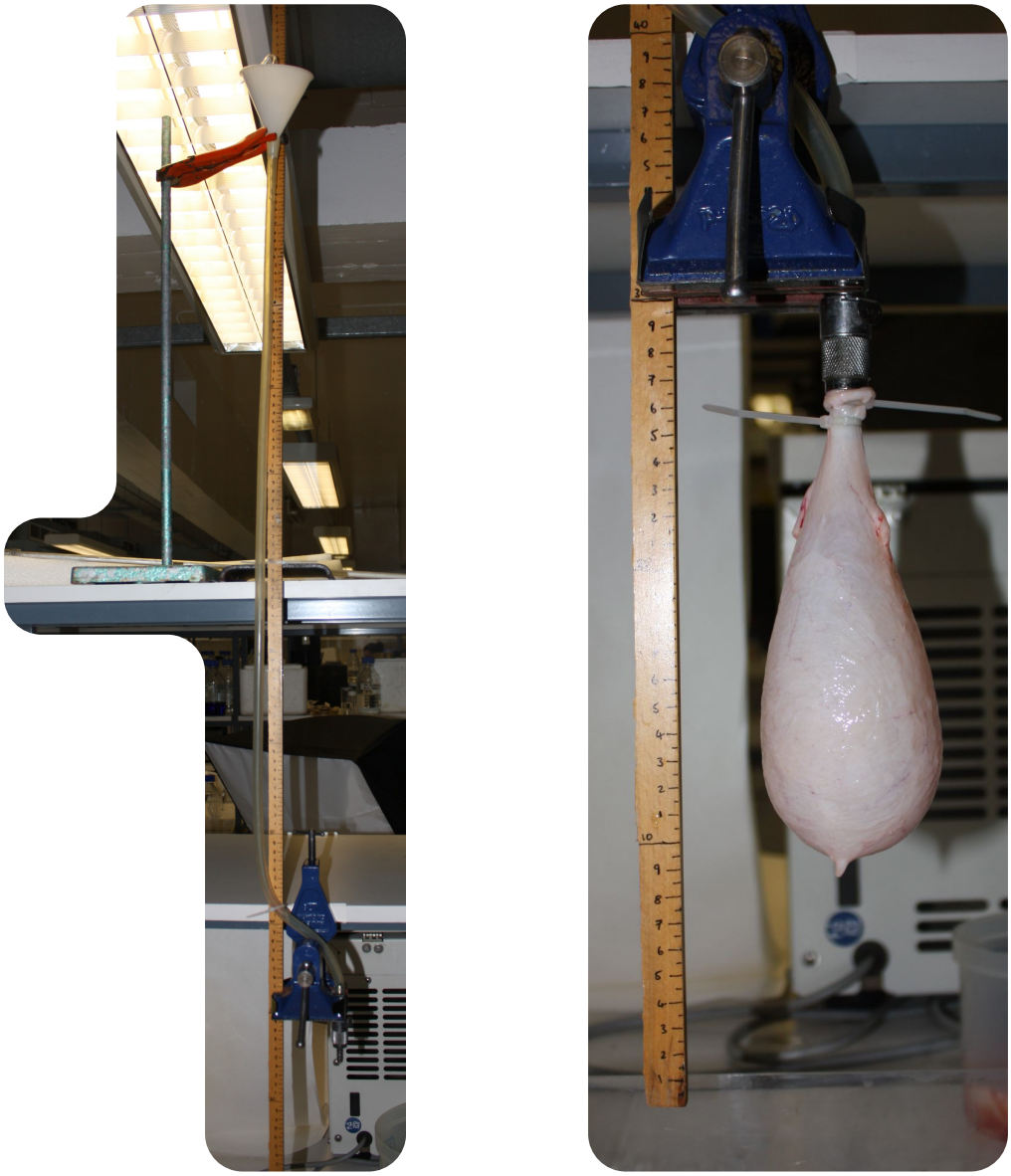

**(a)** Equipment used for the experiment. A ruler was held by a vice (blue, below) and a retort stand clamp (orange, above). Transparent tubing connected the funnel (where liquid was added) to the pipe fitting (where bladders were suspended).

**(b)** A bladder during testing. A vice was used to hold a pipe fitting, which was connected to a second pipe fitting. Cable ties were used to secure each bladder to the second pipe fitting.

**Figure 2.7: Equipment setup for the suspended bladder distension experiment.**

### 2.7.3 Preparation of bladders

Before testing, each bladder was laid flat with its dorsal surface facing upwards, as described in Section 2.4.4. A ruler was placed next to each bladder and an image of the bladder was taken, normal to the dissection board from a distance of approximately 30 cm. The width, elliptical length and tissue volume of bladders were found by the method described in Section 2.4.7. The width and elliptical length were measured to a precision of $\pm 1$ mm. The tissue volume was measured to a precision of $\pm 1$ ml.

### 2.7.4 Image analysis

The captured images were used to find the apex-to-ureter length and area of the bladders. Image were loaded into ImageJ, and the multi-point selection tool was used to place points at the base of the ureters and around the outline of each bladder. A grid was overlaid on each image to improve the consistency of placing markers on the outline. Two additional points were placed 5 cm apart on the ruler to later calibrate the scale of the images. After placing the points on each image, the $x$- and $y$-coordinates of the points were exported to a `.txt` file. A Matlab script was written to read the coordinate data files.

The apex-to-ureter length was calculated by finding the distance between the bladder apex and the midpoint of the ureters, and the width was calculated at the widest point of the bladder. Using the images, these lengths were measured with a precision of $\pm 0.2$ mm The below-ureter area was calculated by finding the area contained by the points on the perimeter of the bladder and points placed at the base of the ureters. The error of the below-ureter area was calculated as the sum of the error associated with the placements of the points and the error associated with calculating the area using the trapezium rule, assuming the perimeter of the bladder was approximately ellipsoid. The initial thickness was calculated by dividing the tissue volume by twice the total bladder area, and the precision of the initial thickness was calculating by summing the respective relative errors of the tissue volume and bladder area.

### 2.7.5 Distension procedure

Bladders were connected via the urethra to a female pipe fitting using cable ties. Each bladder was connected to the equipment by connecting the pipe fitting on the bladder to the pipe fitting in the vice, so that the bladder suspended from the

equipment as shown in Section 2.7.2. Bladders were distended by placing 50 ml PBS into the funnel every 45 sec. If a head of water was visible in the tube shortly after each filling, bladders were gently squeezed to ensure no air was trapped inside them. Thirty seconds after each bladder filling, any visible head of PBS was recorded. The head of water was measured with an error of $\pm 2.5$ mm. Bladder capacity was measured with the same relative error as water head. Each test ended when the weight of the filled bladder caused it to detach from the pipe fitting.

## 2.8 Immersed bladder distension

### 2.8.1 Rationale

The immersed bladder distension experiment was a mechanical test designed to determine the state of deformation of the bladder wall during filling. Each bladder was filled when immersed in a tank in order to mimic the conditions of bladder decellularisation, i.e. suspended in a fluid.

During filling, the internal pressure and dimensions of the bladder wall were recorded in order to later calculate the stress and strain in the bladder wall. Unlike the suspended bladder distension experiment, the immersed distension method applied a uniform internal pressure to each bladder.

### 2.8.2 Materials

#### 2.8.2.1 Solutions

**Coloured PBS**

Coloured PBS was made by adding 38 ml black food colouring to 3 L PBS.

#### 2.8.2.2 Equipment setup

A diagram of the arranged equipment is shown in Figure 2.8. An image of a bladder being tested with the equpiment is shown in Figure 2.9. A glass tank (30 cm $\times$ 30 cm $\times$ 20 cm) was filled with PBS so the level was approximately 50 mm below the top of the tank. A vice was attached to a laboratory shelf and a pipe fitting (male) was placed in the jaws. The pipe fitting was positioned in the tank so that it just touched the surface of the PBS. Tubing ran from the top of this pipe

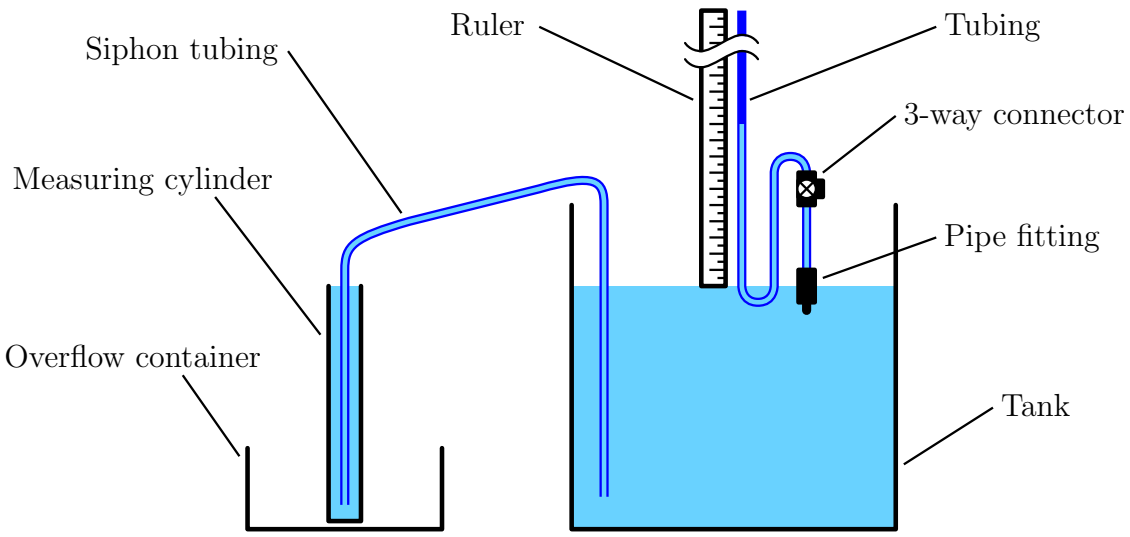


**Figure 2.8: Diagram of the equipment used in the immersed distension of bladders.** Clamp is not shown.

fitting to the bottom of a 3-way tubing connector. The 3-way connector allowed bladders to be filled using a syringe without trapping air in the system. Another piece of tubing ran from the top of the 3-way connector, down to below the pipe fitting, then back upwards, to make an 'S' shape. This tubing continued vertically upwards for 120 cm. The 'S' shaped section of tubing allowed the 3-way connector to be positioned above the water line for ease of use. A 120 cm ruler was placed alongside the vertical section of tubing, so that the bottom of the ruler was level with the PBS level. The bottom of the ruler was secured in the vice, and the top of the ruler was secured with a retort stand and clamp. The top of the vertical tubing was secured to the clamp.

An overflow container was placed outside the tank. A measuring cylinder was placed in the overflow container so that the top of the measuring cylinder was level with the PBS level. Tubing ran from inside the tank to inside the measuring cylinder. The tubing between the tank and the measuring cylinder was filled so that PBS was able to siphon freely between these two containers. Any PBS added to the tank resulted in the tank PBS level being higher than the measuring cylinder PBS level, which resulted in PBS siphoning from the tank to the measuring cylinder. This resulted in the measuring cylinder overflowing, and the PBS level in the tank eventually returning to its previous level.

A 50 ml syringe was connected to the 3-way connector, and used to fill the tubing between the 3-way connector and the pipe fitting with coloured PBS. Similarly, the tubing in the 'S' shape was filled until the PBS in the tubing was level with the bottom of the 120 cm ruler.

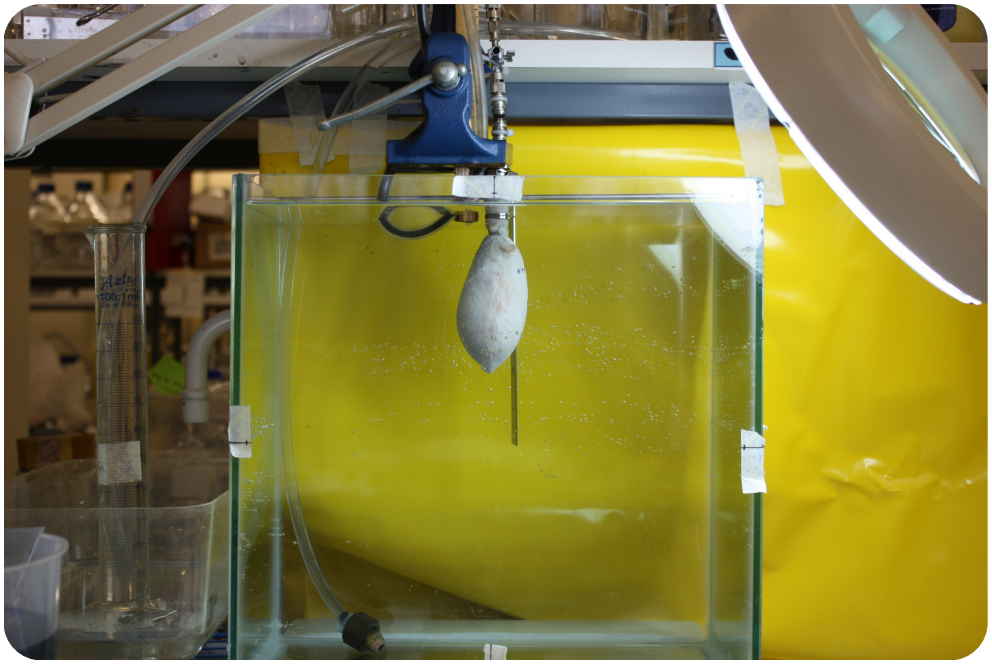

**Figure 2.9: Equipment setup of immersed distension experiment.** A bladder is seen, being tested. The ruler continues to run upwards from the tank.

A camera stand was used to place a Canon 450D camera approximately 50 cm away from the tank, normal to the centre of the front side of the tank. The stand allowed the camera to be quickly detached from the stand after taking a front-angle image. To take the side- and top-angle images, the camera was positioned freehand at a distance of approximately 50 cm normal to the side and top of the tank respectively. During the tests, photographs were taken successively from the front, side and top of the tank. To improve photograph quality, a magnifying lamp was used to illuminate the tank.

A rod was placed across the top of the tank, and a 150 mm ruler was suspended from the rod. This allowed the ruler to be suspended from any point in the tank. From the angle of the front-facing camera, this ruler was suspended just to the right of each bladder.

## 2.8.3 Procedure

### 2.8.3.1 Marker placement

Bladders were laid flat so their dorsal surface was facing upwards (Section 2.4.4). Tissue paper was used to blot the surface of bladders in order to remove excess liquid. Bladders were blotted three times to prevent the haematoxylin from running. A 20 µl pipette was used with a 10 µl tip to place small (2 mm diameter) drops of

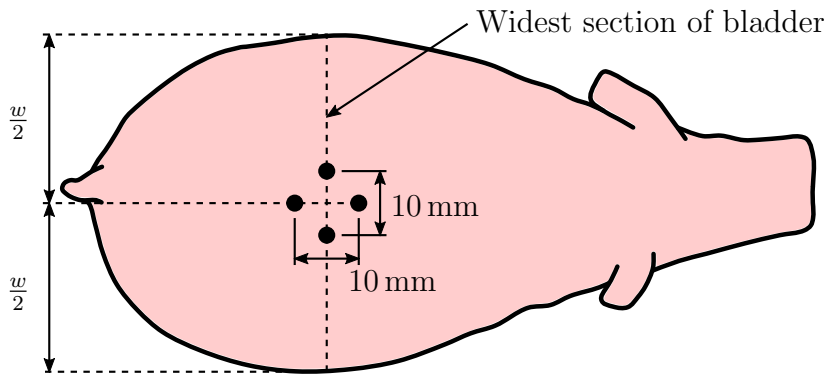


**Figure 2.10: A diagram showing the position of markers placed on bladders.** Circles indicate the position of the markers. The dorsal surface of the bladder is facing upwards. The apex can be seen on the left side of the diagram and the ureters and neck of the bladder can be seen on the right. Haematoxylin was used to stain markers onto the tissue.

haematoxylin on the surface of bladders. Four drops of haematoxylin were placed near the midpoint of the widest section of bladders. Each marker was placed 5 mm from the midpoint, in each direction along the longitudinal and axial axes, as shown in Figure 2.10. The haematoxylin was incubated for 2 min then washed off using PBS.

#### 2.8.3.2 Preparatory measurements

The volume of each bladder was recorded using a measuring cylinder to a precision of $\pm 1$ ml. A balance was used to record the mass of each bladder to a precision of $\pm 0.05$ g.

#### 2.8.3.3 Preparation

In turn, bladders were laid flat, dorsal side upwards (Section 2.4.4), and a ruler was placed next to them. A pre-test photograph was taken of the bladder, normal to the dissection board from a distance of $\approx$30 cm. The neck of the bladder was placed over the end of a female pipe fitting, and secured using two cable ties. Ureters were occluded using cable ties.

The bladder was placed in the tank by connecting the female pipe fitting to the pipe fitting in the vice. Bladders were rotated so that the markers were positioned towards the front side of the tank. Bladders were photographed from the front, side and top as described previously. A 50 ml syringe was filled with coloured PBS.

#### 2.8.3.4 Distension

Every 60 sec, a 50 ml syringe was used to add 50 ml coloured PBS to the bladder to a precision of ±0.5 ml. Each filling was performed over approximately 15 sec. After each filling, the syringe was re-filled with coloured PBS and the bladder was observed for leakage. To account for bladder movement during filling, bladders were rotated so the markers resumed facing the front of the tank and the ruler in the tank was re-adjusted if required. Thirty seconds after filling the head of PBS in the tube (internal bladder pressure) was recorded with an error of ±0.25 $cmH_2O$. Photographs were then taken of the bladder from the front, side and top as described previously.

Each test was concluded when the bladder burst, the internal bladder pressure was >120 $cmH_2O$ or the bladder leaked excessively due to tissue wall damage. Bladders were excluded from analysis if the leakage was due to inadequate sealing of the ureters or urethra.

### 2.8.4 Analysis

In order to simplify the analysis, a coordinate system was used whereby the directions $x$ and $y$ were used to represent the circumferential and longitudinal axes of the bladder respectively. This coordinate system is shown in Figure 2.11a.

#### 2.8.4.1 Image Analysis

Four types of images were analysed: pre-test, front-angle, side-angle and top-angle. Examples of these images are shown in Figure 2.11. The multi-point selection tool in ImageJ was used to select a number of points of interest in each image. These points included the edges of the tank; the bladder markers; the base of the ureters; the apex; the neck; and the bladder outline. A grid was overlaid on each image to improve the consistency of placing markers on the outline. Points were placed on images with a precision of ±0.2 mm. This tolerance was used to calculate the error associate with each parameter. The standard error of the mean was used as a measure of error for parameters calculated using numerous points of measurement, such as bladder area.

After placing the points on each image, the $x$ and $y$ coordinates of the points were exported to a `.txt` file. The volume data, pressure data, and bladder measurements (width, length, sex, mass, volume) were placed in `.txt` files. A Matlab script was written to read and analyse these data files.

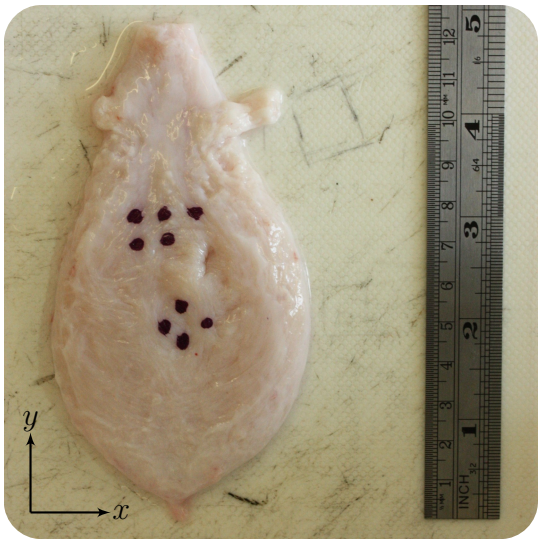


**(a)** Pre-test image

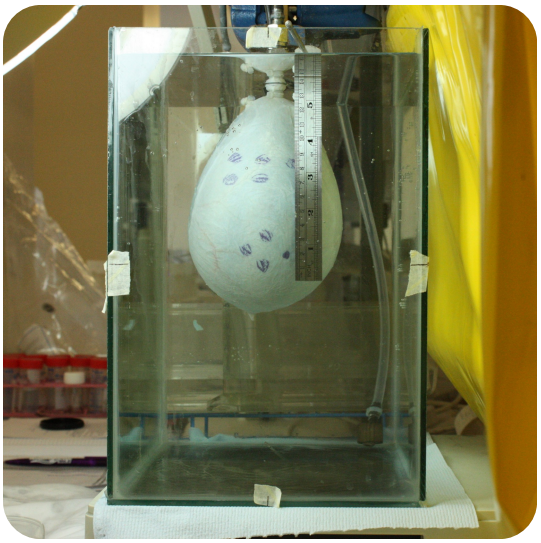

**(b)** Front-angle image

**(c)** Side-angle image

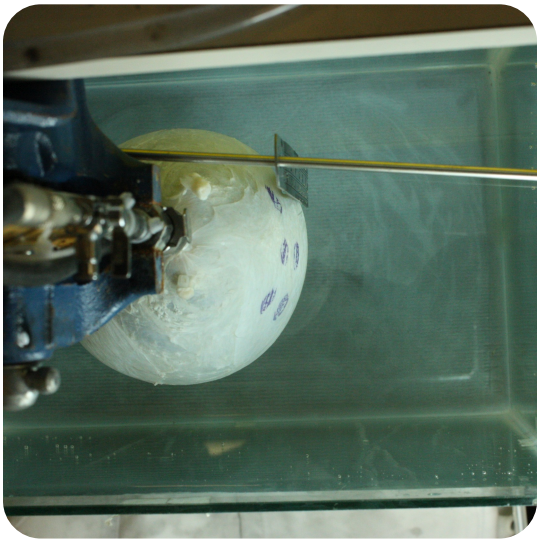

**(d)** Top-angle image

**Figure 2.11: Images taken during the immersed distension experiment.** A single pre-test image was taken before the start of each test. A front-angle, side-angle and top-angle image was taken at each time point during testing. These images were analysed using ImageJ and Matlab. The coordinate system used to analyse the bladders is shown in (a).

### Calibration

Pre-test images were calibrated by scaling them relative to the points placed on the ruler. Front-angle images were also calibrated using the points on the ruler. Once calibrated, the height and width of the bladder could be calculated from the front-angle images.

Side- and top-angle images were calibrated by reference to the height and width respectively of the bladder in the corresponding front-angle image.

### Pre-test image measurements

The distances between the top and bottom markers and the left and right markers were calculated. The width and apex-to-ureter length of each bladder was calculated. The perimeter and the area inside the perimeter of the bladder was calculated.

### Front-angle image measurements

The distances between the left and right markers (marker $x$ distance) and the top and bottom markers (marker y-distance) were calculated.

The trigone height was calculated as the longitudinal distance between the bottom of the bladder neck and the base of the ureter. The bottom height was calculated as the longitudinal distance between the base of the ureter and the apex. The total height was the longitudinal distance between the bottom of the bladder neck and the apex.

### Side- and top-angle image measurements

The side- and top-angle images captured the side and top profiles respectively of each bladder at each time point, including the side and top profile of the bladder marker region. The Matlab `polyfit` function was used to calculate the coefficients of a quartic polynomial using the points in the bladder marker region. The distance between the markers along the curve of the polynomial was approximated using 2000 straight lines. The straight-line distance between the markers was also calculated.

The length of the perimeter of the bladder was calculated. The area inside this perimeter—the total cross-sectional area—was also calculated.

#### 2.8.4.2 Calculation of variables describing bladder deformation state

The curved distances between markers were divided by the straight-line distances between markers to give curvature ratios in the $x$ and $y$ directions. The marker $x$ and $y$ distances were multiplied by the $x$ and $y$ curvature ratios respectively to give the true (curvature-corrected) marker $x$ and $y$ distances.

Stretch, $\lambda$, is defined as the new length, $\ell$, divided by the original length, $L$. The stretch in each direction, $\lambda_{x,y}$, was found by dividing the true marker distances, $\ell_{x,y}$, by the pre-test marker distances, $L_{x,y}$. The relative error of stretch was calculated the sum of the relative measurement errors of the new length and the original length.

$$\lambda_x = \frac{\ell_x}{L_x}, \quad \lambda_y = \frac{\ell_y}{L_y} \tag{2.4}$$

Strain, $\varepsilon$, is defined as the change in length, $\Delta L = \ell - L$, divided by the original length L. The bladder strains in each direction, $\varepsilon_{x,y}$, were found by subtracting one from the stretches (Equation 2.5). The error of the strain was found by multiplying the relative stretch error by the strain.

$$\varepsilon_x = \frac{\Delta L_x}{L_x} = \frac{\ell_x - L_x}{L_x} = \lambda_x - 1, \quad \varepsilon_y = \frac{\Delta L_y}{L_y} = \frac{\ell_y - L_y}{L_y} = \lambda_y - 1 \tag{2.5}$$

The preparatory thickness of the bladder, $z_0$, was calculated by dividing the bladder tissue volume, $V_{\text{tissue}}$, by twice the pre-test bladder area, $A_0$. The relative thickness measurement error was equal to the sum of the tissue volume error plus twice the pre-test bladder area.

$$z_0 = \frac{V_{\text{tissue}}}{2A_0} \tag{2.6}$$

The tissue thickness, $z_t$, at each time point was estimated by assuming incompressibility ($\lambda_x \lambda_y \lambda_z = 1$). It was therefore calculated by dividing the preparatory thickness by the stretches in the $x$ and $y$ directions ($\lambda_x, \lambda_y$). The error associated with tissue thickness found from the measurement errors of the $x$ stretch, $y$ stretch and initial thickness (initial thickness error was calculated from pre-test area and tissue volume, as above).

$$z_t = \frac{z_0}{\lambda_x \lambda_y} \tag{2.7}$$

The cross-sectional area of the bladder wall in the $x$ plane was estimated by multiplying the perimeter of the bladder in the top-angle image by the tissue thickness. The $y$ plane bladder wall cross-sectional area was similarly calculated using the perimeter of the bladder in the side-angle image. The error of these cross-sectional areas were calculated from the errors of the perimeters of the bladder in each plane

and the tissue thickness, which was calculated from the errors of the tissue volume and bladder pre-test area.

$$A_{\text{wall}} \approx z_t d_{\text{perimeter}} \tag{2.8}$$

The cross-sectional area of the bladder lumen in the $x$ plane was estimated by subtracting the $x$ plane bladder wall cross-sectional area from the $x$ plane total cross-sectional area. The $y$ plane lumen cross-sectional area was similarly found. The measurement error associated with the lumen cross-sectional area was a sum of the total size-angle area and the area of the wall (which was calculated from the side-angle perimeter, $x$ and $y$ stretches, tissue volume and pre-test area errors).

$$A_{\text{lumen}} = A_{\text{total}} - A_{\text{wall}} \tag{2.9}$$

True stress was calculated in order to prevent a bias which may have resulted from the error associated with calculating the initial thickness. The $y$ direction stress, $\sigma$, was found by multiplying the internal pressure, $p_i$, by the $x$ plane lumen area, $A_i$, and dividing by the $x$ plane bladder wall area, $A_{\text{wall}}$. The $x$ direction stress was similarly found using the $y$ plane lumen area and $y$ plane bladder wall area. The measurement error of the stress in each direction was found from the errors of the internal pressure, size-angle cross-sectional areas and perimeters, $x$ and $y$ stretches, tissue volume and pre-test area.

$$\sigma_{\text{true}} = \frac{F}{A} = \frac{pA_{\text{lumen}}}{A_{\text{wall}}} \tag{2.10}$$

To find a mean stress-strain curve for multiple bladders, the strain values of each bladder were linearly interpolated from the original stress–strain data for stress values between 0 MPa and 1.8 MPa in intervals of 0.01 MPa. At each of these stress intervals, the mean of the corresponding strain values for multiple bladders was found.

## 2.9 Modelling bladder deformation

Distending bladders during the decellularisation process was not a suitable method for a commercial manufacturing process. Biaxially stretching flat sheets of bladder tissue would be compatible with such a process. The finite element modelling (FEM) was used to model the deformation of flat sheets of bladder to ensure adequate strains would be applied to the tissue.

A Matlab script was written to automatically generate meshes of the bladder tissue based on a number of input parameters. The script also defined boundary conditions

and prescribed node displacements, and generated an XML file which could be processed by FEBio.

### 2.9.1 The finite element method

Finite element modelling (FEM) is used to calculate the distribution of some material variables of a body which is subjected to a known set of initial conditions and boundary conditions. The technique is used when a solution is required for a problem which is too complex to be solved analytically. The method involves dividing the material body up into numerous elements. This allows the distribution of the material variables of each of these elements to be approximated numerically. By using many small elements, the material variables for the entire model can be found to give an estimate of the variables in the real world situation. FEM is often used in steady-state mechanics problems to find the stresses and strains in a body subjected to known forces and displacements. The method can also be applied to dynamic problems, and other types of problem such as heat transfer.

To analyse a problem using FEM, the body is first subdivided into numerous small regions, each of them a single element. Common shapes for elements include hexahedrons and tetrahedrons. Elements are connected by their nodes, which typically lie at the vertices of each element. Nodes can also be placed along the edges of elements. The body is divided up into a sufficient number of elements so that the features of the body are represented in sufficient detail by the elements. This construct which represents the material body, consisting of all the elements, is known as the mesh.

After the body is meshed, initial conditions and boundary conditions are applied to the nodes. These dictate how certain variables (such as force and displacement) are said to act on the material body. The distribution of the predefined variables on the elements is approximated using a polynomial. A constitutive equation is selected to represent the material properties of the body. This determines the behaviour of an element in response to the predefined variables and the interactions with other elements.

To compute the result, the equations which govern each element are brought together to generate equations which represent the entire model. These equations for the entire system are solved numerically to compute the required variables, such as displacement, stress and strain. Because the analysis is simplified by discretizing the problem, only an approximate solution is found. More accurate solutions can be computed by using a greater number of elements in the body (a finer mesh).

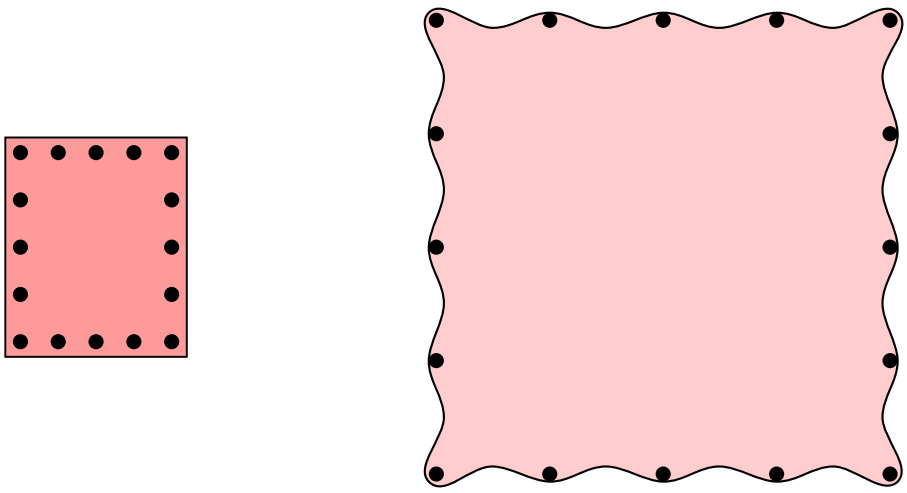

**(a)** Unstretched **(b)** Stretched

**Figure 2.12: Bladder tissue (a) before and (b) after stretching using pins.** Movement of the pins causes the bladder to stretch. Stretching the bladder using discrete points will result in the bladder being stretched unevenly.

However, coarse meshes can produce realistic results for problems with simpler geometries.

### 2.9.2 Geometry of bladder tissue

It was decided to use pins to biaxially stretch flat sheets of bladder. Once placed into the tissue, pins would be displaced in order to apply the required strain to the tissue. Stretching the bladder in this way—using discrete points—would result in uneven stretching and wavy edges. This is shown in Figure 2.12.

The bladder tissue was modelled as a rectangular cuboid. The dimensions of the cuboid in the $x$, $y$ and $z$ directions corresponded to the transverse length (width), longitudinal length (height) and thickness (depth) of the bladder tissue. The cuboid comprised of two areas. The main area was the region contained by the pins, and it is this area which the final bladder patch material would be made from. The border was the area outside the region contained by the pins. This area was not expected to be decellularised, and would be cut off from the main area after decellularisation.

The bladder patch requirements dictated that the final size of the bladder patch should be 80 mm × 80 mm. From the immersed distension experiment, the strains which were needed to be applied to bladders during decellularisation were 2.0 and 1.4 in the $x$ and $y$ directions. The initial size of the bladder patch should therefore be 26.67 mm and 33.33 mm in the $x$ and $y$ directions respectively.

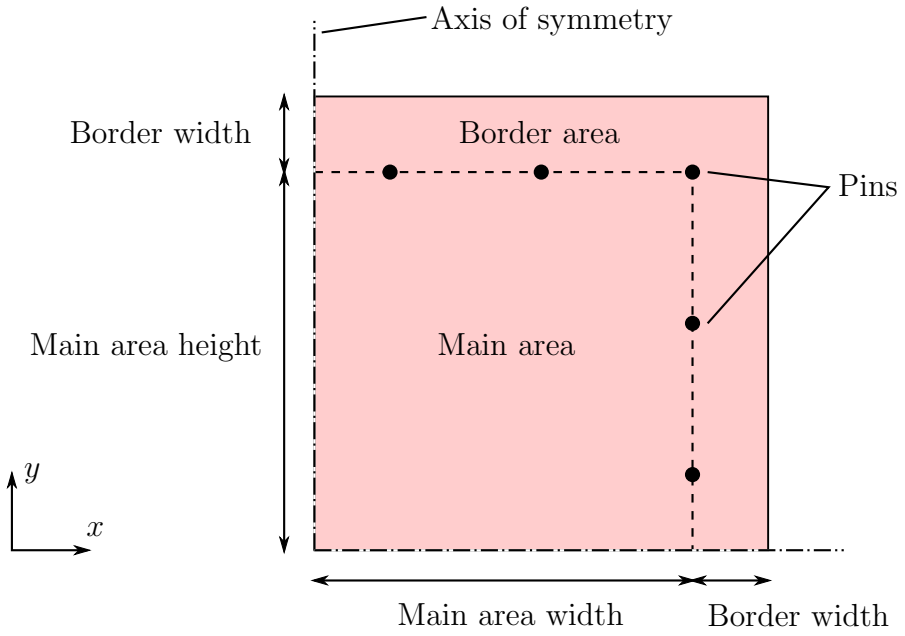


**Figure 2.13: Schematic of the geometry of the tissue model.** The bladder tissue comprises a main area and a border area. The tissue also has a thickness, which is not shown.

The initial thickness of the bladder patch model was calculated from experimental data. The preparatory tissue volume and area of bladder footprint (when laid flat) of 24 bladders (12 fresh, 6 once-frozen, 6 twice-frozen) were found using the methods described in Section 2.4.7 and Section 2.8.4.1. The initial thickness of each bladder was calculated by dividing the tissue volume by the top-down area. The mean of these thicknesses was 5.0 mm.

Because of symmetry one eighth of the bladder tissue was modelled; half of the material in each of the three dimensions. Therefore the initial (before deformation) dimensions of the main tissue area were 13.33 mm, 16.67 mm and 2.50 mm in the $x$, $y$ and $z$ directions respectively. The detailed calculations used to determine these figures are given in Appendix B.

The size of the entire area was equal to the main area plus the border area. The length of the entire area in the $x$ direction was equal to the $x$ length of the main area plus the border width. The length of the entire area in the $y$ direction was equal to the $y$ length of the main area plus the border width. All the dimensions are shown in Figure 2.13.

### 2.9.3 Mesh design

The tissue was meshed using hexahedral elements. The number of elements in the main area in the $x$ and $y$ directions was set by the variables `hexnumx` and `hexnumy`. The elements were all of equal size in each dimension. The number of elements in the $z$ direction was set by the variable `hexnumz`, and all were of equal size. The number of elements in the border was equal to the border width (`borderwidth`) divided by border element size (`hexbordersize`), rounded up to the nearest whole number.

### 2.9.4 Prescribed displacements

According to the design specifications, the final stretched size of the bladder patch was required to be 80 mm × 80 mm . The strains which should be applied to bladders during decellularisation were 2.0 and 1.4 in the $x$ and $y$ directions. The extensions which should be applied to the bladder patch were therefore 53.33 mm and 46.67 mm in the $x$ and $y$ directions respectively.

Because of symmetry, half of the material in each of the three dimensions was modelled. Therefore the extensions applied to the main area of the bladder tissue model were 26.67 mm and 23.33 mm in the $x$ and $y$ directions. The calculations used to determine these figures are given in Appendix B. These displacements were applied to the pins in the model.

During the decellularisation process, it was decided to stretch bladder tissue using discrete points. It was thought that some form of pin, hook or eyelet would be used to hold the bladder. Preliminary tests showed that it would be best to push such a pin right through the tissue It was though that such a pin would be most effective with a diameter of 1–2 mm. Therefore a diameter of 1.5 mm was used in the model. In the model, pins were simulated by applying a prescribed displacement to a number of nodes. Nodes were displaced if they were within a radius of 0.75 mm from the pin locations. Pin locations were positioned at the interface of the main area and the border area. The number of pins along each side of the main area was defined by the variable `pins`. A pin was always placed at the corner of the tissue.

Pins were displaced so that strain was linearly applied to the main area of the tissue until the required strains were reached. The corner pin moved by the $x$ and $y$ extensions that were previously calculated. The other pins moved so that all the pins stayed in a rectangular formation and evenly stretched the main area of the

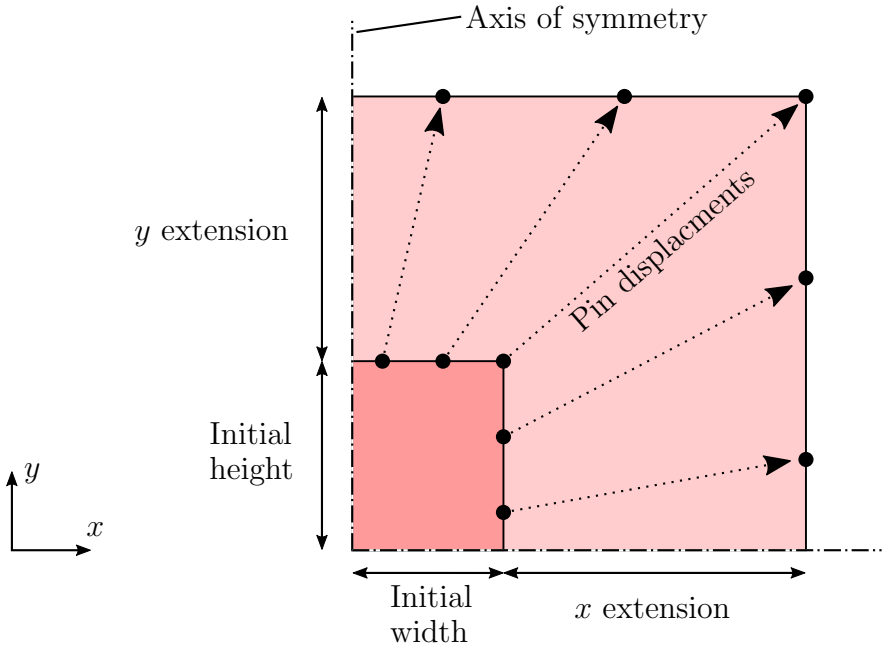


**Figure 2.14: Schematic of the displacements applied to the tissue model.** The initial size of the tissue is shown in darker red, and the final size of the tissue is shown in lighter red. Pins are respresented as black circles. The dotted arrows indicate the displacements of the pins. The tissue also has a thickness, which is not shown. The border is not shown.

tissue. These displacements are shown in Figure 2.14.

### 2.9.5 Boundary conditions

Zero displacement boundary conditions were applied to the front, left and bottom sides of the model because they were coincident with the planes of symmetry. The nodes on these faces were prevented from moving out of the planes of these faces. Nodes moved by pins were constrained to prevent movement in the z direction.

### 2.9.6 Solver parameters

A structural mechanics time step was used. A summary of the solver parameters which were used is shown in Table 2.3.

### 2.9.7 Material parameters

The constitutive equation used to model the bladder tissue was the incompressible hyperelastic Ogden material. The strain-energy equation for this model is given in

| Parameter | Value |
|---|---|
| Time steps | 1000 |
| Step size | 0.001 |
| Max step size | $10^{-3}$ |
| Min step size | $10^{-6}$ |
| Max retries | 50 |
| Optimal iterations | 10 |
| Auto time stepper | Aggressive |
| Nonlinear solution method | BFGS |
| Energy tolerance | $10^{-3}$ |
| Displacement tolerance | $10^{-4}$ |
| Residual tolerance | 0 |
| Line search tolerance | 0.9 |
| Minimal residual | 0 |
| Max reformations | 15 |
| Max BFGS updates | 10 |

**Table 2.3:** FEBio solver parameters

Equation 2.11.

$$W = \sum_{i=1}^{N} \frac{c_i}{m_i^2} \left(\lambda_1^{m_i} + \lambda_2^{m_i} + \lambda_3^{m_i} - 3\right) + U(J) \tag{2.11}$$

Parameters $(c_i, m_i)$ for this model were calculated by fitting the equation to experimental stress–strain data. The parameters which were used to model the tissue are as given in Equation 2.12. The calculation of these parameters is described in Chapter 5. The material bulk modulus was set to 1000.

$$c_1 = 0.006623, \quad m_1 = -1.73837, \quad c_2 = 0.000220, \quad m_2 = 7.59122 \tag{2.12}$$

### 2.9.8 Mesh generation

A Matlab script was written to automatically generate an `xml` file which could be processed by FEBio.

Given a set of input parameters (Table 2.4) the script calculated the node coordinates, applied boundary conditions to the nodes and determined the prescribed displacments which should be applied to nodes. This information was written into an `xml` file in the syntax required for processing with FEBio. Also included into

| Parameter | Value |
|---|---|
| Width ($x$ length) | 13.33 |
| Heigh ($y$ length) | 16.67 |
| Thickness ($z$ length) | 2.5 |
| Displacement, $x$ direction | 26.67 |
| Displacement, $y$ direction | 23.33 |
| Border size | `borderwidth` |
| Number of pins per side | `pins` |
| Pin radius | 0.75 |
| Number of x-dimension elements | `hexnumx` |
| Number of y-dimension elements | `hexnumy` |
| Number of z-dimension elements | `hexnumz` |
| Size of elements in the border | `hexbordersize` |

**Table 2.4:** Bladder mesh parameters

the file were the solver parameters and material parameters. Two finite element problems generated using the script are shown in Figure 2.15.

### 2.9.9 Software: FEBio

FEBio is an open-source software package designed to solve FEM problems. FEBio was developed specifically for use in solving biomechanical problems, and it can be used to model structural mechanics, heat transfer, biphasic and multiphasic physics, both statically and dynamically. Many of the available constitutive models are able to model complex tissue behavior. Its problem creator, PreView, is a useful tool for generating single FEM problems and for understanding the capabilities of FEBio. PostView is the post-processing software designed to view FEBio output files.

FEBio was used to compute the FEM problems generated using Matlab. The software was chosen because of its ability to model large material deformations with nonlinear stress–strain responses. Its ability to process custom generated `xml` files allowed meshes with varying parameters to be solved sequentially using an automated system. PostView was the post-processing software used to analyse and observe the results computed by FEBio. PreView version 1.17.1, FEBio version 2.3.1, and PostView version 1.9.0 were used.

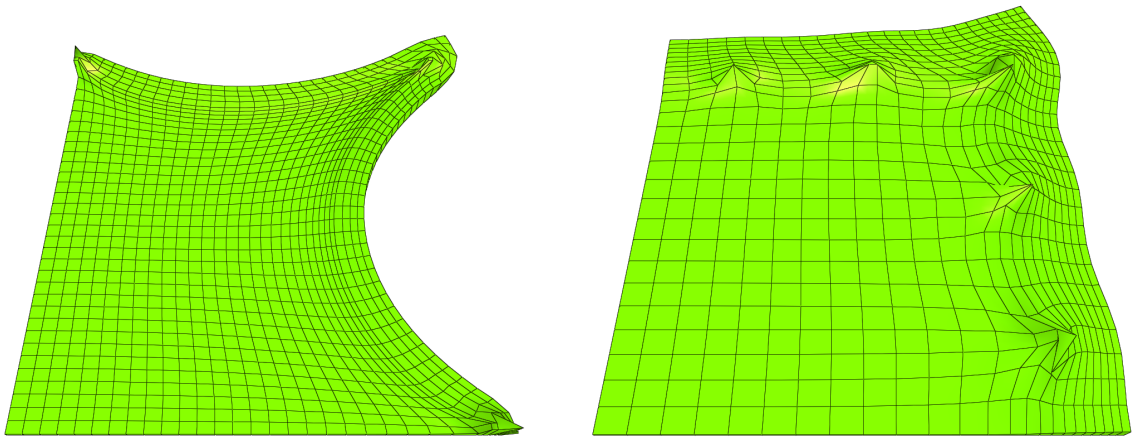

**(a)** A mesh simulating the deformation of bladder tissue with a border of 4 mm using 3 pins per side. The main area had an initial mesh density of 2 elements/mm along the $x$ and $y$ axes and the border had an initial mesh density of 1 element/mm along the $x$ and $y$ axes.

**(b)** A mesh simulating the deformation of bladder tissue with a border of 10 mm using 6 pins per side. The main area had an initial mesh density of 1 element/mm along the $x$ and $y$ axes and the border had an initial mesh density of 1 element/mm along the $x$ and $y$ axes.

**Figure 2.15: Examples of finite element problems simulating the deformation of flat sheets of bladder tissue.** The problems were generated using a Matlab script and solved using FEBio. The different problems were generated by varying the values of the input parameters. Planes of symmetry are along the left and bottom edges of each model.

# Chapter 3

# Determination of bladder filling criteria for successful decellularisation

## 3.1 Introduction

A variety of different tissues have been reported to be successfully decellularised in the literature, such as porcine cardiac valves (Booth *et al.*, 2002), porcine small intestine submucosa (SIS; Badylak *et al.*, 1995), porcine aortic root (Korossis *et al.*, 2005), ovine forestomach matrix (OFM; Lun *et al.*, 2010) and porcine urinary bladder matrix (UBM; Freytes *et al.*, 2004). The techniques used to decellularise these tissues typically involve combinations of physical and chemical processes in order to remove immunogenic material. The chemical processes rely on the diffusion of the chemicals (enzymes, detergent, etc.) into the tissue for them to act on the cellular material.

The diffusion of these chemicals is affected by time, temperature, concentration gradient, the permeability of the material, and the diffusion distance (tissue thickness) over which the chemicals must diffuse. The concentration of the solution and the incubation time of the tissue must both be limited to prevent excessive action on the tissue near the tissue/solution boundary. The incubation temperature is limited to the working temperature range of the solution, and must also be within a range which does not cause damage to the tissue (e.g. below the denaturation temperature of collagen). Material permeability is defined by the tissue, and is not a controllable factor. Given these restrictions, there must therefore be a critical thickness of tissue, above which a tissue is not able to be decellularised for a given decellularisation

method.

The thickness of undistended full-thickness porcine bladder wall is approximately 5 mm. When placed in decellularisation solutions with no liquid actively placed in the lumen, the effective thickness of the tissue is double this. Similar tissues which have been decellularised in the literature—such SIS, OFM and UBM—are mechanically delaminated in order to isolate a particular layer of the tissue. SIS, UBM and OFM have thicknesses of 0.1 mm, 0.24 mm and 0.3 mm respectively (Badylak *et al.*, 1989; Davis *et al.*, 2011; Lun *et al.*, 2010), and when placed in solutions the buffers have been able to access both the inner and outer surfaces. Therefore, in an undistended configuration, it is unlikely that full-thickness porcine bladder would be able to be successfully decellularised.

Previously a process was developed to decellularised porcine bladders (Bolland *et al.*, 2007). To overcome the problem of bladder thickness, the method involved distending bladders by not only placing them in, but filling them with, decellularisation buffers. Distending the organs utilised the natural ability of bladders to distend to large volumes during normal physiological function and resulted in the application of biaxial strain to the bladder walls. This caused the bladder walls to reduce in thickness, which allowed adequate diffusion of the buffers into the tissue.

The original porcine bladder decellularisation process used 500 ml of decellularisation buffer to fill bladders (Bolland *et al.*, 2007). This amount of fluid was put into bladders at each stage of the process regardless of their initial size. Preliminary tests demonstrated that this filling criterion did not always result in successful bladder decellularisation. It was hypothesised that larger bladders would need to be filled with greater volumes of liquid to ensure adequate application of biaxial strain to bladder walls. A filling criterion which fills bladders with varying volumes of fluid depending on their size might result in successful decellularisation of porcine bladders of all sizes. Bladders filled to these amounts must, however, not be damaged by the stretching process, otherwise the final acellular biomaterial may not be suitable for use.

### 3.1.1 Rationale

The thickness of bladder wall tissue must be reduced for decellularisation. This occurs when the organ is distended and the tissue stretched. Bladders which have been distended a small amount have collagen fibres which are tightly coiled and randomly orientated. During stretching the coils become extended and these collagen fibres become aligned so that they are parallel with the surface of the lumen. These

structural changes result in a reduction of the thickness of the bladder wall (Chang *et al.*, 1998). When a bladder is fully distended, all the collagen fibres are aligned parallel to the surface of the lumen, and the fibre coils are fully extended. This point corresponds to the transition point on the stress-strain curve of the tissue. Filling bladders to this point would be ideal for bladders undergoing decellularisation because the tissue thickness would be at a minimum.

During filling, the bladder initially undergoes a period of low-pressure filling (Scott *et al.*, 1982). Over this period, there is a large increase in volume and little increase in pressure until the transition point is reached. Any filling beyond this point results in a large increase in bladder stiffness and intraluminal pressure. It was hypothesised that the transition point would be reached by suspending bladders from the neck and filling them until the liquid level inside them rose to the top of the neck. This method of suspending bladders should fill bladders by application of low pressure to the lumen. Filling bladders by suspending from the neck is more consistent and reproducible than manually holding the bladders using forceps, as used in the original decellularisation process. When the transition point of the tissue is reached, the pressure should steeply rise. A steep rise in pressure will cause the liquid level in the bladders to rise quickly, and the end-point of the experiment will be reached.

This chosen filling criterion would minimise the risk of tissue damage due to over-stretching. Some internal pressure must be applied to bladder tissue for it to stretch and the organ to fill. This method of distension would use the length of each bladder to provide the pressure head. The normal pressure range for a bladder is 0–40 $cmH_2O$ (Clayton *et al.*, 2010), so there would be no risk of tissue damage provided the bladders do not distend to a length greater than 40 cm. Previously decellularised bladders have been around 20 cm in length, so bladders are not likely to become over-pressurised.

If a relationship could be found between bladder capacity and the initial dimensions of bladders, then bladder capacity could be calculated with minimal bladder manipulation. Using this capacity as the filling criterion for bladders being decellularised should result in adequate bladder distension and successful decellularisation. This explicit relationship for bladder volume may result in a greater likelihood of bladder decellularisation than the original criterion of filling bladders with a set volume of 500 ml.

### 3.1.2 Aims and objectives

#### Aims

The aim of this chapter was to find a relationship between porcine bladder size and capacity such that porcine bladders filled with this volume during the decellularisation process would be successfully decellularised, regardless of initial size.

#### Objectives

1. To perform mechanical tests to determine the low-pressure capacity of bladders of various sizes.
2. To calculate the relationships between bladder capacity and initial bladder size. Use statistical methods to select one relationship which is able to accurately predict bladder capacity from initial measurements.
3. To decellularise porcine bladders using the capacity relationship as the filling criterion at each stage of the process.
4. To assess the effects of tissue freezing on the efficacy of the decellularisation process.

## 3.2 Methods

A summary of experiments is shown in Table 3.1.

| | Experiment | Samples (number) | Outputs |
|---|---|---|---|
| 1 | Bladder decellularisation, original method | Bladders 3.1.a–c (3) | Histology: H&E |
| 2 | Bladder capacity investigation | Bladders 3.2.a–h (8) | Relationships between dimensions and capacity: initial and revised |
| | Additional data | Bladders 3.2.a–l (12) | Additional data points for the highest correlated of the revised capacity relationships |
| 3 | Bladder decellularisation using the highest correlated of the initial capacity relationships | Bladders 3.3.a–c (3 from fresh) | Histology: H&E and DAPI; DNA assay; Contact cytotoxicity assay |
| 4 | Bladder decellularisation using the highest correlated of the revised relationships (with additional data points) | Bladders 3.4.a–c (3 from frozen) | Histology: H&E and DAPI; DNA assay; Contact cytotoxicity assay |

**Table 3.1: A summary of the experiments featured in Chapter 3.**

### 3.2.1 Bladder decellularisation, original method

Two bladders were procured, transported in transport medium and and dissected as described in Sections 2.4.2, 2.4.3 and 2.4.6.1. Measurements were not taken. These bladders were decellularised using the original method (Bolland *et al.*, 2007) as described in Section 2.5, using 500 ml filling volumes and nuclease solution to remove the DNA.

### 3.2.2 Bladder capacity investigation

In order to determine relationships between the low-pressure capacity of bladders and their initial measurements, eight bladders were procured, transported in transport medium and dissected to remove excess connective tissue as described in Sections 2.4.2, 2.4.3 and 2.4.6.1, and stored in transport medium until testing. The width, elliptical length, and tissue volume of the bladders were recorded as described in Section 2.4.7. Bladders were photographed and their low-pressure capacity was found by performing the suspended bladder distension experiment, described in Section 2.7.

#### Initial relationships

Matlab was used to perform simple linear regression to calculate straight-line relationships with bladder capacity as the criterion variable, and each of the following parameters in turn as the predictor variable: width, elliptical length, tissue volume and width × elliptical length. The linear regression coefficients were calculated by minimising the sum of the squared errors of prediction. The $R^2$ value for each straight-line relationship was also calculated. A Grubbs' test was performed on the data to identify outliers. The relationship which was best able to predict bladder capacity was taken forward to use as the filling criterion for bladders during decellularisation (the 'initial method').

#### Revised relationships

Image data was later used to calculate the apex-to-ureter length, below-ureter area and initial thickness of each bladder. Matlab was used to perform simple linear regression with bladder capacity as the criterion variable, and each of the following parameters as the predictor variable: apex-to-ureter length, below-ureter area, width × apex-to-ureter length, and initial thickness. Linear regression coefficients,

$R^2$ values, and a Grubbs' test were calculated as above. These relationships were compared with the previous relationships, and the one best able to predict bladder capacity was later used to calculate the filling volume of bladders during decellularisation (the 'revised method').

#### Additional data

The low-pressure capacity and initial measurements of a further four bladders were determined using the methods described above. Simple linear regression was performed using the data collected using all ($n = 12$) bladders, with bladder capacity as the criterion variable and width × apex-to-ureter length as the predictor variable.

### 3.2.3 Bladder decellularisation with initial calculated filling volumes, from fresh

To test whether filling bladders according to the previously calculated initial relationships would result in the successful decellularisation, three bladders were collected from Traves abattoir and transported to the laboratory in transport medium according to the method described in Sections 2.4.2 and 2.4.3. All subsequent work was carried out aseptically in a class II safety cabinet. Excess tissue was removed from the bladders using the method described in Section 2.4.6. The width and elliptical length of bladders were recorded as described in Section 2.4.7.

The fresh bladders were decellularised according to the method described in Section 2.5 with the following changes. Two litres of each of the decellularisation solution were used per bladder for each step of the process. Each bladder was filled with a calculated volume of decellularisation solution using a syringe (day 1) or measuring cylinder (subsequent days). The volume bladders were filled with was calculated using Equation 3.1. This relationship was developed as an output of the capacity investigation, chosen as the best predictor of capacity from the initial relationships. It related the capacity ($v_c$) to the width ($w$) and elliptical length ($l_e$) of bladders.

$$v_c = (0.143 \times w \times l_e) + 78.8 \tag{3.1}$$

Based on these calculations, the three bladders were distended with 653 ml, 707 ml and 824 ml of each decellularisation solution. These fill volumes and the preparatory

| Bladder | Width (mm) | Elliptical length (mm) | Fill volume (ml); $(0.143 \times w \times l_e) + 78.8$ |
|---|---|---|---|
| 1 | 55 | 73 | 653 |
| 2 | 61 | 72 | 707 |
| 3 | 62 | 84 | 824 |

**Table 3.2:** The preparatory dimensions and filling volumes of bladders decellularised with calculated filling, initial method

dimensions of the bladders are shown in Table 3.2. Following decellularisation the bladders were placed into 3 L beakers containing the volume of solution remaining after bladder filling. Beakers were covered with heat-sterilised foil. Bladders were dissected flat using two cuts by the method described in Section 2.4.6.2.

### 3.2.4 Bladder decellularisation with revised calculated filling volumes, from twice-frozen

from twice-frozen

To test whether filling bladders according to the previously calculated revised relationships would result in successful decellularisation, and to investigate the effects of freezing on the decellularisation process, three bladders were collected from the abattoir and transported to the laboratory without transport medium according to the method described in Sections 2.4.2 and 2.4.3. All subsequent work was carried out aseptically in a class II safety cabinet. Bladders were rinsed internally and externally with wash buffer (Section 2.4.5), air dried for 5–10 min, placed into Sterilin pots, and frozen at −20 °C. Bladders were thawed at ambient temperature for 4 h, refrozen at −20 °C, and thawed for a second time at ambient temperature for 4 h. Excess tissue was removed by the method described in Section 2.4.6, but leaving the urethras as long as possible. The width and apex-to-ureter length of bladders were recorded as described in Section 2.4.7.

The frozen-twice bladders were decellularised as described above in Section 3.2.3. The volume bladders were filled with was calculated using Equation 3.2. This relationship was found during the capacity investigation, and was chosen from the initial and revised relationships as the best predictor of bladder capacity. The equation calculated capacity ($v_c$) from width ($w$) and apex-to-ureter length ($l_a$).

$$v_c = (0.173 \times w \times l_a) + 41.7 \tag{3.2}$$

| Bladder | Width (mm) | Apex-to-ureter length (mm) | Fill volume (ml); $(0.173 \times w \times l_a) + 41.7$ |
|---|---|---|---|
| 1 | 56 | 67 | 680 |
| 2 | 58 | 69 | 722 |
| 3 | 58 | 74 | 772 |

**Table 3.3:** The preparatory dimensions and filling volumes of bladders decellularised with calculated filling, revised method

The three twice-frozen bladders were distended with 680 ml, 722 ml and 772 ml of decellularisation solution. These fill volumes and the preparatory dimensions of the bladders are shown in Table 3.3. Following the decellularisation process, bladders were dissected flat using three cuts by the method described in Section 2.4.6.3 for subsequent analysis of the success of the decellularisation process.

## 3.2.5 Tissue characterisation

### 3.2.5.1 Histology

Square samples, approximately 1 cm × 1 cm in size, were taken for histological analysis from fresh bladders, and bladders decellularised using the methods outlined above. Samples were taken from the centre of the dorsal surface and the right lateral side of each bladder decellularised using the original method and the revised calculated filling method, and from three fresh bladders. Two samples were taken from the dorsal surface of each bladder decellularised using the initial calculated filling method due to tissue in the right lateral side being required for other purposes.

Samples were fixed in neutral buffered formalin (NBF), processed, embedded in paraffin wax, sectioned, de-waxed and re-hydrated as described in Sections 2.6.1.2 to 2.6.1.5. Tissue sections were stained with either haematoxylin and eosin (H&E) or DAPI then dehydrated and mounted as described in Section 2.6.1.6.

### 3.2.5.2 DNA extraction and quantification

Samples for DNA extraction and quantification were taken from fresh and decellularised bladders (decellularised using the initial and revised calculated filling methods) and processed as described in Section 2.6.2. Samples from bladders decellularised using the initial and revised calculated filling methods were taken from the

left lateral region of each bladder. Samples from fresh bladders ($n = 3$) were also taken form the left lateral region.

#### 3.2.5.3 Contact cytotoxicity testing

Square samples, 5 mm × 5 mm in size, were taken from bladders decellularised using the initial and revised calculated filling methods. Samples were taken from the centre of the right lateral side of decellularised bladders. Six samples were taken from each decellularised bladder; three samples for each cell type. Six of each type of control sample (cyanoacrylate contact adhesive, collagen gel, cell-only) were used; three per cell type. All samples were placed into 6-well plates and tested for contact cytotoxicity using BHK and L292 cell types by the method described in Section 2.6.3.1.

## 3.3 Results

### 3.3.1 Bladder decellularisation, original method

Two bladders were decellularised using the original method. At each step of the process, bladders were distended with 500 ml decellularisation solution, and placed in a jar containing a further 500 ml of the same solution. Following processing, bladders were assessed for acellularity using histology and gross observation. The colours of both bladders were significantly changed during the decellularisation process. The final colour of one bladder was completely white, whereas the other bladder was mostly white but with a slightly pink hue.

Images of sections taken from bladders decellularised using the original method and stained with H&E are shown in Figure 3.1. A urothelium was present in the fresh control samples but not the decellularised samples. The smooth muscle fibres in the native sections (Figures 3.1a and 3.1b) were dense and cellular, with nuclei present. The muscle fibres in the sections taken from the first decellularised bladder (Figures 3.1c and 3.1d) were loose and fibrous, indicating the tissue was fully decellularised. The muscle fibres in the sections taken from the second bladder (Figures 3.1e and 3.1f) were partly broken up but still dense, indicating that the tissue was only partially decellularised.

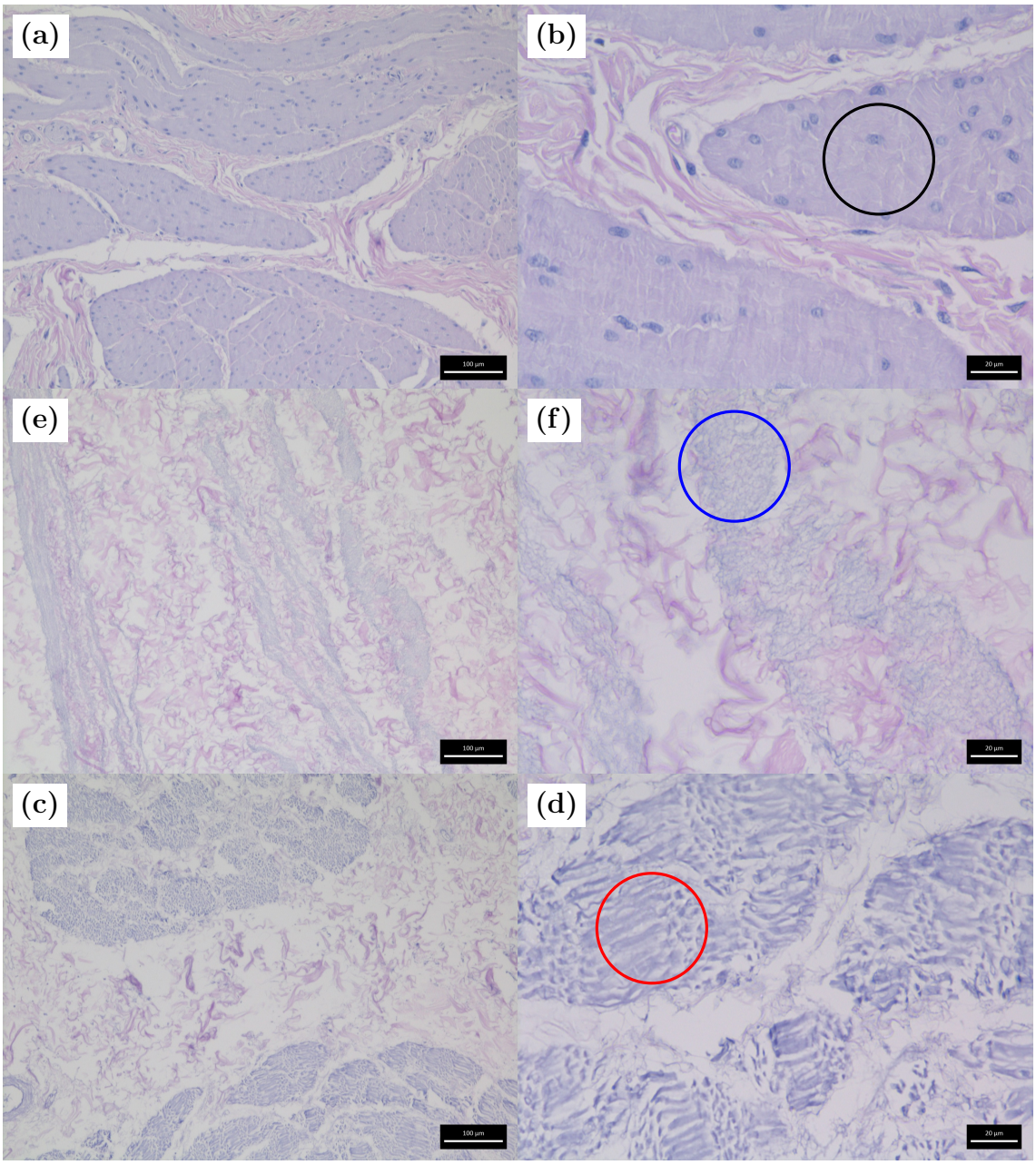


**Figure 3.1: Images of H&E stained sections from bladders decellularised using the original method.** (a) and (b) are native controls; (c) and (d) are sections from the first decellularised bladder and (e) and (f) are sections from the second decellularised bladder. (a), (c) and (e) were captured at 10× magnification, scale bars are 100 µm. (b), (d) and (f) were taken at 40× magnification, scale bars are 20 µm. All images are of the muscular layer of the bladders. Circles indicate the muscle fibres of native tissue (black), the decellularised tissue of the first bladder (blue) and the partially decellularised tissue of the second bladder (red).

### 3.3.2 Relationships between bladder capacity and preparatory measurements

Of the eight bladders initially assessed for bladder capacity by suspended distension, it was only possible to obtain a pressure reading in six of the bladders before failure. Therefore, bladder capacity was determined in six out of eight bladders. The relationships found between bladder capacity and the preparatory measurements are shown in Figure 3.2. The measurement errors of the parameters were relatively small compared to the magnitude of the measurements, and consequently all errors were contained within the width and height of the plotted points. No outliers were found using the Grubbs' test. There was a good positive correlation between bladder capacity and width, elliptical length, and width × elliptical length, In the case of bladder width and width × elliptical length, there was a strong correlation ($R^2 > 0.8$). There was no correlation between bladder capacity and tissue volume ($R^2 < 0.1$). The relationship between capacity and width × elliptical length had the highest $R^2$ value ($R^2 = 0.888$). This relationship (Equation 3.3) was used to calculate the fill volumes of bladders during decellularisation (initial method) shown in Table 3.2.

$$v_c = (0.143 \times w \times l_e) + 78.8 \tag{3.3}$$

Further parameters were later calculated and relationships found between these and bladder capacity, shown in Figure 3.3. The measurement errors of the parameters were relatively small compared to the magnitude of the measurements, and consequently all errors except some for initial tissue thickness were contained within the width and height of the plotted points. Apex-to-ureter length, below-ureter area, width × apex-to-ureter length, and initial thickness all had good correlations with bladder capacity. These were all positive correlations, except for initial thickness which gave a negative correlation. In the cases of below-ureter area and width × apex-to-ureter length, these were strong correlations ($R^2 > 0.8$). The strongest correlation was between capacity and below-ureter area. The Grubbs' test found no outliers.

For a greater number of data points, the test was repeated with four additional bladders. Bladder capacity was successfully recorded in only one bladder out of the further four which were tested. Following this, the relationship between bladder capacity and width × apex-to-ureter length was as shown in Equation 3.4. This relationship was used to calculate bladder fill volumes (Table 3.3) for the revised decellularisation method.

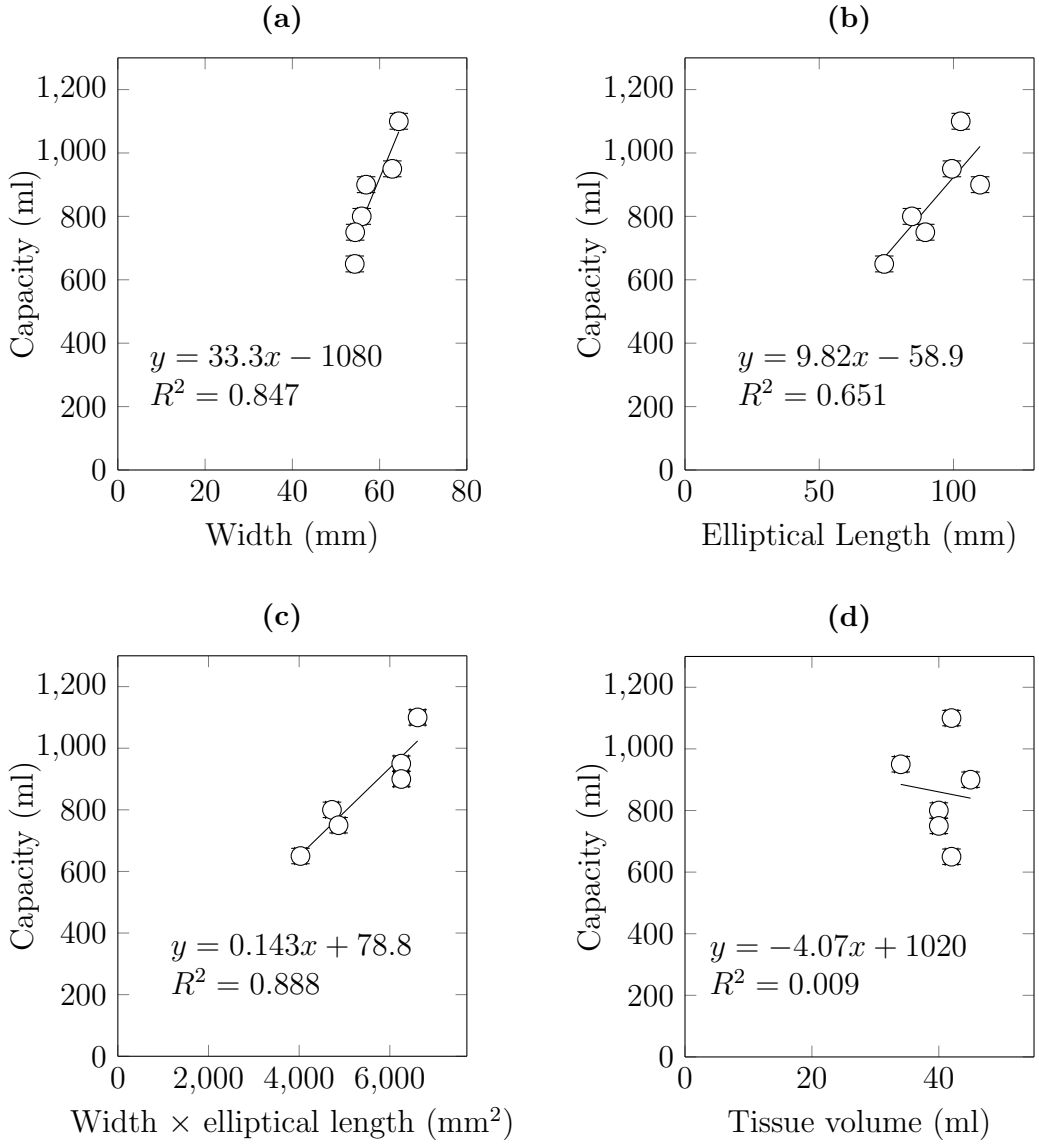


**Figure 3.2: Initial relationships between bladder capacity and the preparatory measurements of bladders.** Each point represents a single bladder. Simple linear regression lines are shown, predicting capacity from the predictor variable. Error bars represent the measurement error associated with each parameter.

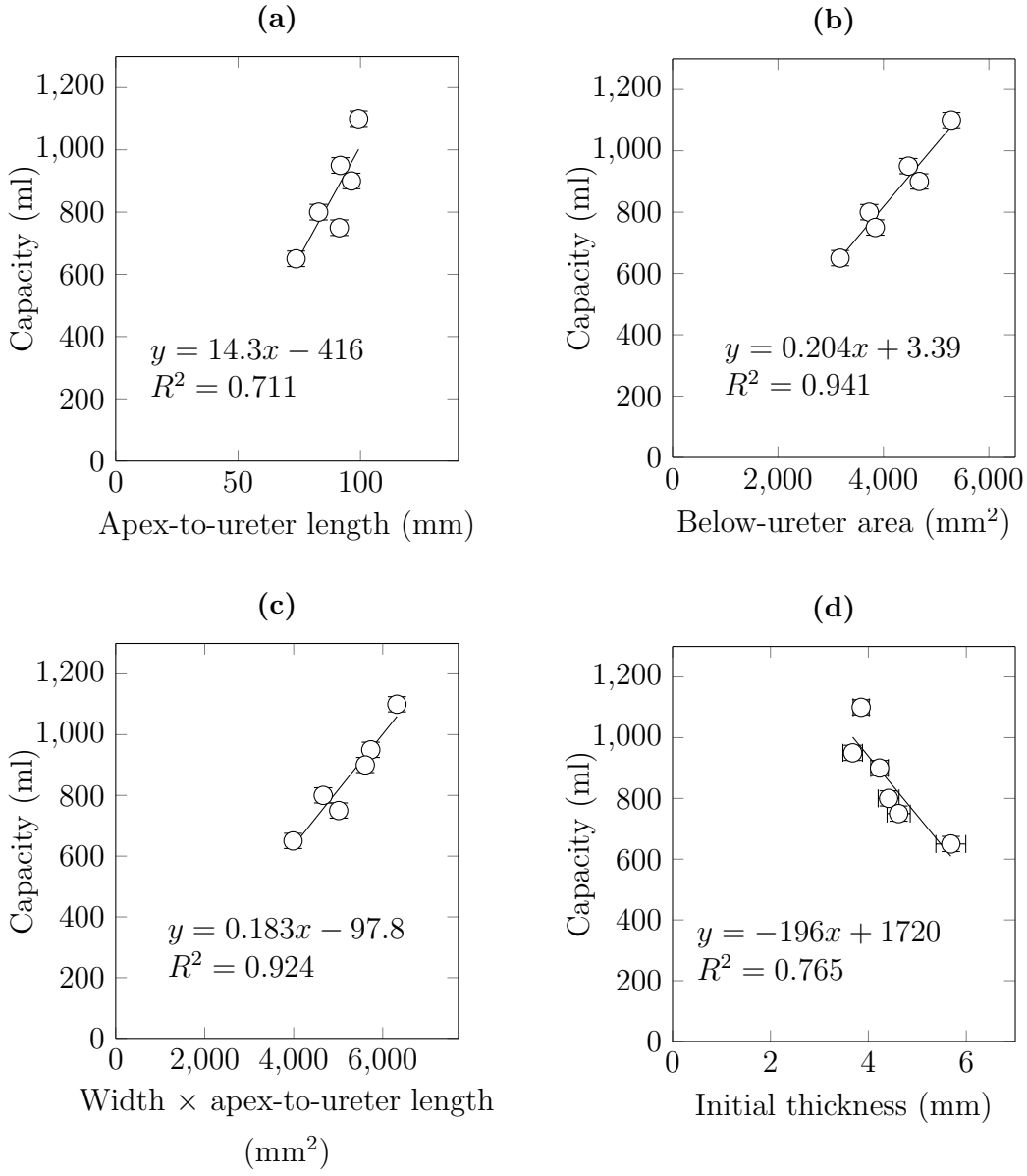


**Figure 3.3: Revised relationships between bladder capacity and calculated bladder parameters.** Each point represents a single bladder. Simple linear regression lines are shown, predicting capacity from the predictor variable. Error bars represent the measurement error associated with each parameter.

$$v_c = (0.173 \times w \times l_a) + 41.7 \tag{3.4}$$

### 3.3.3 Bladder decellularisation with calculated filling

Fresh bladders ($n = 3$) were decellularised, and filled during each step of the process using a formula calculating bladder capacity from width × elliptical length (Equation 3.3). Preparatory measurements were taken, and bladders were filled with 653 ml, 707 ml and 824 ml. This represented a mean increase of 46 % compared to the original process. This resulted in bladders being placed in over 1 L of decellularisation solution during each stage, rather than 500 ml in the original process. Figure 3.4 shows bladders being decellularised in these larger volumes of solutions. When the bladders were dissected using two cuts, the bladder opened out easily into a U-shape, but it was noted that the tissue near the apex was a little gathered-together.

Twice-frozen ($n = 3$) bladders were decellularised, and during the filling phase were filled using a formula predicting bladder capacity from width × apex-to-ureter length (Equation 3.4). When dissected before decellularisation, leaving the urethras as long as possible meant that they were 55 mm, 68 mm and 75 mm long, compared to cutting them to 3 cm long as carried out previously. The increased length of urethra made it easier to fill bladders because the end of the urethras could be more easily wrapped round the forceps holding them to prevent leaking during filling. The preparatory dimensions of bladders were recorded, and the equation used to fill bladders with 680 ml, 722 ml and 772 ml; a mean volume increase of 45 % compared to the original process. When dissected using three cuts, the bladders easily fell out into a square shape.

#### Histology

Samples were taken from bladders decellularised using the initial and revised calculated filling methods and histological sections stained with either H&E or DAPI. Sections stained with H&E are shown in Figure 3.5. Native bladder tissue sections showed that the tissue comprised the urothelium, an underlying layer of lamina propria, and an outer muscular layer. Cell nucleii were present in all layers of the tissues. Sections of the decellularised bladder tissue revealed that the tissues were devoid of a urothelium and there was no evidence of any cells or cell fragments in the other tissue layers. Following decellularisation the overall tissue histoarchitecture was maintained. Sections stained with DAPI are shown in Figure 3.6. These images

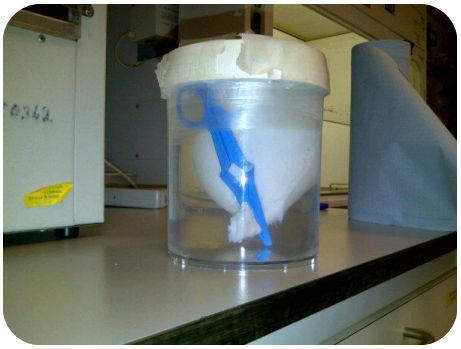

**(a)** Bladder being decellularised using the original process. Total volume of solution per bladder is 1 L.

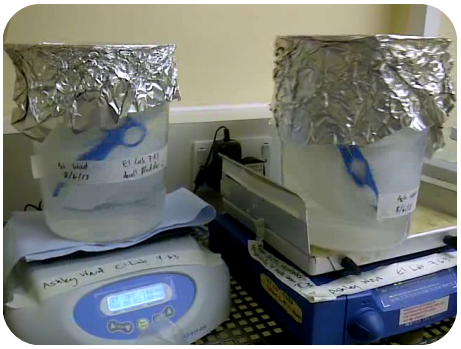

**(b)** Bladdders being decellularised using the initial calculated filling process. Total volume of solution per bladder is 2 L.

**Figure 3.4: Bladders immersed in solutions of varying volumes during different decellularisation processes.** The forceps are of identical size in both pictures.

| | | DNA content per dry weight ($ng \cdot mg^{-1}$) | | | |
|---|---|---|---|---|---|
| | | Samples | | | Mean ± 95 % CI |
| Initial method | Fresh controls | 3940 | 3900 | 5260 | 4370 ± 1930 |
| | Decellularised | 30.2 | 77.7 | 29.2 | 45.7 ± 68.8 |
| Revised method | Fresh controls | 2570 | 3020 | 2140 | 2580 ± 1090 |
| | Decellularised | 13.6 | 16.6 | 9.1 | 13.1 ± 9.4 |

**Table 3.4: DNA content of bladder tissues decellularised using the calculated bladder fill volume methods.**

of the sections of the fresh tissue staind with DAPI showed numerous blue nuclei, which were absent in the sections of the decellularised tissues.

### Total DNA quantification

DNA was extracted from samples taken from fresh and decellularised bladders and quantified using spectrophotometry. Samples from bladders decellularised using the initial calculated filling process had a mean DNA content per dry weight of $45.7\,ng \cdot mg^{-1}$; a reduction of 99.0 % relative to the native controls. Samples from bladders decellularised using the revised process had a mean DNA content per dry weight of $13.1\,ng \cdot mg^{-1}$; a reduction of 99.5 % relative to the native controls. The data are shown in Table 3.4.

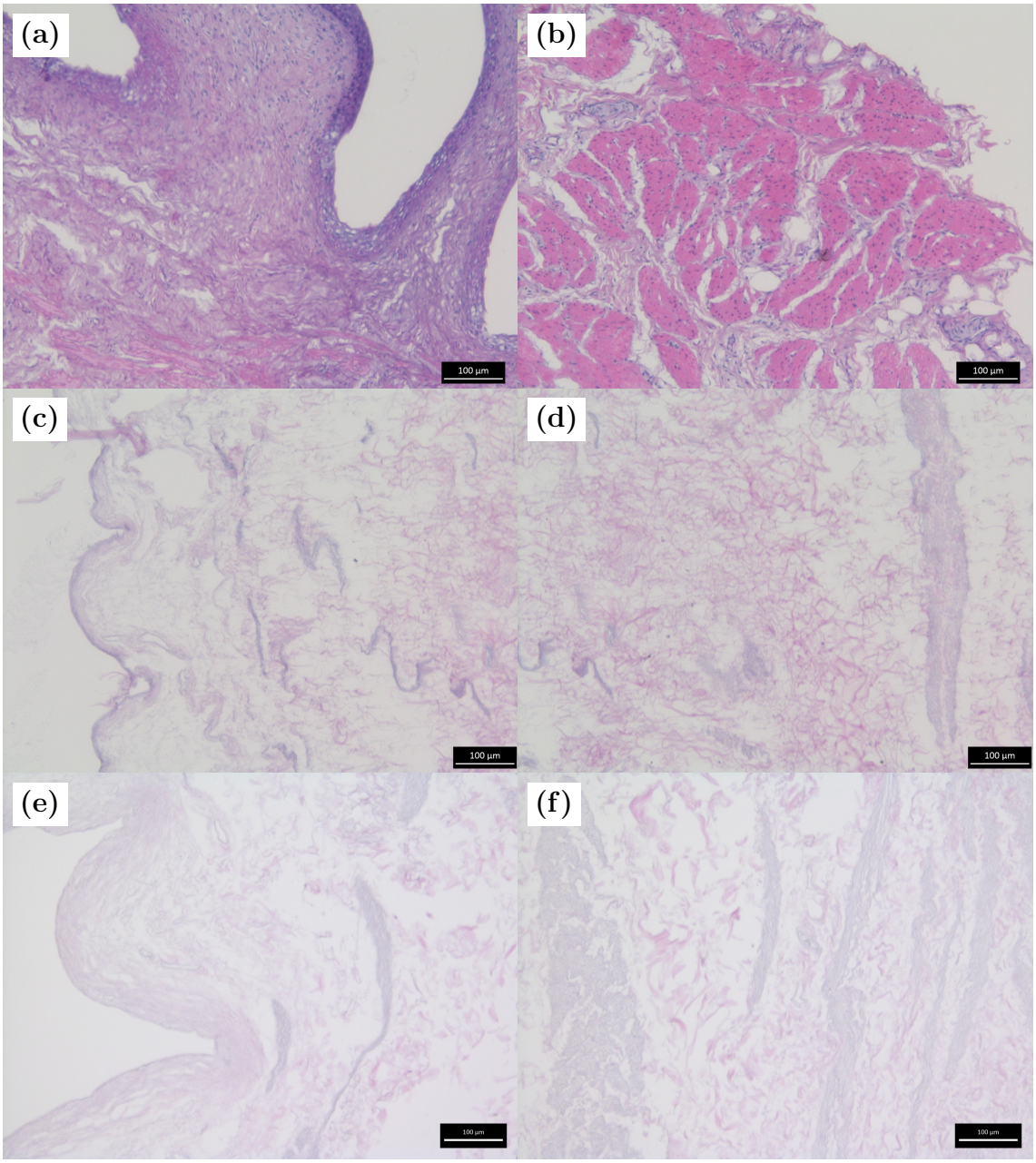


**Figure 3.5: Images of H&E stained slides from bladders decellularised using the calculated filling methods.** (a) and (b) are fresh controls; (c) and (d) are from bladders decellularised by the initial method; (e) and (f) are from bladders decellularised by the revised method. (a), (c) and (e) are images of the luminal surface and (b), (d) and (f) are images of the muscular layer. All images were captured at 10× magnification. Scale bars are 100 µm.

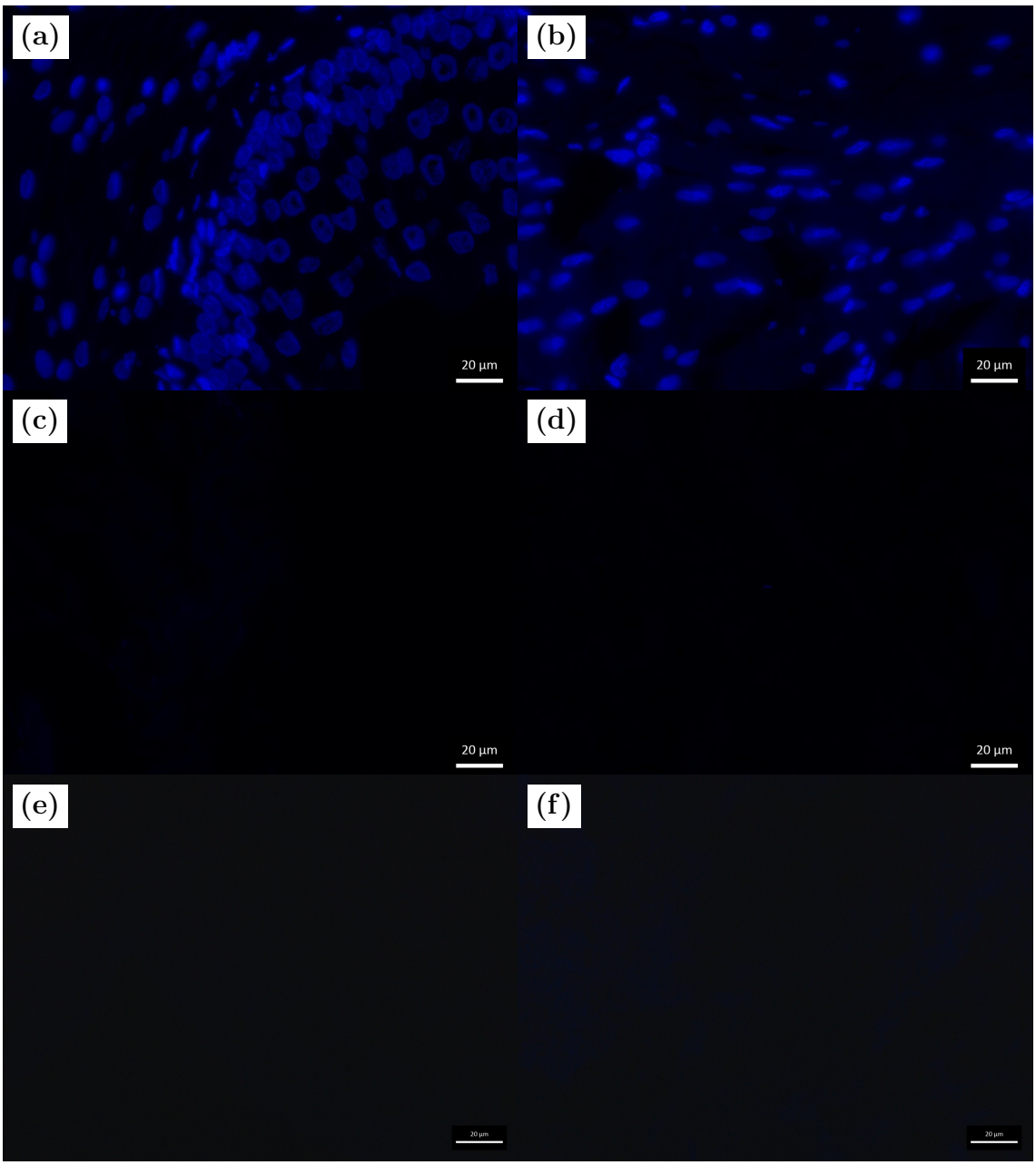


**Figure 3.6: Images of DAPI stained sections of bladders decellularised using the calculated filling methods.** (a) and (b) are fresh controls; (c) and (d) are from bladders decellularised by the initial method; (e) and (f) are from bladders decellularised by the revised method. (a), (c) and (e) are images of the luminal surface and (b), (d) and (f) are images of the muscular layer. All images were captured at 40× magnification. Scale bars are 20 µm.

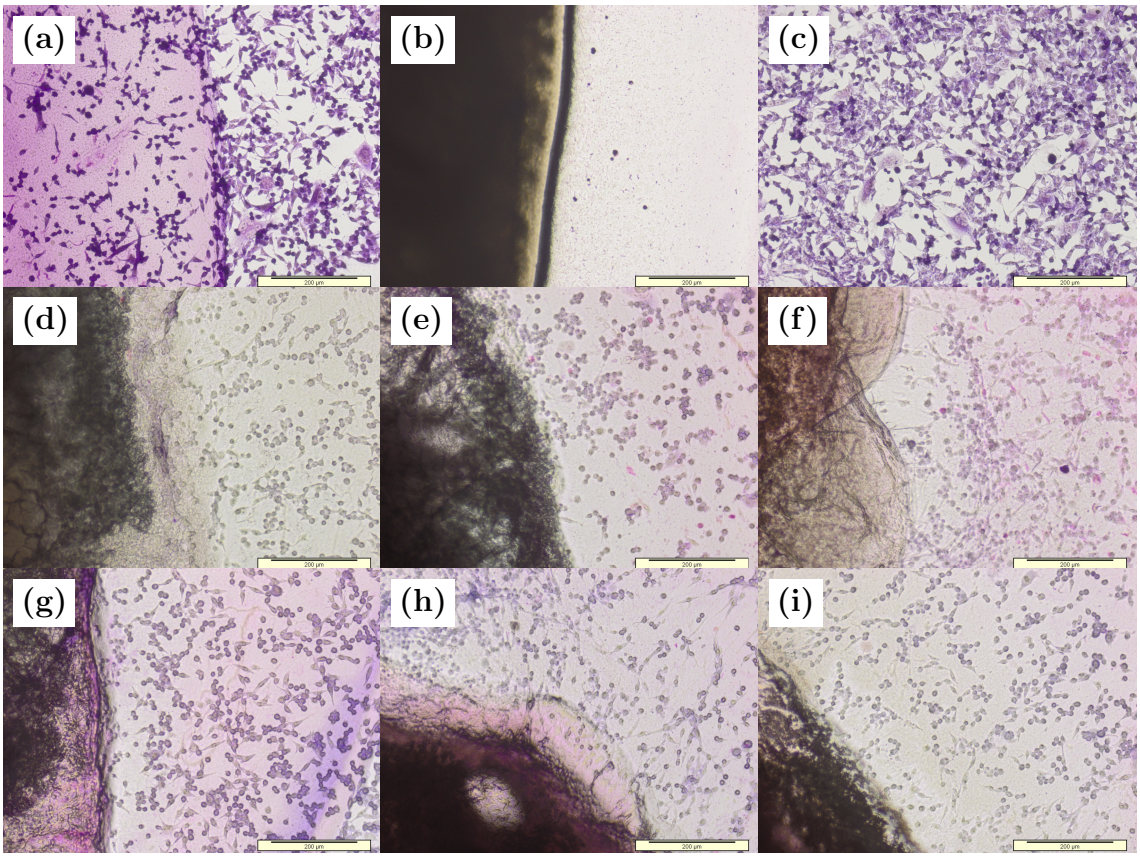


**Figure 3.7: Contact cytotoxicity assay using BHK cells of bladder tissue decellularised using calculated filling volumes.** Controls are (a) collagen gel, (b) cyanoacrylate glue and (c) cells only. Initial method tissue samples are (d), (e) and (f). Revised method tissue samples are (g), (h) and (i). Giemsa stain was used to help visualise the cells. All images were captured using a 10× magnification. Scale bars are 200 µm.

### Contact cytotoxicity assays

Decellularised tissue samples were incubated with either BHK cells (Figure 3.7) or L929 cells (Figure 3.8) for 48 h to determine any residual cytotoxicity. Cell growth in the cell-only control wells appeared normal, showing a high density of cells which had adhered well to the substrate. The confluence of cells grown in wells containing collagen gel only was slightly less than that of the cell-only controls. On the gel, cells were slightly more rounded with fewer projections. The areas next to the drops of cyanoacrylate contact adhesive were sparsely populated with cells, and all were rounded and shrunken in morphology. Decellularised tissue samples did not appear to significantly inhibit cell growth. Cells were able to grow up to the tissue and were comparable in density to the collagen gel control samples. Most cells had a normal morphology with cytoplasmic projections. Cell behaviour was similar to the collagen gel only control group.

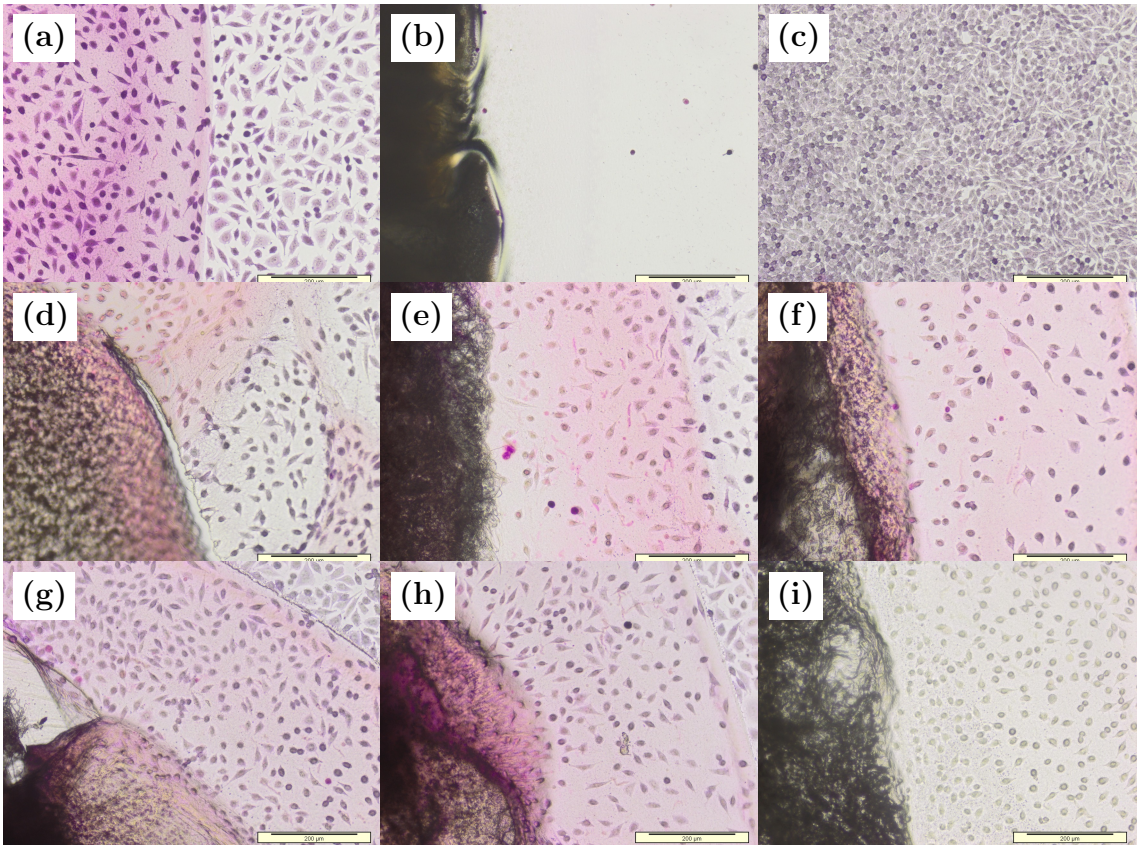


**Figure 3.8: Contact cytotoxicity assay using L929 cells of bladder tissue decellularised using calculated filling volumes.** Controls are (a) collagen gel, (b) cyanoacrylate glue and (c) cells only. Initial method tissue samples are (d), (e) and (f). Revised method tissue samples are (g), (h) and (i). Giemsa stain was used to help visualise the cells. All images were captured using a 10× magnification. Scale bars are 200 µm.

## 3.4 Discussion

Decellularised tissues have the potential to provide alternative means of repairing and replacing tissues of the body with improved clinical outcomes compared to materials which are currently used in surgery. Many types of tissues are currently decellularised using a combination of physical and chemical processes (Badylak *et al.*, 2011). Tissues which are decellularised by chemical processes are typically placed into a series of solutions, and these tissues are typically thin enough for the chemicals to diffuse fully into the tissue, such as ovine forestomach matrix (Lun *et al.*, 2010) and amniotic membrane (Wilshaw *et al.*, 2006), thus providing the required chemical action throughout the entire thickness of the tissue. Previously a process was developed to decellularise full-thickness porcine bladders. In order for the chemicals to fully diffuse into the thick walls of the bladders they were distended with 500 ml of solution, thereby stretching the tissue and reducing its thickness. Because chemicals diffuse more readily over smaller distances, this thinning of the tissue allowed the chemicals to diffuse throughout the full thickness of the tissue. This study investigated the effects of filling bladders using different volumes of decellularisation solutions in order to stretch—and therefore reduce the thickness of—the tissue adequately for complete decellularisation to occur.

In preliminary experiments, two bladders were decellularised using the original decellularisation method, which was developed by Bolland *et al.*, (2007). At each stage of the process, the bladders were each filled with 500 ml decellularisation solution and placed in a container filled with a further 500 ml of the same solution.

Following processing, the larger 'decellularised' bladder had a pinkish hue and the H&E-stained sections of this bladder (Figure 3.1) demonstrated that the muscular layer of the tissue was not loose and fibrous, but densely packed with an appearance similar to that of native tissue. The smaller bladder was completely white by gross observation, and the histological sections exhibited a muscular layer which was loose and fibrous. These findings suggested that the tissue of the larger bladders was not fully decellularised.

Filling one bladder with 500 ml of solution during each stage of the process appeared to result in complete decellularisation, whereas filling the other bladder with this volume did not. It was hypothesised that the bladder was not being sufficiently stretched in order for the thickness to be reduced to a suitable distance for the decellularisation chemicals could to fully diffuse into to tissue. The smaller bladder was successfully decellularised by the process, therefore it was further hypothesised that bladders of differing sizes would need to be distended by different volumes of

decellularisation buffers in order for the required stretch to be applied.

Other chemical-based decellularisation processes which have been developed have used varying amounts of decellularisation solutions depending on the size of the tissue which was processed. For example, (Hogg *et al.*, 2013) used a method of decellularisation whereby 100 ml of solution was used for each 85 mm segment which was processed. Similarly for the bladder decellularisation process—a combination of physical deformation and chemical exposure— it was hypothesised that a relationship existed between the undistended dimensions of bladders and the volume they should be filled to for complete decellularisation to occur. The use of such a relationship would result in larger bladders being filled with greater volumes to apply adequate stretch to the tissue, and smaller bladders not being over-filled. The unstretched dimensions of bladders were recorded, and bladders were in turn suspended at the neck and filled to capacity. Relationships were calculated in order to find a relationship between bladder capacity and the initial dimensions of bladders. This would allow the capacity to be calculated for filling during the decellularisation process.

Initially, eight bladders were tested and six of these were tested successfully. Data was not gathered for two bladders which slipped from the equipment before the tests could be completed. Of the initial relationships between bladder dimensions and capacity (Figure 3.2), the relationships between capacity and width, elliptical length, and width × elliptical length were able to predict capacity with positive correlations, demonstrating that bladders with greater dimensions tended to have greater capacities. The relationship between capacity and width × elliptical length showed the strongest correlation, with an $R^2$ value of 0.888. The $R^2$ values indicated that width ($R^2 = 0.847$) was a better predictor of capacity than length ($R^2 = 0.651$), and the larger gradient of the relationship for width ($y = 33.3x - 1080$) indicated that a change in width would increase capacity more than an equivalent change in length ($y = 9.82x - 58.9$).

There was no correction between tissue volume and capacity, indicated by the low $R^2$ value of 0.009 (Figure 3.2d). This was a surprising result, because tissue volume is a measure of the mass of the tissue, and it is somewhat intuitive that the greater the bladder mass the more of it there would be to expand into a larger shape. However, in the context of bladder tissue, it is important to consider how the collagen fibres extend during distension. Highly coiled collagen fibres unwind and move relative to one another, and there is a limit at which the collagen fibres become tightly coiled and fully stretched out (Chang *et al.*, 1998). This means that each individual collagen fibre is only available to be stretched to a certain maximum strain before damage occurs. Therefore, several collagen fibres in parallel are only able to be

stretched to this same maximum strain. Hence, an increase of the number of collagen fibres would not always result in an increase in the maximum extension of a biological material. This could explain why a greater amount of tissue would not necessarily result in a bladder with a greater maximum capacity.

More relationships were found using detailed measurements taken from images of the bladders (Figure 3.3). Relationships predicting capacity from apex-to-ureter length and initial thickness showed good correlations, with $R^2$ values of 0.711 and 0.765 respectively. Relationships predicting capacity from below-ureter area and width $\times$ apex-to-ureter length showed strong correlations, with respective $R^2$ values of 0.941 and 0.924 respectively. The strongest correlation was between capacity and below-ureter area, and it was expected that tissue area would correlate well with capacity, because area is a measure of the surface area of a distended bladder and a greater surface area would result in a larger volume. However, calculating the below-ureter area of a bladder required an image to be captured and a computer to analyse the image. This process was time-consuming and impractical to perform during the laboratory decellularisation process. However, the correlation between capacity and width $\times$ apex-to-ureter length ($R^2 = 0.924$) was almost as strong as that between capacity and below-ureter area ($R^2 = 0.941$), and both of these measurements could be taken without the use of a camera. Width multiplied by length for an oval shape, such as the bladder, is proportional to the area, which means that width multiplied by length was a good estimate of the area of the bladder. Therefore this relationship was the most favourable relationship to use in the laboratory environment during processing.

There was a negative correlation between capacity and initial tissue thickness, demonstrated by the negative relationship $y = -196x + 1720$ (Figure 3.3d). Thickness was the only variable which had been calculated from other variables rather than measured directly. It was calculated by dividing the tissue volume by twice the below-ureter area. It has already been shown that tissue volume did not correlate with capacity, therefore this negative correlation between thickness and capacity can be explained by the strong positive relationship between capacity and below-ureter area because thickness was calculated as proportional to the reciprocal of area.

There was a stronger correlation between capacity and apex-to-ureter length ($R^2 = 0.924$) than there was between capacity and elliptical length ($R^2 = 0.651$), as shown in Figures 3.2b and 3.3a. This was surprising because the elliptical length of bladders is affected by bladder shape, which in turn is highly likely to affect capacity. Additionally, apex-to-ureter length measurements do not take into account the contribution of the size of the trigone to the length of the bladder, however it has been reported in the literature that the trigone region is less extensible than the other tis-

sue which makes up the wall of the bladder (Lapides & Nesbit, 1976), and therefore is unlikely to contribute as much to the capacity of the bladder. Measurements of elliptical length require human judgement, whereas measurements of apex-to-ureter length do not. Apex-to-ureter length may have resulted in a stronger correlation because elliptical length measurements are more susceptible to human error. The difference in the correlations may have been due to this difference in measurement error. As a result of this, it was determined that bladder capacity should be calculated from the equation which calculates bladder capacity from width × apex-to-ureter length (the revised capacity equation) rather than width × elliptical length (the initial capacity equation).

There were measurement errors associated with each of the parameters used to calculate relationships for bladder capacity. Measurement errors of the width and length of each bladder (measured using a ruler) were small, with a mean error of ±1.4 % for each dimension, and consequently the errors for the derived parameter width × elliptical length was doulbe this (±2.8 %). As it was a derived parameter, the compounded error was unavoidable. The precision for tissue volume was comparable to this, with a mean magnitude of ±2.5 %, but could have been measured more precisely, for example by measuring the mass using a balance and dividing by the tissue density. Measurement errors of the apex=to=ureter length of bladders were smaller than the errors of dimensions taken using a ruler, and had a mean relative error of ±0.2 %. This therefore represented a more precise method for measuring dimensions. Consequently, the measurement error for width × elliptical length was also very small (mean error of ±0.6 %). The below-ureter areas of bladder had errors which were a combination of error due to measurement and error due to the approximation used to calculate the area using the trapezium rule. These were minimised by measuring the area from the images using a large number of points, and therefore the error was small (1.2 %). The measurement error of initial bladder thickness was the largest of all parameters with a mean relative error of ±4.9 %. It was likely that this was because thickness was calculated from both tissue volume and below-ureter area, resulting in a compounding of these errors. However, the small distances involved in measuring bladder thickness resulted in the absolute error of this measurement being ±0.2 mm. This method was chosen because it reduced the amount the bladder was manipulated during measurements, and although it it likely that more precise measurements could have been acquired by taking several measurements using calipers, this method was likely to have had a low accuracy due to the soft and flexible nature of the material. Bladder capacity had a moderately large measurement error, with a mean relative magnitude of ±3.0 %. This could have been reduced by filling each bladder with a smaller volume of phosphate

buffered saline (PBS) at each filling interval. However, all parameters had a mean measurement error below ±5 %, which is within an acceptable measurement range to calculate meaningful relationships between them.

In order to determine whether filling bladders with calculated volumes of decellularisation solutions based on their initial volumes would result in reliable bladder decellularisation, two sets of bladders ($n = 3$ each) were decellularised. The first set was decellularised using the initial relationship, which was used to calculate bladder capacity from width × elliptical length. The second set was decellularised using the revised relationship, which was used to calculate bladder capacity from width × apex-to-ureter length. Although these relationships were different, they used data from the same data set, with the exception that the revised relationship was calculated with an additional data point added to the set. The only other difference was that the first set used elliptical length and the second used apex-to-ureter length in the relationships. These two distances are two different methods of measuring the length of bladders. Therefore, these formulae for calculating capacity were approximately equivalent.

The original process developed by Bolland *et al.*, 2007 used 500 ml decellularisation solution during each step. In this chapter, the initial and revised relationships for bladder capacity were used to calculate bladder fill volumes for two sets ($n = 3$ each) of decellularised bladders. Using these relationships resulted in bladders being filled with mean volumes of 728 ml and 725 ml of decellularisation solutions during the initial and revised decellularisation processes respectively, corresponding to mean relative volume increases of 46 % and 45 % compared to the original decellularisation process. Is was therefore possible that bladders above a certain size would not have been distended sufficiently when being filled for decellularisation using the original method (Bolland *et al.*, 2007).

The histological analysis of bladders decellularised using these methods showed that the bladder tissue no longer contained signs of cellular material (Figures 3.5 and 3.6). The results of DNA extraction and quantification demonstrated that a negligible amount of DNA remained. The mean DNA content of the tissues of each set was less than the $50\,\mathrm{ng} \cdot \mathrm{mg}^{-1}$ level specified by Crapo *et al.*, (2011). These data suggested that this method of filling bladders with calculated volumes based on their initial size resulted in successful decellularisation of bladders of different sizes.

It is not feasible for fresh bladders to be decellularised as part of a manufacturing process. However, it has previously been shown that freezing and thawing tissue prior to decellularisation can reduce the effectiveness of the decellularisation process (Tuan-Mu *et al.*, 2014). To determine whether tissue freezing had a detrimental

impact on the effectiveness of the decellularisation process, bladders were subjected to different freezing conditions before decellularisation using calculated filling methods. The first set ($n = 3$) of decellularised bladders were transported in transport medium and processed fresh. The second set ($n = 3$) of decellularised bladders were transported without transport medium, and were subject to two freeze-thaw cycles before processing. The acellular nature of the processed tissue demonstrated that freezing the tissue did not affect the decellularisation process. Studies in the literature have shown that freezing and thawing tissue before processing is sometimes necessary for successful decellularisation (Fermor *et al.*, 2015). This is because ice crystal formation during the freezing process is thought to open up the ECM to increase the diffusion of solutions into the tissue (Kheir *et al.*, 2011). It is likely, therefore, that freezing the tissue assisted rather than hindered the decellularisation process. However, the freeze-thaw cycles may have caused some permanent changes to the mechanical properties of the tissue, as it is known that the formation of ice crystals can disrupt ECM (Huang *et al.*, 2013). To further investigate this, mechanical tests could be performed to compare the mechanical properties of fresh and frozen bladder tissue.

The original decellularisation process involved transporting bladders in transport medium in order to preserve the tissue. Urothelium deteriorates quickly when left in contact with urine, hence transport medium was used to minimise tissue degradation. However, filling bladders with transport medium immediately after retrieval is a time-consuming and costly process. A scalable manufacturing process is unlikely to be compatible with this procedure, and the laboratory-based decellularisation process would benefit from not having to perform this step. The intended application of transport medium is to maintain viable urothelial cells in bladder tissue samples (Southgate *et al.*, 2002). It was hypothesised that transporting bladders in transport medium was an unnecessary precaution for bladders which would later be decellularised because the urothelium is removed during the decellularisation process anyway. The experiments in this chapter demonstrated that bladders transported without transport medium were able to be successfully decellularised. By not inhibiting deterioration of the urothelium, transporting bladders without using transport medium may even have assisted in removing the cells from the tissue. However, prolonged exposure of the lumen to urine during transportation may have lead to degeneration of the urothelial barrier and exposure of the underlying layers of tissue to urine (Southgate *et al.*, 2002). This may have resulted in damage to extracellular matrix components which would otherwise have been preserved during the decellularisation process. This could alter the mechanical properties or biochemical composition of the decellularised bladder with changes localised to the regions

of the tissue near the urothelium. Any such changes could be determined using mechanical testing, biochemical assays or immunohistochemistry.

When bladders were dissected before decellularisation, the urethras of bladders prepared for the initial processing method were dissected to a length of 30 mm. The urethras of bladders prepared for the revised processing method were left as long as possible, resulting in urethra lengths in the range 55–75 mm. The increased length allowed the bladders to be more easily filled during decellularisation because a greater and more even pressure could be applied to bladders. The extra length also enabled the bladders to be more easily filled because the urethras could be wrapped round the forceps holding them to prevent any solution leaking from the bladders during the filling process.

Bladders decellularised using the initial calculated filling method were dissected flat using the two-cut method, whereas bladders decellularised using the revised method were dissected flat using the three-cut method. Bladder tissue dissected using the two-cut method formed an irregular semicircle shape when laid flat, and the material was drawn together around the apex. Bladder tissue dissected using the three-cut method formed a rectangular shape after decellularisation, and did not show any signs of holding tension when laid flat. This demonstrated that taking a square of tissue from the dome of each bladder enabled production of a piece of material which easily formed a rectangular shape. It also showed that cutting the bladder with 3 cuts was preferable to using 2 cuts because samples taken from tissue in a low-stress state are subject to minimal changes of dimension after being isolated. This has implications for production of a patch of a required surgical size from the decellularised biomaterial.

The original decellularisation process was based on a similar process developed by Booth *et al.*, 2002 to produce decellularised porcine heart valves. This procedure was later adapted by introducing DNase and RNase to break down nucleic acids in the tissue so that the chains of nucleotides would be short enough to be flushed out by subsequent decellularisation solutions (Wilcox *et al.*, 2005). The original bladder decellularisation process also used DNase and RNase in order to assist in the removal of nuclear material from the tissue (Bolland *et al.*, 2007). A later adaptation of the same process used Benzonase rather than DNase and RNase to digest nucleic acids in the tissue (Herbert *et al.*, 2015). Benzonase is a nuclease which is able to degrade both DNA and RNA, and is more economical. Additionally, Benzonase does not require the addition of bovine serum albumin (BSA) to the nuclease solution. This indicated that Benzonase is more suited for a commercial manufacturing process. Benzonase was used during bladder decellularisation using calculated filling volumes. The successful decellularisation of both sets of bladders indicated that Benzonase

was a suitable replacement for DNase and RNase in this bioprocess.

## 3.5 Conclusions

Preliminary tests showed that distending bladders with 500 ml decellularisation solution during processing—as per the original process—did not always result in complete decellularisation. A bladder filling experiment was performed which found several relationships between bladder capacity and initial bladder dimensions. The strongest of these relationships were those which predicted bladder capacity from bladder width × length.

These relationships were used to calculate the filling volumes of two sets of bladders which were decellularised using a modified version of the original decellularisation process. Filling bladders with these calculated volumes during decellularisation resulted in bladders being filled with a mean volume increase of 45 % relative to the volume used in the original process. No signs of cellular remnants were present in samples of these decellularised bladders analysed using histology. DNA extraction and quantification showed that 99 % of the DNA was removed by the decellularisation processes using calculated filling volumes. These tissue characterisation methods demonstrated that adequate biaxial strain was applied for the decellularisation solutions to diffuse sufficiently into the bladder tissue decellularisation.

Transporting bladders without using transport medium and subjecting bladders to two freeze-thaw cycles before decellularisation did not affect the efficacy of the process. Dissecting bladders so that the urethras were left as long as possible allowed bladders to be filled with greater ease during decellularisation. Using three cuts rather than two cuts to dissect the tissue into a flat sheet during decellularisation allowed the tissue to lay in a low-stress state more suitable for samples of specific dimensions to be isolated from it. Benzonase was an efficacious substitute for DNase and RNase during the decellularisation process.

# Chapter 4

# Determination of the deformation state required for bladders to become successfully decellularised

## 4.1 Introduction

In the previous chapter, bladders were suspended and distended to find relationships between their capacities and their initial dimensions. A relationship between bladder capacity and width × length was found which exhibited a high correlation. Bladders were then successfully decellularised using these calculated capacities as the filling criterion. This demonstrated that filling bladders to these volumes applied a suitable amount of biaxial strain to bladders for the solutions to adequately diffuse into the tissue for successful decellularisation to occur.

However, distending bladders with solutions is a procedure which is not compatible with a scalable manufacturing process. In order for the process to be able to be scaled up, new methods of deforming the bladder had to be possible. Bladders stretched using a new method would require being adequately deformed in order to facilitate complete decellularisation. Filling bladders with calculated volumes of solutions results in biaxial strain being applied to the bladder tissue. If the deformation state of bladders filled to these volumes was known, this biaxial deformation state could be applied to bladder tissue using alternative deformation methods. It was hypothesised that applying this known state of biaxial deformation to bladder tissue during decellularisation would then result in acellular tissue. It would then

be possible to develop new methods for deforming the bladder which did not require bladders to be distended, which would be compatible with a manufacturing process.

In the previous chapter it was shown that bladders transported without transport medium that underwent two freeze-thaw cycles before decellularisation resulted in bladder tissue which was completely acellular after processing. Previous studies had however shown that freezing biological tissue can result in changes to the structure of biological tissue (Huang *et al.*, 2013). Hence it was possible that the modified transportation and storage regime may have caused some damage to the tissue, resulting in changes to the mechanical properties. Bladders are able to store large volumes of urine at low pressures due to the highly compliant nature of the tissue (Scott *et al.*, 1982). This compliance is required for normal bladder function (Mundy *et al.*, 2004). Therefore a decellularised bladder patch should sufficiently retain its mechanical properties if it is to perform adequately *in vivo*. This decellularisation process had already been shown to increase the stiffness and reduce the failure strain of the bladder tissue (Bolland *et al.*, 2007). It was therefore important to conduct mechanical tests on the tissue in order to find out whether the change in transportation and storage regime had any additional effect on the biomechanics of decellularised bladder.

Decellularised bladder patches produced by a commercial manufacturing process should be manufactured to a specified size. The specific dimensions should be determined by surgical requirements, and will be discussed later in this thesis. The final size of decellularised bladder material is determined by its initial size and any size changes which occur during the process. Each bladder has a certain measurable size and shape before decellularisation. During decellularisation, bladders are stretched by filling with a predetermined known volume. Is was noticed that after decellularisation, bladders were larger than when they were before processing, but not as stretched as when filled during processing. This lead to the conclusion that bladders adopted an intermediate final size which was larger than their initial (fresh) size but smaller than the size stretched to during decellularisation. The size bladders are stretched to during decellularisation, and the final size of bladders after decellularisation represent two states of deformation of the tissue relative to the original fresh tissue. It was hypothesised that these two deformation states would correlate. This indicated that it would be possible to find a relationship which would be able to predict the final size of bladder tissue given the initial dimensions before decellularisation and the state of deformation during decellularisation.

### 4.1.1 Rationale

During decellularisation, bladders are distended with and immersed in several solutions. In order to determine the deformation state of bladders during decellularisation, it would be necessary to take measurements of bladders which are in the same state as they would be in during decellularisation. It was therefore necessary to distend bladders whilst they were fully immersed in solution, mimicking the decellularisation environment. To maximise repeatability, bladders were held from the neck using a clamp during filling to ensure they were kept stationary. Bladders were filled at a constant quasi-static filling rate.

The mechanical properties of biological tissues can be compared by calculating material parameters from their stress–strain curves. The parameters which are often calculated are the toe region elastic modulus, linear region elastic modulus, transition stress, transition strain, failure stress and failure strain (Korossis *et al.*, 2002; Korossis *et al.*, 2005; Wilshaw *et al.*, 2006). These parameters are only calculable from the stress–strain curves if the materials are tested in uniaxial tension. When bladders were distended in a tank bladders were deformed biaxially, which produced two stress–strain curves (one for each direction). Material parameters cannot be directly extracted from biaxial stress–strain curves because deformation of the material in each direction is dependant on the deformation in the other direction. Therefore the parameters extracted from raw biaxial stress–strain curves would be incomparable.

In order to calculate these parameters from the curves in a way that would allow the samples to be meaningfully compared, a variable was derived which allowed modified stress-strain curves to be plotted. This variable was given the name uniaxial equivalent strain (UE strain). When plotting stress against UE strain, the gradient of the curve is equal to the elastic modulus of the material. This allowed material parameters in each direction to be calculated and used to compare how the bladders mechanically deformed.

### 4.1.2 Aims and objectives

#### Aims

The main aim of this chapter was to determine the mechanical deformation state of bladders during decellularisation, and confirm that application of this state to bladders during decellularisation would result in tissue which was acellular. Another

aim was to find out a way of determining the final size of bladder patch which would be produced from a given initial size of bladder.

**Objectives**

1. To immerse bladders in liquid and distend them to simulate decellularisation conditions. To take measurements at points during distension so the mechanical state of bladders can later be calculated.
2. To compare the deformation mechanics of fresh and frozen bladders.
3. To use the formula for bladder capacity to determine the state of deformation of bladder tissue when filled to this calculated capacity.
4. To decellularise bladders so they are filled to achieve this state of deformation.
5. To measure how bladders deform after decellularisation to determine the size of patch that could be produced from a given size of fresh tissue.

## 4.2 Methods

A summary of experiments is shown in Table 4.1.

| | Experiment | Samples (number) | Outputs |
|---|---|---|---|
| 1 | Immersed distension | Bladders 4.1.a–l (12 from fresh)<br>Bladders 4.1.m–r (6 once-frozen)<br>Bladders 4.1.s–x (6 twice-frozen) | Curves: pressure-volume, strain-volume, $x$–$y$ strain, stress-strain |
| 2 | Finding the deformation state of bladders filled to their (calculated) capacities | Bladders 4.1.a–l (12 from fresh) | Relationships between bladder capacity and pressure, tissue thickness, stress and strain |
| 3 | Investigation of the effect of freezing on bladder tissue | Bladders 4.1.a–l (12 from fresh)<br>Bladders 4.1.m–r (6 once-frozen)<br>Bladders 4.1.s–x (6 twice-frozen) | Calculation of stress–strain parameters from curves, and comparison using ANOVA and Tukey test |
| 4 | Bladder decellularisation with controlled strain, suspended | Bladders 4.4.a–c (3 from fresh) | Gross observation |
| 5 | Bladder decellularisation with controlled strain, immersed | Bladders 4.5.a–c (3 from fresh) | Histology: H&E and DAPI; DNA assay; Contact cytotoxicity assay |
| 6 | Contraction of bladders after decellularisation | Bladders 4.5.a–c (3 from fresh) | Relationship between decellularisation strain and final strain |

**Table 4.1: A summary of the experiments featured in Chapter 4.**

### 4.2.1 Immersed distension

Bladders ($n = 12$) were collected from the abattoir, transported to the lab in transport medium, dissected to remove excess connective tissue and stored in transport medium until use (Sections 2.4.2, 2.4.3 and 2.4.6). On the same day as collection, bladders were tested using immersed distension by the method described in Section 2.8.

A second set of bladders ($n = 12$) was collected from the abattoir, transported to the lab without transport medium and dissected to remove excess connective tissue as above. Bladders were blotted with tissue paper to removed excess moisture, placed in a container containing gauze moistened with phosphate buffered saline (PBS), and frozen at −20 °C. Half of these ($n = 6$) were thawed at room temperature for 4 h and subsequently refrozen at −20 °C ('twice frozen' bladders). The other half were kept frozen during this time ('once-frozen' bladders). All bladders were thawed at room temperature for 4 h and tested by immersed distension by the method described in Section 2.8.

To find the state of mechanical deformation of bladders when filled to capacity, material variables describing the deformation state (pressure, thickness, strain and true stress) were calculated for the first 12 (fresh) bladders. These were calculated for every time point of each bladder using the methods described in Section 2.8.4.2. The capacity of each bladder was calculated using the revised relationship between bladder width, apex-to-ureter length and capacity (Equation 3.2) found in Chapter 3. The material quantities when each bladder was filled to its calculated capacity were found by linear interpolation. A Grubbs' test was performed to find outliers.

Straight line relationships were found between the material variables and bladder volume at the calculated capacities. Statistical analyses were carried out on these straight line relationships: $R^2$ was calculated, and the probability the gradient of each graph was found to be not different from zero was calculated using a two-tailed t-test.

To investigate the effects of freezing on the mechanical properties of bladder tissue, the stress–strain curves of all the bladders were analysed to calculate material parameters. So these parameters could be calculated for biaxial stress–strain data, parameters were found from plotting stresses against the UE strain in the $x$ and $y$ directions. For a material in plane (biaxial) stress, plotting stress against UE strain results in the gradient of the curve being the modulus of the material, as shown in Appendix C. The UE strains are defined in Equation 4.1.

$$\varepsilon_{\mathrm{UE},x} = \frac{\varepsilon_x + \nu\varepsilon_y}{1+\nu^2}, \quad \varepsilon_{\mathrm{UE},y} = \frac{\varepsilon_y + \nu\varepsilon_x}{1+\nu^2} \tag{4.1}$$

The UE strains were calculated for all 24 bladders, and the $x$ and $y$ stresses were plotted against the $x$ and $y$ UE strains respectively. The toe region modulus, linear region modulus, transition stress and transition UE strains of these curves was calculated. In order to discern any differences in mechanical properties between the fresh, once-frozen, and the twice-frozen bladders, two-way ANOVA was used to compare the quantities calculated from the curves. The two factors which were tested were freeze condition (fresh, once-frozen, twice-frozen) and direction ($x$ and $y$). The significance level for the ANOVA was taken as $p < 0.05$. A Tukey HSD (honest significant difference) test was used to compare the differences between means, with a significance level of $p = 0.05$. Significant differences between the $x$ and $y$ directions were ignored (directional differences were expected and were therefore not of interest).

### 4.2.2 Decellularisation with controlled strain

#### Suspended filling

In order to test whether application of bladder wall strains of 2.00 and 1.40 in the $x$ and $y$ directions would lead to successful decellularisation, bladders ($n = 3$) were collected, transported with transport medium and dissected to remove excess tissue by the methods described in Sections 2.4.2, 2.4.3 and 2.4.6. All laboratory work was carried out in a class II safety cabinet. Bladders were then laid flat in a Petri dish and oriented so the dorsal surface was facing upwards (Section 2.4.4). Sutures were tied into the surface of the tissue to act as markers. Sutures were placed in the locations described in Section 2.8.3.1.

Bladders were then decellularised using the method described in Section 2.5 with the following exceptions: 1) at each step of the process a total of 2 L decellularisation solution was used for each bladder; 2) bladders were decellularised in 3 L beakers covered with foil; 3) Benzonase was used to remove the DNA; and 4) bladders were filled when suspended by the neck, as described below.

Each bladder was filled with decellularisation solution by suspending it inside a beaker which was partially filled with approximately 500 ml of decellularisation solution. Bladders were suspended by using a pair of forceps to grip the neck. In order to measure the strain of the bladder wall during filling, a transparent grid was placed on the side of the beaker. This is shown in Figure 4.1. The grid allowed the displacements of the bladder markers to be monitored so that bladder filling could be terminated once the required strains were reached. After bladders were filled, the remaining solution was poured into the beaker.

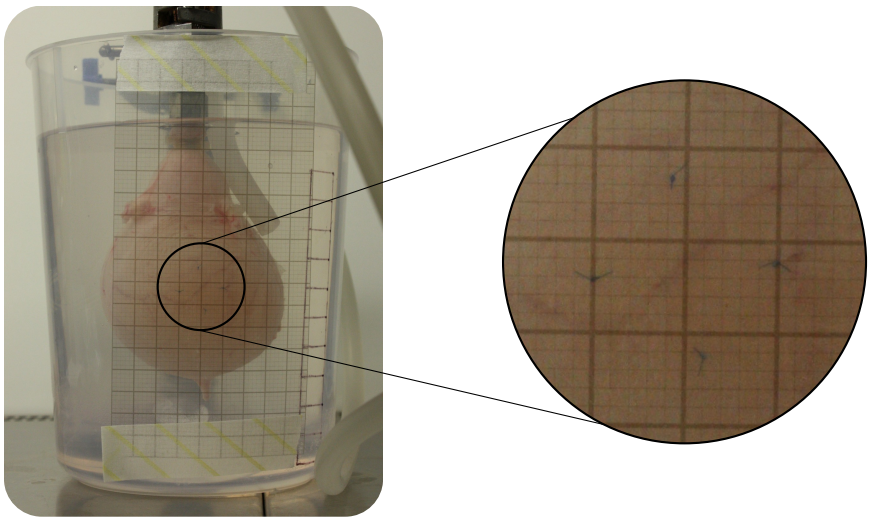

**Figure 4.1: A transparent grid placed on the side of a beaker used to contain bladders during decellularisation.** The grid was used to monitor marker displacement to ensure the required strains were applied to bladder tissue. Blue sutures were used for markers.

### Immersed filling

A second set of bladders ($n = 3$) was collected, transported, dissected and orientated as above. Markers were also placed on bladders as described above. A male pipe fitting was secured to the neck of each bladder using cable ties. Bladders were decellularised using the method described in Section 2.5, except that Benzonase was used to remove the DNA, and bladders were filled when immersed in solution as described below.

During the filling phase, bladders were filled using a method which imitated the way bladders were filled during the immersed distension experiment. In a class II cabinet 2 L decellularisation solution was placed into a 3 L beaker. A retort stand and clamp were used to position a female pipe fitting above the beaker. One end of the tubing was connected to the pipe fitting and the other end was placed in the beaker. The middle of the tubing was brought outside the class II cabinet and placed into a peristaltic pump. A transparent grid was placed on the side of the beaker so the displacement of the bladder markers, and therefore the strain of the tissue, could be monitored during filling (Figure 4.1). Each bladder was connected to the apparatus by connecting the two pipe fittings. The clamp was repositioned so that each bladder became fully immersed in the decellularisation solution. The peristaltic pump was used to pump decellularisation solution from inside the beaker to inside the bladder. Bladders were filled until the strain in both directions were at least the required strain in their respective directions. This setup is shown in

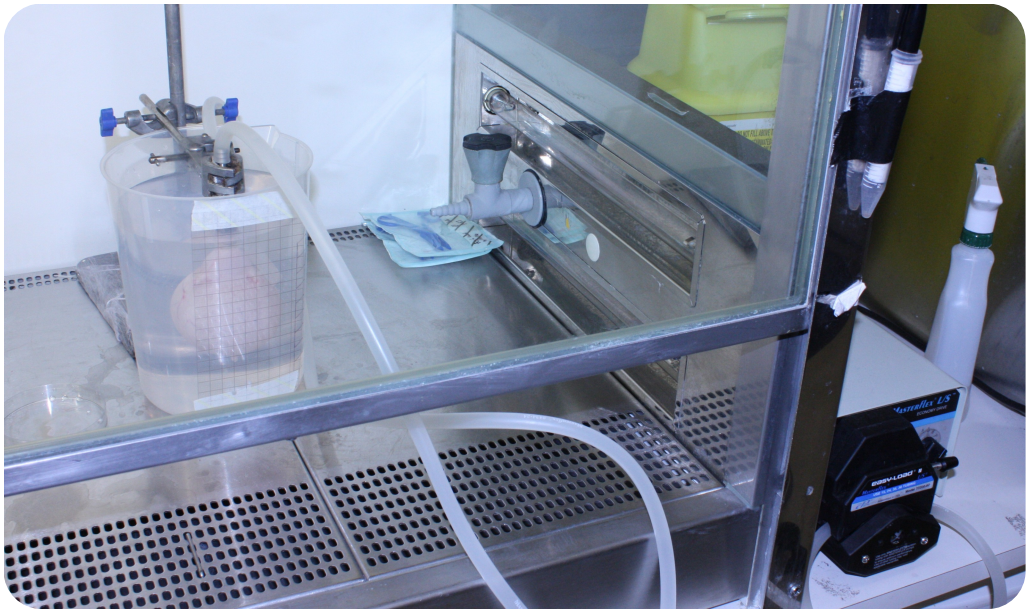

**Figure 4.2: Apparatus used to distend bladders whilst immersed during the fill phase of decellularisation.** The filled beaker can be seen in the top left of the image. The stand and clamp are holding the pipe fitting above the beaker, which is connected to the pipe fitting which the bladder is attached to. The peristaltic pump can be seen in the bottom right of the image, outside the class II cabinet. The tubing is connected to the pipe fitting, travels outside the cabinet, through the pump, back into the cabinet, then into the beaker.

Figure 4.2. At each step of the process, the strain that was applied to bladders was recorded.

#### 4.2.2.1 Contraction of bladders after decellularisation

The hypothesis to be tested was that the strain applied to bladders during the dcell process, $\varepsilon_{\text{dcell}}$, was correlated with the final strain of bladders $\varepsilon_{\text{final}}$. These parameters are defined in Equations 4.2 and 4.3, where the initial, decellularised and final dimensions are the distances between the markers before decellularisation, during decellularisation and after decellularisation, in either the $x$ or $y$ directions.

$$\varepsilon_{\text{dcell}} = \frac{\text{decellularised dimensions - initial dimensions}}{\text{initial dimensions}} \tag{4.2}$$

$$\varepsilon_{\text{final}} = \frac{\text{final dimensions - initial dimensions}}{\text{initial dimensions}} \tag{4.3}$$

For the bladders decellularised with controlled strain using immersed filling, during decellularisation the strain applied to bladders during each stage of the process was

recorded to a precision of $\pm 1\,\mathrm{mm}$ using the grid on the beaker. The mean of these values was calculated for each bladder in each direction.

Images were taken of the bladders before decellularisation (day 1), after decellularisation (day 8), and for three subsequent weeks (days 16, 23 and 30). Bladders were laid flat in a petri dish, placed on graph paper, and photographed. The distance between the markers in the $x$ and $y$ directions was measured using ImageJ, and calibrated using the graph paper. The mean of the final dimensions (post-decellularisation) was calculated for each bladder in each direction to a precision of $\pm 0.2\,\mathrm{mm}$.

A graph was plotted of final strain against decellularisation strain. Linear regression was performed to find a relationship between the two so that final strain could be predicted from the decellularisation strain. The $R^2$ value for this line was calculated.

## 4.3 Results

### 4.3.1 Immersed distension

#### 4.3.1.1 Raw data obtained during immersed distension

The mass and tissue volume of bladders was recorded before testing. This data is shown in Figure 4.3. The high $R^2$ value indicated a very strong relationship between mass and tissue volume. The line of regression passed close to the origin, but not through it. The coefficient of the predictor variable in the regression line equation represented a specific mass of bladder tissue of $1010\,\mathrm{m^3 \cdot kg^{-1}}$, equivalent to a density of $990\,\mathrm{kg \cdot m^{-3}}$.

The majority (11/12) of the fresh bladders failed by bursting, and only one failed by excessive leakage. Of the six once-frozen bladders, 3 failed by bursting, 2 failed by excessive leakage, and 1 failed because the pressure rose above the acceptable limit. Of the six twice-frozen bladders, 2 failed by bursting, 1 failed by excessive leakage, and 3 failed due to excessive pressure.

The raw pressure and volume data for the fresh, once-frozen and twice-frozen bladders is shown in Figure 4.4. The majority of fresh bladders showed an initial pressure rise, followed by a period of low-pressure filling, and finally a steep rise in pressure as the bladders approached their maximum capacity. Two of the once-frozen bladders also followed that mode of deformation, however three once-frozen bladders exhib-

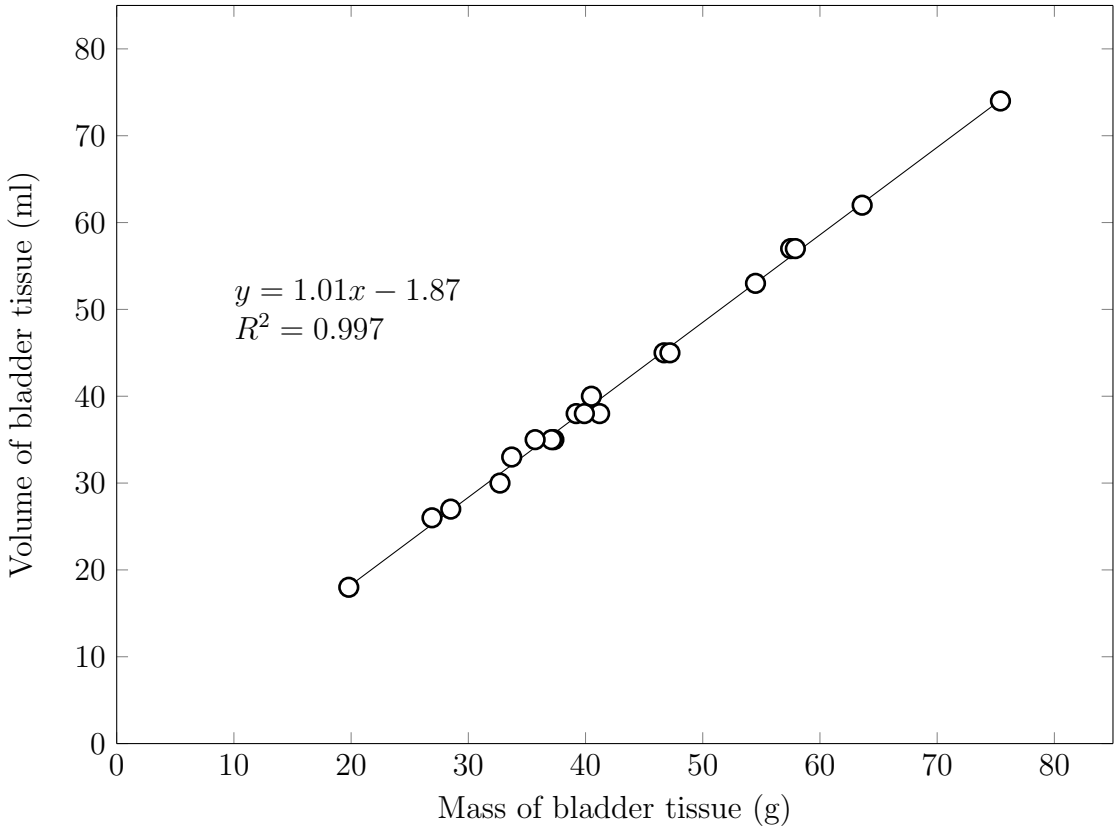


**Figure 4.3: A graph of tissue volume plotted against tissue mass.** Each point represents a single bladder. Error bars representing the measurement errors of each variable are contained within the footprint of each point.

ited steep rises in pressure which continued to rise until failure, with only slight stiffness changes over this period. One once-frozen bladder had a curve which was between these two types of deformation. Most of the twice-frozen bladders (5/6) had steep near-linear pressure-volume curves, often with a definite gradient change at a single point. One twice-frozen bladder demonstrated a consistent moderate stiffness with a slight dip in stiffness in the centre of the curve.

The relationships between filled volume and wall strain for all tested bladders are show in Figure 4.5. The strain initially rose quickly with a small volume increase, but as the bladders filled the gradients gradually decreased. Fresh, once-frozen and twice-frozen bladders all demonstrated this response, However there appeared to be less variation between samples for the twice-frozen bladders.

The strain of the bladders in each direction were not equal during distension. The relationship between $x$ strain and $y$ strain for each fresh, once-frozen and twice-frozen bladder is shown in Figure 4.6. Most fresh bladders (11/12) demonstrated greater strain in the $x$ direction than in the $y$ direction and all plots were approximately linear. Once-frozen bladders also exhibited this response, with a comparable variation between samples to that observed with fresh bladders. Twice-frozen bladders followed the same response, however all samples appeared to be closer to the $y = x$ line, with one sample demonstrating greater strain in the $y$ direction than in the $x$ direction.

The stress–strain curves of fresh, once-frozen and twice-frozen bladders are shown in Figure 4.7. These curves showed an initial phase of low-stress elongation (the toe region), followed by a transition into a phase of steep rise in stress (the linear region). Many of the fresh bladder curves demonstrated this behaviour very well. The once-frozen bladders showed less of a distinction between these two phases, and the twice-frozen bladders even less so. For the majority of bladders, the stress–strain curve was higher in the $y$ direction compared to the $x$ direction, and also rose to a greater magnitude in the $y$ direction. There appeared to be less of a difference between the $x$ and $y$ curves the more times the bladders had been frozen, although there was much variability between the bladder samples.

#### 4.3.1.2 Material variables of bladders when filled to capacity

Various material variables were calculated at the calculated capacity of each fresh bladder. These variables (pressure, thickness, stress and strain) described the deformation state of bladders. The plots of these variables against bladder capacity are shown in Figure 4.8. The relationship between pressure and capacity (Figure 4.8a)

**(a)** Fresh bladders.

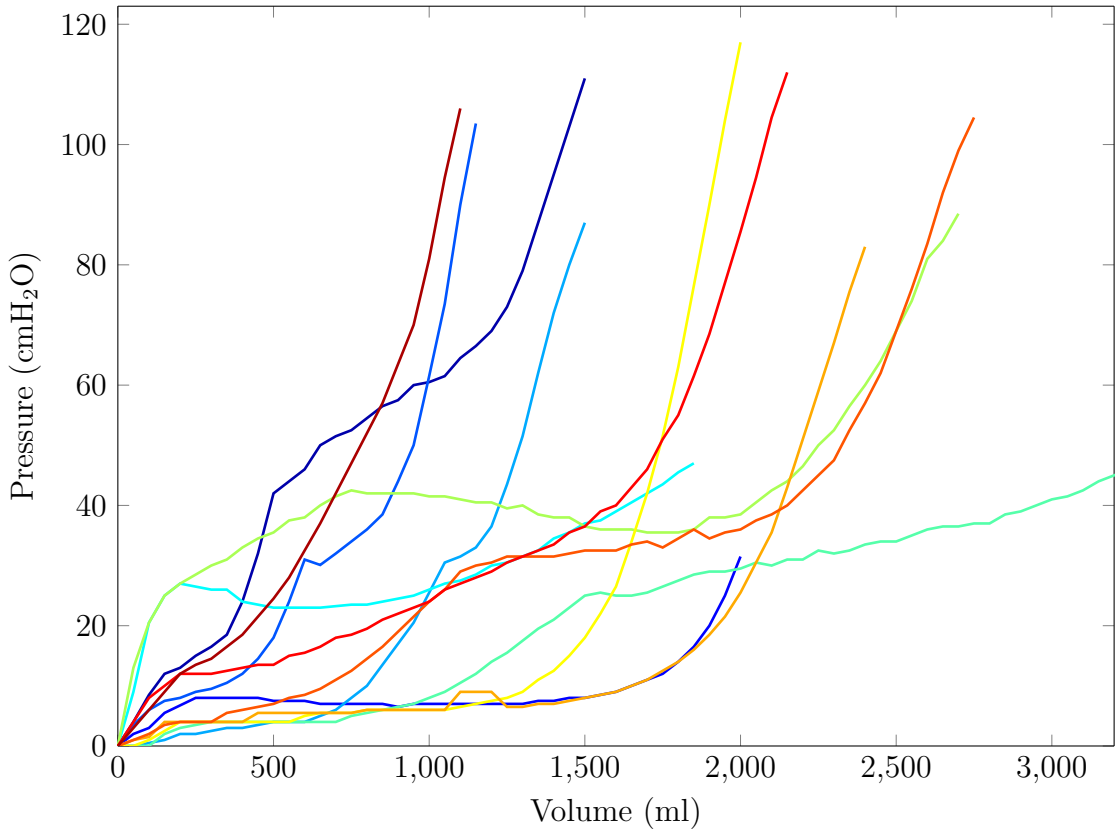


**Figure 4.4: Pressure–volume curves of bladders tested by immersed distension.** Each colour represents a single bladder.

**(b)** Once-frozen bladders.

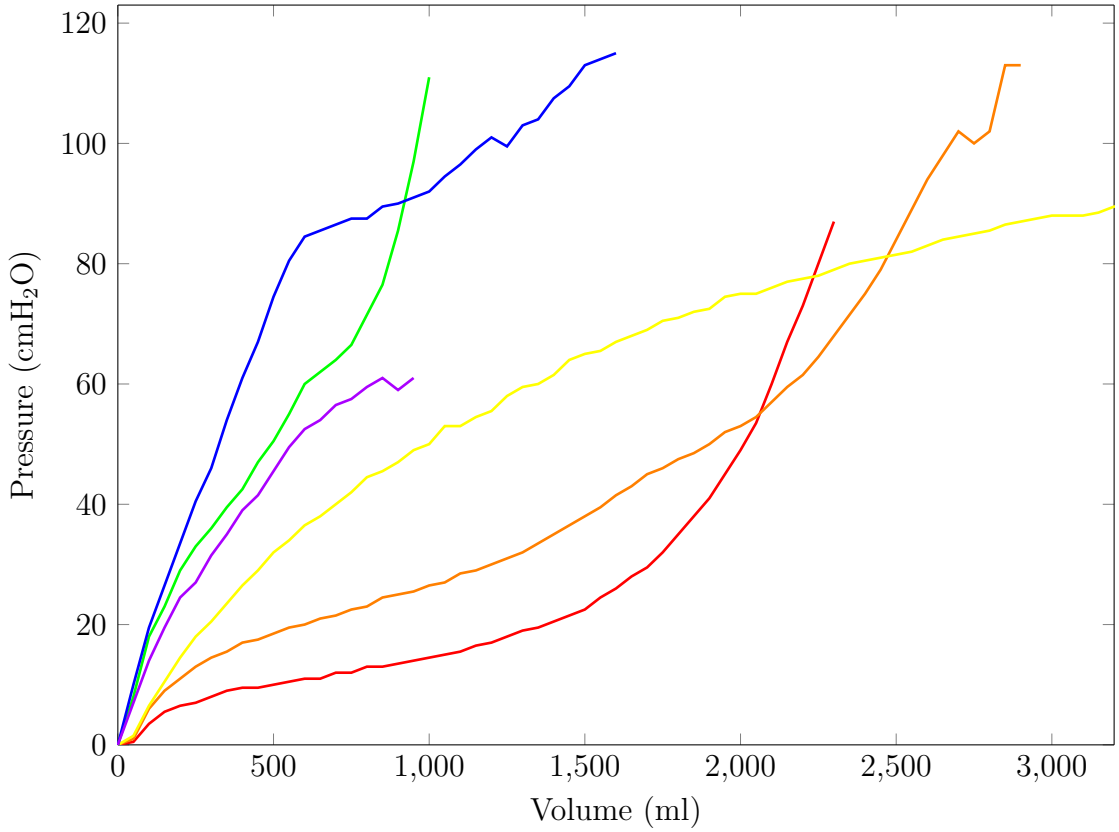


**(c)** Twice-frozen bladders.

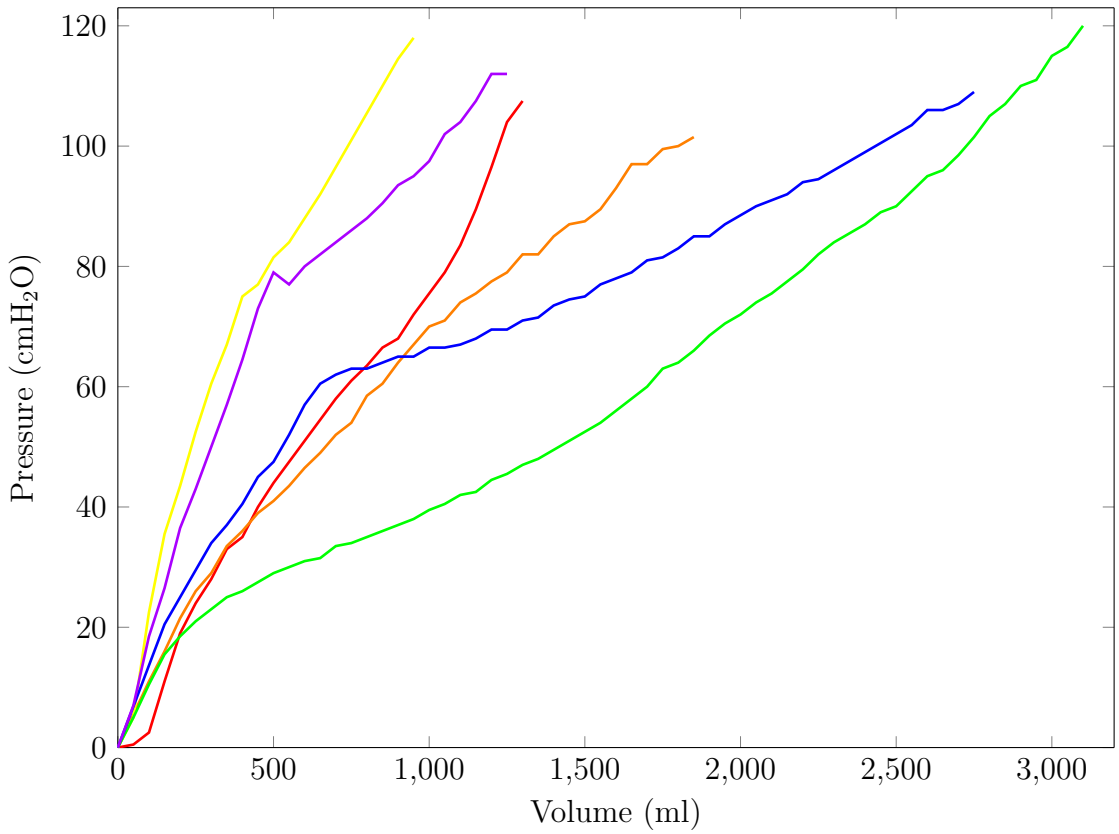


**Figure 4.4: Pressure–volume curves of bladders tested by immersed distension.** Each colour represents a single bladder.

**(a)** Fresh bladders.

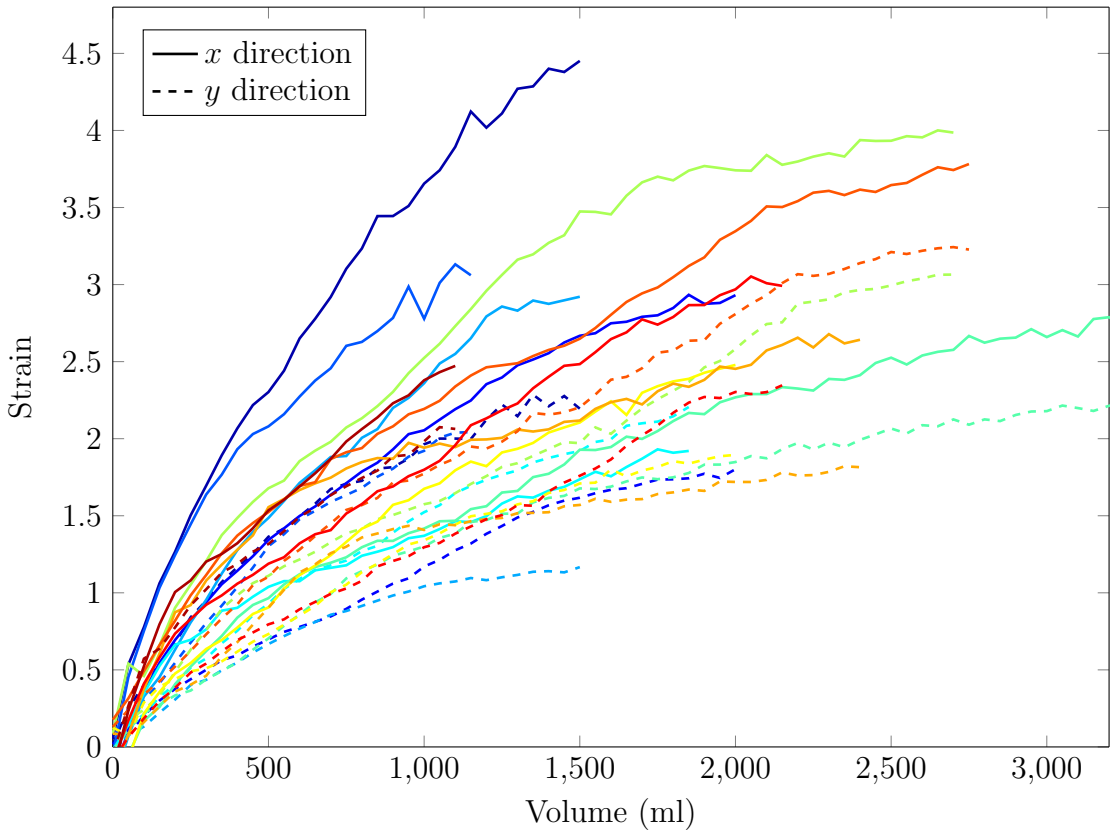


**Figure 4.5: Strain–volume curves of bladders tested by immersed distension.** Each colour represents a single bladder.

**(b)** Once-frozen bladders.

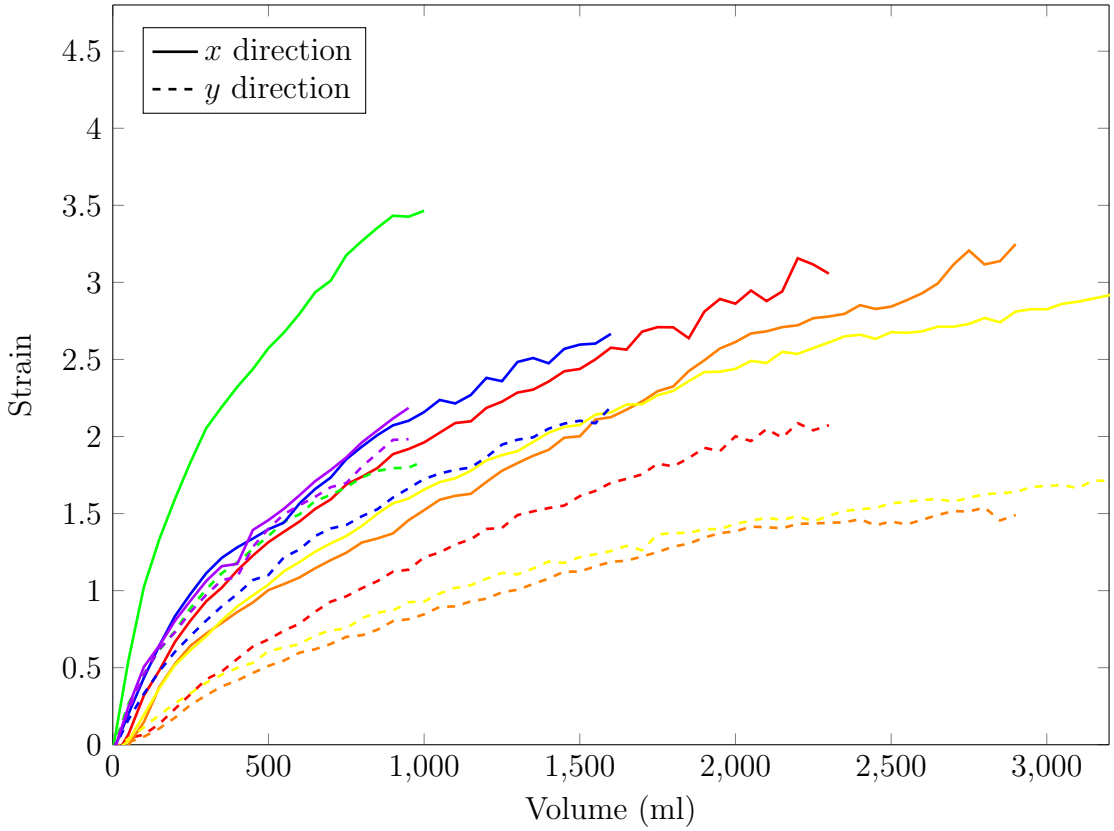


**(c)** Twice-frozen bladders.

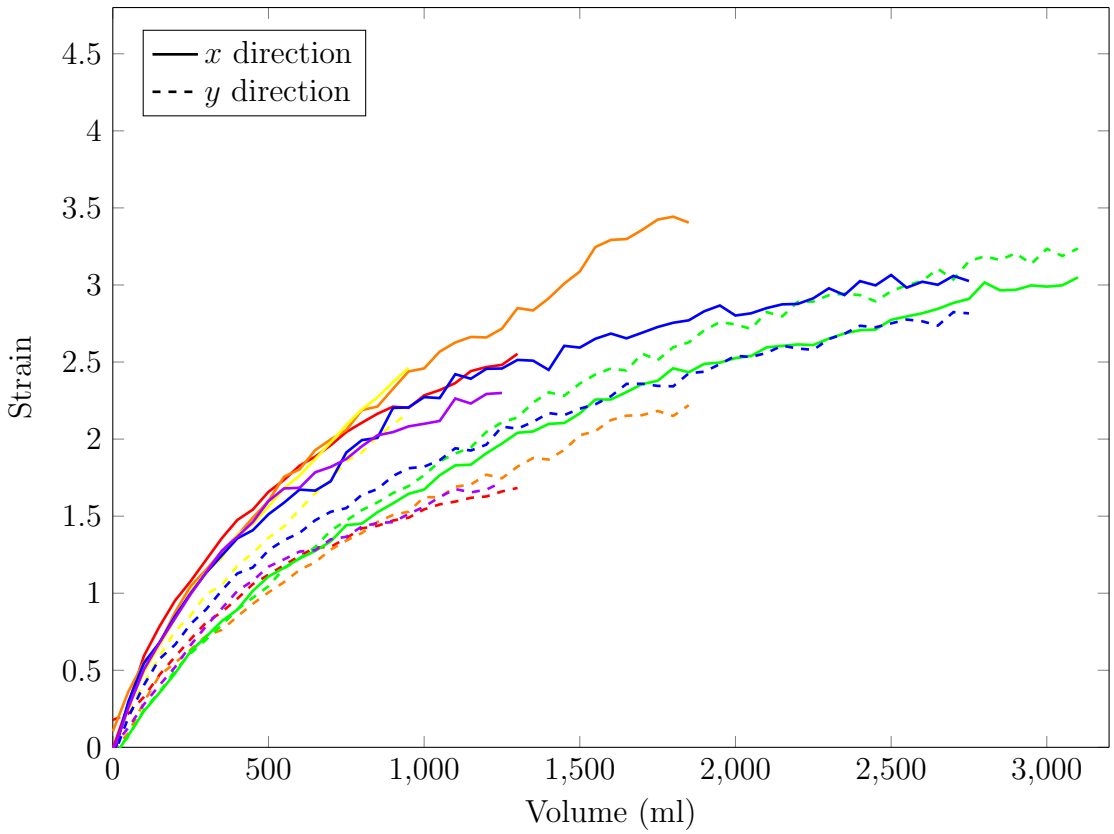


**Figure 4.5: Strain–volume curves of bladders tested by immersed distension.** Each colour represents a single bladder.

**(a)** Fresh bladders.

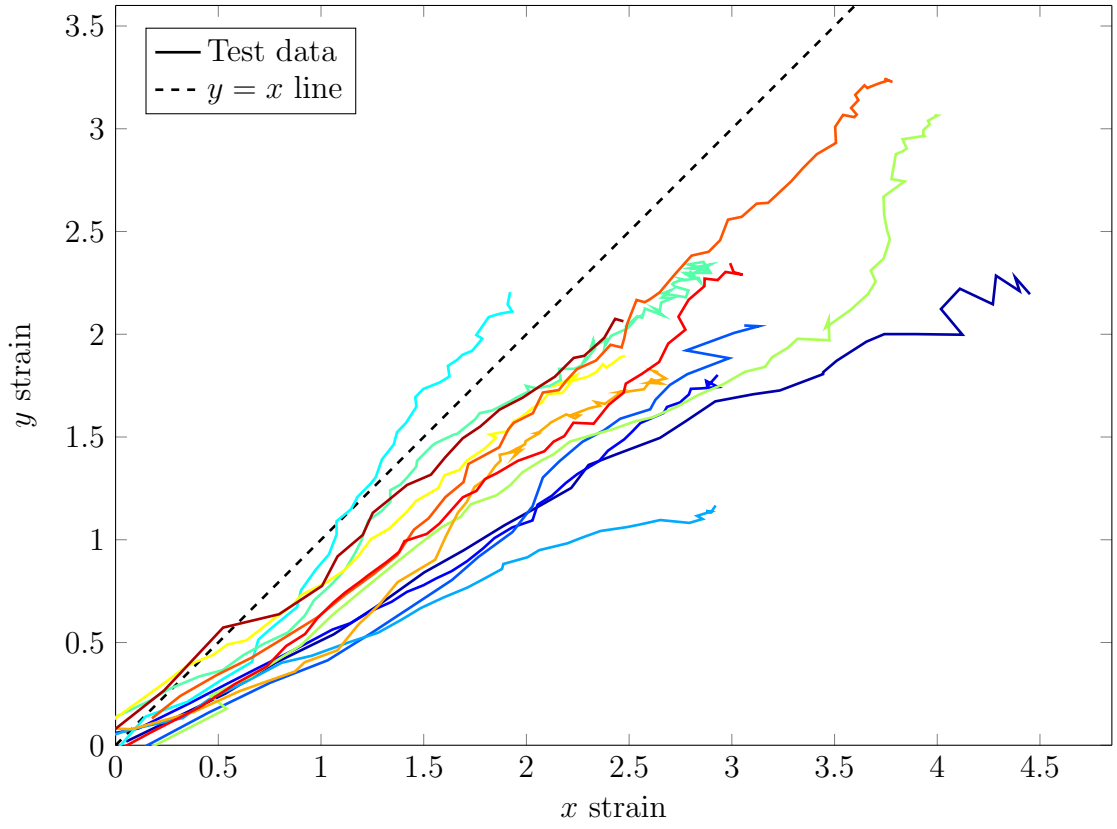


**Figure 4.6: Curves of $y$ strain plotted against $x$ strain of bladders tested by immersed distension.** Each colour represents a single bladder. The $y = x$ line represents a curve of equibiaxial strain.

**(b)** Once-frozen bladders.

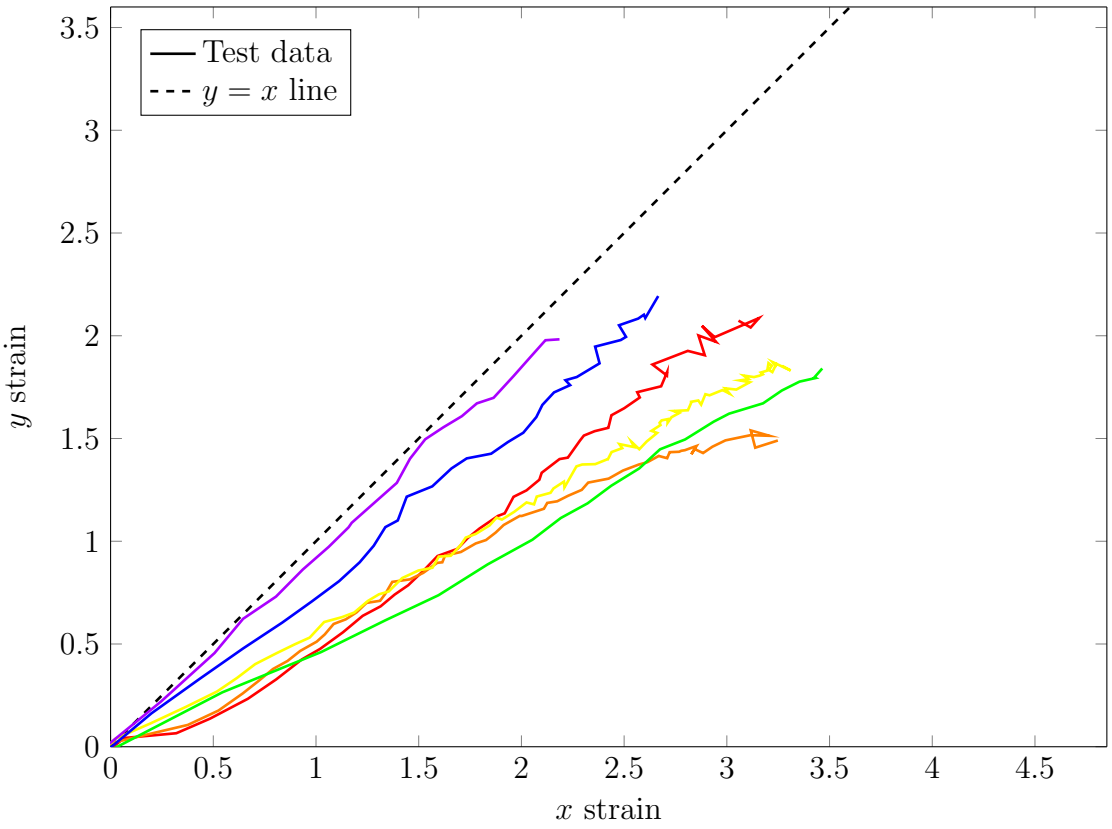


**(c)** Twice-frozen bladders.

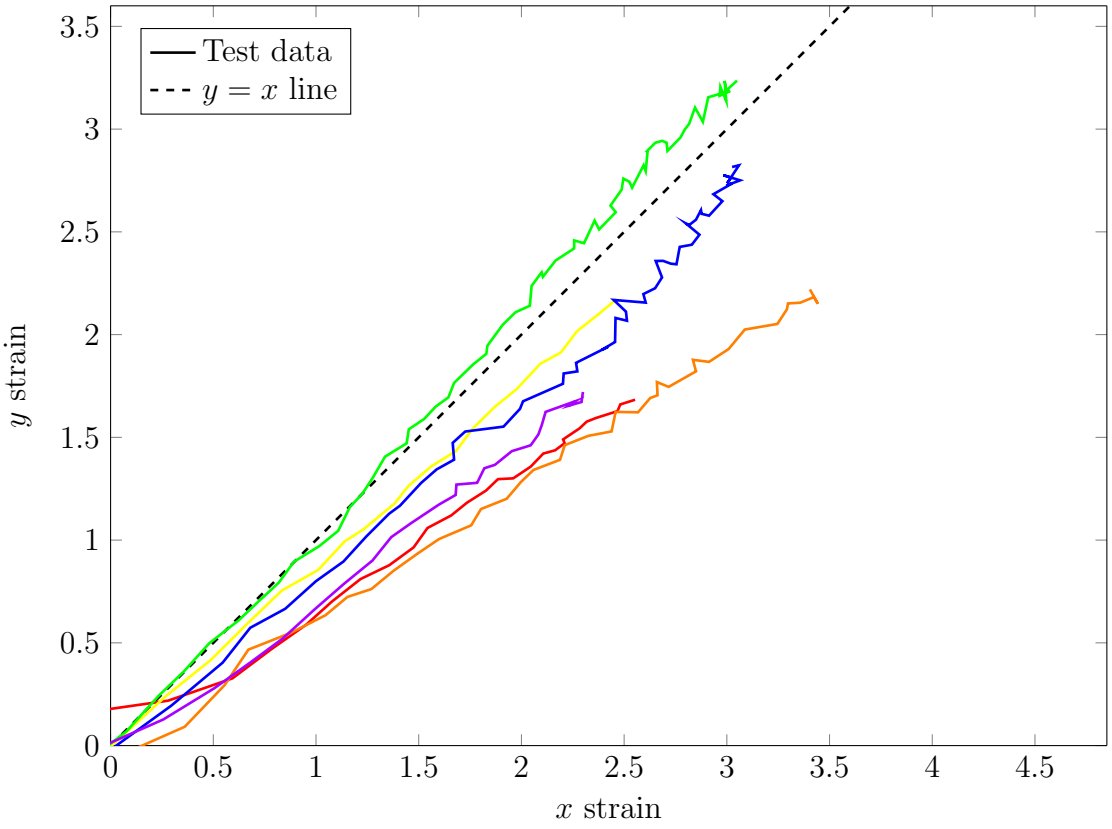


**Figure 4.6: Curves of $y$ strain plotted against $x$ strain of bladders tested by immersed distension.** Each colour represents a single bladder. The $y = x$ line represents a curve of equibiaxial strain.

**(a)** Fresh bladders.

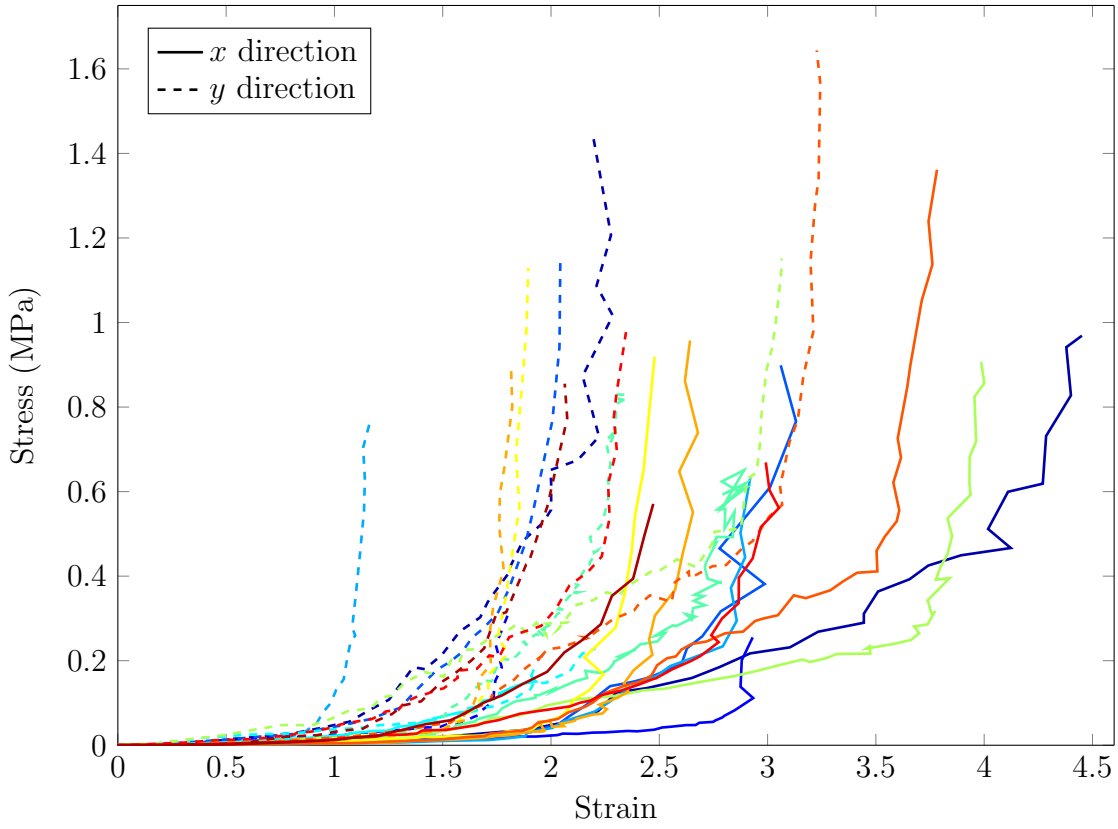


**(b)** Once-frozen bladders.

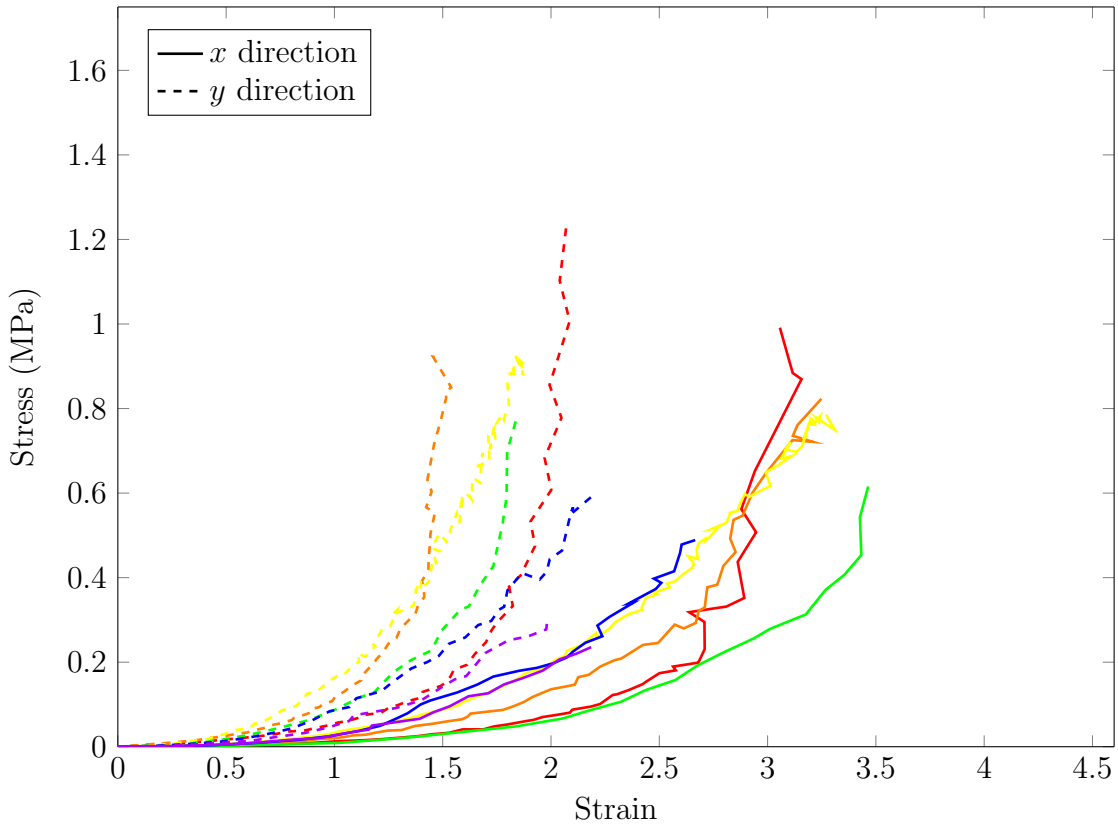


**Figure 4.7: Stress–strain curves of bladders tested by immersed distension.** Each colour represents a single bladder.

**(c)** Twice-frozen bladders.

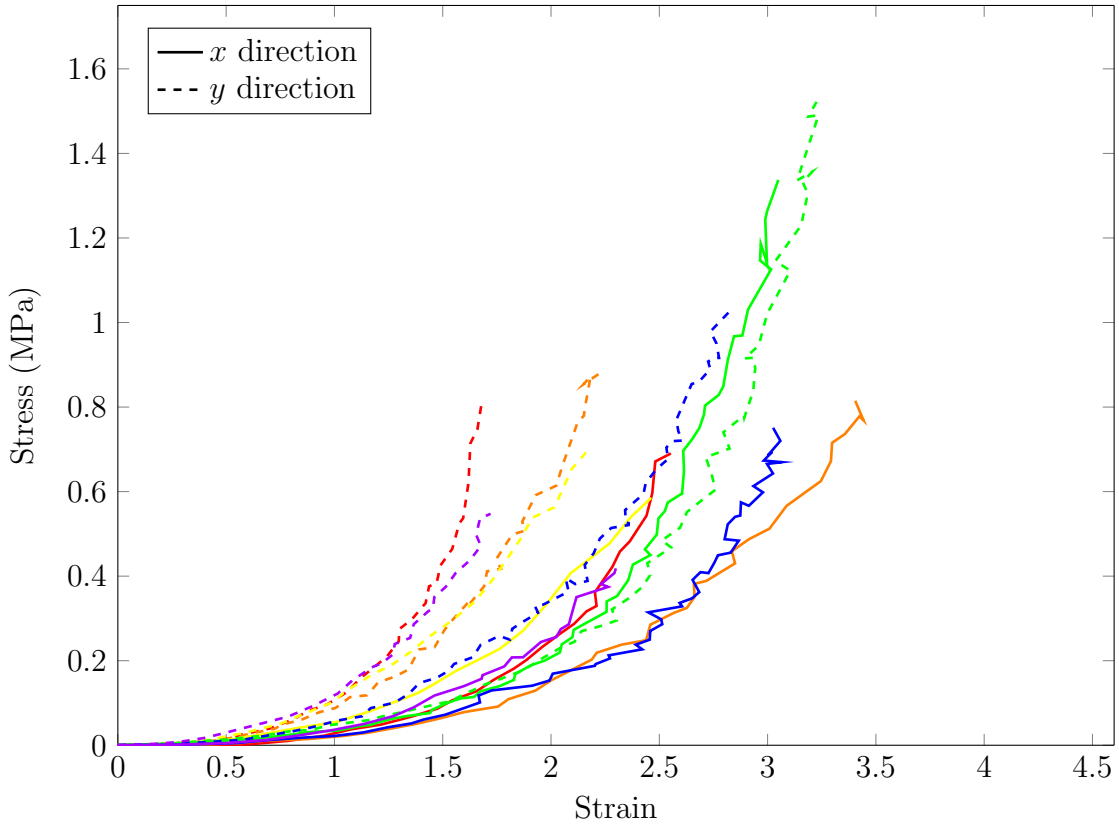


**(d)** Average curves for fresh, once-frozen and twice-frozen bladders.

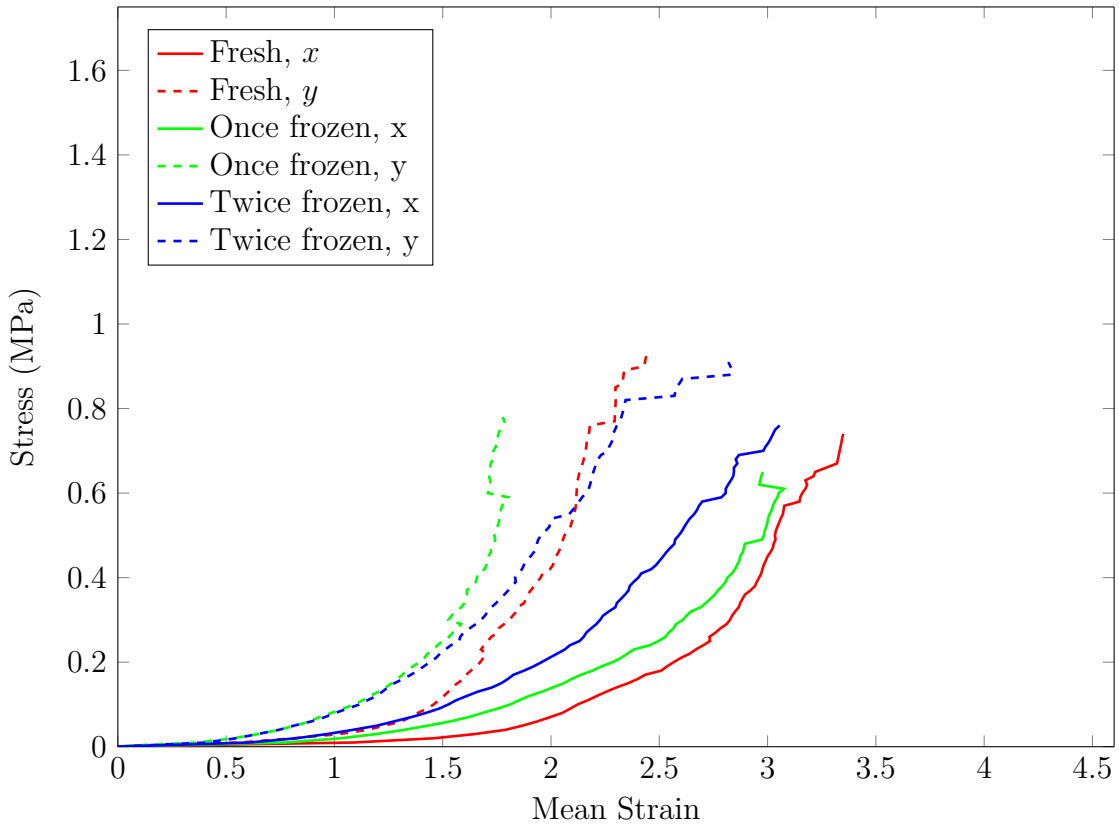


**Figure 4.7: Stress–strain curves of bladders tested by immersed distension.** Each colour represents a single bladder.

showed a negative correlation between pressure and capacity. The gradient $p$ value of 0.014 showed that there was a relationship between the two variables, and the $R^2$ value of 0.470 indicated that this relationship was moderate in strength. The relationship between tissue thickness and capacity is shown in Figure 4.8b. Sequential application of the Grubb's test discovered two outliers. The $p$ value of 0.631 gave confidence that the thickness of the bladder tissue was invariant with change in bladder capacity. The mean of the bladder thickness was 0.617 mm. The relationship between stress and capacity is shown in Figure 4.8c. The $p$ values of 0.073 and 0.052 in the $x$ and $y$ directions respectively indicated that there may have been relationships between stress and capacity, however the $R^2$ values of 0.286 and 0.327 demonstrated that these relationships were weak. The relationship between strain and capacity is shown in Figure 4.8d. The $p$ values of 0.331 and 0.667 in the $x$ and $y$ direction respectively gave confidence that the strain of the bladder tissue was invariant with change in bladder capacity. The means of these strains in the $x$ and $y$ directions were 2.00 and 1.40 respectively.

#### 4.3.1.3 Comparing the mechanical properties of fresh, once-frozen and twice-frozen bladders

The stress–UE strain curves of the bladders were analysed to calculate the material parameters of the bladders. The toe region modulus, linear region modulus, transition stress and transition strain of these curves were calculated in the $x$ and $y$ directions Two-way ANOVA was used to analyse this data. The results are shown in Table 4.2.

These $p$ values showed that freezing did not result in a significant change to the toe region modulus or the transition stress, but freezing did significantly effect the linear region modulus and the transition UE strain ($p < 0.01$). There was a significant difference ($p < 0.05$) between the means of the linear phase slope in the two directions. Differences in the directions were expected since the material was anisotropic.

Plots of the material properties of the fresh, once-frozen and twice-frozen bladders are presented in Figure 4.9. There were significant differences between the means for the linear region modulus and the transition strain (Tukey HSD test). In both cases, the means of the fresh samples were significantly higher than the means of the frozen samples ($p < 0.05$). There were no significant differences between the once-frozen and twice-frozen bladders.

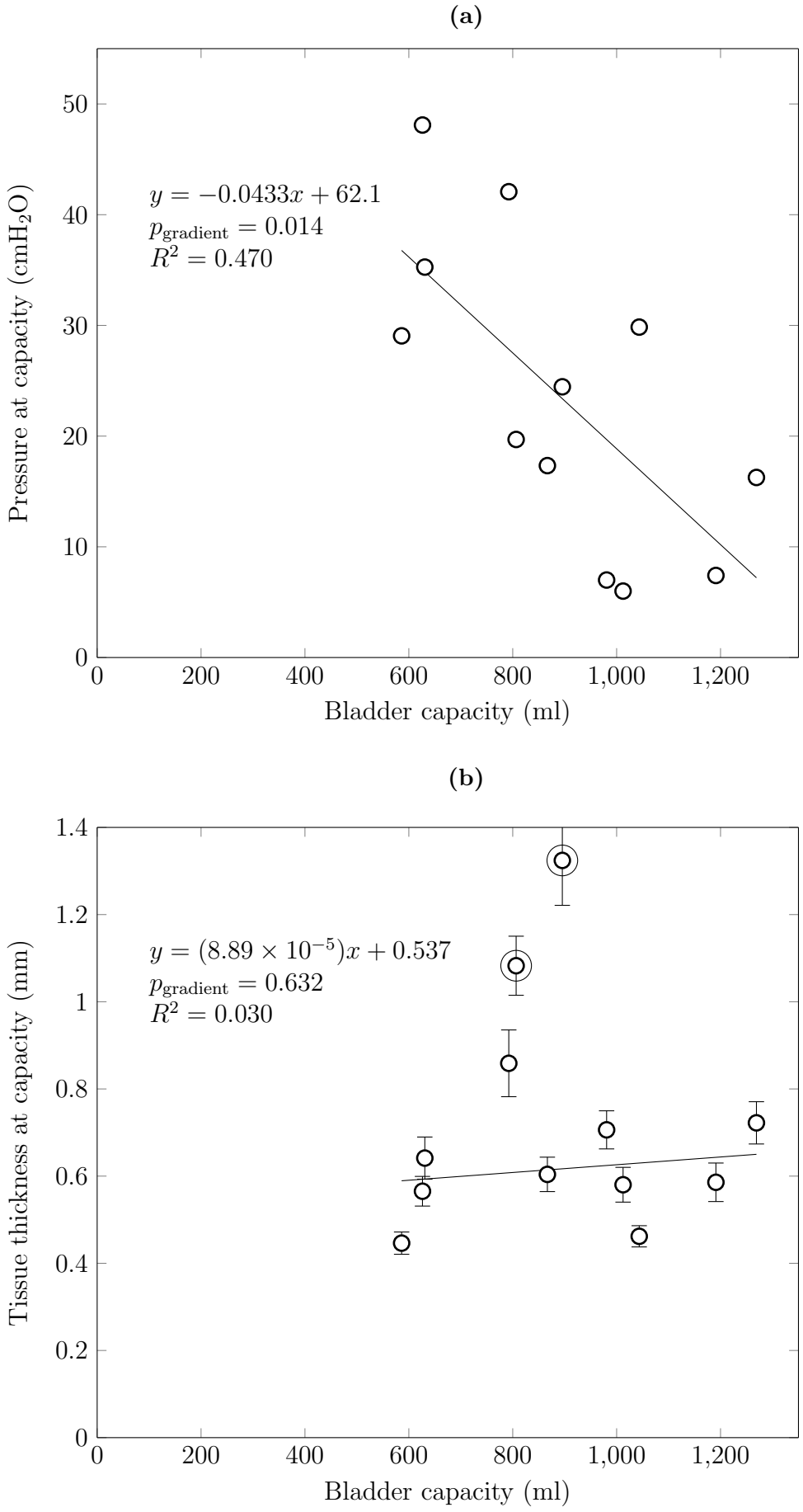


**Figure 4.8: Material variables of fresh bladders filled to their calculated capacities.** Each point represents a single bladder. Measurement errors are shown.

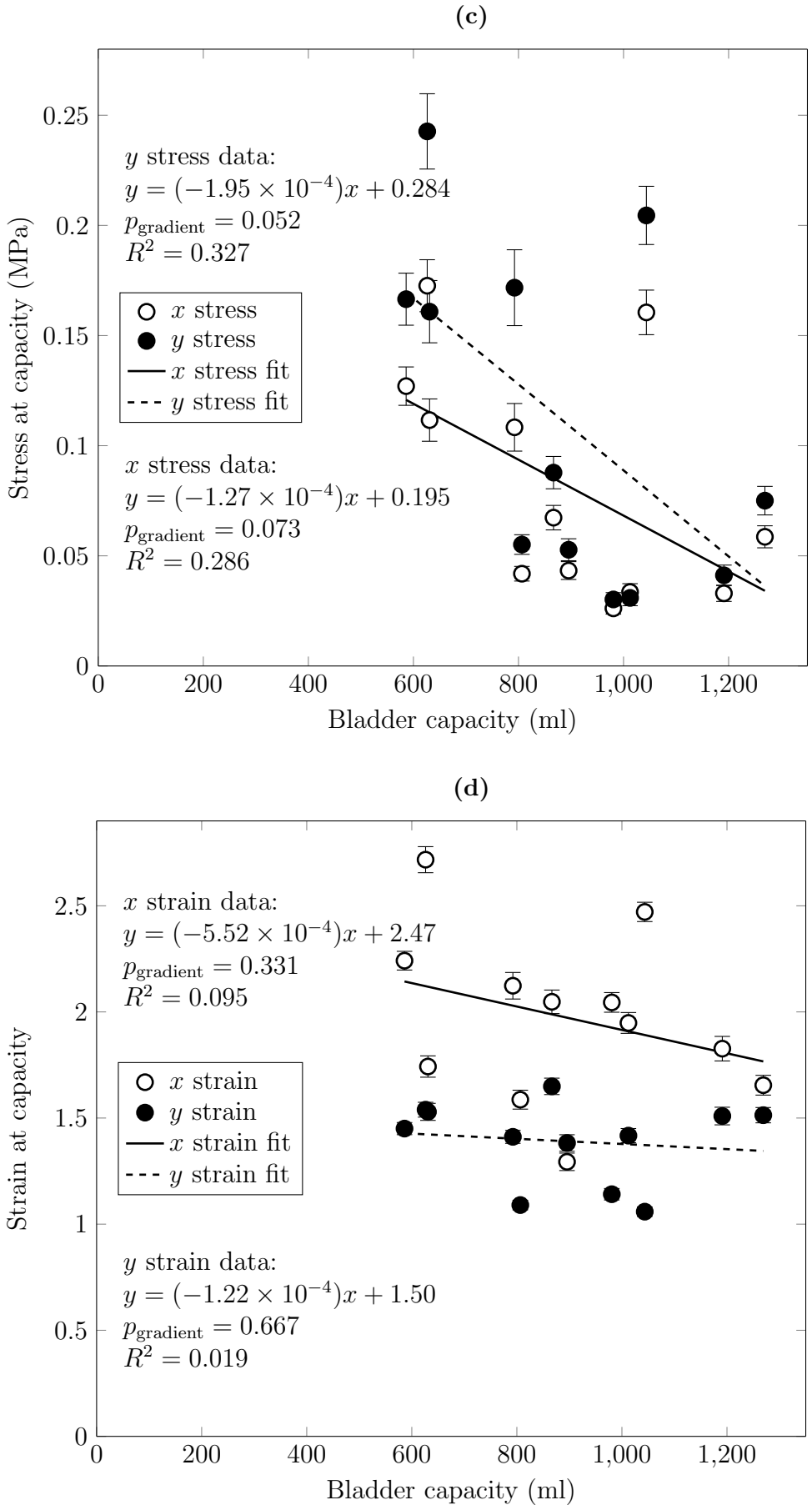


**Figure 4.8: Material variables of fresh bladders filled to their calculated capacities.** Each point represents a single bladder. Measurement errors are shown.

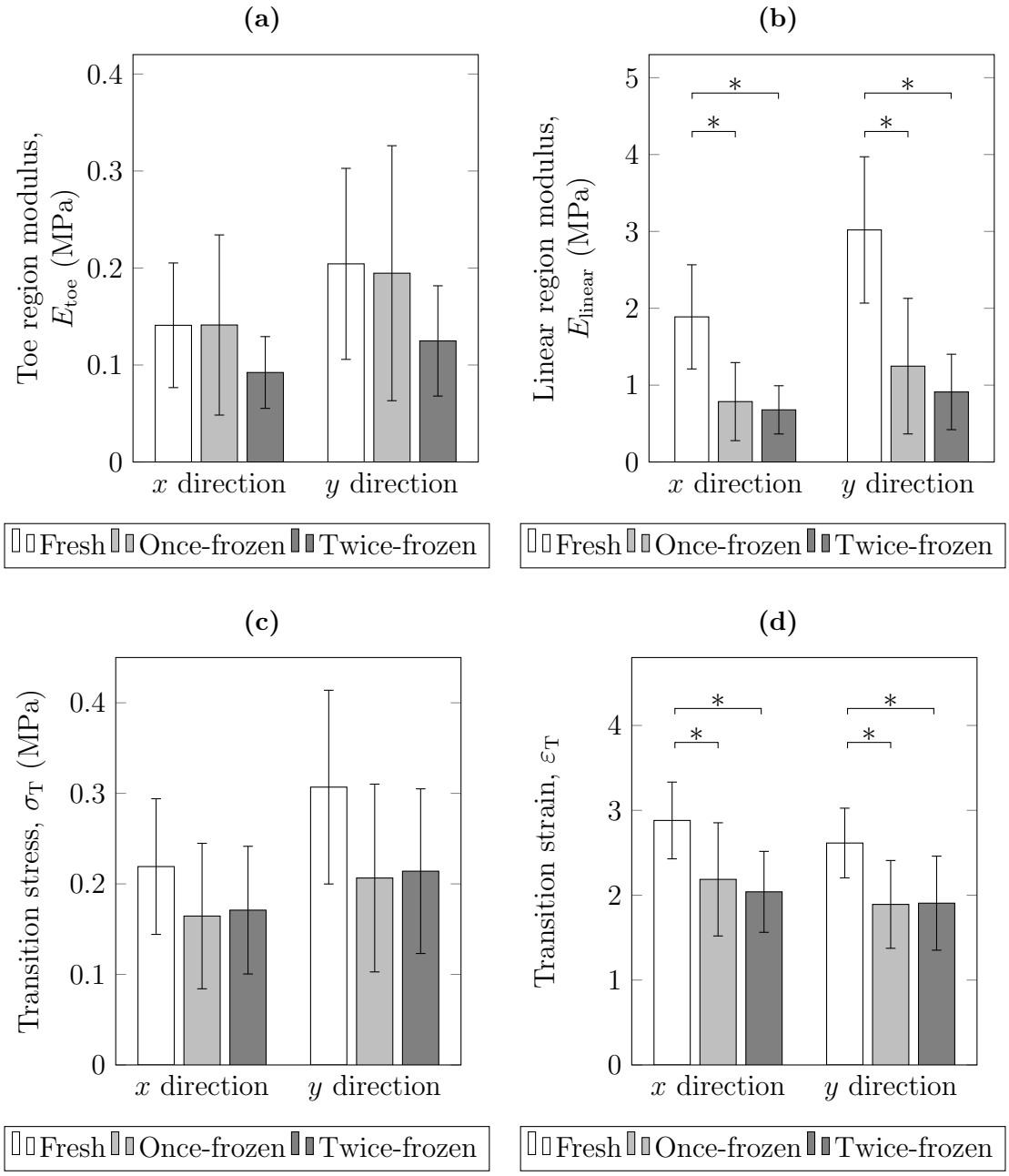


**Figure 4.9: A comparison of stress–UE strain curve parameters of fresh, once-frozen and twice-frozen bladders.** Bars represent the means of the parameters, and error bars represent the 95 % confidence intervals. The differences between the means for each parameter were compared using a Tukey test, ignoring significant differences between the two directions. Significant differences between means are indicated with *.

| | $p$ value | |
|---|---|---|
| Mechanical property | Freeze condition | Direction |
| $E_{\text{toe}}$ | 0.234 | 0.097 |
| $E_{\text{linear}}$ | ***0.000 | *0.015 |
| $\sigma_{\text{T}}$ | 0.104 | 0.062 |
| $\varepsilon_{\text{T}}$ | ***0.001 | 0.173 |

**Table 4.2: Comparison of the means of bladder material properties as affected by freezing condition and direction.** Data for each parameter was analysed by 2-way ANOVA with freeze condition and direction as the two factors. Significant results are marked with *.

### 4.3.2 Bladder decellularisation with controlled strain

The hypothesis to be tested here was that the strains found in the bladder walls when filled to capacity were the strains bladders need to be stretched to in order to be successfully decellularised.

#### 4.3.2.1 Suspended filling

In order to find out whether the strains in the bladder wall when filled to the calculated capacity were sufficiently large to ensure successful decellularisation, bladders were decellularised by controlling the strain in the bladder walls. Sutures were placed in the walls and the bladders were distended until the stretch in the walls reached at least 2.00 and 1.40 in the $x$ and $y$ directions. During the initial decellularisation process, bladders were filled by holding them using forceps and filling them with either a syringe or funnel until the required strains were reached. For the revised process, bladders were filled using a stand and clamp to hold them inside a beaker filled with decellularisation solution. A peristaltic pump was used to fill the bladders until the required strains were reached.

Bladders filled using the suspended method did not stretch in the ratio of 2.00 : 1.40 in the $x$ and $y$ directions. The strain in the $y$ direction was greater than the strain in the $x$ direction for all bladders filled during decellularisation.

#### 4.3.2.2 Immersed filling

Three bladders were decellularised by immersing them in decellularisation solutions and using a peristaltic pump to fill them. The equipment setup allowed the bladders

| | Dimensions (mm) | | Strains | |
|---|---|---|---|---|
| Bladder | $x$ | $y$ | $x$ | $y$ |
| 1 | 30 | 28 | 2.0 | 1.8 |
| 2 | 30 | 37 | 2.0 | 2.7 |
| 3 | 36 | 24 | 2.6 | 1.4 |

**Table 4.3: The mean deformation of the bladder markers when bladders were decellularised by immersed filling.** The distance between the markers in each direction was recorded at each stage of the process for each bladder. The mean of these values for each bladder is shown. The initial distance between each pair of markers was 10 mm .

to be filled in a controlled manner until the required strains were applied to the bladder wall tissue. Markers were placed on the bladders in the form of sutures. The initial distance between each pair of markers was 10 mm. During filling, bladders were stretched so the distance between markers in the $x$ direction was 30 mm and the distance between markers in the $y$ direction was 24 mm. These displacements corresponded to strains of 2.0 and 1.4 in the $x$ and $y$ directions respectively.

When bladders were immersed and distended using the peristaltic pump, the ratios of the $x$ strain to $y$ strain in the tissue (as indicated by the markers) were not equal to exactly $2.0 : 1.4$. That is, if the $x$ strain of the tissue was increased to 2.0, the $y$ strain was either less than or greater than 1.4, depending on the particular bladder. To overcome this problem, bladders were stretched until the strains had reached a minimum of 2.0 in the $x$ direction and a minimum of 1.4 in the $y$ direction. This condition resulted in the strain in one direction reaching the required values, and the strain in the other direction exceeding the required value. The strain applied to the bladders was recorded at each step of the decellularisation process. The mean strains which were applied to bladders during the process are shown in Table 4.3.

### Histology

Samples were taken from bladders decellularised using the immersed filling methods using controlled strain, and stained with either haematoxylin and eosin (H&E) or DAPI. Sections stained with H&E are shown in Figure 4.10.

Decellularised matrices were devoid of a urothelium and no cell fragments could be seen in the other tissue layers. The overall tissue histoarchitecture was maintained. Sections stained with DAPI are shown in Figure 4.11. These images showed complete

| | DNA content per dry weight ($ng \cdot mg^{-1}$) | | | |
|---|---|---|---|---|
| | Samples | | | Mean ± 95 % CI |
| Fresh controls | 3880 | 4100 | 3950 | $3970 \pm 272$ |
| Decellularised | 0.0* | 31.5 | 16.9 | $16.1 \pm 39.2$ |

*Not detectable.

**Table 4.4: The DNA content of samples taken from bladders decellularised using the strain-controlled method.** Means and confidence intervals were calculated from $n = 3$ bladder samples. The DNA content of one decellularised sample was too low to be detected.

absence of cell nuclei.

### DNA Assay

A DNA extraction and quantification assay was performed on samples taken from fresh and decellularised bladders. Samples from decellularised bladders had a mean DNA content per dry weight of of $14.5\,ng \cdot mg^{-1}$. The DNA content of bladders decellularised by each method was reduced by 99.6 % relative to the native controls. The data from the DNA assay are shown in Table 4.4.

### Contact cytotoxicity assay

Residual tissue cytotoxicity was determined by incubating decellularised tissue samples with either BHK cells (Figure 4.12) or L929 cells (Figure 4.13) for 48 h. The cell-only control wells contained a high density of cells which had adhered well to the substrate, and were normal in appearance. Cells in the collagen gel control wells were slightly less confluent than those in the cell-only control wells, and were more rounded in appearance with fewer projections. The regions of the wells around the drops of cyanoacrylate glue were sparsely populated with cells. The cells which were present in these regions had a rounded and shrunken morphology. The growth of cells did not appear to be significantly inhibited by the presence of decellularised tissue samples in the wells. Regions adjacent to tissue samples were populated with cells. Cell behaviour was similar to that observed with the collagen gel only control group. Cells were comparable in density to the collagen gel control samples and had a normal morphology and cytoplasmic projections.

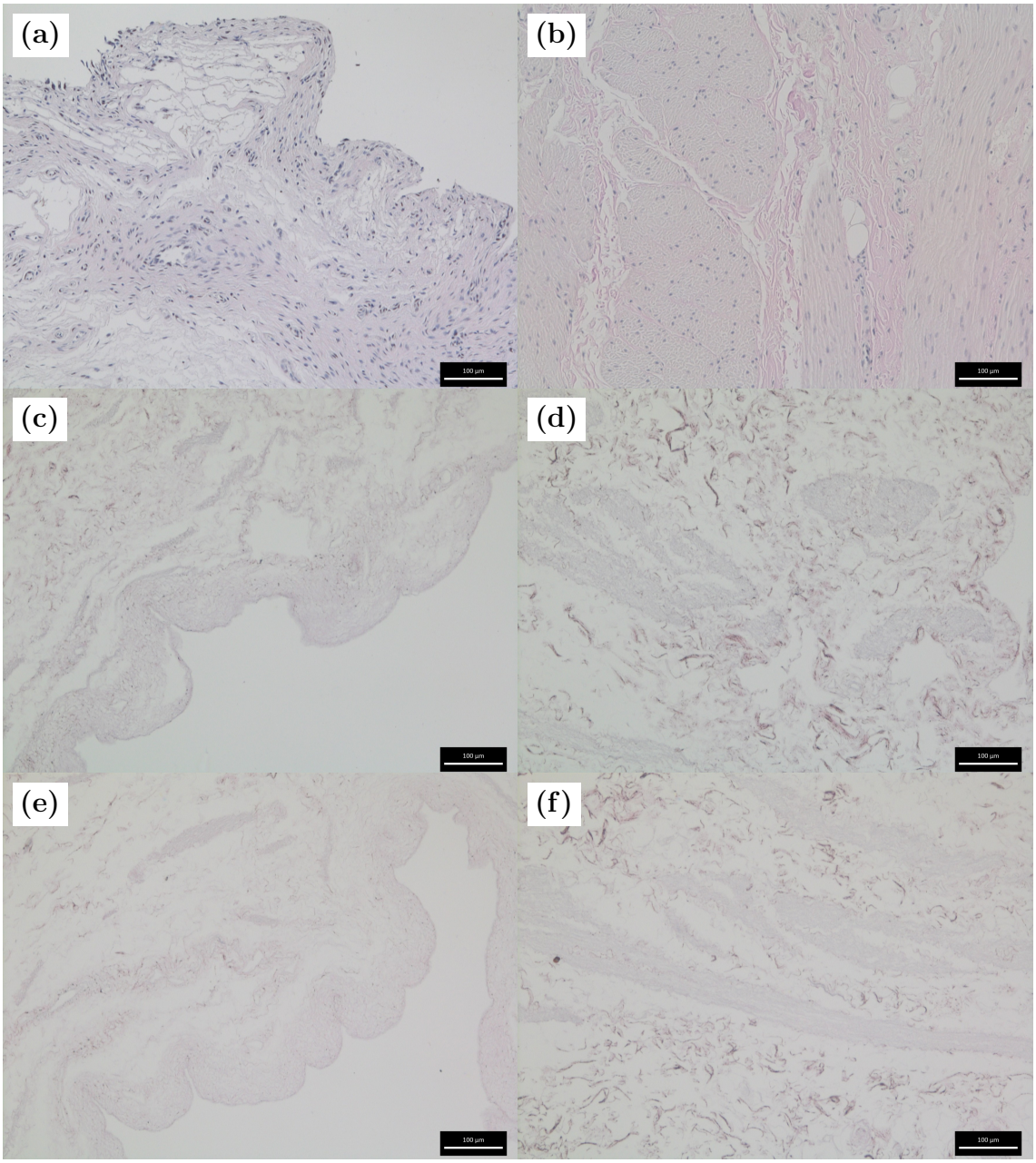


**Figure 4.10: Images of H&E stained section from bladders decellularised using the controlled strain method.** (a) and (b) are fresh controls; (c), (d), (e) and (f) are from decellularised bladders. (a), (c) and (e) are images of the luminal surface and (b), (d) and (f) are images of the muscular layer. All images were captured at 10× magnification. Scale bars are 100 µm.

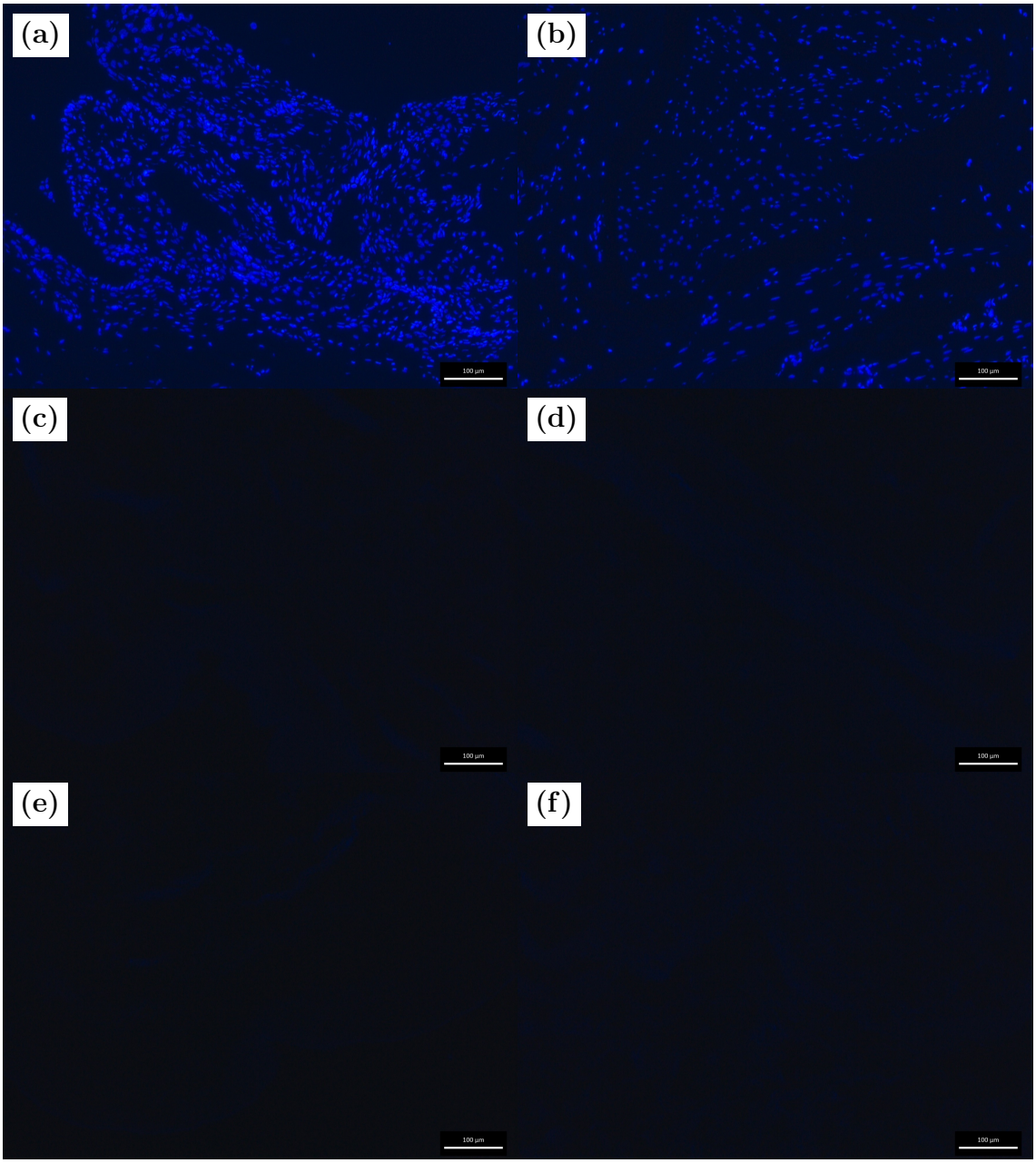


**Figure 4.11: Images of DAPI stained sections from bladders decellularised using the controlled strain method.** (a) and (b) are fresh controls; (c), (d), (e) and (f) are from decellularised bladders. (a), (c) and (e) are images of the luminal surface and (b), (d) and (f) are images of the muscular layer. All images were captured at 10× magnification. Scale bars are 100 µm.

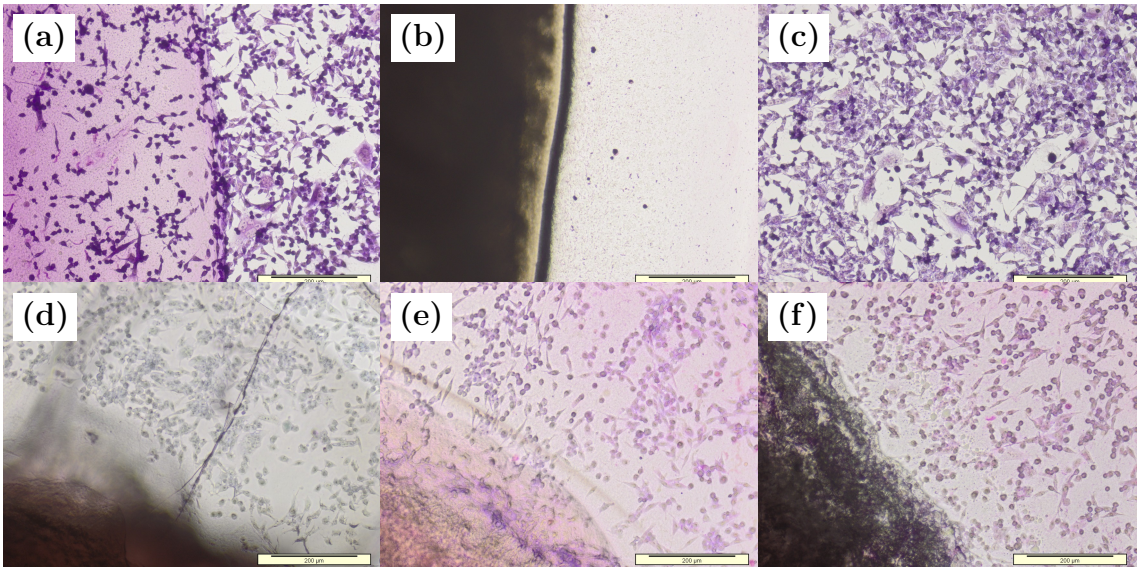


**Figure 4.12: Contact cytotoxicity assay using BHK cells of bladder tissue decellularised using controlled strain.** Controls are (a) collagen gel, (b) cyanoacrylate glue and (c) cells only. Bladder tissue samples are (d), (e) and (f). All images were captured at 10× magnification. Scale bars are 200 µm.

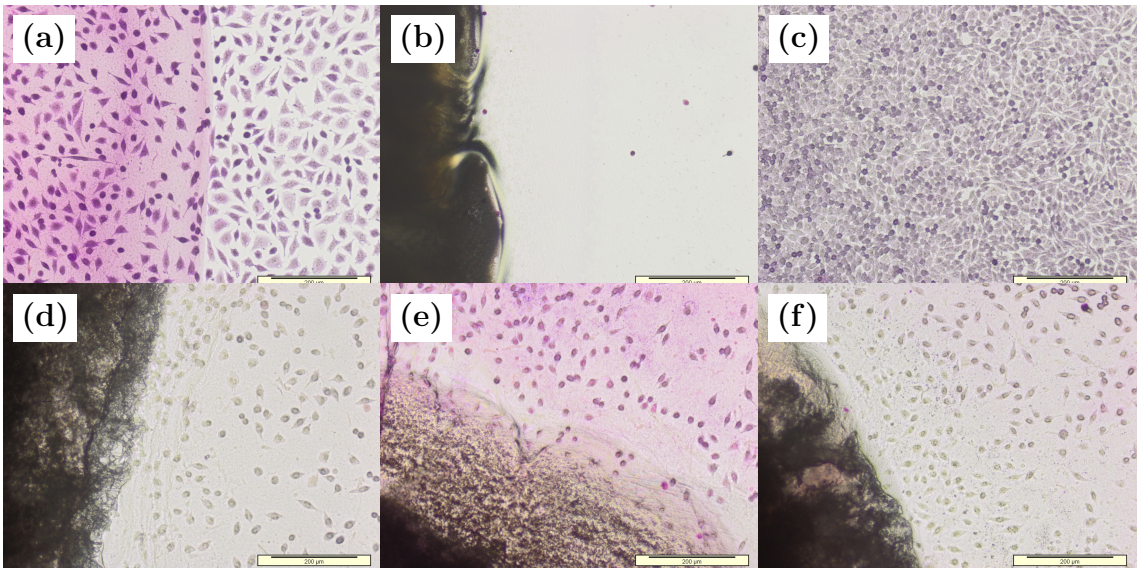


**Figure 4.13: Contact cytotoxicity assay using L929 cells of bladder tissue decellularised using controlled strain.** Controls are (a) collagen gel, (b) cyanoacrylate glue and (c) cells only. Samples are (d), (e) and (f). All images were captured at 10× magnification. Scale bars are 200 µm.

#### 4.3.2.3 Tissue dimensions after decellularisation

Markers (blue sutures) were placed on bladders which were decellularised using the controlled strain distension method. After placing markers approximately 10 mm apart, an image was taken to more accurately measure the distance between markers. The initial distances between the bladder markers for all bladders in all directions were $10.4 \pm 0.2$ mm (mean $\pm$ standard error). The distances for individual bladders are given in Table 4.5.

During decellularisation the required strains were applied to each bladder by monitoring the displacement of the markers during filling. The dimensions of the $x$ direction markers during decellularisation were $30.0 \pm 0.0$ mm, $30.0 \pm 0.0$ mm and $35.8 \pm 0.3$ mm for each of the bladders; and the dimensions of the $y$ direction markers during decellularisation were $28.4 \pm 0.3$ mm, $36.6 \pm 1.0$ mm and $24.0 \pm 0.0$ mm for each of the bladders (mean $\pm$ standard error). The decellularisation strain, $\varepsilon_{\text{dcell}}$, was calculated for each bladder in each of the $x$ and $y$ directions using the initial marker dimensions and the mean of the marker dimensions during decellularisation. These strains are shown in Table 4.5.

Distances between the bladder markers were recorded after decellularisation. These final dimensions were recorded immediately after decellularisation, and for three subsequent weeks. The dimensions of the $x$ direction markers after decellularisation were $18.8 \pm 0.3$ mm, $19.9 \pm 0.8$ mm and $22.1 \pm 0.6$ mm for each of the bladders; and the dimensions of the $y$ direction markers after decellularisation were $18.3 \pm 0.4$ mm, $24.5 \pm 0.2$ mm and $14.7 \pm 0.3$ mm for each of the bladders (mean $\pm$ standard error). The final strain, $\varepsilon_{\text{final}}$, was calculated for each bladder in each direction using the initial marker dimensions and the mean of the marker dimensions after decellularisation. These strains are shown in Table 4.5.

In order to predict final strain from decellularisation strain, linear regression was performed with decellularisation strain as the predictor variable and final strain as the response variable. There was a very strong correlation between the two variables, with a high $R^2$ value of 0.963. A graph of final strain plotted against decellularisation strain and the corresponding straight line relationship is shown in Figure 4.14. Substituting $\varepsilon_{\text{dcell}} = \{2.00, 1.40\}$ into the relationship gives $\varepsilon_{\text{final}} = \{0.926, 0.488\}$.

| | | Dimensions (mm) | | | Strains | |
|---|---|---|---|---|---|---|
| Bladder | Direction | Initial | Decell. | Final | Decell. ($\varepsilon_{\text{dcell}}$) | Final ($\varepsilon_{\text{final}}$) |
| 1 | $x$ | 11.2 | 30.0 | 18.8 | 1.68 | 0.68 |
| | $y$ | 10.3 | 28.4 | 18.3 | 1.77 | 0.78 |
| 2 | $x$ | 10.0 | 30.0 | 19.9 | 1.99 | 0.98 |
| | $y$ | 10.3 | 36.6 | 24.5 | 2.57 | 1.39 |
| 3 | $x$ | 10.7 | 35.8 | 22.1 | 2.35 | 1.08 |
| | $y$ | 10.0 | 24.0 | 14.7 | 1.40 | 0.47 |

**Table 4.5: Distance between bladder markers over the decellularisation process, and the corresponding strains.** The decellularisation and final dimensions were a mean of the strains recorded during and after decellularisation respectively.

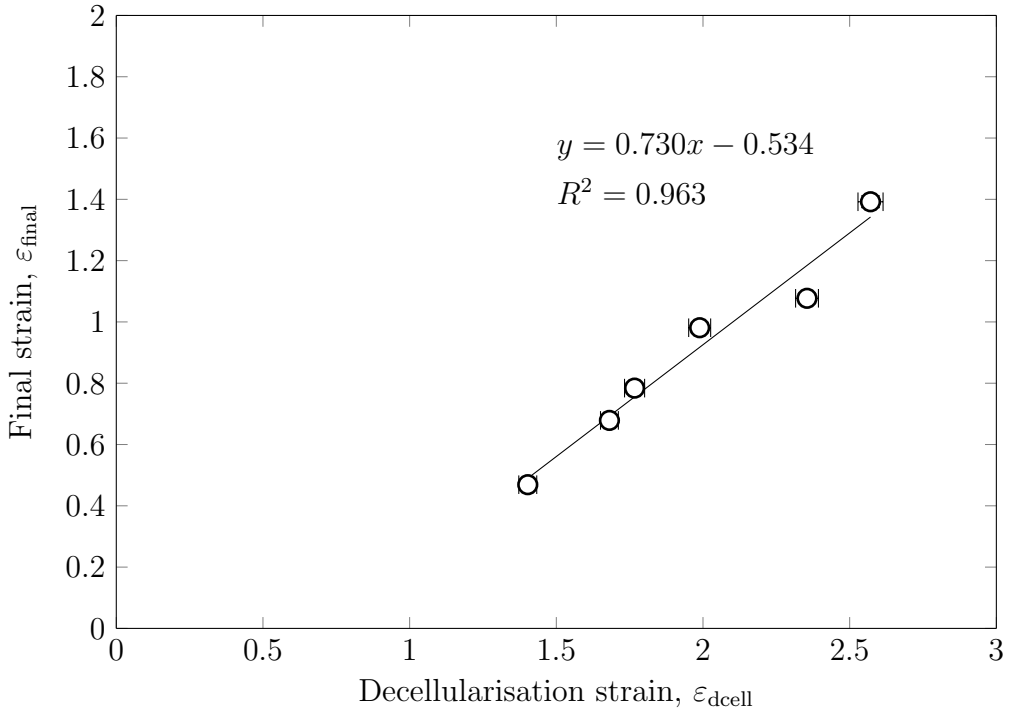


**Figure 4.14: The relationship between final strain and decellularisation strain.** Each point represents a measurement of bladder strain in either the $x$ or $y$ direction. Simple linear regression was used to find a relationship to predict final strain from decellularisation strain. Measurement errors are shown.

## 4.4 Discussion

In the previous chapter, filling experiments were performed to determine relationships for calculating bladder capacity. Bladders filled with these calculated filling volumes during decellularisation appeared to be acellular after processing. In this chapter, a filling experiment was performed to measure and calculate material variables for bladders when filled to their calculated capacities. Filling was performed whilst bladders were immersed in solution in order to mimic the decellularisation environment. This was carried out so that the calculated material variables would describe the mechanical deformation state that they were subject to during decellularisation. Once known, this state of deformation could be applied to bladder tissue to enable decellularisation regardless of gross geometry.

Before bladders were immersed and distended, their masses and tissue volumes were recorded so that the required material variables could be later calculated. A strong relationship was found between mass and tissue volume, demonstrating that it could be used to calculate tissue volume from bladder mass. The high $R^2$ value of 0.997 indicated that the density of the different bladders were very similar This was not unexpected, since it has been reported in the literature that all soft tissue has a density which lies in a narrow range, between $916\,\mathrm{kg}\cdot\mathrm{m}^{-3}$ and $1060\,\mathrm{kg}\cdot\mathrm{m}^{-3}$ (Wells & Liang, 2011). The gradient of the graph represented a specific mass of bladder tissue of $1010\,\mathrm{m}^3\cdot\mathrm{kg}^{-1}$, equivalent to a density of $990\,\mathrm{kg}\cdot\mathrm{m}^{-3}$, which is within the range reported in the literature. The regression line did not intersect the origin, and instead intersected the $x$ axis (zero volume) at $x = 1.9\,\mathrm{g}$ and the $y$ axis (zero mass) at $y = 1.9\,\mathrm{ml}$. This suggested that one or both of these measurements were measured with a consistent bias. The measurement errors associated with bladder mass were very small ($\pm 0.05\,\mathrm{g}$). The error of $\pm 1\,\mathrm{ml}$ for tissue volume was larger, however it is unlikely that multiple measurements with this magnitude of error would contribute to an offset of 1.9 ml due to the effect of diminishing standard error when a greater number of measurements are used. The intersection of the $x$ axis may explained because these measurements were performed in a particular sequence and when the tissue was wet. It is possible that this method resulted in more solution being present on the surface of bladders for one measurement than the other, resulting in the observed offset. The method for measuring tissue volume using a measuring cylinder was more susceptible to human error and not as accurate as measuring mass using a balance. The method for measuring mass was also easier to perform than measuring volume, particularly if the measurement was taken aseptically. If either of these values are needed, it therefore follows that mass should be measured, and volume calculated from that.

The strain–volume curves of distended bladders (Figure 4.5) showed an initial steep increase of strain as each bladder was initially filled followed by a decrease in curve gradient as each bladder became more full. In order to analyse whole-bladder deformation mechanics, Korossis *et al.*, 2009 approximated the shape of bladders to be spherical. Using this, a relationship was found between the volume ($V$) bladders are filled with and the resulting strain ($\varepsilon$) in the bladder wall: $V = V_0(1 + \varepsilon)^3$. The strain–volume data of bladders in this chapter appeared to follow this cubed relationship, with the differing gradients of each graph explained by the different initial volumes of each particular bladder.

The graphs of $y$ strain against $x$ strain showed that most bladders stretched more in the circumferential ($x$) direction than in the longitudinal ($y$) direction (Figure 4.6). This was consistent with the literature (Korossis *et al.*, 2009). This anisotropy allows bladders *in vivo* to distend up into the abdomen during filling (Bullock *et al.*, 1994). All these curves were approximately linear, indicating that the bladder tissue stretched in equal proportions in each direction throughout the filling process.

The stress–strain curves (Figure 4.7) exhibited a response typical for biological tissue, with an initial toe region of low-stress extension followed by a transition into a steeper linear region (Korossis *et al.*, 2002). There was significant variation between the samples, as expected for biological tissue. The toe region of the frozen bladders appeared to be steeper (stiffer) than the toe region of fresh bladders, with a longer period of transition between the two phases of the curves. These effects were more pronounced in the twice-frozen bladders than the once-frozen bladders.

The pressure–volume curves of fresh distended bladders typically showed an initial increase in pressure followed by a long period of low-pressure filling (Figure 4.4). This initial pressure increase is seen when any spherical balloon is inflated (Ogden, 1972). Low-pressure filling is observed with normal bladders *in vivo* (Scott *et al.*, 1982). During these phases, collagen fibres in the tissue were uncoiling and straightening out and the tissue was in the toe region of the stress–strain curve. After the low-pressure filling, a steep increase in pressure was observed. During this phase the collagen fibres had finished uncoiling and the linear region of the stress–strain curve was reached. Any extra volume increase in the bladders was a result of elongation (rather than the uncoiling) of the collagen fibres, resulting in a material with a high stiffness. The overall shape of the pressure-volume curves can therefore be considered as a superposition of the pressure–volume curve of a spherical balloon and the stress–strain curve tissue response. However, there was a large degree of variation between samples, particularly regarding the extent to which bladders exhibited an initial steep pressure rise. This was likely to have resulted from biological variation due to the compounding effects of variation due to initial tissue stiffness, tissue thick-

ness and variation in initial bladder size, with initial tissue thickness ranging from 3.04 to 7.11 mm and initial bladder area ranging from 2700 to 6020 $mm^2$. For example, a small bladder with particularly stiff and thick wall tissue is likely to exhibit a large initial steep pressure rise, whereas a large bladder with particularly compliant and thin wall tissue is likely to exhibit a much lower initial pressure rise.

The equation for bladder capacity found in the previous chapter (Equation 3.4) was used to calculate the capacity for fresh bladders immersed and distended in this chapter. These volumes were used to interpolate several material variables which described the state of mechanical deformation of bladders filled to these points. Relationships were found between these variables and bladder capacity, as shown in Figure 4.8. Hypothesis testing revealed that the gradient of the relationship between pressure and capacity differed significantly from zero ($p = 0.014$) and had a moderate negative correlation ($R^2 = 0.470$), which indicated that internal bladder pressure could be used as the controlled variable during bladder decellularisation. The gradients of the relationships between stress and capacity were close to being significantly different from non-zero ($p_x = 0.073, p_y = 0.052$), indicating that more data may be necessary to establish significance. The poor correlations ($R_x^2 = 0.286, R_y^2 = 0.327$) also revealed a poor fit to the data, which may have been a result of the large errors associated with some of the data points. Strain and tissue thickness were invariant with bladder capacity. This was evident because the gradients of the relationships did not significantly differ from the null hypothesis that the gradients were equal to zero ($p_{x\text{-strain}} = 0.331,\ p_{y\text{-strain}} = 0.667,\ p_{\text{thickness}} = 0.632$). This suggested that either strain or thickness could be used to measure whether bladders have been sufficiently stretched for decellularisation. Of these, it would be more feasible to control the strain which is applied to bladder tissue because tissue thickness is more difficult to measure, and in either case strain must be applied to stretch the tissue anyway. The mean strains of bladders filled to their decellularisation volumes were 2.00 in the circumferential ($x$) direction and 1.40 in the longitudinal ($y$) direction.

The measurement errors of bladder pressure and bladder capacity were small, with relative errors of less than 0.5 %. Similarly the errors of strain were also small with the vast majority (22 out of 24) of strain measurements having a relative error under 3 %. It is likely that the errors for strain were larger than those for pressure and capacity because strain was calculated from two measurements, whereas pressure and capacity were measured directly. The small errors therefore allowed meaningful relationships between these parameters to be calculated with confidence. The errors of tissue thickness and stress were significantly larger, with relative errors of 5–9 % and 6–11 % respectively. These large measurement errors were a consequence of calculating these parameters from several other parameters, resulting in a com-

pounding of these errors. The relationships found using thickness and stress were therefore not as reliable as those found using pressure and strain, and these large errors may have contributed to the poor correlations found between capacity and stress ($R^2 = 0.286$ for $x$ stress and $R^2 = 0.327$ for $y$ stress). Both of these errors could have been reduced by measuring tissue thickness directly during the experiment rather than calculating it from initial thickness and experimental strain data. Tissue thickness could have been measured using ultrasound, however this would have been limited to finding the thickness at a particular location which may not have been representative of the mean tissue thickness, and multiple measurements would likely have restricted the view of the camera, which would have reduced the accuracy of measurements taken from images.

Previously, bladders were filled with a calculated volume during decellularisation. It was therefore logical that the strain could also be used to control the deformation of bladders during decellularisation given the geometrical relationship between strain and volume for ovoid shapes such as porcine bladders. There were two outliers in the scatter graph of tissue thickness plotted against capacity. This indicated that although the thickness of most bladders when filled to capacity will fall around a mean value, there is a chance that some bladders will be thicker than this. This increased thickness could restrict decellularisation solutions from fully penetrating a bladder wall during processing, resulting in inadequate decellularisation.

In order to determine the effects of freezing on the mechanical properties of bladder tissue, biaxial stress–strain data was gathered for fresh, once-frozen and twice frozen bladders. Because of the intrinsic link between orthogonal strains due to the Poisson effect, the material parameters typically calculated from stress–strain curves cannot be found from biaxial stress–strain curves. Variables such as the toe region modulus or transition strain would not be comparable between samples if calculated from the biaxial stress–strain curves. In order to find these material parameters, a new variable was derived. Plotting stress against UE strain allowed these material parameters to be calculated. The values for these parameters allowed them to be compared between samples, and the effects of freezing investigated.

A two-way ANOVA was performed to determine if freezing resulted in any significant changes to the toe-region modulus, linear region modulus, transition stress or transition strain of the stress–strain curves of distended bladders. As shown in Figure 4.9, freezing was not found to significantly affect the toe region modulus or transition stress of bladder tissue ($p = 0.234$ and $p = 0.104$ respectively, 2-way ANOVA), however significant differences were found for the means of the linear region modulus and transition strain ($p < 0.001$ and $p = 0.001$ respectively). Freezing bladder tissue resulted in a significant decrease in both the linear region modulus

and transition strain of tissue samples in both the longitudinal and circumferential directions (2-way ANOVA). There were no significant differences between the once-frozen and twice-frozen bladders. These results suggested that the different tissues performed similarly in the toe region of the curves, but the transition point was occurring at a lower strain resulting in a lesser gradient between the transition point and failure.

Reports on the effects of freezing on the mechanical properties of bladder tissue could not be found in the literature. Similarly no data could be found for intestine, which is similar in structure to bladder tissue. However, blood vessels share some structural properties with bladders as both have an inner epithelial layer and a thick layer of smooth muscle, and the effects of freezing on their mechanical properties has been well documented. Freezing and thawing porcine femoral arteries has been reported to result in a change in mechanical properties, specifically a reduction in both the linear region modulus and transition strain of the uniaxial stress–strain response (Grassl *et al.*, 2004; Venkatasubramanian *et al.*, 2006). These changes in the stress–strain response also occurred in the of bladder tissue which was tested in this chapter, indicating that the same changes may have occurred in both types of tissue. The studies also reported an increase in initial length and a decrease in mass. These parameters were not measured for bladder tissue, but could be investigated in the future. It was hypothesised by the authors that the changes were caused by a mixture of tissue dehydration, reduction in smooth muscle cell function, and damage due to ice crystal formation resulting in alignment changes and damage to collagen crosslinks.

A study performed by Venkatasubramanian *et al.*, 2010 investigated the mechanisms behind the changes in mechanical properties due to porcine artery freezing. They used a combination of dehydration, cell-death and freezing treatments to assess smooth muscle cell contraction, collagen distribution, and uniaxial tensile testing mechanical properties to do this. Freezing was found to cause cell damage, death, and lack of smooth muscle cell function, which was linked to an increase in tissue length and reduction in transition strain. Collagen fibres were also seen to become more aligned and uniformly distributed, which was thought to be the cause of the observed increase in initial length and consequently result in the tissue bearing load at a lower strain. Changes were also attributed to the observed tissue dehydration caused by the freezing process. However, our samples were tested in water, which is seen to reverse the effects of dehydration (Venkatasubramanian *et al.*, 2006). It is therefore highly likely that the changes observed in bladder tissue are similarly caused by a reduction in smooth muscle function and collagen fibre re-distribution. These altered biomechanics may affect the *in vivo* performance of the decellularised

bladder because the differences in strain as a result of changes in ECM stiffness are known to affect cell behaviour (Farhat & Yeger, 2008).

Despite these changes in mechanical properties, all frozen bladders were able to be distended to similar, if not greater pressures compared to the fresh bladders. This suggested that it is unlikely that damage has been caused to the fibres. Therefore, the forces and strains which are required for successful decellularisation were able to be applied to once-frozen and twice-frozen bladders without the tissue nearing its failure point.

The parameters in this study were calculated from calculations of true stress rather than engineering stress, and therefore could not be directly compared to those found by Korossis *et al.*, (2009). This was done in order to minimise the compounding of measurement errors associated with calculating the stress. However, estimates of transition engineering stress and transition strain were found to differ from the values found by Korossis *et al.*, (2009) by factors of approximately 2.5 and 0.5 in the transverse and apex-to-base directions respectively. These differences may have been brought about by the two different modes of testing, especially the effect of testing only a small strip of bladder, as the deformation of the bladder could be dependant on whether the adjacent collagen fibres have been cut away or left intact. The different testing conditions, such as temperature and strain rate, may also have played a role.

In order to control the strain of bladders being decellularised, markers were placed on the surface of the tissue. This allowed the displacement of the tissue to be monitored as bladders were filled using the same method as the original decellularisation process. To do this, bladders were suspended from the neck with forceps and filled via the urethra using a syringe. This resulted in bladders being overly stretched in the longitudinal direction, so that the strain the bladder wall in the two directions was not in the ratio of 2.00 to 1.40. Filling the bladders by this method applied much more longitudinal stretch than circumferential stretch because the wall of the bladder must support the mass of the decellularisation solution in the bladder. Using this method it was therefore not possible to fill bladders to the same state of deformation they would be found in during decellularisation.

So that bladders could be filled to the same deformation state as they would be during decellularisation, a method was developed to immerse bladders in decellularisation solution during the filling phase of the decellularisation process. Unlike the previous process, the resulting strain in the wall of the bladders did occur approximately in the ratio of 2.00 to 1.40 in the circumferential and longitudinal directions respectively. This exact ratio was not reached in all of the bladders due to biolog-

ical variation. Bladders decellularised using this method were shown to be devoid cellular material and the matrix resembled the structure of native bladder tissue (Figures 4.10 and 4.11). Analysis of the DNA content showed that 99.6 % of the DNA was removed by the process, and the DNA content of each bladder was less than $50\,\mathrm{ng} \cdot \mathrm{mg}^{-1}$. These results supported the hypothesis that stretching bladder tissue to strains of 2.00 in the circumferential direction and 1.40 in the longitudinal direction was sufficient to allow adequate diffusion of decellularisation solutions, and consequently successful decellularisation.

A manufacturing process for decellularising porcine bladders must be able to produce patches of a specific size. In order to do this, the final size of the decellularised tissue must be known. It was noticed that at the end of the process, bladder tissue appeared to be larger than the initial size of the fresh tissue before the process, but smaller than the size that the tissue was stretched to during processing. It was subsequently hypothesised that the strain applied to bladders during the process would correlate with the final resulting strain of the bladder tissue after decellularisation. This hypothesis was tested by recording the dimensions of bladder markers during and after decellularisation, and calculating the strains for these states relative to the initial size of the markers. A strong correlation was found between the decellularisation strains and the final strains ($R^2 = 0.963$, Figure 4.14). This demonstrated that the greater the size a bladder is stretched to during decellularisation, the greater its dimensions will be at the end of the process. This suggested that the decellularisation process irreversibly changed the tissue so that the tissue was stretched relative to the original tissue when in the ground (relaxed) state, which was likely caused by an increase in collagen fibre alignment. The relationship which was found between decellularisation strain and final strain was used to calculate that if decellularisation strains of 2.00 and 1.40 are applied to bladder tissue, the final strains will be 0.926 and 0.488. These values can therefore be used to calculate the initial size of bladder tissue required to produce a patch of a specific final size.

## 4.5 Conclusions

A filling experiment was performed in order to determine the deformation state of bladders which were distended when immersed in solution. The previously found relationship for bladder capacity was used to calculate that the strains of bladders filled to their decellularisation capacities were 2.00 and 1.40 in the circumferential and longitudinal directions respectively. Applying these strains to bladder tissue during decellularisation produced bladder tissue which appeared to be completely devoid

of cellular material when examined histologically. DNA extraction and quantification showed that more than 99 % of the DNA was removed by the process. These data demonstrated that applying prescribed strains of 2.00 and 1.40 to bladder tissue, in the circumferential and longitudinal directions respectively, was a suitable method for stretching bladder tissue adequately to allow complete decellularisation to occur.

In order to compare the mechanical properties of fresh and frozen bladder tissue, a parameter—uniaxial equivalent strain—was derived so that the required material parameters could be derived from biaxial stress–strain data. The mechanical performance of the different types of tissues compared with the application of this new variable. Once- and twice-frozen bladders were able to be filled to pressures comparable to those of fresh bladders. All frozen bladders could be filled to the point where the strains required for decellularisation were applied to the tissue. There was no statistical difference between the toe region modulus and the transition stress of fresh, once-frozen and twice frozen bladders. The linear region modulus and transition stress of fresh bladders were significantly greater than those of once- and twice-frozen bladders. No significant differences of these variables were found between once-frozen and twice-frozen bladders.

There was a strong correlation between the dimensions bladders were stretched to during decellularisation and the resulting dimensions of the tissue at the end of the process. A relationship between decellularisation strain and final strain was used to calculate that applying strains of 2.00 and 1.40 to bladder tissue during decellularisation would result in final strains of 0.926 and 0.488. This information could be used to calculate the initial size of tissue required to produce a decellularised patch of a specific size.

# Chapter 5

# Concept design of decellularisation equipment and modelling of bladder material under new deformation regime

## 5.1 Introduction

The original porcine bladder decellularisation method involved manually distending bladders with solutions at each stage of the process. Distension was performed in order to stretch the bladder wall to make it thin enough for the decellularisation solutions to diffuse into it. This step was necessary for successful decellularisation (Bolland *et al.*, 2007). However, this method of manipulating the bladder was time consuming, difficult to perform, and high volumes of decellularisation solutions were required to fill and surround the bladders at each stage of the process. This process was subsequently deemed impractical to execute on a large scale as part of a commercial manufacturing process. A way of stretching the bladder which does not require repeated organ distension would be compatible with a manufacturing process.

In the previous chapter, it was shown that bladder wall strains of 2.00 and 1.40 in the circumferential and longitudinal directions were found to stretch the tissue sufficiently for successful decellularisation to occur. It was hypothesised that applying these strains to bladder tissue which is held in a different shape would still reduce the thickness of the tissue to facilitate decellularisation. The specifications of a commercial bladder patch were discussed with surgeons. They specified that a patch

should be a flat, square sheet with a minimum size of 8 cm × 8 cm. Decellularising a piece of tissue which is no larger than the required size would minimise wastage and increase efficiency in the production process. To produce a final patch which was square in size, it was decided to decellularise the bladder in the form of a flat square sheet. This 2D form also meant that there would be a minimum amount of decellularisation solution which would be required to fully submerge the tissue in solution, unlike the distension method. This would be advantageous over other shapes which a square sheet of tissue could take, such as a cylinder, because a volume of solution would be required to fill the void of any 3D shape, possibly resulting in larger volumes of solution being required to decellularised the tissue.

In order to biaxially stretch flat sheets of tissue, it was decided to stretch the tissue using discrete points. This method is one which has been adopted previously in the literature (Cooney *et al.*, 2016). This method involves placing several pins (e.g. needles or hooks) into the border of the tissue, and applying a displacement to these pins, which in turn stretch the tissue. A diagram of a piece of material stretched using discrete points is shown in Figure 5.1. However, biaxial stretching using discrete points does not result in a material which is uniformly stretched. Both the number of points the material is stretched with and the thickness of border left outside the region contained by the pins both affect the distribution of strain throughout the tissue. Biaxially stretched tissue should be stretched sufficiently to apply the strains required for complete decellularisation to occur. Stretching the tissue with a greater number of pins will result in a more uniform stretching, but will add complexity into the design of the equipment. A border of a minimum size is required so that there is material for the pins to pass through and support the tissue. Having a thicker border around the tissue will provide support which will stretch the main region of material more uniformly, but will require a larger piece of tissue to be used.

Previously, measurements were taken of bladders before, during and after decellularisation in order to be able to calculate the initial size of bladder tissue required to produce a decellularised patch of a specific size. Due to the nature of stretching a material using discrete points, there will be some regions of the tissue which are not stretched to within the required limits for decellularisation, particularly the edge regions of the tissue close to the pins. Tissue in these regions may not be suitable for use as part of the final patch due to insufficient stretching. The final patch would likely have to be taken from a central region of the stretched tissue.

The finite element method is a numerical method for calculating the distribution of certain material variables of a body which is subjected to a set of known conditions. Is is often employed to estimate the stress and strain within a material when a known

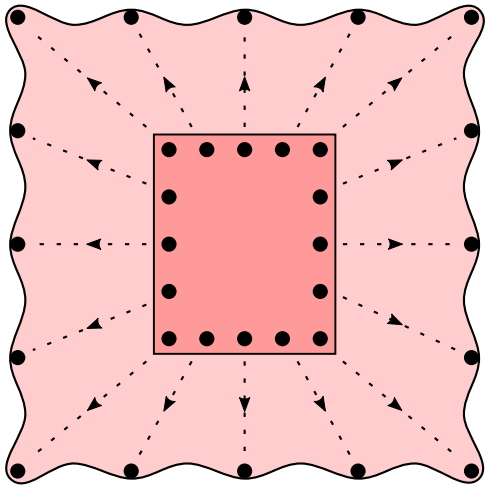

**Figure 5.1: Stretching a material biaxially using discrete points.** The dark red region represents the unstretched material, and the lighter region represents the stretched material. The black circles represent the discrete points which are used to stretch the material. The dotted lines and arrows represent the movement of the points, which may take the form of hooks placed into the material. The wavy edges of the stretched material demonstrates how the resulting deformation is not uniform when discrete points are used.

force or displacement has been applied to it. Finite element modelling (FEM) was therefore a suitable method of finding the optimal parameters, such as number of discrete points and border size, for stretching bladder tissue, and to subsequently find a suitable mode of stretching the tissue to ensure that a sufficient strain was applied to the required region of tissue during decellularisation.

### 5.1.1 Rationale

The software package FEBio was used to compute FEM problems. FEBio was developed with the purpose of solving biomechanical structural mechanics problems, as well as other types of problems (Maas *et al.*, 2012). It is able to model large material deformations with nonlinear stress–strain responses, and can process custom-generated `xml` problem files. This allowed Matlab scripts to be written to generate problems which could be processed by FEBio.

Any material modelled using FEM must be represented using a constitutive equation. A constitutive model dictates how the material responds to the applied conditions. The Ogden Hyperelastic strain–energy function was used as the constitutive model for the bladder material because it is able to model complex stress–strain responses. It was reasonable to assume the material was incompressible because soft

tissue has a Poisson's ratio which is close to 0.5 (Wells & Liang, 2011). Other constitutive models were considered, such as the Mooney-Rivlin and Veronda-Westmann models. However, these models are limited in the variety of stress–strain response they are able to represent as they are each governed by only two constants (Veronda & Westmann, 1970), and preliminary tests demonstrated that they were unsuitable for modelling the stress–strain data which had been collected. Conversely, the Ogden model strain–energy function is a sum of multiple exponent terms (Ogden, 1972), is therefore able to represent a more varied stress–strain response, and was consequently able to model the stress–strain data.

It was previously shown that applying orthogonal strains of 2.00 and 1.40 (in the circumferential/$x$ and longitudinal/$y$ directions respectively) to bladder tissue stretches the tissue enough for successful decellularisation to occur. Application of this biaxial strain results in a negative strain in the third direction, and therefore a thinning of the bladder wall so that solutions are able to fully diffuse into the tissue. The strain in the third dimension was therefore deemed a suitable measure of the success of the deformation of the modelled material.

The Ogden material model assumes isotropy. The material properties of bladder material has previously been shown to be directional (Korossis *et al.*, 2009). Therefore, modelling the bladder using the Ogden model would not account for the anisotropic nature of bladder material. However, the stress–strain response of the two directions of the material were shown to be similar (see Chapter 4), and this approximation would therefore suffice for these purposes.

### 5.1.2 Aims and objectives

#### Aims

The main aim of this chapter was to model the deformation of flat sheets of bladder material using FEM in order to find the optimal mode of stretching the tissue for decellularisation. A suitable stretching regime using discrete points had to be found which would apply adequate biaxial strain to the required region of tissue.

#### Objectives

1. To use experimental data to determine the constitutive model parameters for the bladder material.
2. To determine a measure of successful tissue stretching, in terms of $z$ direction strain.

3. To find an adequate mesh for modelling the stretching of flat bladder tissue sheets.
4. To model bladder stretching to determine the number of stretching points and the thickness of the outside border required for the optimal stretching regime.
5. To model bladder stretching to determine the required size of tissue to produce an adequately stretched patch of a specific size.

## 5.2 Methods

A summary of experiments is shown in Table 5.1.

A Matlab script was written to generate FEM meshes so that various different models of the bladder tissue could be generated by varying the input parameters. In order to properly simulate tissue deformations, material constants for the bladder were calculated using experimental data. A mesh convergence study was performed to find an optimal mesh density to use in the main studies. The bladder was modelled using different numbers of attachment points and different thicknesses of border in order to find optimal values for these parameters which would result in flat sheets of bladder tissue being sufficiently stretched.

| | Experiment | Samples (number) | Outputs |
|---|---|---|---|
| 1 | Calculation of Ogden Model parameters | Bladders 4.1.a–l (12 from fresh)<br>Bladders 4.1.m–r (6 once-frozen)<br>Bladders 4.1.s–x (6 twice-frozen) | Parameters calculated using stress–strain data |
| 2 | Determination of criterion for successful bladder stretching | — | Target $z$ strain range of $-0.861 \pm 10\%$ |
| 3 | Mesh design | — | Parameterised finite elements mesh |
| 4 | Mesh density in the border area | — | Modified mesh design |
| 5 | Mesh convergence study | — | Optimised mesh density |
| 6 | Finite element modelling of flat sheets of bladder tissue | — | Determination of the optimal parameters for stretching flat bladder sheets |
| 7 | FEM model of full-size bladder tissue sheet | — | Determination of the size of tissue required to stretch in order to produce a piece of tissue of the requisite size |

**Table 5.1: A summary of the experiments featured in Chapter 5.**

### 5.2.1 Calculating the Ogden model parameters

The Ogden model was chosen to model the material deformation of the bladder. The constitutive equation for this model is given in Equation 5.1.

$$W = \sum_{i=1}^{N} \frac{c_i}{m_i^2} \left(\lambda_1^{m_i} + \lambda_2^{m_i} + \lambda_3^{m_i} - 3\right) + U(J) \tag{5.1}$$

In order to use the Ogden model in FEM, the elasticity parameters of the material $(c_i, m_i)$ required calculation. The complexity of the model is increased by using a greater number of pairs of these material parameters. This is done by increasing the integer value of $N$. These parameters were calculated by fitting the model to experimental stress–strain data.

Stress–strain relationships were derived from the strain–energy equation of the model. These derivations are shown in Appendix D. The relationship between stress and stretch for a material in equibiaxial tension was used (Equation 5.2).

$$\sigma_1 = \sum_{i=1}^{N} \frac{c_i}{m_i} \left(\lambda_1^{m_i} - \lambda_1^{-2m_i}\right) \tag{5.2}$$

#### 5.2.1.1 Experimental data

Experimental stress–strain data from the immersed distension experiment was used to calculate the Ogden model parameters. The mean stress–strain curves for the once-frozen and twice-frozen bladders (biaxial data) were used. Because the model assumes the material is isotropic, the mean stress–strain curve of the two ($x$ and $y$) directions was found. The mean stress–strain curve was calculated using the method described in Section 2.8.4.2 and data above the mean maximum stress was ignored. These curves are shown in Figure 5.2.

#### 5.2.1.2 Least-squares curve-fitting

The nonlinear least-squares curve-fitting Matlab function `lsqcurvefit` was used to find optimal values for the parameters in Equation 5.2 in order to fit the Ogden model to the experimental data. A similar method was used to the one outlined by Ogden *et al.*, 2004.

Values for the elasticity parameters were found for $N = \{1, 2, \ldots, 6\}$. For each of these, the calculation was performed 10 times (variations `a`–`j`), because there may be multiple solutions for each value of $N$, particularly for greater values of $N$.

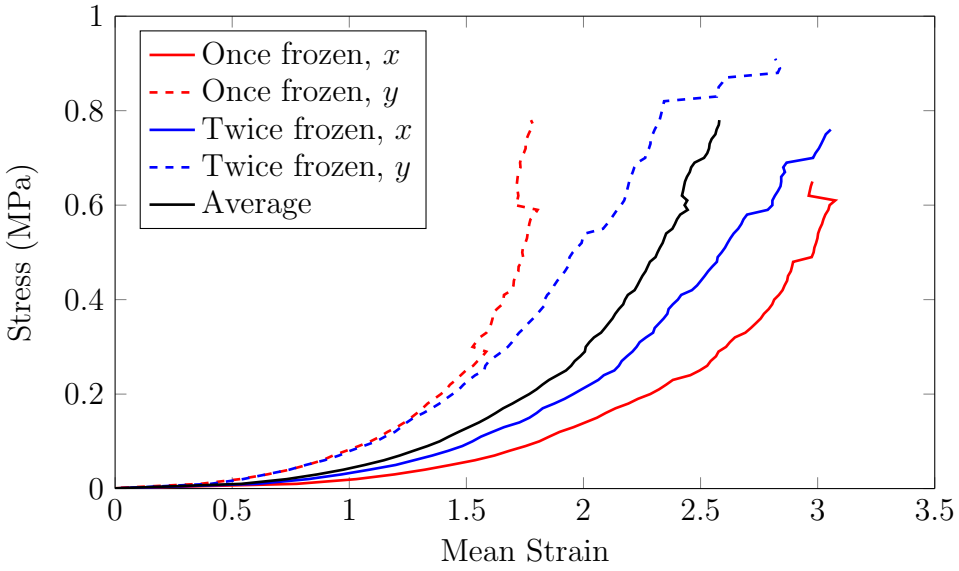


**Figure 5.2: The average stress strain curve the Ogden Model Data was fitted to.** Taken from immersed distension experiment ($n = 12$ for fresh bladders, $n = 6$ for once-frozen and twice-frozen bladders).

A random number generator function in Matlab, `rand`, was used to generate initial values for the material parameters $c_i, m_i$ ($i = \{1, \ldots, N\}$). Initial values were generated in the range $0 < c_i, m_i \leq 10$. Values for these parameters in this range are typical (Twizell & Ogden, 1983).

The `lsqcurvefit` function was set to stop when either the tolerance on $X$ (`TolX`) dropped below $10^{-8}$, the tolerance on the function value (`TolFun`) dropped below $10^{-12}$, or when the total number of function evaluations (`MaxFunEvals`) reached a total of 3000. The squared 2-norm of the residual and the stopping criteria for each solution was recorded. A solution was chosen which had a minimum norm of the residual for a number of parameter pairs which did not over-parameterise the function. This set of parameters was used in the FEM model.

### 5.2.2 Criterion for successful FEM bladder stretching

Positive strain applied to bladder tissue in the $x$ and $y$ directions results in negative strain in the $z$ direction. It was hypothesised that this reduction in thickness allowed greater diffusion of decellularisation solutions into the wall of the bladder due to the lesser distance these solutions must diffuse over. Therefore the bladder could be considered adequately stretched if the $z$ strain of the bladder reached a required value, which corresponded to a required final thickness for bladders with similar initial thicknesses.

If the $x$ strain, $y$ strain and Poisson's ratio of a material is known, the $z$ strain

can be calculated. The $x$ and $y$ strains required for successful decellularisation were calculated in the previous chapter. The tissue was assumed to be incompressible with a Poisson's ratio of $\nu = 0.5$ because the Poisson's ratio of soft tissue is known to lie between 0.49 and 0.50 (Wells & Liang, 2011). It was therefore possible to calculate the $z$ strain of bladder tissue during decellularisation.

FEBio does not calculate $z$ strain, so this could not be directly used as the criterion for successful bladder stretching. Instead, an equivalent value for the $z$ Lagrange strain of the tissue was found. This measure of strain was computed by FEBio, and could be used to quantify bladder stretching in the $z$ direction. A relationship for $z$ Lagrange strain in terms of $z$ strain is given in Equation 5.3. The derivation for this can be seen in Appendix E.

$$\varepsilon_{Lz} = \frac{1}{2}[(\varepsilon_z + 1)^2 - 1] \tag{5.3}$$

Due to incompressibility, the stretches in the 3 dimensions must equal unity when multiplied.

$$\lambda_x \lambda_y \lambda_z = 1 \tag{5.4}$$

The $z$ direction stretch was calculated for the case when the required strains of 2.00 and 1.40 are applied in the $x$ and $y$ directions.

$$\lambda_z = \frac{1}{\lambda_x \lambda_y} = \frac{1}{(2.00 + 1)(1.40 + 1)} = 0.139 \tag{5.5}$$

This $z$ stretch is equivalent to a strain in the z direction of $\varepsilon_z = -0.861$, and a $z$ Lagrange strain of $\varepsilon_{Lz} = -0.490$. It was decided to apply a tolerance of $\pm 10\,\%$ to this target $z$ strain of bladder tissue. This is equal to a strain range in the $z$ direction of $-0.861 \pm 10 = [-0.775, -0.947]$. This strain range corresponds to a $z$ Lagrange strain range of [-0.475,-0.499].

Ideally the entire sheet of bladder tissue should be stretched to within these strain ranges. However, stretching the bladder using discrete points would cause some regions of the tissue to be under-stretched. Therefore, a measure of the efficacy of a particular mode of stretching is the fraction of the tissue which has been stretched to within this specification. The efficacy of bladder stretching of the FEM models was quantified by calculating the fraction of the elements which have a $z$ Lagrange strain within the limits calculated above.

### 5.2.3 Mesh design

The design of the mesh is detailed in Section 2.9. Briefly, the material body was modelled as a cuboid, and consisted of a main area (cuboid) and a border area

which was a perimeter to the main area on two faces. The main area was 13.3 mm, 16.7 mm and 2.50 mm in the $x$, $y$ and $z$ directions respectively. The program variables `hexnumx`, `hexnumy` and `hexnumz` were used to set the number of elements in the $x$, $y$ and $z$ directions respectively of the main area. The width of the border area was defined by the program variable `borderwidth`. The number of elements in the border was equal to the border width (`borderwidth`) divided by border element size (`hexbordersize`), rounded up to the nearest integer. The program variable `pins` was used to set the number of discrete points along each side of the bladder model which applied strain to the model.

### 5.2.4 Mesh density in the border area

Preliminary FEM problems were computed with `hexbordersize` set to a value such that elements in the border of the model were similar to the size of the elements in the main area of the tissue. This was to test the model using a uniform meshes so that the element density was similar in the main area and the border. FEM problems were computed using the methods described in Section 2.9.

It was noticed that meshes which were too fine would often cause FEBio to terminate with an error. Further tests were performed by varying `hexbordersize` whilst not changing the values of the other variables. These indicated that it was the meshing of the border which caused errors to occur; FEBio would solve all problems for very fine meshes in the main area, but meshes in the border which were too fine were not always able to be solved.

To overcome this problem, it was decided to limit the minimum size of the border elements to maximise the chances of a solution being found. A study was carried out to determine a minimum value of `hexbordersize` which would result in very few solutions terminating with an FEBio error.

It was thought that the errors were being caused by an overly fine mesh in the border, resulting in excessive deformations of the elements close to the pins. Inspection of the deformation of these fine meshes showed that elements near the pins were indeed highly deformed. These high deformations appeared greater when fewer pins were used, and when the border width was approximately 10 mm. A greater incidence of FEBio errors seemed to occur when `hexbordersize` was set to approximately 1 mm or less. It was hypothesised that there existed a value of `hexbordersize` below which meshes would be produced which were too fine and would result in FEBio errors, and above which there would be few errors. Errors could then be curtailed by limiting `hexbordersize` to a minimum of this value.

To find this critical value of `hexbordersize`, Matlab was used to generate numerous meshes using combinations of values for `pins`, `borderwidth` and `hexbordersize` in order to find the critical value for a wide range of mesh types. The different values for each parameter is listed below.

- (`hexnumx`, `hexnumy`, `hexnumz`) = (20, 20, 1)
- `hexbordersize` = [0.2, 0.4, 0.6, 0.8, 1.0, 1.2, 1.4, 1.6, 1.8, 2.0] mm
- `borderwidth` = [5, 10, 15] mm
- `pins` = [3, 4]

These sixty meshes were processed using FEBio, and the outcome of each problem (success/error) was recorded.

### 5.2.5 Mesh convergence study

Using a greater number of elements in an FEM model typically results in a more accurate result. However, using more elements required a greater amount of time and computing power to compute the problem. A mesh convergence study was done to find an optimal mesh density which is close to the real-world solution but which can be computed in a realistic time frame.

Models were generated using Matlab with varying mesh densities in the main area of the tissue using the methods described in Section 2.9. The number of elements in the border was calculated so the elements were equal to the size of the elements in the main area, rounded to the nearest whole number of elements. The number of elements in the border was limited so that `hexbordersize` was not less than 1 mm. This was to prevent the FEBio errors which were known to occur with overly fine border meshes. All models had identical geometries, with a border width of 10 mm and three pins along each side of the tissue. Each combination of the follow program parameters were generated using Matlab.

- (`hexnumx`, `hexnumy`) = [(20, 20), (30, 30), (40, 40), (50, 50), (60, 60), (70, 70)]
- `hexnumz` = [1, 2, 3, 4, 5]
- `hexbordersize` = $\geq$1 mm
- `borderwidth` = 10 mm
- `pins` = 3

These thirty FEM problems were solved by FEBio using the methods described in Section 2.9. The percentage of main area elements within 10 % of the target strain was found for each problem. Graphs were plotted of the percentage of elements within 10 % of the target $z$ strain against the number of elements in the $x$, $y$ and $z$

directions. An optimal mesh was chosen by selecting a mesh which had converged close to the most accurate, but using a minimum number of elements.

### 5.2.6 Determination of optimal parameters for stretching flat bladder sheets

In order to determine an optimal mode of stretching flat sheets of bladder tissue for decellularisation, FEBio was used to compute FEM models of flat sheets of bladder tissue stretched with combinations of different border widths and numbers of pins.

Matlab was used to generate FEBio problems using the methods described in Section 2.9. The number of elements in the main area was equal to the optimal mesh density which was found previously. The number of elements in the border was such that the elements were of the same size as the main area, but with a minimum width of 1 mm, rounded to the nearest number of elements. Border widths of 2 mm to 20 mm in 2 mm increments were tested. Pin numbers between 3 and 9 were tested. The parameter combinations which were used are summarised below.

- $(\texttt{hexnumx}, \texttt{hexnumy}, \texttt{hexnumz}) = (30, 30, 1)$
- $\texttt{hexbordersize} = \geq 1\,\text{mm}$
- $\texttt{borderwidth} = [2, 4, 6, 8, 10, 12, 14, 16, 18, 20]\text{mm}$
- $\texttt{pins} = [3, 4, 5, 6, 7, 8, 9]$

These seventy problems were solved using FEBio using the methods described in Section 2.9. The fraction of elements in the main area within 10 % of the target $z$ was calculated. For all of the solved problems, the percentage of elements within the target strain range was plotted against border width and the number of pins. An optimum case was chosen in order to maximise the fraction of elements within the target strain range, but whilst minimising the number of pins and border width. This optimum case was further analysed by observing it in PostView and plotting a histogram of the distribution of the $z$ strains of the elements within the main area.

### 5.2.7 Final FEM model of full-size bladder sheet

All dimensions and strains in this section are given in the $x$ and $y$ directions respectively.

### Tissue dimensions before, during and after decellularisation

After bladder tissue is decellularised it returns to a size which is greater than its original size, but less than the size it is stretched to during decellularisation. Previously it was shown that strains of 2.00 and 1.40 (stretches of 3.00 and 2.40) applied during decellularisation resulted in final strains of 0.926 and 0.488 (stretches of 1.93 and 1.49).

Information was collected from surgeons about the size requirements of an acellular bladder biomaterial. A useful size for such a material was reported to be 80 mm × 80 mm. This is the required final size of a flat sheet of decellularised bladder. The dimensions of the bladder tissue which would produce patches of this size were calculated by dividing these dimensions by the final stretches. These initial dimensions were 41.6 mm × 53.8 mm. The stretched dimensions of bladder tissue during decellularisation were calculated by multiplying these initial dimensions by the decellularisation stretches of 3.0 and 2.4. These decellularisation dimensions were 124 mm × 129 mm. Bladder sheets should be stretched to this size during decellularisation.

### Compensating for insufficient bladder stretching

Modelling the stretching of flat sheets of bladder demonstrated that there were some regions of the tissue which were not stretched to within the required strain range. The regions of the tissue which were under-stretched were localised to the edges of the main area. It was hypothesised that a piece of bladder which was larger than the required size could be stretched, so that there would exist a region within that piece (of the required size) which would be stretched to within the required strain range. This central region could then later be cut out from the entire region to produce a sheet of bladder of the required size, the entirety of which was stretched to within the required strain range.

To test this hypothesis, the FEM model was modified to consist of three distinct regions: i) the patch area, out of which the final patch would be made (sufficiently stretched during decellularisation); ii) the inside border, which surrounds the patch area and is within the region contained by the pins; and iii) the outside border, which surrounds the inside border and is outside the region contained by the pins. If the elements in the patch area were to have a $z$ strain which is within the required range, then this would support the hypothesis, and it would be likely that a tissue patch could be made from the patch area.

In order to model this scenario, the initial and stretched dimensions of the main area (patch area + inside border) need to be known. The dimensions of the patch area were calculated above. To calculate the size of the inside border, it was assumed that the border area would have a uniform width along all sides of the patch area. It was shown that stretching the bladder using five pins along each side results in approximately 80 % of the main area of the bladder being stretched to within the required $z$ strain range. For a stretched patch area of 125 mm × 129 mm, the inside border width which results in the patch area contributing to 80 % of the total of these two areas is 7.5 mm. This calculation is detailed in Appendix F. The size of the main area (patch area + inside border) is therefore 140 mm × 144 mm when stretched and 46.5 mm × 60.0 mm unstretched.

### Modelling and analysis

FEM problems were generated using Matlab using the method described in Section 2.9. The number of elements in the main area were equal to the number used previously. However, extra nodes were placed in the main area along the interface between the patch area and the inside border area. This was to ensure that no elements crossed the boundary between these two areas, and resulted in there being an extra element in each of the $x$ and $y$ directions in the main area of the model. The mesh density in the outside border was equal to the density in the density in the main area, but limited to a minimum width of 1 mm. Five pins were used to stretch the tissue. Previous FEM models showed that this was an optimal number of pins to stretch flat sheets of bladder tissue. Various border widths were tested because the size of the main area was very different to when an optimal size for the border width was found previously. The program parameters which were used are summarised below.

- $(\texttt{hexnumx}, \texttt{hexnumy}, \texttt{hexnumz}) = (31, 31, 1)$
- $\texttt{hexbordersize} = \geq 1$ mm
- $\texttt{borderwidth} = [0, 1, 2, 3, 4, 5, 6, 7, 8]$mm
- $\texttt{pins} = 5$

These problems were solved using FEBio using the methods described in Section 2.9. The percentage of elements in the patch area within the required $z$ strain range was calculated for each problem. A graph was plotted of this percentage against the border width. An optimal border width was chosen to maximise bladder stretching whilst minimising border width. A histogram was plotted of percentage against $z$ Lagrange strain for the optimal border width. The deformation of elements in the patch area of the optimal case was visualised using PostView.

| | `lsqcurvefit` stopping criterion | | |
|---|---|---|---|
| Number of terms | Function tolerance | $X$ tolerance | Maximum function evaluations |
| 1 | abcdefghij | | |
| 2 | adefghij | c | b |
| 3 | | j | abcdefghi |
| 4 | | | abcdefghij |
| 5 | | | abcdefghij |
| 6 | | | abcdefghij |

**Table 5.2: The `lsqcurvefit` stopping criteria for solutions of Ogden model parameters when fitted to experimental data.** Each letter represents a solution variation using a distinct set of randomised starting parameters.

## 5.3 Results

#### 5.3.0.1 Calculation of Ogden model elasticity parameters

The Matlab `lsqcurvefit` function was used to calculate Ogden model parameters from experimental stress–strain data. Elasticity parameters were calculated for a number of Ogden model terms from 1 to 6. Ten solutions were calculated for each term, each solution using a different set of randomised starting parameters. Solutions were calculated for each order, each using ten sets of starting parameters. A solution was found when either the function tolerance dropped below $10^{-12}$, the $X$ tolerance dropped below $10^{-8}$ or when the total number of function evaluations reached a total of 3000. A local minimum was possible if the stopping criterion of a solution was a result of the function tolerance or the $X$ tolerance.

Function tolerance was the stopping criteria for all solutions found for a single Ogden model term. For two Ogden model terms, function tolerance was the stopping criterion for eight solutions, $X$ tolerance was the stopping criterion for one solution and maximum function evaulations was the stopping criterion for one solution. For three terms, $X$ tolerance was the stopping criterion for one solution and maximum function evaluations was the stopping criterion for nine solutions. Solutions with greater than 3 terms were all stopped by a maximum number of function evaluations. These data indicate that Ogden model parameters with three terms or more resulted in the fitted curve being over-parameterised. This information is summarised in Table 5.2.

| | Number of Ogden model terms | | | | | |
|---|---|---|---|---|---|---|
| Variation | 1 | 2 | 3 | 4 | 5 | 6 |
| a | 0.01615 | 0.01212 | 25.98584 | 118442.968 | 52302.8 | 73626 |
| b | 0.01615 | 0.01662 | 0.07295 | 511.635 | 12410.7 | 35007 |
| c | 0.01615 | 0.02412 | 1.07250 | 365.244 | 375733.8 | 301635 |
| d | 0.01615 | 0.01212 | 0.01185 | 1405.391 | 21787.1 | 32898 |
| e | 0.01615 | 0.01212 | 0.34445 | 2.158 | 198890.0 | 973419 |
| f | 0.01615 | 0.01212 | 0.28158 | 1956.656 | 2402.6 | 1461678 |
| g | 0.01615 | 0.01208 | 0.16013 | 269.663 | 496.5 | 997368 |
| h | 0.01615 | 0.01212 | 0.01265 | 632.748 | 6477.9 | 7076 |
| i | 0.01615 | 0.01212 | 0.69802 | 661.371 | 20117.7 | 5726 |
| j | 0.01615 | 0.01208 | 0.12492 | 1.973 | 16390.1 | 7623 |

**Table 5.3: Residuals for each solution of the Ogden model parameters calculated using `lsqcurvefit`.** Each value is the squared 2-norm of the residual of each solution.

The residuals for each of the solution variations are shown in in Table 5.3. The residuals for single-term solutions were all small and of equal value. Two-term solutions had smaller residuals than the single-term solutions, and there were four different residual values. Three-term solutions had residuals which were slightly larger than the one- and two-term solutions, and all had different values. Solutions with greater than three terms had residuals which were very large. The low residuals for the two-term solutions indicate that two terms are enough to provide a very close fit of curve.

A solution was selected to be used when modelling bladder tissue using FEM. Solutions with the smallest residuals and a number of Ogden model terms fewer than three were chosen, corresponding to variations `g` and `j` of the two-term solutions. These two variations represented a single solution. The elasticity parameters for this solution are shown in Equations 5.6 and 5.7. These parameters were used to calculate an equibiaxial stress–strain curve. This data shows good correlation with experimental data (Figure 5.3).

$$c_1 = 0.006623 \qquad m_1 = -1.73837 \tag{5.6}$$

$$c_2 = 0.000220 \qquad m_2 = \quad 7.59122 \tag{5.7}$$

FEBio was used to calculate the outcome.

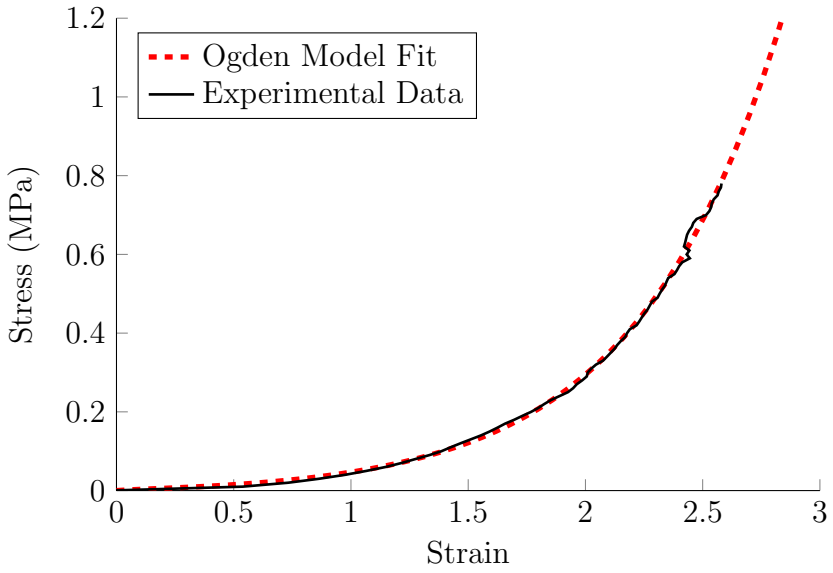


**Figure 5.3: Equibiaxial stress–strain curve of the Ogden model and the corresponding experimental data.** Parameters for the Ogden model were selected to optimise the fit with the experimental data.

### 5.3.1 Mesh density in the border area

Preliminary FEM computations demonstrated that FEBio was unable to compute problems which had a high mesh density in the border area. The mesh density in the border area was controlled by the variable `hexbordersize`. It was hypothesised that a minimum value of `hexbordersize` could be set which would result in the majority of generated meshes being albe to be sucessfully computed by FEBio. A study was done to find this critical value of `hexbordersize`.

FEBio problems were generated with 10 different values of `hexbordersize` varying from 0.2 mm to 2 mm. Six meshes were generated for each value of `hexbordersize`. The parameters controlling the border width and the number of pins were also varied. Of the 60 meshes which were generated, 51 were computed successfully and 9 resulted in errors. Errors only occurred for meshes with `hexbordersize` less than 1 mm. No errors resulted when meshes were computed with `hexbordersize` set to greater than or equal to 1 mm. The success rates for each value of `hexbordersize` is shown in Figure 5.4. This data supported the hypothesis that there is a critical value of `hexbordersize`, below which there is an increased chance of the resulting mesh being unsolvable. The critical value chosen to limit the minimum width of border elements in subsequent meshes was 1 mm.

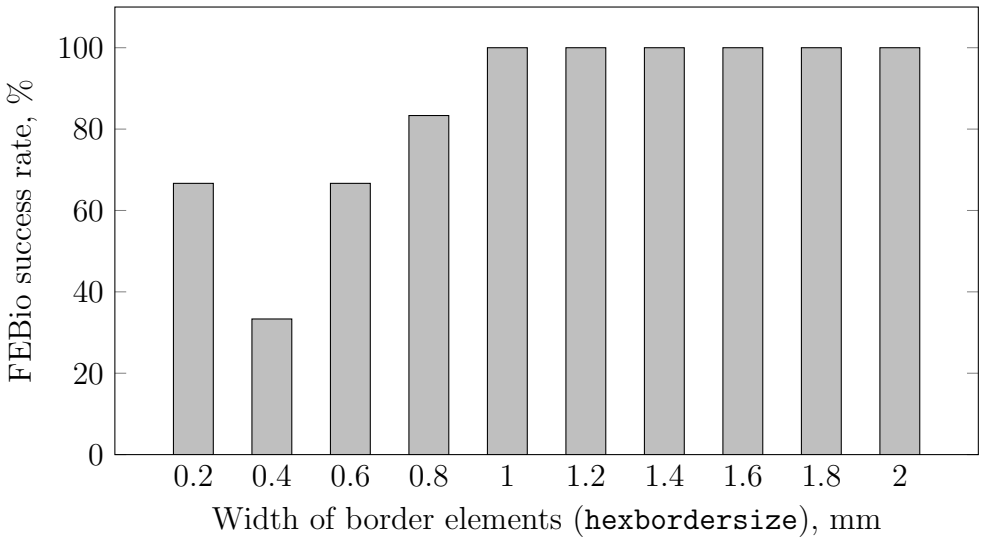


**Figure 5.4: The percentage of successful FEBio computations for various widths of border elements.** Each border element width represents meshes computed with border widths of 5 mm, 10 mm and 15 mm and numbers of pins of 3 and 4.

### 5.3.2 Mesh convergence study

A mesh convergence study was carried out in order to find an optimal mesh density to use in the main finite element studies. A single model geometry with 3 pins and a border size 10 mm was used. Numerous meshes were generated with the number of elements in the $x$ and $y$ directions varying from 20 to 70 (in 10 element increments) and the number of elements in the $z$ direction varying from 1 to 5 in unit increments. The width of elements in the border area was set to match the size of elements in the main area, but limited to a minimum of 1 mm. The number of elements in the main area within 10 % of the target $z$ strain was used to compare the accuracy of the different meshes.

All thirty problems except one successfully solved by FEBio. Figure 5.5 shows that the number of elements within 10 % of the desired strain increases as the number of elements in both the $x$ and $y$ directions increases. There is a dramatic increase from 20 elements to 30 elements, however there it little change for numbers of elements greater than 30. Figure 5.6 shows how the number of element within 10 % of the desired strain varies with the number of elements in the $z$ direction. Changing the number of elements in the $z$ direction has little effect on the tested result.

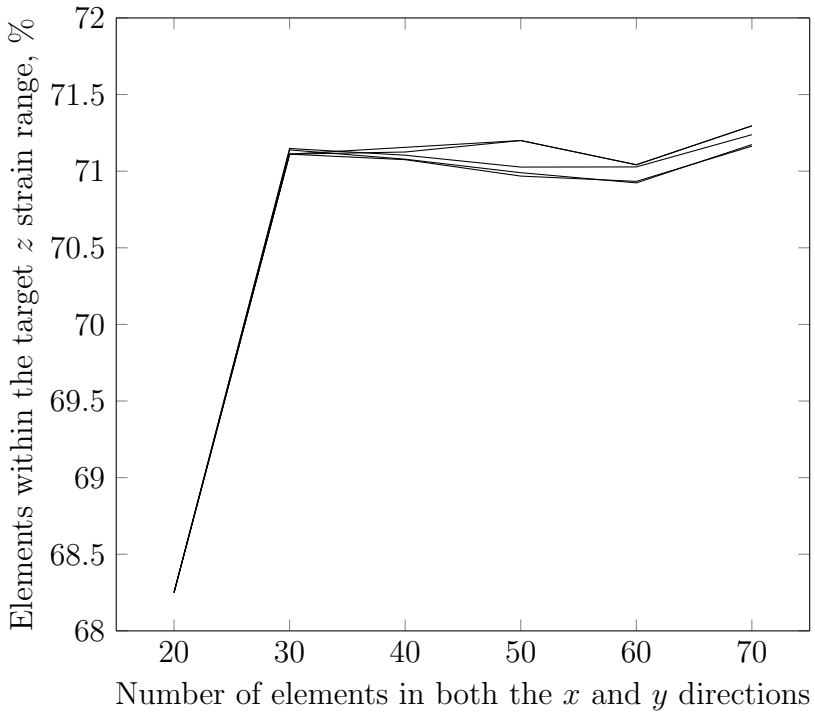


**Figure 5.5: Mesh convergence for a varying number of elements in the $x$ and $y$ directions.** Each line represents meshes with an equal number of elements in the $z$ direction.

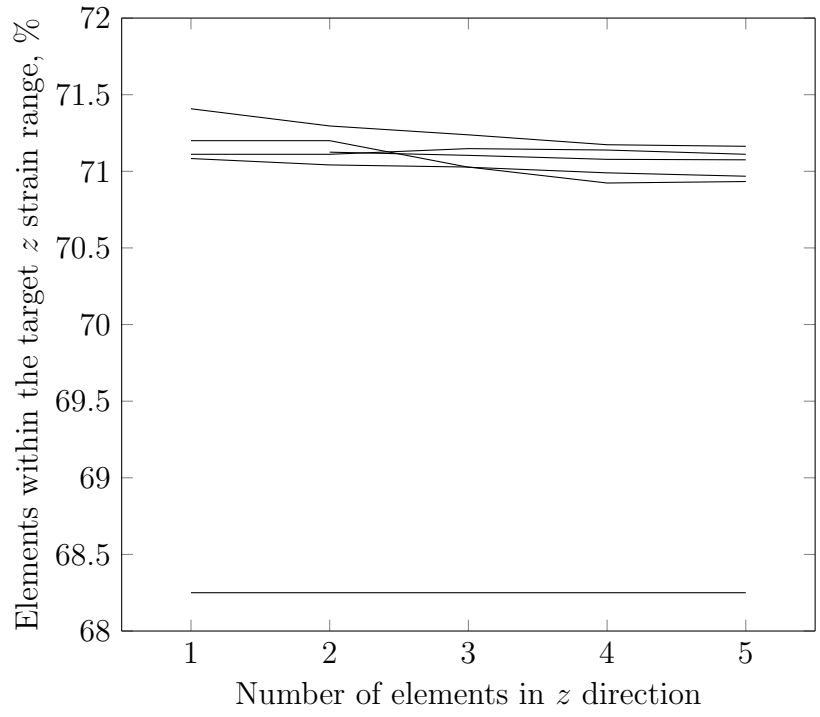


**Figure 5.6: Mesh density investigation, varying mesh density in the z direction.** Each line represents meshes with an equal number of elements in the $x$ and $y$ directions.

### 5.3.3 Finding an optimal configuration for stretching flat sheets of bladder tissue

In order to find an optimal regime for stretching flat sheets of bladder tissue, FEBio was used to model different configurations of stretching the tissue by varying the number of pins the tissue was stretched with and the width of border around the main area of the tissue. The effectiveness of each regime was compared by calculating the number of elements in the main area which were within 10 % of the target $z$ strain.

The $z$ strain of the elements varied with the number of pins used to stretch the bladder. The relationships between these variables are shown in Figure 5.7. The number of elements within the required $z$ strain limits generally increased as a greater number of pins were used to deform the tissue. There was a large increase in the number of elements within the required strain range as the number of pins increased from 3 to 4, but less of an increase as the number of pins was increased from 4 to 5. Increasing the number of pins above 5 had little effect on the $z$ strain of elements.

Figure 5.8 shows how the width of the border affected the $z$ strain of the elements. A wider border generally increased the number of elements being within the required strain range. For small border widths, increasing the width resulted in a significant increase in the number of elements within the required $z$ strain limits. For large border widths (approximately 8 mm and above), the $z$ strain of the interested elements was invariant with changes in the border width. The greater number of pins, the less effect the border width had on the strain of the elements. For 5 pins, there is only an increase in the number of elements within the required strain range of 2.5 % if the border width is increased from 4 mm to 12 mm.

A histogram of the $z$ strain of the elements of a bladder modelled with 5 pins and a border of 4 mm is shown in Figure 5.9. The vast majority of the elements are within the required strain range. A small number of elements (10 out of 400) are over the desired strain. Most of the elements not within the required strain range are close to the required $z$ strain. Visual representations of the distribution of the $x$ and $y$ strains in this scenario are shown in Figure 5.10. The distributions of each of these strains were not uniform throughout the model, and there were some regions of the model which were over-stretched, and other regions of the tissue which were under-stretched. Projecting horizontally from each pin were regions where the $x$ strain was high and the $y$ strain was low, and projecting vertically from each pin were regions where the $x$ strain was low and the $y$ strain was high. Therefore,

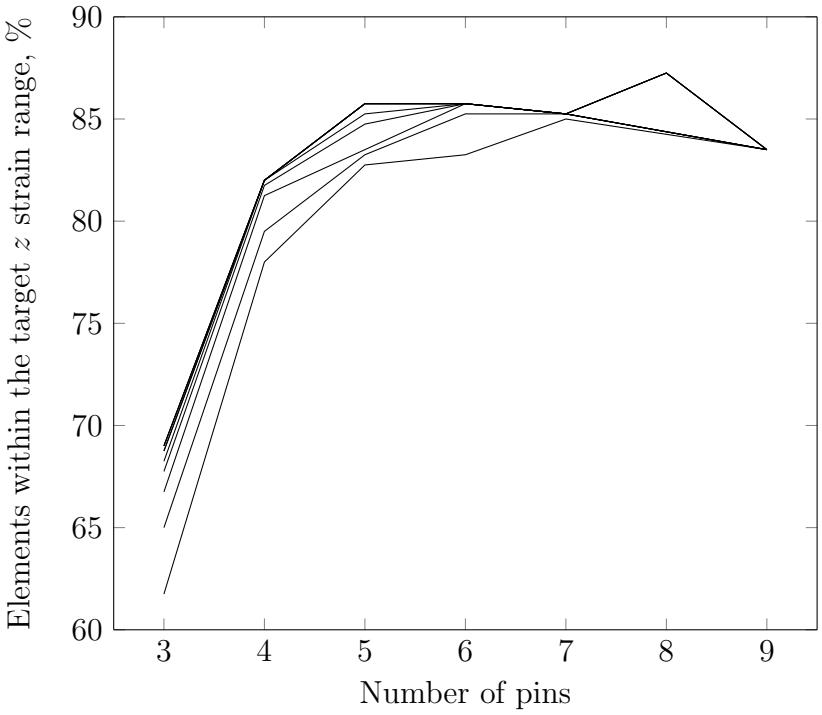


**Figure 5.7: Variation of the number of elements within the target strain range with the numbers of pins used to stretch the modelled tissue.** Each line is plot of a single border width.

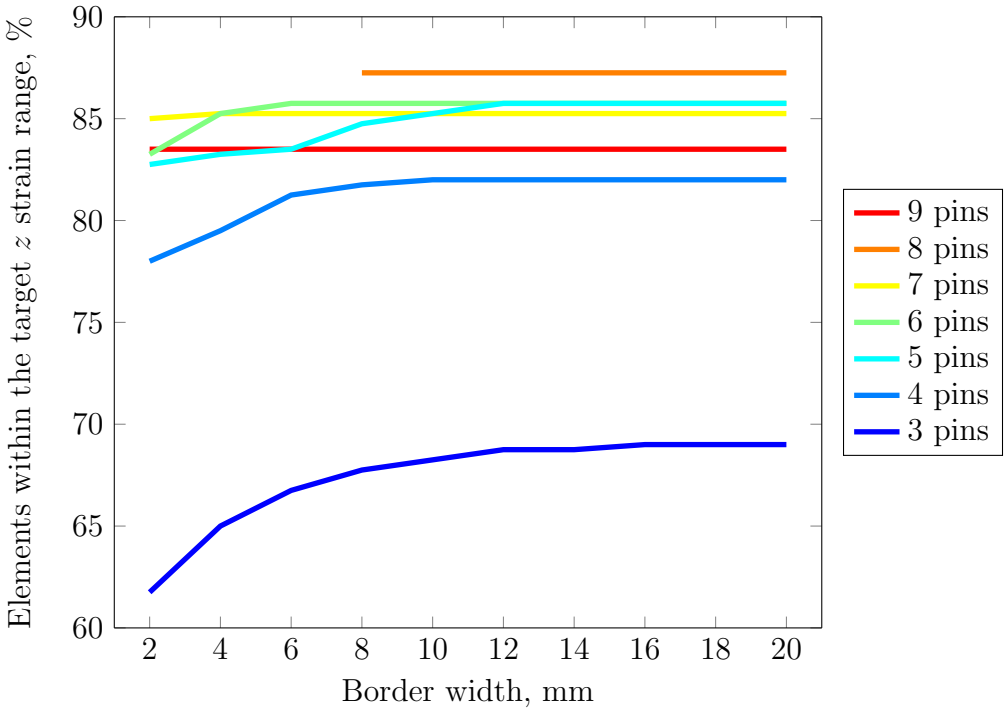


**Figure 5.8: Variation of the number of elements within the target strain range with the border width of the modelled tissue.** Each line is a plot of a single number of pins.

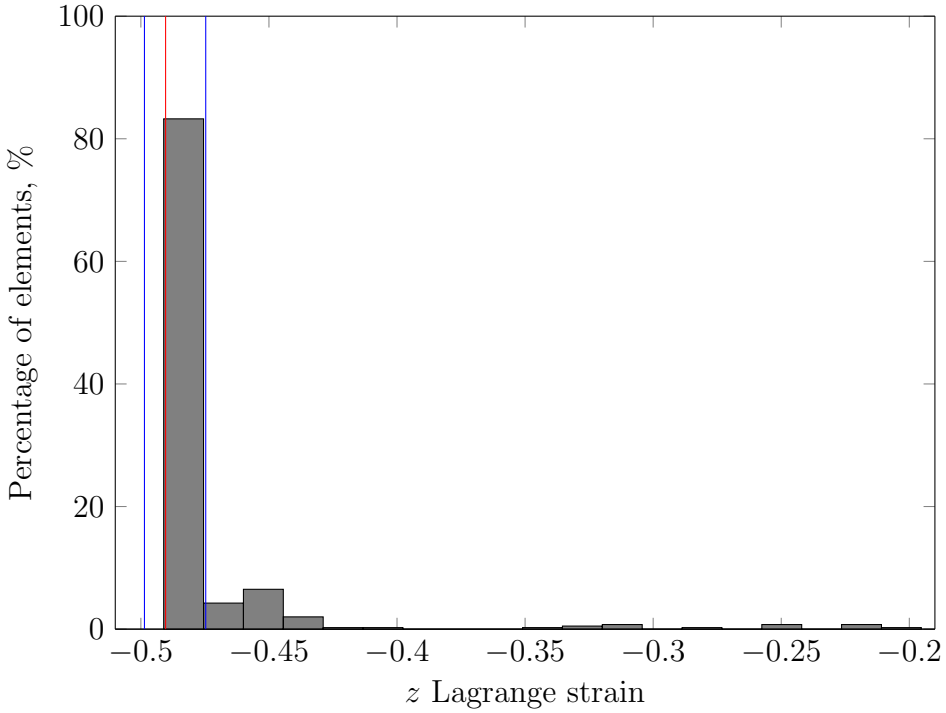


**Figure 5.9: Histogram of the $z$ Lagrange strains of elements for a model stretched using 5 pins and a border of 4 mm.** The red line is the target $z$ strain, and the blue lines are the upper and lower limits of the $\pm 10\,\%$ target $z$ strain range.

regions where the $x$ strain was high coincided with regions where the $y$ strain was low, which resulted in a uniform distribution of the $z$ strain throughout the majority of the tissue. This can be seen in Figure 5.11. The border region and the areas close to the pins remained under-stretched.

### 5.3.4 Modelling of a fully-stretched patch area of the required size

In order to test the hypothesis that stretching a sheet of bladder tissue which was larger than required would result in a central region of the tissue that was all stretched to within the required strain specifications, FEBio was used to model a bladder tissue sheet, and a central region was analysed. The contraction of the tissue following decellularisation was also taken into account so that a biomaterial of the required clinical size could theoretically be produced from the size of the modelled graft. Several different models were solved using varying border widths.

One model could not be computed by FEBio successfully. This model had a border width of 8 mm. All computed models had a number of elements with a $z$ strain within the required range of over 94 %. Figure 5.12 shows how the percentage of

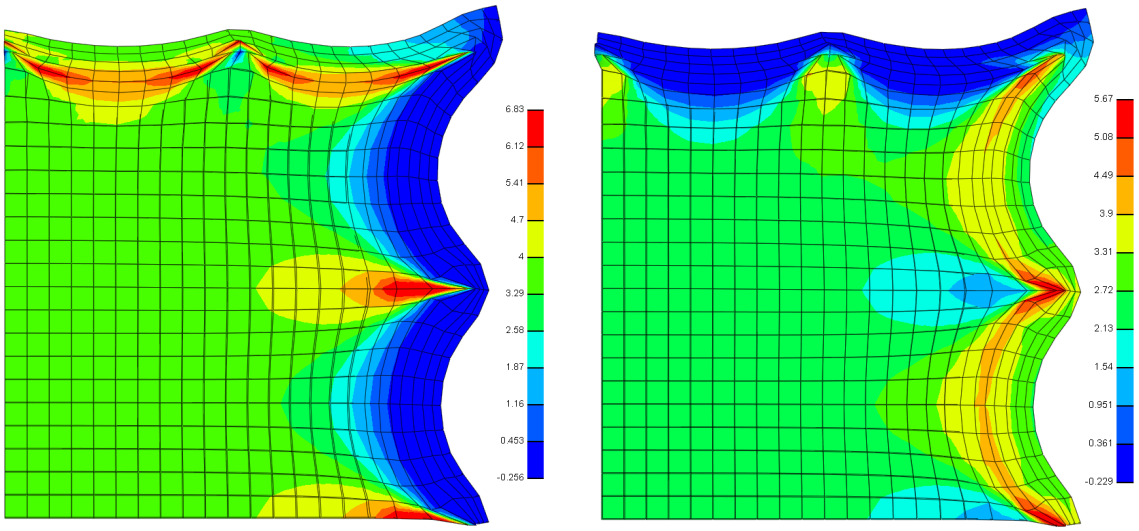


**(a)** $x$ strain **(b)** $y$ strain

**Figure 5.10: Distribution of the $x$ and $y$ strains in the model of bladder tissue stretched using 5 pins and border width of 4 mm.** Individual elements can be seen. The colouring indicates the magnitude of the Lagrange strain.

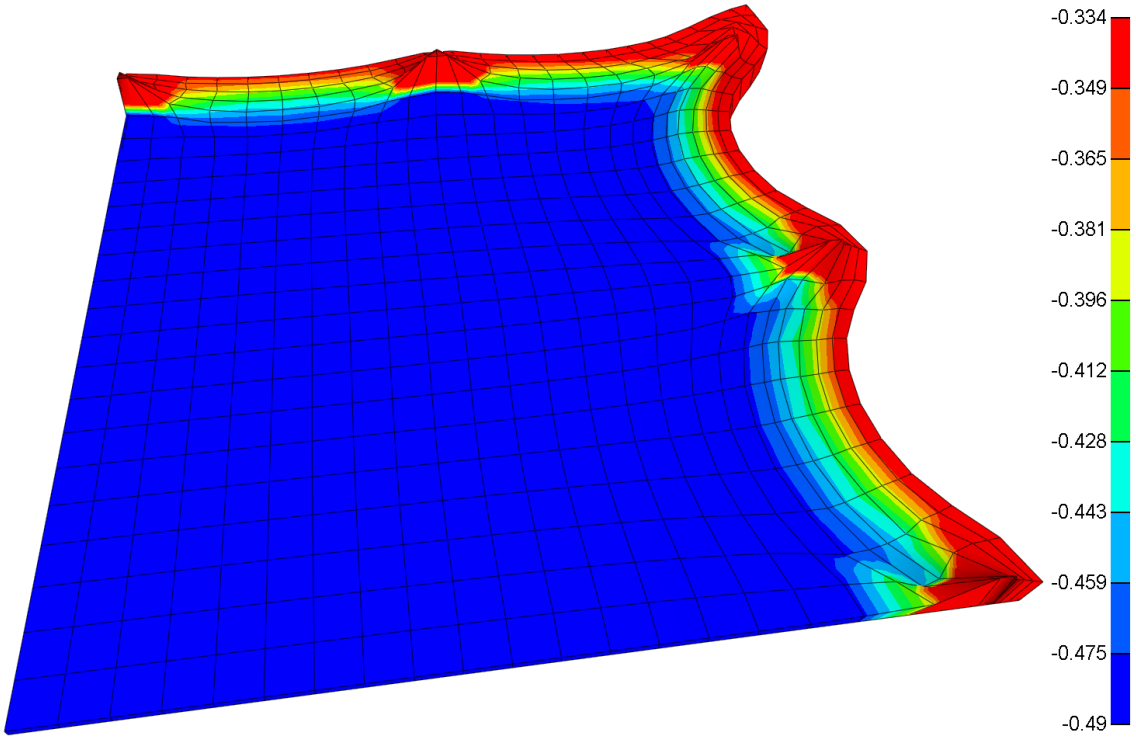


**Figure 5.11: Distribution of the Lagrange $z$ strain in the model of bladder tissue stretched using 5 pins with a border of 4 mm.** Individual elements can be seen. The colouring indicates the magnitude of the strain. The darkest blue shading represents the target $z$ strain range.

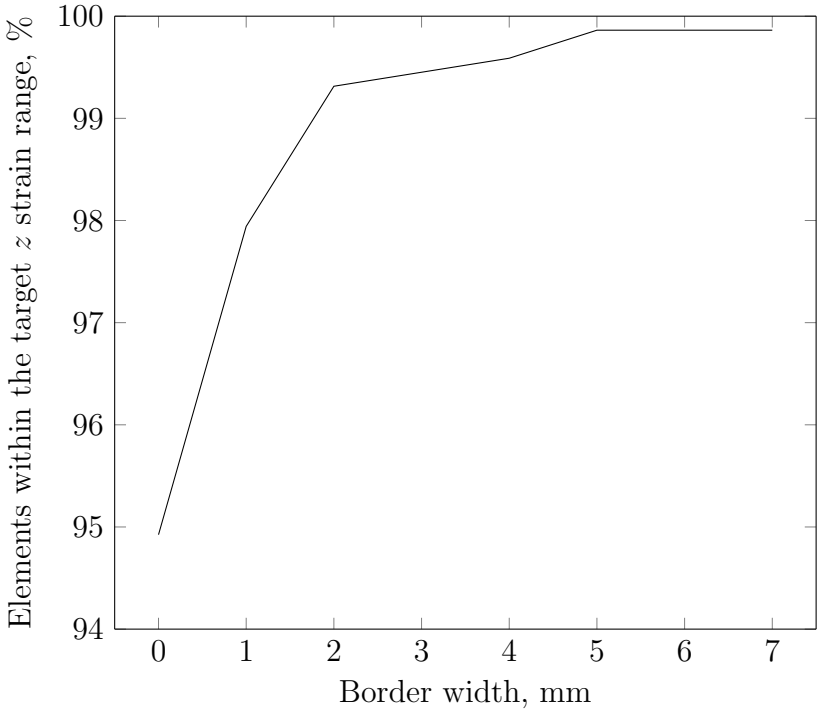


**Figure 5.12: The percentage of elements within the required $z$ strain range of the final model for different border widths.**

elements within specification varies with changes to the border width. Models with border widths greater than or equal to 2 mm had over 99 % of the elements within the required limits.

A histogram of the $z$ strain of the elements for the model with a border width of 2 mm is shown in Figure 5.13. The majority of elements are close to the target strain and within the target strain range. A negligible minority of elements have a strain which is outside the required range.

A graphical representation of the tissue model is shown in Figure 5.14. Elements near the pins and along the edges of the tissue are distorted, but elements nearer the centre of the tissue are less distorted. The edges of the central region of interest follow the scalloped shape of the edges of the tissue, but the shape is less pronounced than that of the tissue edges.

## 5.4 Discussion

Stretching bladder tissue in a flat sheet configuration would be compatible with a scalable manufacturing process. This may be a viable method of applying biaxial strain to the tissue so that it is sufficiently stretched for decellularisation. In order to apply uniform biaxial strain to a rectangular material, a continuous clamp would

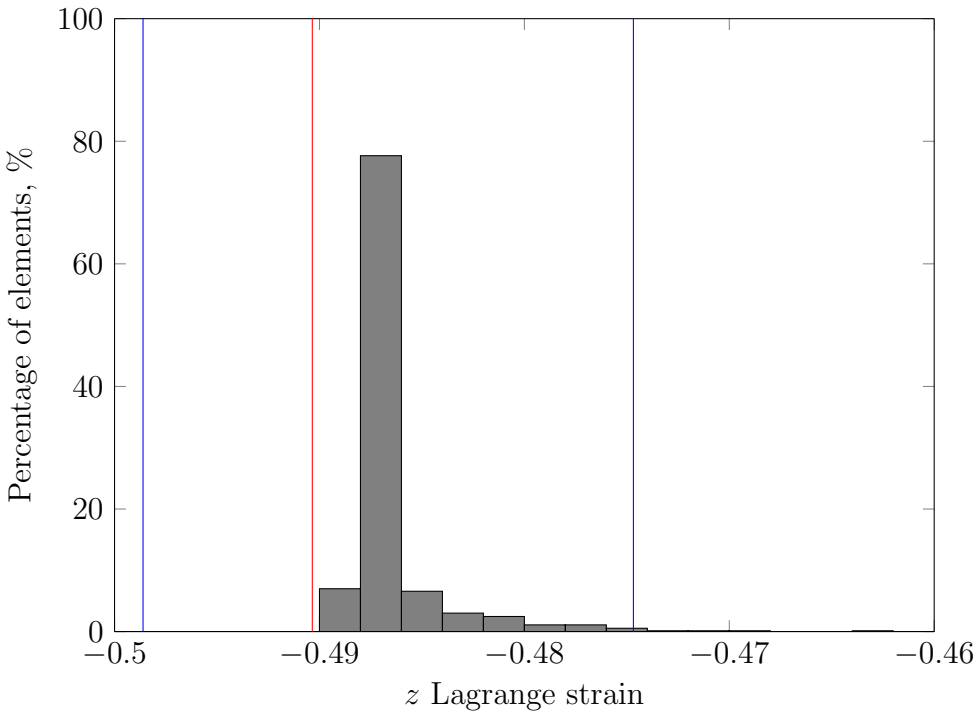


**Figure 5.13: Histogram of the element strains in the central 80 % of the main bladder area, for a border width of 2 mm.** The red line is the target $z$ strain, and the blue lines are the upper and lower limits of the ±10 % target $z$ strain range.

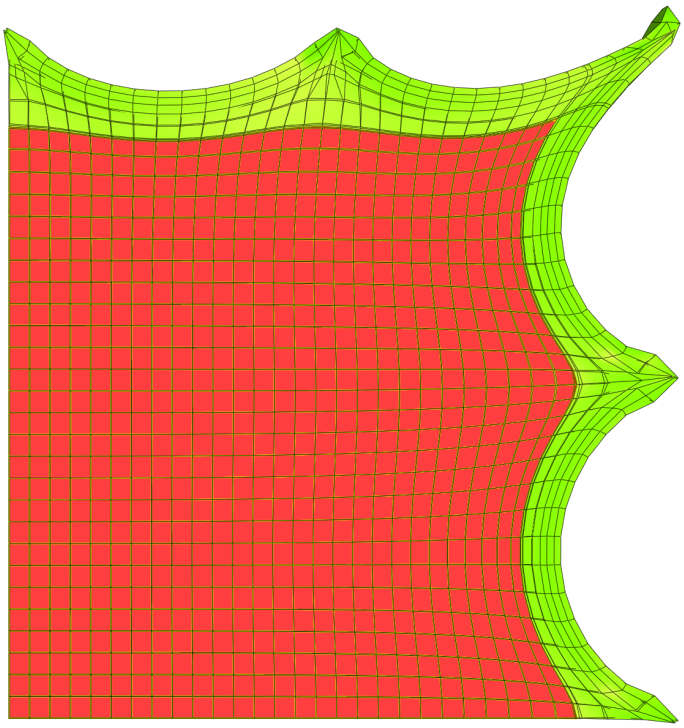

**Figure 5.14: A view of the bladder tissue model designed so the central region of the tissue should be stretched to within the required strain range, with an outside border width of 2 mm.** The elements in the central 80 % of the main area of the tissue are highlighted in red.

need to be applied to each side of the material. However, these clamps would restrict the deformation of the tissue, and so could not be used to apply biaxial strain to materials which undergo large deformations, such as soft tissue. An alternative method of applying biaxial strain is to use discrete points. This is a viable method which is commonly used in the literature for deforming biological tissue (Cooney *et al.*, 2016; Shahmansouri *et al.*, 2016; Khoiy & Amini, 2016; Macrae *et al.*, 2016). However, when materials are stretched using discrete points, the region of material bounded by the points is not uniformly stretched. Stretching the bladder tissue using discrete points would be suitable for the decellularisation process because the tissue does not need to be uniformly stretched; the tissue only needs to be stretched adequately for decellularisation to occur. In order to ensure that bladder tissue would be sufficiently stretched using discrete points, tissue stretching was modelled using FEM. This enabled several stretching configurations to be analysed in order to find an optimal method of stretching so that the required strains were applied to a tissue region of the required size.

No articles were found in the literature which aimed to use finite element modelling in order to model the deformation of porcine bladder tissue. However, the Ogden constitutive model has been used to model many other types of soft tissues, including porcine brain tissue (Rashid *et al.*, 2013) and porcine linea alba (Cooney *et al.*, 2015). The Ogden constitutive equation was therefore chosen because of its ability to model complex nonlinear stress–strain relationships. Lyons *et al.*, 2014 used the Ogden model to model the uniaxial and biaxial behaviour of porcine rectus sheath. An average stress–strain response was used to calculate the models, which resulted in the computation of numerous solutions. Similarly in this chapter, multiple solutions were also computed from a single stress–strain response due to the nonlinear nature of the model. The stress–strain data of porcine cerebellum tissue was modelled by Li *et al.*, 2015 using the Gent, Fung, Ogden and exponential models. All models demonstrated a good fit to the data, however the best fit to the data was found using the exponential model, followed by the Ogden model. It is likely that a better fit would have been found if a greater number of terms had been used, compared to the single term used in the study. In contrast, Zuo *et al.*, 2016 performed uniaxial tensile testing on human and ovine mitral valves using three Ogden terms to fit the model to the experimental data. This was able to capture the nonlinear stress–strain response of the human tissues in sufficient detail, however the ovine test data did not appear to be adequately represented, and may have benefited from being modelled using a greater number of terms or a different model. Therefore, when the mechanics of bladder tissue were modelled in this chapter, multiple solutions to the model were found for multiple numbers of terms in order to find an optimal number

of terms which would suitably fit the model to the experimental data.

The elasticity parameters of the Ogden model were found for ten different sets of starting parameters for a number of model terms from 1 to 6. An Ogden model which uses a single term is able to exactly model a stress–strain response which follows the shape of an exponent, and adding a second term means that the model is able to exactly model a response which is the superposition of two exponent curves. The stress–strain curve of the experimental data appeared to roughly follow the shape of a single exponent. If this had been the case, a single term would have sufficed and using two terms would have over-parameterised the function. However, biological tissue is known to have a toe region, followed by a transition into a linear region. Because such a curve has two phases, this response may benefit from being modelled using two terms. The results demonstrated a good fit with the data for a single term, but a better fit for two terms, with the means of the residuals equal to 0.0161 and 0.0138 respectively. This supports the theory that the stress–strain response mostly follows an exponential curve, but that a second term to correct for the linear region was a better model of the response. Using three or more terms was likely to have over-parameterised the model of the two-phase experimental data. The stopping criteria for these functions were equal to 'Maximum function evaluations' for all sets of starting parameters except one, and the residual means for three, four, five and six terms were equal to 2.88, $5.03 \times 10^3$, $6.52 \times 10^6$ and $1.23 \times 10^6$ respectively, which indicated that those solutions were indeed over-parameterised. The fit of the model curve against experimental data (Figure 5.3) demonstrated that the calculated parameters were able to model the required stress–strain response accurately up until the maximum strain of 2.6 given by the data. The strains which were later applied to the model (2.00 and 1.40) were below this, so deformation of the material was kept to within the known range of deformation.

Distending bladders during decellularisation applies biaxial strain to the tissue, which results in a reduction of the tissue thickness. It has been reported that the reduced thickness allows adequate diffusion of decellularisation solutions into the tissue (Bolland *et al.*, 2007). In order to quantify the efficacy of the stretching in each FEM model, a single measurand was required. The $z$ strains of the elements of the models were used to compare the stretching efficacy of the models because a change in $z$ strain corresponded to a specific change in tissue thickness. In the previous chapter it was seen that strains of 2.00 and 1.40 in the circumferential ($x$) and longitudinal ($y$) directions were suitable strains to apply to the tissue to result in complete decellularisation. Soft tissue is known to have a Poisson's ratio which is close to 0.50 (Cooney *et al.*, 2016), and subsequently the material was assumed to be incompressible. Strains of 2.00 and 1.40 in the $x$ and $y$ directions for such tissue

correspond to a strain of $-0.861$ in the $z$ direction. Although applying these strains to tissue had been seen to result in complete decellularisation, it was hypothesised that stretching the tissue to within a strain range close to this value would still result in successful decellularisation. It was decided that the tissue would be considered suitably stretched for decellularisation if it fell within $\pm 10\,\%$ of the target $z$ strain. As a result of this, models were compared by calculating the fraction of elements in each model which had a $z$ strain which was within this range. This was a relevant and effective measure of stretching efficacy which was able to be used to compare the different models.

Several studies in the literature, and previous studies in this thesis, have demonstrated that the mechanical properties of bladder tissue are anisotropic (Bullock *et al.*, 1994; Korossis *et al.*, 2009). The Ogden model is effective at modelling complex nonlinear stress–strain responses, however it is only able to do this for isotropic materials. To fit the model to the biaxial experimental data, a stress–strain curve was used which was the average of the circumferential ($x$) and longitudinal ($y$) stress–strain curves. Bladder tissue is stiffer in the $y$ direction than in the $x$ direction, and therefore would deform more in the $x$ direction and less in the $y$ direction than is shown in the models. However, in the biaxial stretching regime which was modelled, it is likely that a shift in stiffness between the $x$ and $y$ directions will still result in a similar $z$ strain, particularly because similar strains were applied in each direction. As a result of this, the effect the isotropic nature of the model has on the stretching measure is likely to be small for this biaxial stretching regime.

Solutions are not always able to be computed for finite element problems. Factors such as mesh density and solver parameters affect whether a problem can be computed successfully. A study of mesh density in the border area demonstrated that setting the width of border elements to less than 1 mm greatly increased the likelihood of the computations terminating erroneously, as shown in Figure 5.4. The combinations of mesh parameters which resulted in failed computations, and inspections of the failed meshes suggested that the errors were a result of excessive deformations of elements in the border region which were close to pins. It was therefore likely that several bladder stretching configurations in later studies would be unable to be computed. This was likely to have resulted in numerous missing data points in the collected data. In order to prevent meshes being generated which were unable to be computed by the finite element solver, a minimum limit was set for the size of the elements in the border region of the model. As a result of this, there was only one failed computation in the study of optimal bladder stretching parameters. It is possible that errors could have been prevented by using a finer mesh which would have modelled the deformation of elements around the pins with

greater accuracy. However, the contribution of the deformation of these elements to the measured outcome—$z$ strain—was likely to be very small, and therefore unnecessary for our purposes, and would have resulted in long computation times.

A more accurate solution is typically found when a greater number of elements is used in the mesh of a finite element model. However, using a large number of elements is computationally demanding and may be unfeasible to compute due to the length of time the computation would take. A mesh convergence study was carried out in order to find an optimal mesh density which would give a solution close to the real-world case without using an unnecessary number of elements. The results showed that a change in the number of elements in the $z$ direction had little effect on the outcome (Figure 5.6). This is not surprising, given that no deformation was applied in the $z$ direction, and therefore the deformation seen in this dimensions was approximately uniform. The number of elements in the $x$ and $y$ directions did affect the outcome, however little change was seen in the result for numbers of elements above 30 in these directions (Figure 5.5). This demonstrated that this was the optimal number of elements for use in the main study. However, the curves did not seem to follow a typical mesh convergence curve. This may be because the mesh density of the border region was being limited so the elements were not wider than 1 mm, as discussed previously. However, it is possible that an optimal solution may have been reached for the stretching regime.

Flat sheets of bladder tissue were modelled in numerous stretching configurations in order to find an optimal configuration for decellularising flat sheets of bladder. Using discrete points appeared to be an effective method for applying biaxial strain in order to reduce the thickness of the bladder tissue, as indicated by the meshes of the deformed models. This was further demonstrated, because although there were regions of the tissue where the $x$ strain was low, in those same regions the $y$ strain tended to be high, and *vice versa*. This can be seen in Figure 5.10. As a result of this, the $z$ strain distribution across the main area of the models was visually uniform, with some variation close to the edges (Figure 5.11).

Increasing either the thickness of the tissue border or the number of pins used to stretch the tissue tended to increase the number of elements within the main region of the tissue which were stretched to within the target strain range (Figures 5.7 and 5.8). This is not surprising, given that using a greater number of pins results in the tissue being more evenly stretched; an infinite number of pins would result in uniform stretching. Also, the border around the tissue acted as a 'frame' which assisted in applying strain to the main area of the tissue in the regions between the pins. As a result of this, a thicker border resulted in the main area being more uniformly stretched. The number of elements stretched to within the target strain

range varied from a mean of 67.4 % with 3 pins, 81.3 % with 4 pins, 84.8 % with 5 pins to a mean of 87.3 % with 8 pins. Because little improvement in the outcome was observed when the number of pins used to stretch the tissue was increased beyond 5, it was concluded that 5 was an optimal number of pins to stretch the bladder tissue. A study by Eilaghi *et al.*, 2009 also found five attachment points to be an optimal number of points for stretching square material, however this number is likely to vary with each intended application. When varying the border width used to stretch the modelled bladder tissue, the number of sufficiently stretched elements ranged from 79.0 % for a border width of 2 mm to 82.6 % for a border width of 20 mm. Therefore, varying the number of pins bladder tissue was stretched with had a greater affect on the uniformity of the strain field than the width of the border. It has also been observed in the literature that the uniformity of the stretched area can be increased by increasing the number of displacement points, and that the number of points has a greater affect on uniformity than the width of the border region (Eilaghi *et al.*, 2009).

In the study by Eilaghi *et al.*, 2009, whereby the stretching of square material using discrete attachments points was investigated, it was found that the more spaced out the pins along each side of the material were, the more uniform the strain field in the centre of the tissue. They also found that the peak strain in the centre of the tissue was always less than the strain applied, as calculated from the displacement of the attachment points. This was not found to be the case when modelling bladder tissue, where the strain in the centre of the material was found to be equal to the gross applied strain (as shown in the histogram in Figure 5.9), but less in other areas. However, the arrangement of pins which were used when modelling the bladder represented the most spaced out the pins were able to be, so that the outer pins of one edge were shared by the outer pins of each adjacent edge, unlike the study by Eilaghi *et al.*, 2009. This suggests that the layout of attachment points used to stretch bladder represented a more optimal method of uniformly stretching tissue biaxially than were tested in the study. However, it may have been of benefit to test other arrangements of discrete attachment points.

Other geometries could have been used to produce a reduction in tissue thickness using biaxial strain. An investigation into the biaxial stretching of hyperelastic material of varying geometries was undertaken by Avanzini & Battini, 2016. They stretched material using various shapes of cruciform, and found that these shapes tended to be easier to mount onto testing equipment. However the square material stretched using discrete points resulted in a strain field which was as uniform as the most uniform of all the different types of cruciform which was tested, despite the non-uniform nature of the loading method. This aligns with the findings of this chapter,

which demonstrated a large region of bladder tissue stretched to within the required specifications. They also found high stress concentrations around the positions of the discrete points, something also found when bladder tissue was modelled, and should be taken into consideration when designing a method of stretching bladder tissue which avoids damaging the tissue. A main advantage of stretching a square piece of tissue using discrete points is that significantly less tissue is required (Zhao *et al.*, 2014), which is a significant advantage for a manufacturing process for bladder decellularisation, where both space and tissue size may be limited.

Increasing the number of pins to 9 resulted in a significant decrease in the measured outcome. This was likely to have been caused by a feature of the mesh design due to how the model was discretized. For a given number of pins, there reached a point where increasing the border width further no longer resulted in more elements being stretched to within the required range. This point should have been chosen in order to maximise tissue stretching for a given number of pins. However, using a thicker border would require a greater amount of tissue to be used in the process, therefore using a smaller border would be a more efficient use of bladder tissue. For a border width greater than 4 mm the improvement in the number of adequately stretched elements was minimal, therefore an optimal border width of 4 mm was chosen for this initial stretching mode.

The model revealed that stretching the bladder using discrete points lead to an uneven distribution of both the $x$ strain and the $y$ strain throughout the tissue. The strains were uniform in the centre of the tissue, however there were regions of high $x$ strain and low $y$ strain projecting horizontally from each pin, regions of low $x$ strain and high $y$ strain projecting vertically from each pin. As a result of this, the distribution of the $z$ strain of the tissue was much more uniform than either the $x$ strain or the $y$ strain, and resulted in 79.5 % of the tissue being stretched to within the target $z$ strain range previously mentioned. This apparent superposition of the $x$ and $y$ strains is a result of the $z$ stretch being equal to the inverse of the product of the $x$ and $y$ stretches (due to material incompressibility), and therefore the $z$ strain is able to be constant for varying $x$ and $y$ strains provided that the $x$ and $y$ strains vary inversely to one another.

Although flat sheets of material cannot be deformed to produce a completely uniform biaxial strain field, Nielsen *et al.*, 1991 reported that stretching material biaxially can lead to a region in the centre of the tissue which is stretched to within a certain range of the applied strain. In order to produce a patch whereby the entire region was made from tissue stretched to within the target $z$ strain range, it was hypothesised that stretching a region of tissue which was larger than required would result in a central region of the tissue which was sufficiently stretched, and a border around this which

was not sufficiently stretched but could be dissected from the central region after processing. The final decellularised bladder patch material would consist of solely this central region of tissue. Information was gathered from surgeons that in order to be of use clinically, a patch of decellularised bladder biomaterial would have to be 8 cm × 8 cm in size. A relationship found in the previous chapter (Figure 4.14) was used to calculate the initial size of tissue required in order to produce tissue of this required final size, and it was demonstrated in this chapter that the central elements of the modelled tissue were stretched to the required thicknesses. Subsequently, this information was combined to model the stretching of bladder tissue with a central region of the required size, with a border around this which would be still inside the region marked out by the pins. The dimensions of these regions were calculated so that the central region made up 80 % of the area of both regions, because stretching bladder tissue using 5 discrete points resulted in 82.8–85.8 % of the elements being stretched to within the desired strain range. The results (Figure 5.12) showed that, for outside border widths of 2 mm or more, over 99 % of the elements in the central region were stretched to within the required $z$ strain range. This supported the hypothesis that a central region of a flat sheet of tissue can be stretched to the required specifications for decellularisation. Although this method of stretching a central region of tissue requires more tissue than the previously investigated method, it gives a much greater assurance that the tissue will be adequately stretched.

When the deformations of these models were observed visually, shown in Figure 5.14, it was observed that when the tissue was stretched, the central regions no longer took on a rectangular shape; there were scooped regions in the areas of the tissue between the pins. The contracted final shape of the tissue would therefore not be rectangular, and an 8 cm × 8 cm square cut from this region would be made up of mostly the central region (80 % of the main area), but also a small amount of the inner border (20 %). This means that there could be regions of the final tissue which were not stretched to within the required specifications. The regions which are at most risk of this are the points half-way between each pin. However, it is highly likely that these regions were stretched so they are very close to being within the required strain range, as shown by the histogram of element strains (Figure 5.13). They are therefore unlikely to be stretched insufficiently for decellularisation. Also, the scooping of the edges will be less pronounced when the tissue is no longer stretched due to contraction of the tissue following decellularisation. Renderings of the deformed models showed that this scooping effect could cause greater problems for tissue stretching in the $x$ direction, because the scooped effect seen in the edges was more pronounced in the $x$ direction than in the $y$ direction. This was due to the greater strain which was applied in the $x$ direction. However, real bladder tissue is

stiffer in the $y$ direction and less stiff in the $x$ direction than in the isotropic material which was modelled, and therefore this effect is likely to be less pronounced with real bladder tissue.

## 5.5 Conclusions

For compatibility with a commercial manufacturing process, it was decided to decellularise bladder tissue in a flat sheet configuration. The deformation of flat sheets of bladder tissue was modelled using FEM in order to find an optimal mode of applying a sufficient amount of strain to the material. Experimental stress–strain data was used to calculate the parameters of a two-term Ogden model. This was a sufficient number of terms for the model to accurately represent the response of the data. The strains required for decellularisation (2.00 and 1.40), found in the previous chapter, represent a strain of $-0.861$ in the $z$ direction. It was decided that the tissue would be sufficiently stretched if it was stretched to within 10 % of this strain. The fraction of elements within this target strain range was used as an effective measure of the efficacy of bladder stretching between different models.

Modelling the stretching of bladder tissue demonstrated that stretching the material using discrete points was an effective method to uniformly reduce the thickness of the tissue. Increasing both the border width and the number of pins increased how uniformly the tissue was stretched. It was concluded that an optimal number of pins to stretch the bladder with was 5 pins along each edge of the material. Elements which were not stretched to within the required strain range were localised to the edges of the material. It was hypothesised that a piece of bladder tissue could be stretched such that a central region would be stretched to within the target strain range. The stretching of a piece of bladder was modelled which had a main area (bounded by the pins) of 46.5 mm × 60.0 mm. Over 99% of the elements in the central 80 % of this area of tissue were stretched to within the required $z$ strain range when an outside border of 2 mm or greater was used. Theory developed in the previous chapter predicts that this central region would become approximately 8 cm × 8 cm square after decellularisation. This is the required size of a decellularised bladder patch, per surgical requirements.

# Chapter 6

# Detailed design and test of novel bladder decellularisation equipment

## 6.1 Introduction

A scalable manufacturing process for decellularising bladders should apply adequate strains to bladder tissue, thereby reducing the thickness of the tissue to enable sufficient diffusion of the solutions into the tissue. Such a process should also apply these strains in a format which allows the solutions to be quickly and easily changed, and does not require large volumes of solution in order to cover the tissue. The previous method of decellularising bladder by filling each organ with solution at each stage of the process was therefore not suitable for commercial manufacture. Decellularising bladder tissue in a flat sheet configuration would overcome the problems with the original process, which were a result of the method involving distending bladders with decellularisation solutions.

The original bladder decellularisation process involved distending bladders so that biaxial strain was applied to the tissue in order to reduce the thickness sufficiently for the solutions to adequately diffuse into the tissue (Bolland *et al.*, 2007). In Chapter 4, it was demonstrated that applying strains of 2.00 and 1.40 (in the circumferential and longitudinal directions respectively) to bladder tissue resulted in decellularisation. These strains corresponded to a strain of $-0.861$ being applied to the tissue in the radial ($z$) direction. It was hypothesised that flat sheets of bladder tissue would be successfully decellularised provided that this $z$ strain, which corresponds to a reduction in tissue thickness, is applied to the tissue.

In the previous chapter, finite element modelling (FEM) was used to model the stretching of bladder tissue in order to determine an optimal mode of applying strain to the biomaterial. It was found that stretching a rectangular piece of bladder tissue using 5 discrete points along each side resulted in a bladder which was suitably stretched. This mode of stretching resulted in a $z$ strain being applied to a central region of the tissue which was within 10 % of the target $z$ strain. It was further hypothesised that stretching the tissue to within this strain range would apply a suitable amount of stretch for decellularisation of this central region.

In order to test these hypotheses, a piece of equipment was required which was capable of deforming sheets of bladder in this specific manner. No piece of equipment could be found which could be used or indeed adapted to apply the required deformations to bladder tissue and also be suited to the various environmental conditions of the decellularisation process. Bespoke equipment was therefore designed and manufactured in order to apply the required stretching regime to bladders, in a manner that was compatible with the procedure. This frame was then used to decellularised flat sheets of bladder tissue.

### 6.1.1 Rationale

This proof-of-principle test had to ensure that specific strains were applied to porcine bladder tissue sheets of a specific size. As a consequence of this, pieces of porcine bladder tissue stretched in this regime would all be stretched to identical sizes. This allowed a single piece of equipment to be designed, on which any porcine bladder tissue could be stretched for decellularisation. In the previous chapter, it was seen that an initial tissue size of 46.5 mm × 60.0 mm stretched with strains of 2.0 and 1.4 resulted in a stretched tissue size of 140 mm × 144 mm. The designed equipment therefore had to be able to stretch bladder tissue to this size. Furthermore, the material decellularised using this flat-bed technology had to be able to produce decellularised bladder patches of a relevant clinical size at the end of the process. It was also predicted in the previous chapter that stretching a piece of bladder tissue of this size in this way would produce a fully decellularised area of tissue which was 8 cm × 8 cm in size. From information gathered from surgeons about the requirements of a bladder patch material, this size of tissue was found to be of a clinically useful size.

This equipment had to be compatible with a sterilisation process, and resistant to the chemicals used in the decellularisation protocol. It also had to be suitable for use with the current lab-based protocol, and therefore had to be compatible with aseptic technique. It therefore had to be able to be placed in the environments

used during decellularisation, including refrigerators and incubators, and on orbital shakers, and therefore to be capable of withstanding temperatures in the range 0–40 °C. A detailed design specification for a decellularisation process involving this equipment is given in Appendix G.

### 6.1.2 Aims and objectives

#### Aims

The main aim of this chapter was to design and test a piece of equipment which would adequately stretch bladders in the way which was previously modelled. The equipment would allow bladders to be subjected to the decellularisation process whilst in their deformed state.

#### Objectives

1. To design a piece of equipment capable of stretching flat sheets of porcine bladder tissue.
2. To decellularise flat sheets of porcine bladder tissue using the equipment.
3. To characterise the decellularised porcine bladder tissue.

## 6.2 Methods

A summary of experiments is shown in Table 6.1.

| | Experiment | Samples (number) | Outputs |
|---|---|---|---|
| 1 | Design and manufacture of equipment for stretching bladders during decellularisation | — | 3D-printed bladder stretching frames |
| 2 | Preliminary test of frame | Bladders 6.2.a&b | Bladder stretching assessed |
| 3 | Bladder decellularisation, 'flat-bed method', using fresh bladders on stretching frames | Bladders 6.3.a–c (3 from fresh) | Histology: H&E and DAPI; DNA assay; Contact cytotoxicity assay |
| 4 | Bladder decellularisation, 'flat-bed method', using twice-frozen bladders on stretching frames | Bladders 6.4.a–c (3 twice-frozen) | Histology: H&E and DAPI; DNA assay; Contact cytotoxicity assay |
| 5 | Differential scanning calorimetry (DSC) | Bladders 3.3.a–c, 3.4.a–c, 4.5.a–c, 6.3.a–c, 6.4.a–c | Assessment of changes to collagen denaturation temperature |

**Table 6.1: A summary of the experiments featured in Chapter 6.**

### 6.2.1 Frame design

In order to test the hypothesis that applying the required strains to flat sheets of bladders would result in successful decellularisation, a frame was designed on which to stretch bladder sheets so that they could be put through the decellularisation process. Such a frame needed to support the bladder in its stretched state, and be compatible with the current lab-based decellularisation process. A method of stretching the bladder onto the frame also had to be considered. Elements of design of the frame were investigated which could later be used as part of a manufacturing process. If the proof-of-principle test demonstrated that flat sheets of bladder could be decellularised, then the principles could be carried forward and further developed.

#### 6.2.1.1 Conceptual design

**Active or passive frame**

For a sheet of bladder to be held in a state of biaxial tension on a frame, the tissue must first of all be stretched to that point. Two ways of stretching the bladder material were considered The stretching action could be provided either by an active frame itself, or the bladder could be deformed through other means and merely supported and held in the deformed state by a passive frame.

An active frame would require it to be an involved mechanical system which was able to provide the force and actuation to stretch the bladder. It would be a complex system, but would have the potential to be much simpler and quicker to operate. The form of a passive frame would be much simpler, and would likely be cheaper to design, manufacture, and take up less space. Another device would be required to stretch the bladder, but this could be done manually for an initial prototype.

To stretch the bladders onto the frame, ideally a piece of equipment would be designed to do this evenly and accurately, and allow the bladder to be easily transferred onto the frame once stretched. However, even and adequate stretching would be achievable if the pins were stretched by hand. This latter method would be suitable for this proof-of-principle experiment.

**The frame–bladder interface**

It was previously decided that stretching the bladder with discrete points was the most effective way to apply strain to sheets of bladder during decellularisation. To

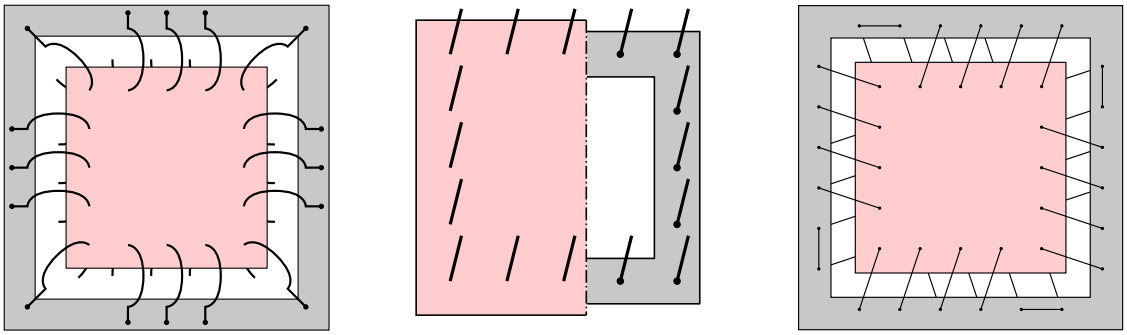

**(a)** Hooks **(b)** Pins **(c)** Sutures

**Figure 6.1: Design ideas for stretching bladder tissue using a frame.** Bladder tissue is shown in red and frames are shown in grey.

implement this two elements of design were considered: how the frame contributed to the frame-bladder interaction, and how the bladder contributed to the frame-bladder interaction.

Three ways the frame could interact with the bladder were considered: using hooks, pins, or sutures (Figure 6.1). Hooks would keep a low profile in the $z$ direction, however they would make the footprint of the frame bigger in the $x$ and $y$ directions. Hooks of different gauges are widely accessible, however it may be difficult to thread the hook through the tissue precisely. Pins would protrude in the $z$ directions, but would keep the frame size small in the $x$ and $y$ dimensions. Placing pins accurately in the tissue would be simple. Sutures would keep a low profile in the $z$ direction, but would require a larger frame in the $x$ and $y$ directions. The process of threading all the sutures may be complex and time-consuming. Also, it may be difficult to precisely apply the required strains as the suture tension would need to be applied in a particular manner.

Three ways the bladder could interact with the frame so that it was able to be stretched were considered. To make holes in the tissue so that discrete points could pull the tissue, holes could be punched out of the tissue, eyelets could be placed in the tissue, or the tissue could be pierced without removing any tissue. Preliminary tests demonstrated that punching holes out of tissue would lead to excess expansion of the holes when stretched, however punched holes would make it easier to locate the pins into the tissue. An even easier method of locating the tissue stretching points would be to use eyelets, however it is likely that they would also result in excess tissue expansion. Piercing through the tissue would make it difficult to later locate the punctured holes, however this problem would be negated if the pins themselves were used to pierce the holes.

### Integration of pins into frame

Features of the frame which would allow pins to be freely attached to the frame include screw-in mechanisms and magnets, or a guided channel. Screwing mechanisms and magnets are more complex designs which may be easier to operate, but would likely require custom-made pins. A guided channel into which a more simple pin would slide would be a simpler design, but would require a lever arm to keep the pin in place. Such a lever could be a feature of the frame, made out of the same material and able to flex or move into position.

### Placing pins into bladder tissue

To place the pins into the correct locations in the bladder tissue, a piece of equipment should be designed. This should ensure the pins are correctly positioned, and be removable so that the pins and tissue can be then moved onto the frame.

### Connecting multiple frames

In a large-scale manufacturing process, numerous bladders would be decellularised simultaneously. This may be achieved by stacking frames closely together in a single tank which contains the decellularisation solutions. One way that frames could be closely stacked would be to design a rack which the frames slide into, and could accommodate many frames. Another way this could be achieved would be to design features onto the frames which allow them to connect together.

There are several geometrical features which were considered to enable frames to connect together. These features should allow the relative movement of two interlocking frames in one direction, but restrict movement in other directions. These geometrical features included dovetail joints, tenon and mortise joints, tongue and groove joints, rebate joints and dowel pins.

The orientation of connected frames relative to one another was considered. The frame could be designed to become positioned linearly, radially, orthogonally, or in a less regular madder such as staggered (e.g. brickwork). To achieve these, the design could be such that all frames are identical, or there may be two or more variations of frame design, which used together would form the desired structure. Frames which have been connected must be able to stay locked together during the decellularisation process. Geometric features typically will leave one direction of movement between two frames unrestrained. This relative movement could be

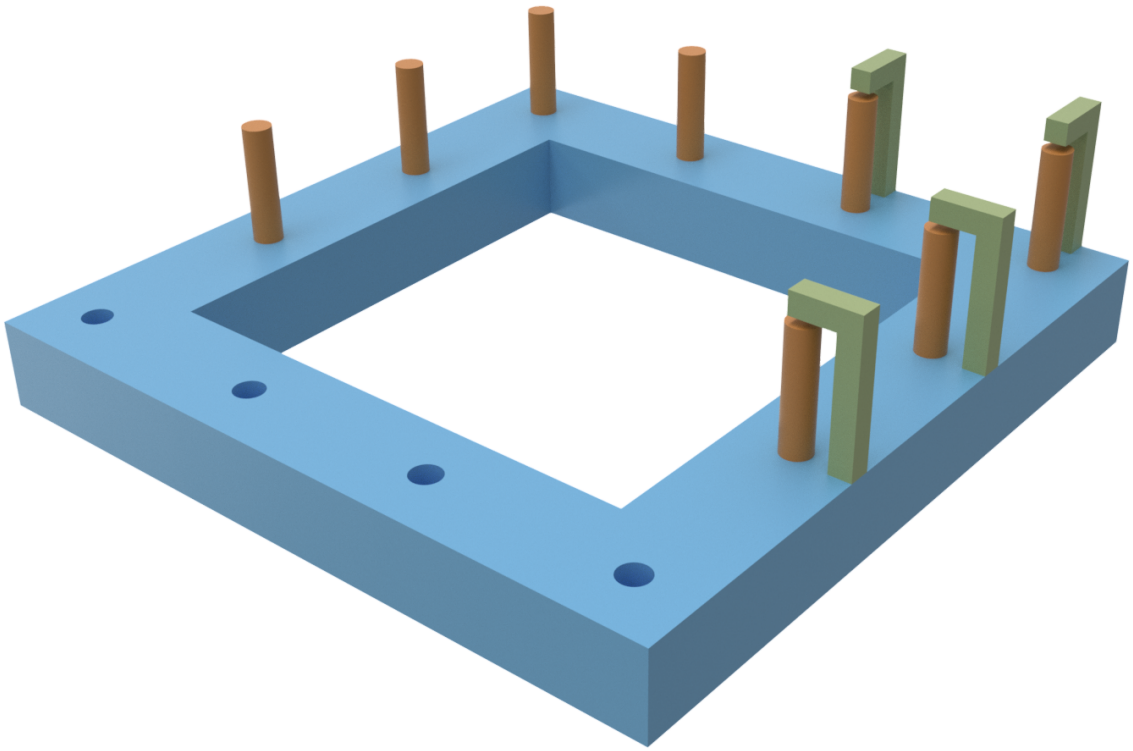

**Figure 6.2: Visualisation of the design concept for the bladder tissue stretching equipment.** The main body of the frame is shown in blue. The pins (orange) are able to be placed into holes in the main body, and levers (green) hold the pins in place. The pins would be designed to pierce the tissue to hold it in position. Some pins and levers have been omitted in order for the frame design to be more clearly seen.

prevented by using gravity, friction, or by employing the use of another component or mechanism.

#### Concept visualisation

Using these ideas, a concept frame design was developed which would passively support bladder tissue via pins which would be held in place round the perimeter of the frame. The pins would pierce the bladder tissue, and would be held in place via a series of retaining levers. A visualisation of this concept is shown in Figure 6.2.

### 6.2.1.2 Embodiment design

Having developed a design concept, details of the design were then developed.

### Manufacturing method

3D printing, also known as additive manufacturing (AM), is a method of manufacturing which is able to produce small batches of objects with complex geometries. A 3D printer produces objects by laying down successive layers of material. Each layer is a 2D slice of the final object, and when printed sequentially the desired object emerges. The starting material is typically a powder, but may be a liquid or a solid wire. A variety of plastic, metal and ceramic materials can be used depending on the type of 3D printing used. Selective laser sintering (SLS) uses a laser to sinter powdered base material.

Objects produced by 3D printing are usually manufactured one at a time, although several objects can be manufactured by a single printer if they are small enough relative to the printer. Although the cost of printing an object is relatively high, there is no setup cost for each bespoke item. This makes 3D printing an ideal method for manufacturing prototypes of components and devices. The wide variety of materials which can be produced using 3D printing means that it is possible to produce visual, proof-of-principle and functional prototypes.

Manufacturing the prototype using 3D printing would also allow a complex design to be easily and quickly manufactured, with minimal considerations for how the frame might be mass-produced. If the proof-of-principle tests showed that the method of stretching did result in successful decellularisation, the frame could be further developed and designed with mass-production in mind.

### Material

The material used to manufacture the frame must be resistant to the solutions used during decellularisation, usable in the temperature range 0–40 °C and compatible with a method of sterilisation. The material must also be strong enough to support the bladder tissue when stretched, and strong and flexible enough to support the geometries required of it during use.

### Pin specifications

It was previously discussed that it would be suitable to stretch the bladder using pins. These pins should be able to pierce the bladder tissue, and allow a user to manually stretch the bladder onto the frame. For this proof-of-principle test it was adequate that the pins not be specially designed, and the frame instead designed to

accommodate the pins. Dissecting needles may prove to be adequate pins because of their ability to easily penetrate tissue, whilst also being strong. Preliminary tests demonstrated that dissecting pins would be able to adequately stretch bladder tissue. Dissecting needles were acquired and their dimensions were recorded.

### Integration of pins into the frame

To integrate the pins into the frame, it was decided to design cavities in the frame which the needles of the pins would sink into. To prevent pins being released from these cavities, it was decided to design pin retaining levers which would cover the handle end of each pin. Therefore cavities would limit pin movement so they would only be able to move along their axis, and levers would full restrain the pins by restricting movement in the axial direction.

Cavities were designed to be of a depth to support the pin, whilst ensuring that there was enough length of pin above the cavity to support the bladder tissue. The dimensions of the pins were used to calculate the required dimensions of the cavities.

Pin handles needed to be of a minimum usable length. However the height of the frame was determined by the length of the pins, and therefore using pins which were longer than required would have resulted in a frame height which was excessive. A minimum handle length was specified and used to calculate the length which dissecting needles should be cut to in order to create pins suitable for the frame.

To keep pins retained in the cavities when placed in the frame, levers were designed to cover their ends. Such levers should cover the handle end of each pin to prevent the pins from moving along their axis. These levers should be positioned close to the end of each pin to ensure minimal movement of the pins when in use. The height of these levers was calculated using the required cavity depth and the required pin length.

For ease of use, the pins should be able to be easily placed into cavities. To ensure this, a cavity diameter was chosen which was larger than the diameter of the pins. However, this size discrepancy would allow the pins to move around in the cavities, resulting in an exaggerated displacement at the top (end of the handle) of each pin. These displacements were calculated to ensure that pins would still be contained by the levers in these circumstances.

### Geometry of pin retaining levers

The pin retaining levers needed to be able to be positioned over the end of the pins when in place, but also be moved aside for pins to be placed in and removed from the frame. The levers had to be designed so they were easy to use to ensure that mounting bladder tissue onto a frame was quick and simple. Producing the frame using 3D printing allowed a complex pin lever geometry to be designed and manufactured which was part of the body of the frame. Using a flexible material for the lever arm allowed a lever to be designed which would elastically deform to allow the pins to be placed into and removed from the frame. Displacement and deformation of the pin retaining levers would result in stresses in the material. These stresses should stay within acceptable limits to ensure the frame is suitable for normal use.

The pin lever geometry should accommodate the easy installation and removal of pins from the frame. A schematic of the dimensions of a pin lever is shown in Figure 6.3. The lengths of each of these dimensions were investigated using the following criteria.

The lever height $L$ must be sufficiently tall to allow a pin to fit under it. The base of the lever ($e$) should be positioned so that the lever stands closely to a positioned pin. The lever cap must protrude over and cover the top of pins by a suitable amount to keeps the pins in place, for all deviations of the top of the pins. Making this cap length $b$ longer than required to hold the pin would require the lever to be pulled back a greater distance, making it more difficult to use. The lever retraction distance $y$ must be large enough for pins to be removed. For easy removal of pins the lever should retract a distance equal to the length of the lever cap, however the retraction distance may be smaller than this when allowing for pin top deviation, but not much shorter otherwise it may prove difficult to remove pins. To limit the lever retraction distance a feature on the frame was considered. This would prevent the levers from being accidentally damaged by being bent too far. The lever and the cap must be thick enough ($a, h$) to be strong enough to hold the lever in place, but not so thick that it would generate stresses in the base of the lever which would cause it to undergo plastic deformation.

Plastic deformation of the levers would prevent them from returning to their original positions after bending. This may prevent the levers from sufficiently keeping the pins in place, leading to the frame no longer being fit for purpose. To ensure the material does not undergo plastic deformation, the stresses in the levers must not exceed the tensile strength of the material. The tensile strengths of Duraform® PA

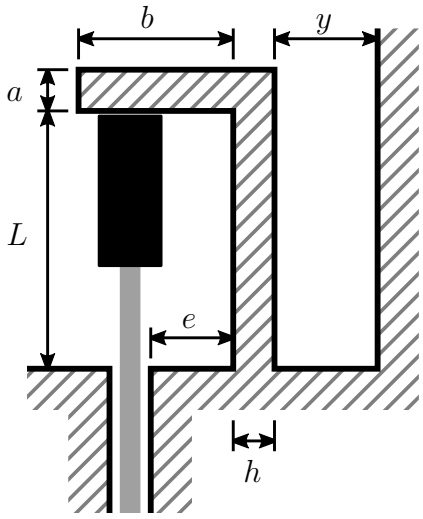


**Figure 6.3: Variables which contribute to the geometry of pin retaining levers.** The hashed section is the frame and the lever. $a$ is the thickness of the cap of the lever, $b$ is the length of the lever cap, $y$ is the retraction distance, $L$ is the height of the lever, $e$ is the distance from the pin cavity and $h$ is the thickness of the lever.

and Duraform® GF are 44 MPa and 38.1 MPa respectively. Incorporating a factor of safety of 1.5, the maximum material stresses should not exceed 29.3 MPa and 25.4 MPa respectively. The flexural moduli of these two materials are 1285 MPa and 3300 MPa respectively.

An expression for the maximum stress in the lever was found using Euler-Bernoulli beam theory (Appendix H.1). The deformation of the lever was modelled as a beam with length $L$ (lever height), height $h$ (lever thickness), unit depth, displacement $y$ (retraction distance) and a flexural modulus $E$. The contribution of the lever cap to the displacement was assumed to be negligible. This expression is given in Equation 6.1. This demonstrates that the maximum stress would increase with lever height and retraction distance, and decrease with lever height.

$$\sigma_{\max} = \frac{3Ehy}{2L^2} \tag{6.1}$$

To find a combination of these parameters which would prevent the lever material from undergoing plastic deformation, the maximum stress of the material was calculated for various values for each of the parameters. The maximum stress was calculated for $L = 25$ mm; $E = 1285$ MPa and 3300 MPa; $y = 5$ mm, 6 mm and 7 mm; and $h = 2$ mm, 3 mm, 4 mm and 5 mm. The stresses for these various parameter combinations were compared against the maximum stresses of the materials, calculated above (29.3 MPa and 25.4 MPa for Duraform® PA and Duraform® GF respectively). A suitable parameter combination was chosen and used to create the final

frame geometry for manufacture.

### Frame supporting structure

The supporting structure of the frame should ensure the pin levers and pin cavities remain in a constant position when a bladder is loaded onto the frame. To achieve this the supporting structure should connect the pin cavities so the frame will undergo a negligible deflection when loaded with bladder tissue. When the bladder tissue is stretched onto the frame, a force is applied by the pins which deforms the tissue. The tissue exerts an equal and opposite force onto the pins, which exert the same force onto the frame, causing it to deform. Deformation of the frame should be kept within acceptable limits to ensure the bladder tissue is sufficiently stretched. To calculate this deflection, the frame was modelled as a simple beam with a bending moment applied to each end.

The amount of force required to stretch the bladder was calculated using experimental data from the immersed distension experiment. The mean stress-strain curves for once-frozen and twice-frozen bladders were used to find the stress in the bladder tissue when strains of 2.0 and 1.4 were applied in the $x$ and $y$ directions. For calculating the deflection of the frame, the largest of these stresses in each direction was used to calculate the bladder stretching force. The areas over which the stresses act were calculated in order to calculate the tissue stretching force. The cross-sectional area of the bladder tissue was calculated by modelling the bladder as an incompressible rectangular cuboid. Bladder stretching force was calculated by multiplying the normal stress by the cross-sectional area of the tissue. These forces were assumed to be acting on the frame when it was supporting the bladder.

The deformation of the frame when supporting bladder tissue was modelled using beam bending theory. When the frame is supporting the bladder, the bladder exerts forces on the frame which are parallel, but not collinear, to the neutral axis of the frame. This scenario was be modelled as a beam with a pure bending moment applied to each end, with the magnitude of these moments equal to the bladder stretching force multiplied by the distance of this force from the neutral axis. Euler-Bernoulli beam bending theory was used to derive an expression for the maximum beam displacement. Parameters of a preliminary design of the frame were used in the model, and the maximum frame deflections in the $x$ and $y$ directions were calculated.

#### Inserting pins into bladder tissue

Pins must be pushed through bladder tissue at specific locations in order to ensure the correct strain is applied to the tissue when it is then stretched onto the frame. A preliminary test demonstrated that laying the tissue onto a cork board allowed for this precise placement of pins. It was decided to design a bespoke plate which would guide the pins into the tissue. The plate should be able to be then removed once the pins are in place, whilst allowing the pins and tissue to remain in their position. The pins and bladder should then be able to be transferred to the frame.

#### Connecting frames by stacking

A large-scale manufacturing process for decellularised bladders may benefit from frames which are able to connect together to form a single unit. Although not necessary for this proof-of-principle prototype, the concept was investigated to explore the benefits, pitfalls and feasibility of connecting bladder decellularisation frames to direct the design of future frame prototypes.

To be compatible with the current lab-based decellularisation process, frames needed to be able to be placed on shakers. Due to their flat shape, frames which connected side-by-side would therefore not be suitable for this because the combined footprint would have been too large for the orbital shakers. Frames stacked on top of one another would have a footprint which was suitable for placing on a shaker. A geometric feature which facilitates frame stacking should allow frames to move and engage in the vertical direction, but restrict relative motion between frames in all other directions.

### 6.2.1.3 Detail design

#### Final prototype design

A final design of the frame was created according to the specifications developed in the previous section (Section 6.2.1.2). SolidWorks software was used to generate a CAD model of the design. A CAD model of the pin guide plate was also created.

#### Final design and manufacture

Three frames and one guide plate were manufactured using 3D printing by Keyworth Rapid Manufactruing Limited (Leeds, UK). The 3D printing method used was SLS using Duraform PA as the additive material. Side cutter pliers were used to cut the handles of the dissecting pins to length.

### 6.2.2 Preliminary test of frame

To test whether the procedure of mounting bladders onto a frame would result in the successful stretching of bladders onto frames, two bladders were acquired from an abattoir, transported without transport medium and dissected to remove excess connective tissue (Sections 2.4.2, 2.4.3 and 2.4.6.1). The bladders were dissected into flat sheets using the three-cut method (Section 2.4.6.3), however a small portion of tissue leading to the apex was left attached to the sheet of bladder so the orientation of the sheet could be discerned. Bladders were placed in Sterilin pots, then frozen and thawed twice before use.

To stretch the bladders onto the frames, each bladder was placed onto a cork board and preconditioned by pushing the back of a scalpel handle across the tissue. The bladder was laid flat and the pin guide plate placed on top of it. Pins were placed through the bladder in the required locations and into the cork board below. The border around the pins of the first bladder was cut to a width of 2 mm, using the guide plate as a guide. The border of the second bladder was left to be larger, with a width of approximately 5 mm. The guide plate was removed, and the pins were carefully removed from the cork board without removing them from the bladder tissue. Bladder tissue and pins were transferred to the frame.

The first bladder was stretched onto the frame by placing pins into the frame in a clockwise sequence; each pin placed in the frame was followed by the pin adjacent to it. The second bladder was stretched onto the frame by placing pins into the frame so the bladder was stretched as evenly and symmetrically as possible. Firstly, the corner pins were placed into the frame in symmetrical pairs (Figure 6.4a), followed by the pins half way along the edges of the bladder (Figure 6.4b), again in opposing pairs. Finally, the other pairs of pins were placed into the frame in a sequence which stretched the bladder evenly (Figure 6.4c). This sequence is shown in Figure 6.4. To minimise the chance of tearing around the pins, both bladders were stretched onto the frames slowly to allow the tissue to creep.

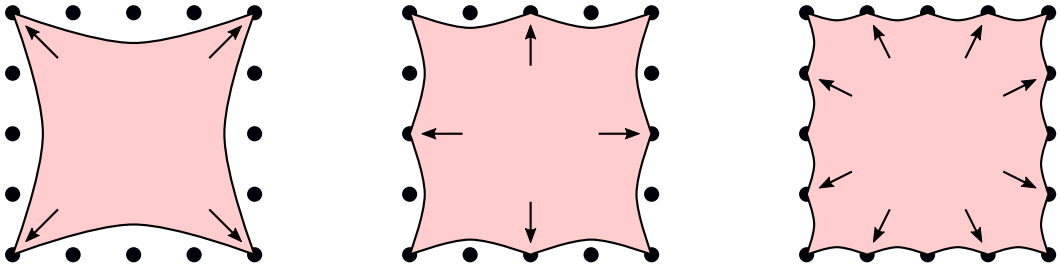

**(a)** Attaching the corner pins to the frame.

**(b)** Attaching the pins at the midpoints of the edges.

**(c)** Attaching the remaining pins.

**Figure 6.4: Sequence for evenly stretching a bladder onto a frame.** Arrows show the pins which were attached at each stage. Firstly the pins at the corners were attached to the frame (a). Secondly the pins at the midpoints of the edges of the bladder were attached to the frame (b). Finally the remaing pins were attached (c). All pins were placed in opposing pairs.

### 6.2.3 Bladder decellularisation using flat-bed method

To find out whether flat sheets of porcine bladder tissue could be successfully decellularised, six bladders were mounted onto the bladder stretching frames and subject to the decellularisation process. Bladders were collected from an abattoir and transported to the laboratory without using transport medium (Sections 2.4.2 and 2.4.3). Each bladder was aseptically dissected to remove excess connective tissue Section 2.4.6.1, and dissected into a flat sheet using 3 cuts as described in Section 2.4.6.3 In order to distinguish bladder orientation a small strip of tissue was left connecting the sheet of bladder to the apex.

Before processing, one set of bladders was frozen and thawed twice, and another set remained fresh. The first set of bladders ($n = 3$) were placed into 150 mm Sterilin pots, frozen at $-20\,^{\circ}\mathrm{C}$ overnight and thawed at room temperature for 4 h. Bladders were then frozen and thawed again before use. A second set of bladders ($n = 3$) were processed without undergoing any freeze-thaw cycles.

Bladders were stretched onto the frames by first laying them flat onto a cork board. The tissue was preconditioned by pushing a scalpel handle over it. The pin guide place was placed on the centre of the bladder tissue, covering the dorsal surface. Pins were pushed through the bladder in the required positions and into the cork below. Excess tissue was cut from the bladder sheets, leaving a border around the pins of approximately 10–15 mm on the twice-frozen bladder set and a border of 5–10 mm on the fresh bladder set. The pins and tissue were transferred to a frame,

where each bladder was stretched using the pins to strains of 2.0 and 1.4 in the $x$ and $y$ directions respectively. Pins were attached to the frame in symmetric pairs in an even fashion, as shown in Figure 6.4, to ensure bladders were stretched evenly. The procedure of mounting bladders onto a frame is shown in Figure 6.5.

Bladders which were stretched onto frames were then decellularised using the method described in Section 2.5. Rather than filling bladders with decellularisation solution and placing them in beakers, stretched bladders were placed into containers which were filled with 2 L decellularisation solution. This was enough for the tissue to be fully immersed in the solutions. All boxes were placed onto a single IKA shaker for the required stages of the process.

Following the peracetic acid treatment stage, bladders were aseptically removed from the frames and placed into 150 ml Sterilin pots. The pots were filled until 125 ml full (including the volume of the bladder) with phosphate buffered saline (PBS) and placed in their required environment. At the end of the process, bladders were stored in fresh 150 ml Sterilin pots containing PBS at 4 °C.

#### 6.2.3.1 Tissue characterisation

After decellularisation, the outside border of the tissue was removed from each bladder patch, leaving the area of tissue which was contained by the pins. Samples for analysis were all taken from the central 8 cm × 8 cm square region in the centre of this biomaterial. The four sides of this square region were made up of the right lateral edge, left lateral edge, anterior edge and posterior edge. The centre of each bladder patch corresponded to the centre of the dorsal surface of the unprocessed bladder.

##### Histology

Square samples, approximately 1 cm × 1 cm in size, were taken for histological analysis from fresh bladders, and both fresh and twice-frozen bladders decellularised by stretching onto a frame. Samples from decellularised bladders were taken from the centre, the midpoint of the right lateral edge, and the right posterior corner of the bladder patches. Samples were taken from the centre of the dorsal surface and the right lateral side of three fresh bladders.

Samples were processed, embedded in paraffin wax, sectioned, de-waxed and re-hydrated as described in Sections 2.6.1.2 to 2.6.1.5. Tissue sections were stained

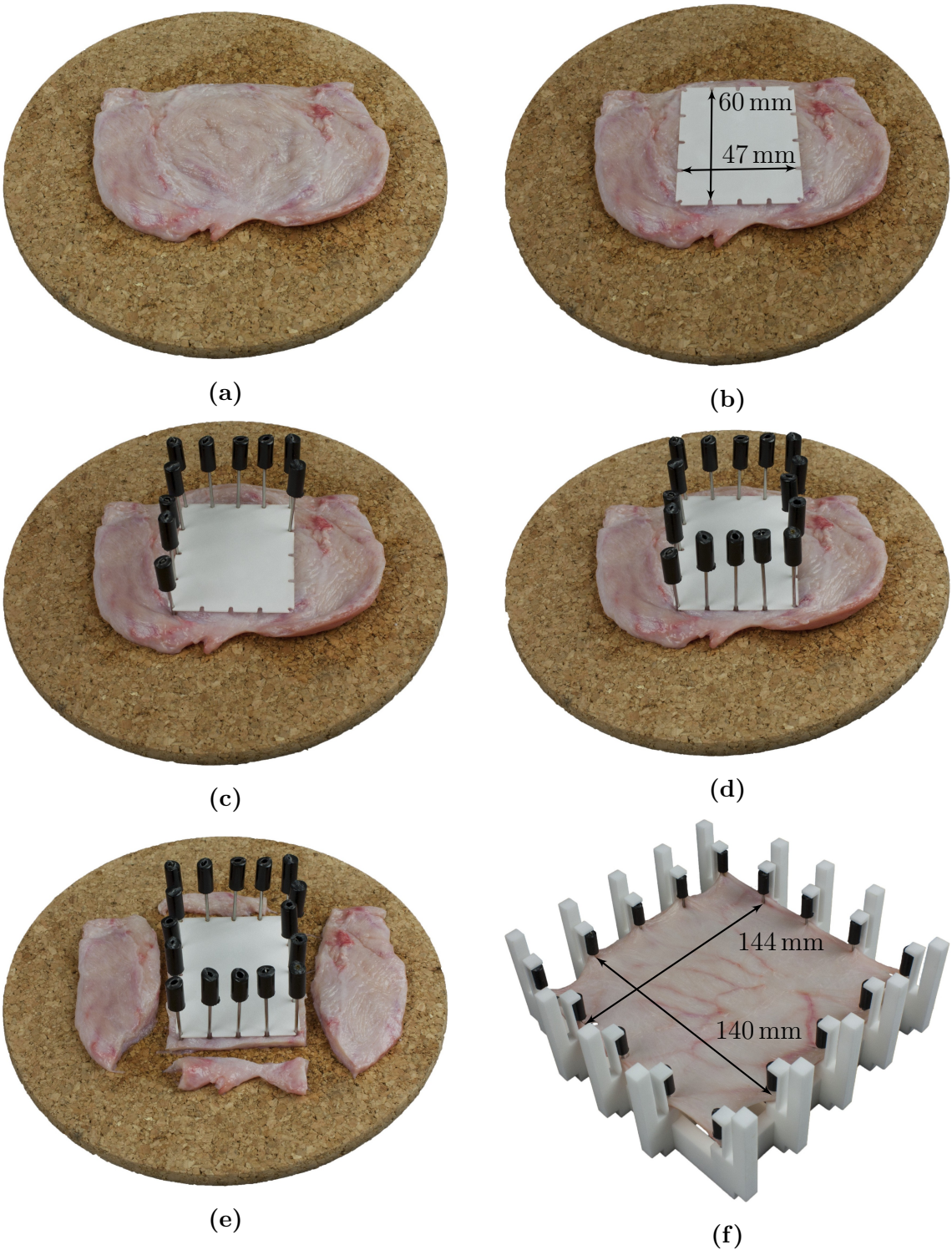


**Figure 6.5: The procedure for stretching bladder tissue on to the frame.** After dissecting into a flat sheet, the bladder was laid flat on a cork board, lumen side down (a). The pin guide plate was placed on the centre of the bladder (b). Notches on the guide plate were used to push pins through the required points on the bladder and into the cork board (c) until all the pins were in place (d). Excess bladder material was removed (e). The pins and bladder were removed form the cork board and evenly stretched onto the frame (f).

with either haematoxylin and eosin (H&E) or DAPI then dehydrated and mounted as described in Section 2.6.1.6.

### DNA extraction and quantification

Samples for DNA quantification were taken from fresh and decellularised bladders and processed as described in Section 2.6.2. Samples from decellularised bladders were taken from the region between the centre and the midpoint of the left lateral edge of the bladder patches. Samples from fresh bladders ($n = 3$) were taken form the centre of the dorsal surface.

### Contact cytotoxicity testing

Square samples, 5 mm × 5 mm in size, were taken from the midpoint of the left lateral side of decellularised bladders. Six samples were taken from each decellularised bladder; three samples for each cell type. Six of each type of control sample (cyanoacrylate contact adhesive, collagen gel, cell-only) were used; three per cell type. All samples were placed into 6-well plates and tested for contact cytotoxicity using BHK and L292 cell types by the method described in Section 2.6.3.1.

### Differential scanning calorimetry

In order to determine whether the bladder decellularisation process had an effect on the quality of the collagen in the tissues, differential scanning calorimetry (DSC) was used to investigate the collagen denaturation temperature of control and decellularised bladder samples. Samples were tested from bladders decellularised using the various methods outlined in Chapter 3 and this chapter. Three samples were taken from each bladder decellularised using the following methods: decellularisation with calculated bladder filling, initial method, from fresh (Chapter 3); decellularisation with calculated bladder filling, revised method, from twice-frozen (Chapter 3); decellularisation as a flat bladder sheet using the frame, from fresh (this chapter); and decellularisation as a flat bladder sheet using the frame, from twice-frozen (this chapter). For all bladders, samples were taken with a 5 mm diameter biopsy punch from the centre of the dorsal surface (region A), the point halfway between the centre of the dorsal surface and the centre of the right lateral side (region B), and the centre of the right lateral side (region C).

Four types of control samples were used: fresh bladder, twice-frozen bladder, formalin-fixed bladder and heated bladder. Fresh bladders ($n = 6$) were collected from an

abattoir and transported in transport medium using the methods described in Sections 2.4.2 and 2.4.3. Three of these bladders were frozen overnight at −20 °C, thawed at room temperature for 4 h, frozen again and thawed a second and final time. A 5 mm diameter biopsy punch was used to take three samples from the centre of the dorsal surface of each of the three fresh bladders. Three of these samples (one from each fresh bladder) were used as fresh bladder controls. Another three samples were placed into bijous containing 2 mm PBS and heated in a water bath set to 80 °C for 15 min in order to partially denature the collagen. A thermometer was used to record the temperature of the water bath when the samples were placed in and taken out of the bath. The temperature dropped from 75 °C to 73 °C over this period. The remaining three samples from each of the fresh bladders were placed into universal containers containing 20 ml neutral buffered formalin (NBF) for 48 h. A 5 mm diameter biopsy punch was used to take a sample from the centre of the dorsal surface of each of the three twice-frozen bladders. These three samples were used as frozen bladder controls.

All samples were tested using the method described in Section 2.6.4. A two-way ANOVA was used to compare the differences between means of the sample transition temperatures. The two factors were bladder condition and region. The groups used for bladder condition were calculated filling, fresh; calculated filling, frozen; stretched on frame, fresh; stretched on frame, frozen; fresh control and frozen control. The groups used for bladder region were A, B, and C, as described above. If a significant variation in the data was detected by the ANOVA, a Tukey HSD test was used to compare the differences between means for groups of that factor.

## 6.3 Results

### 6.3.1 Frame design

A frame was designed which enabled the application of the required strains to flat sheets of porcine bladder tissue The design of the frame underwent a conceptual design stage, and an embodiment design stage before a final prototype was generated. The final model of the frame design is shown in Figure 6.6.

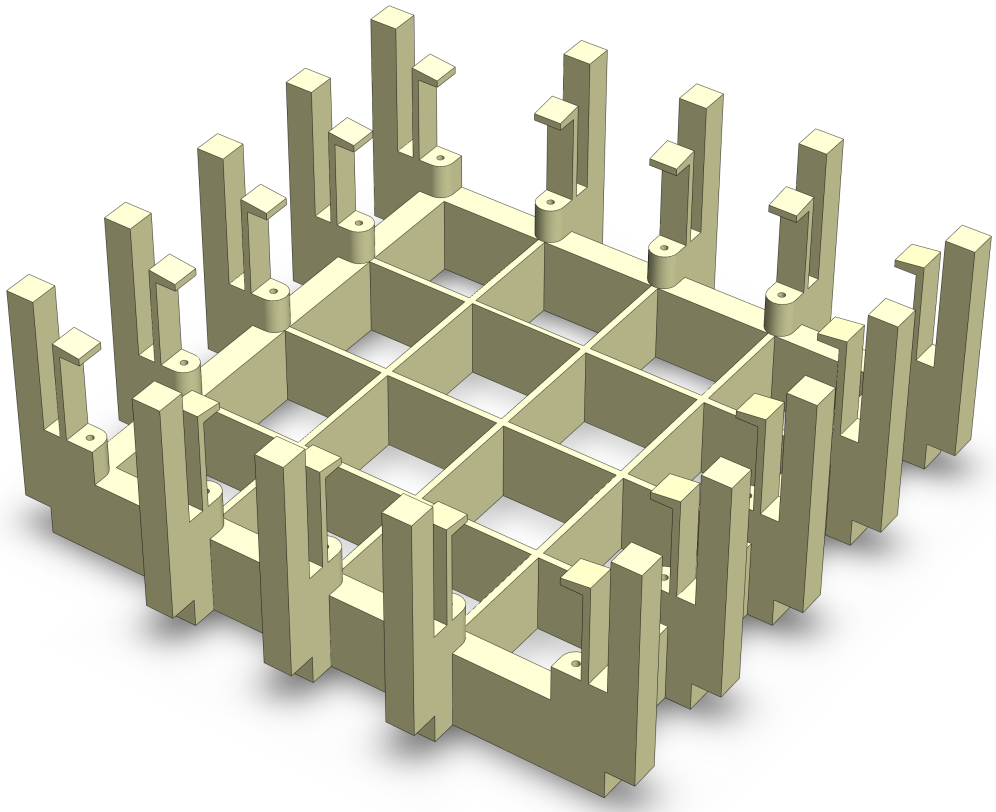

**Figure 6.6: Final CAD model of the frame.** The model shows pin cavities (circular holes) adjacent to pin retaining levers. Behind each pin retaining lever is a post to prevent excessive lever deformation and enable frame stacking. These features are connected by a supporting structure which is comprised of a thick perimeter border and an inner strut mesh.

#### 6.3.1.1 Conceptual design

**Active or passive frame**

It was decided to design a passive frame onto which bladder tissue would be stretched using a separate device. This enabled the frame to be far simpler than an active frame would have been. A complex active frame may be preferable to save time during a manufacturing process, but stretching the bladder manually onto a passive frame was considered suitable for this prototype lab-based design.

**The frame–bladder interface**

In order to stretch the bladder using discrete points, hooks, pins and sutures were considered to support the bladder, which in turn would be held in place on the frame. It was decided to take pins forward as the interface between bladder and frame because of the minimal size they would take up in the same plane as the bladder sheet, and the ease with which they could be accurately placed into bladder tissue.

Three methods of placing the pins through the bladder were considered: placing eyelets in the tissue, punching holes in the tissue, or directly piercing the tissue. Piercing directly through the tissue was the option taken forward because making holes in the tissue poses a risk of insufficient strain being applied to the tissue due to the likelihood of the holes expanding.

**Integration of pins into frame**

To connect pins onto the frame, customs pins could potentially be made which could attach to the frame using screw-in mechanisms or magnets. However a guided channel system was chosen for its simplicity, and so that custom pins would not have to be designed and made. To hold pins in place, it was decided to design a lever to hold the ends of pins. It was decided to design a flexible lever built into the frame which would flex into position.

**Placing pins into bladder tissue**

To guide pins into the correct places in bladder tissue, it was decided to design a device which would be used to indicate the places pins should be pushed through the tissue.

#### Connecting multiple frames

Frames could be designed so they are able to connect together and form a single unit which could be placed in and out of decellularisation solutions. This may simplify the processing of numerous bladder sheets. A simple method of connecting frames was deemed suitable for this proof-of-principle design in order to explore the practicalities of this idea, because it was not necessary to connect bladder frames for these laboratory-based prood-of-principle experiments.

### 6.3.1.2 Embodiment design

#### Manufacturing method

It was decided to manufacture the prototype frame using 3D printing, which allows small batches of complex designs to be easily made, and out of materials which would be compatible with the decellularisation processing environment. It is therefore an ideal method of production for producing a prototype frame for stretching bladders.

#### Material

Two materials were identified which were suitable for manufacturing the frame using with SLS. Duraform PA and Duraform GF are both nylon-based polymers which have a high chemical resistance and are autoclavable. Duraform GF is much stiffer than Duraform PA, so having the choice of either helped maintain a flexibility of design.

#### Pin specifications

Dissecting needles were chosen as the pins to use to stretch bladder sheets onto the frame. These were deemed adequate for this preliminary method. A dissecting needle was chosen which would be suitable for piercing bladder tissue, and with a plastic handle which could be easily cut to a custom size if required.

Measurements were taken of the dissecting needles. There was some variation in the length of the handle and the length of the needle of each dissecting needle. The length of the needles were 36–38 mm and the length of the handles were 101–102 mm. The diameter of each needle was 1.5 mm and the diameter of each handle was 6.8 mm. These dimensions are shown in Figure 6.7.

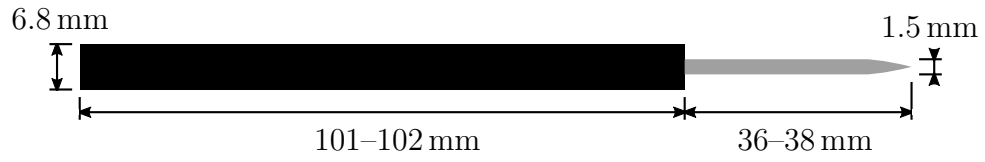


**Figure 6.7: The dimensions of the dissecting needles used to stretch bladder tissue onto the frame.** The handle is shown in black and the needle in gray.

### Integration of pins into the frame

To allow pins to be secured into frames, cavities were designed for the pins to sink into, and levers were designed to prevent pins from leaving the cavities.

When placed in a cavity, the exposed section of the needle of a pin must be long enough to support the bladder. The needle lengths of a selection of pins ranged from 36 mm to 38 mm. A range of 34–40 mm was chosen to accommodate a possible wider variation in needle lengths than the acquired sample. These ranges of needle lengths defined how deep the cavities should be. Allowing a minimum space of 4 mm for the tissue, the cavities should be 30 mm in length. This is shown in Figure 6.8a.

The lengths of the handles of the acquired dissection needles were longer than were required. It was decided to cut the handles to a shorter length to minimise the size of the frame. A range of 34–40 mm was assumed for the needle lengths of pins. It was decided that pin handles should be a minimum of 15 mm for the pins to be manipulable by the user. It was decided that 55 mm was a sufficient length for the dissecting needles. This is shown in Figure 6.8b.

Levers were needed to keep pins in place in the frame. It was calculated that pins should be cut to a length of 55 mm and placed in cavities with depths of 30 mm. Therefore, the levers should cover the area at the end of the pins at a distance of 25 mm from the top of the cavity. This arrangement is shown in Figure 6.8c.

To ensure pins could easily be placed into cavities, a large diameter of cavity was chosen than the diameter of the pins. The diameter of the pins was 1.5 mm, so a diameter of 2.0 mm was chosen for the the cavities. This size discrepancy allows the pins to move around in the cavities, resulting in a displacement of the tops of the pins. The maximum magnitude of this displacement was calculated. Figure 6.8d shows that with pins, with a diameter of 1.5 mm and length of 55 mm, placed in cavities, with a diameter of 2 mm and depth of 30 mm, will have a maximum deviation at the end of 2.3 mm.

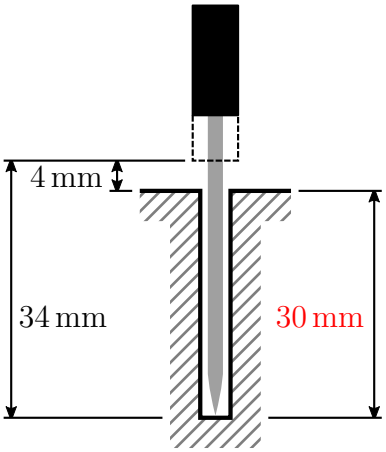


**(a)** The cavity depth was calculated from the minimum needle length (34 mm) and the mimimum allowed space for the tissue (4 mm).

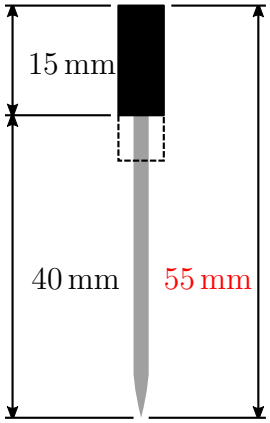


**(b)** Pin length was calculated from the maximum needle length (40 mm) and the minimum allowed handle length (15 mm).

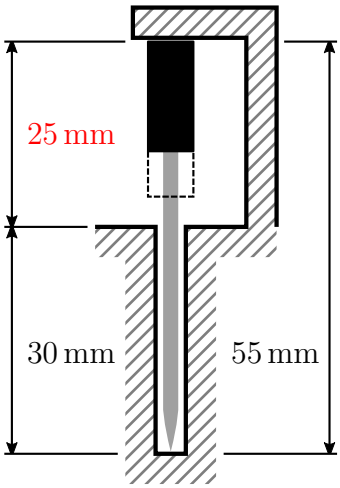


**(c)** The lever height was calculated from the cavity depth (30 mm) and the pin length (55 mm).

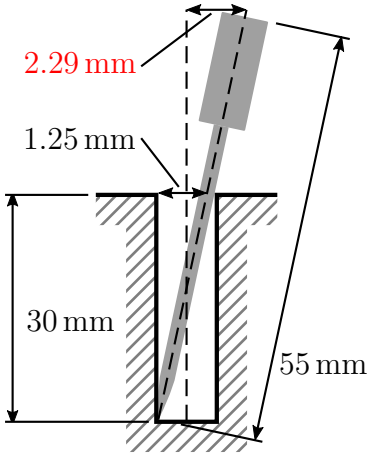


**(d)** The maximum movement of the top of pins (55 mm long, 1.5 mm diameter) when placed into cavities (30 mm deep, 2 mm diameter).

**Figure 6.8: Determining the frame cavity depth, pin handle length, height of pin retaining levers and the deviations of the top of pins.** The frame is signified using hashed lines. Dotted lines show the variation in needle lengths which were assumed. Calculated values are shown in red.

### Geometry of pin retaining levers

A pin retaining lever was designed to be integral to the frame and which would be capable of securing pins into the frame. Different dimensions were considered for the geometry of the pin levers (Figure 6.3).

The lever height $L$ must be 25 mm to allow a pin to fit under it, as previously calculated. The radius of the pins handles was 3.4 mm. It was decided to position the lever base 4 mm from the centre of the pin cavity ($e = 3$ mm). For the lever cap to cover at least half of the pin lever diameter, it should be at least 5.7 mm long. The cap length of 6 mm or 7 mm would therefore be appropriate. The lever retraction distance $y$ must be equal to the cap length so pins can be removed. But allowing for pin top deviation (2.3 mm) the retraction distance was chosen to be up to 1 mm shorter than the cap length. For a cap length of 6 mm or 7 mm, this would therefore be 5 mm, 6 mm or 7 mm. Lever retraction limiters were designed to prevent the user deforming the levers beyond the usable range. Vertical posts were used to provide this function, which may also protect the levers from damage during storage or if the frame is dropped. The lever and the cap must be sturdy enough $(a, h)$ to hold the lever in place without inducing excessive stresses in the lever when it is deformed. A thickness of 1 mm was likely to too fragile, but a thickness of 2 mm or greater would be sufficient.

The levers were designed to allow the pins to be placed in and out of the frame by undergoing deformation. Levers had to be easy to use, and not undergo plastic deformation under normal modes of use. To accommodate these design criteria, different geometries and material types were considered for the levers. Lever deformation was modelled using beam bending theory, and the maximum lever stresses were calculated for a variety of lever geometry configurations.

The calculated maximum stresses for the various configurations of lever geometries which were considered are shown in Figure 6.9. The graphs show which configurations are above the maximum tensile stress of these materials (incorporating a factor of safety of 1.5). For the Duraform® PA material, all maximum stresses for a lever thickness of 1 mm were below the maximum tensile stress. A lever thickness of 2 mm resulted in stresses which were just above the maximum tensile stress, and lever thicknesses above this ($\geq$3 mm) were well above the maximum tensile stress. All the configurations for the Duraform® GF material were greater than the maximum tensile stress of the material.

**(a)** Duraform® PA material ($E = 1285\,\text{MPa}$).

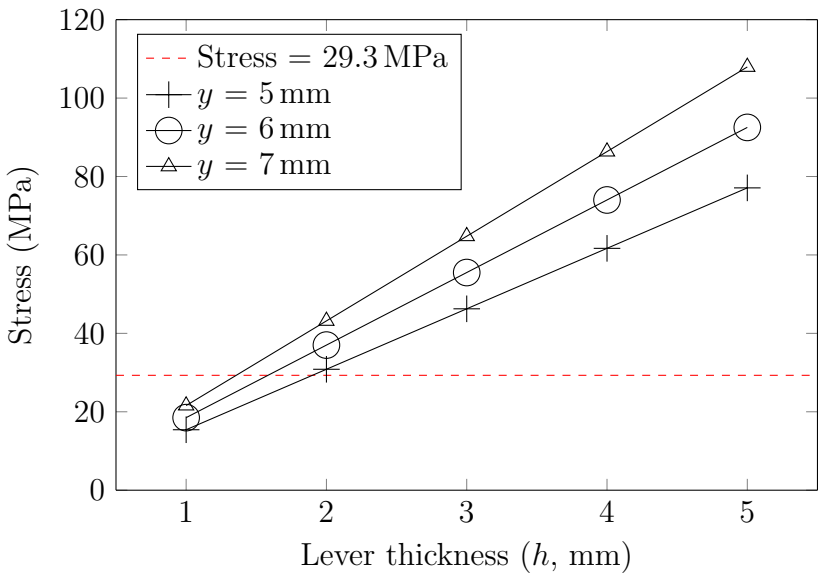


**(b)** Duraform® GF material ($E = 3300\,\text{MPa}$).

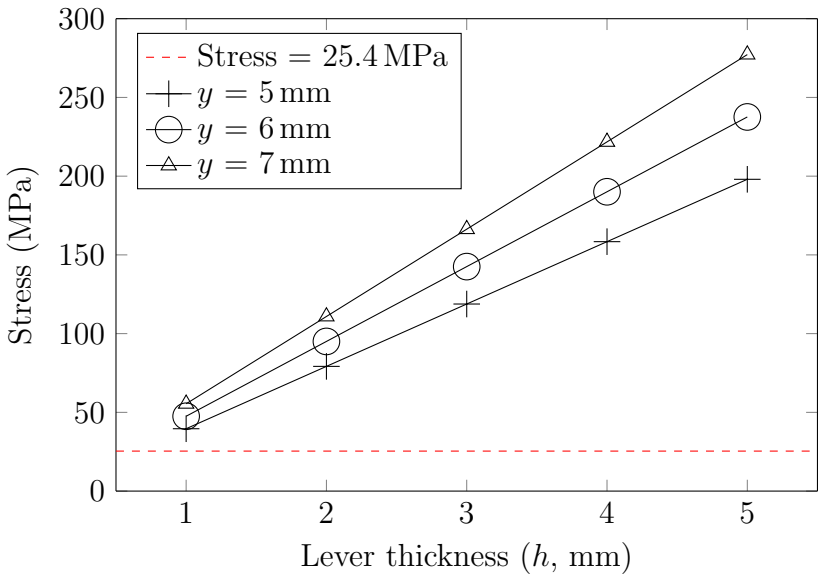


**Figure 6.9: Maximum lever stresses for different lever geometry configurations.** The stress is shown for (a) Duraform® PA and (b) Duraform® GF. Stress was calculated for lever thicknesses $h$ of 1 mm, 2 mm, 3 mm, 4 mm and 5 mm, and retraction distances $y$ of 5 mm, 6 mm and 7 mm respectively. The lever height $L$ was 25 mm for all calculations. The red dotted lines indicate the maximum tensile stress of the materials with a factor of safety of 1.5.

**Frame supporting structure**

In order to prevent the pins from moving by a significant amount when the frame was loaded with bladder tissue, a simple rectangular prism was deemed suitable for connecting the pin cavities and levers. This rectangular prism was designed to connect all these features to form a square, leaving a hollow region in the centre of the frame. It was decided to reinforce this centre of the frame using cross beams. This would add strength to the frame and prevent the edges of the frame from deflecting towards the centre when bladder tissue is mounted.

Mounting bladder tissue onto the frame will cause the frame to undergo deformation. To ensure that these deflections were not excessive, the force the bladder would apply to the frame was calculated from experimental stress-strain data, and a mean bladder thickness was used. Beam bending theory was used to model the maximum deflection of the frame when it is supporting stretched bladder tissue.

The force the bladder would apply to the frame was calculated from experimental stress-strain data. When deformed to the required strains the largest stress in the $x$ direction was $\sigma_x = 0.212\,\text{MPa}$ and the largest stress in the $y$ direction was $\sigma_y = 0.204\,\text{MPa}$. From Chapter 5, the initial dimensions of bladder tissue to be stretched onto the frame (incorporating an outside border of 4 mm) were $54.5\,\text{mm} \times 68.0\,\text{mm} \times 5.0\,\text{mm}$ in the $x$, $y$ and $z$ directions respectively. Applying strains of 2.00 and 1.40 to this tissue (assuming incompressibility) results in final dimensions of $164\,\text{mm} \times 163\,\text{mm} \times 0.694\,\text{mm}$. This rectangular cuboid has faces in the $xy$, $xz$, and $yz$ planes with areas $A_{xy} = 26\,700\,\text{mm}^2$, $A_{xz} = 114\,\text{mm}^2$, $A_{yz} = 113\,\text{mm}^2$. The bladder stretching forces in the $x$ and $y$ directions were therefore $F_x = \sigma_x A_{yz} = 24.1\,\text{N}$, $F_y = \sigma_y A_{xz} = 23.1\,\text{N}$.

Using Euler-Bernoulli beam bending theory, an expression was found for the maximum deflection of the frame when a sheet of bladder was stretched on it. The derivation is detailed in Appendix H.2. This expression is shown in Equation 6.2. The maximum deflection $y$ is given in terms of the flexural modulus $E$, bladder stretching force $F$, perpendicular distance between the bladder stretching force and the beam neutral axis $d$, beam length $L$, beam width $w$ and beam height $h$.

$$y = \frac{3FL^2d}{2Ewh^3} \tag{6.2}$$

A prelimiary design of the frame used the following values for the above variables: $E = 1285\,\text{MPa}$, $F_x = 24.1\,\text{N}$, $F_y = 23.1\,\text{N}$, $d = 22\,\text{mm}$, $L_x = 140\,\text{mm}$, $L_y = 144\,\text{mm}$, $w = 10\,\text{mm}$, $h = 22\,\text{mm}$, These values were used to calculate the maximum frame deflections in the $x$ and $y$ directions. These maximum deflections were 0.114 mm

and 0.116 mm in the $x$ and $y$ directions respectively.

#### Inserting pins into bladder tissue

A pin guiding device was designed to guide pins into the correct positions into bladder tissue. This was a rectangular plate the same size as the area of bladder to be stretched plus a 2 mm border, as per the requirements for sheets of bladder tissue. Grooves were placed along the edges of this plate, indicating the locations the pins should be placed into the tissue.

#### Stacking frames

For this frame prototype, geometric features were designed into the frame which would allow them to connect together vertically. Lever retraction limiters were designed into the frame to limit the maximum distance pin levers could deflect. It was decided to enable frame stacking by extending these limiters so they would be able to fit into a groove, which was placed directly below the limiters. This system would allow frames to connect by placing one frame upon another and bringing together the two halves of the joints. When the posts were placed into the the grooves, relative frame movement would be prevented in the horizontal plane, and gravity would prevent the joints from disengaging vertically.

### 6.3.1.3 Detail design

#### CAD model

A model of the final design of the prototype frame was created using Solidworks. The frame consisted of pin cavities—cylindrical holes—each adjacent to a pin retaining lever. Behind the levers were posts to limit the retraction distances of the levers, designed to prevent the levers from undergoing plastic deformation due to excessive deflection. The posts extended above the height of each lever so they were able to dock with a second bladder placed above the first. Directly below each post a recess facilitated the other half of the frame-frame connection. These pin retaining features were connected via a supporting structure which consisted of a rectangular-sectioned frame perimeter and an inner mesh of struts. The top of the lever cavities were elevated from the supporting structure of the frame to prevent the centre of the frame frame from being in contact with the tissue. Engineering drawings of the design are shown in Figure 6.10

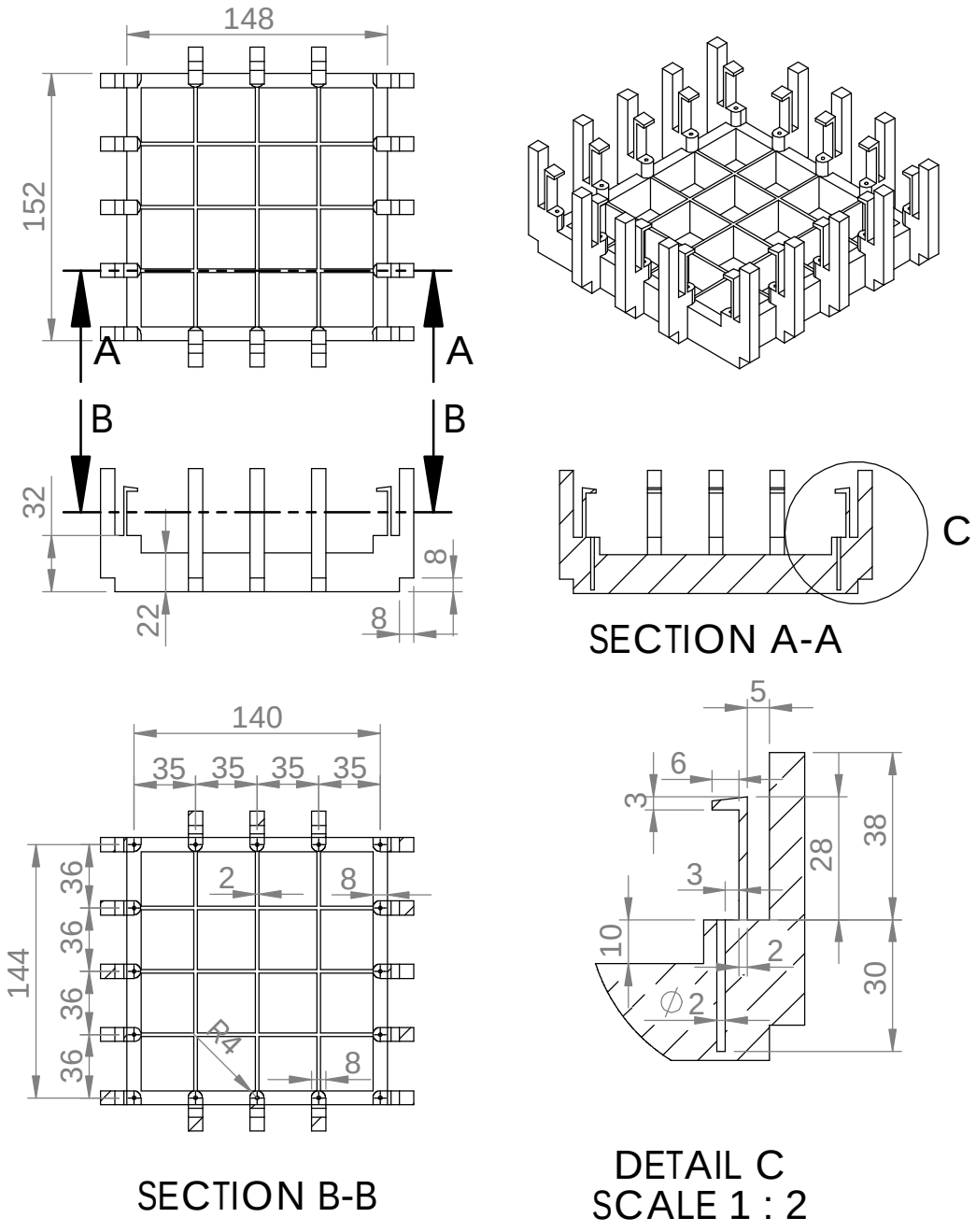


**Figure 6.10: CAD drawings of the final frame design.** Scale is 4:1.

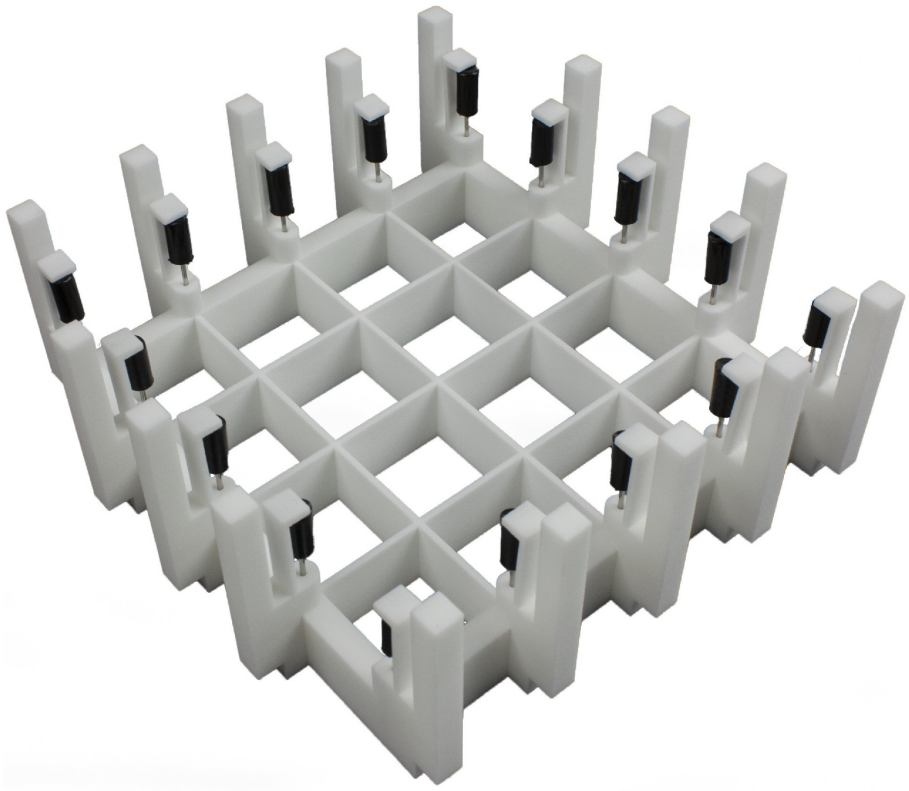

**Figure 6.11: Manufactured frame.** Pins are shown placed into position in the frame.

#### Frame manufacture

Three frames were manufactured using 3D printing by Keyworth Rapid Manufacturing Limited. SLS was used as the manufacturing method with Duraform® PA as the additive material. Dissecting needles were cut to thier required lengths so they were able to fit into the frame. Pins were able to be placing in and out of the frame with ease. The manufactured frame is shown in Figure 6.11.

### 6.3.2 Preliminary test of frame

In order to test the procedure of mounting bladders onto frames, two bladders were acquired and frozen and thawed twice. Bladders were prepared by placing them onto a cork board and using a guide plate to place pins into the required locations in the bladder tissue. Excess bladder tissue was then removed. Pins and bladders were transferred to the frame for stretching.

When pins were placed into the bladders and cork boards, a small amount of tissue was dragged down into the cork, pinning the bladder to it. To circumvent this, the pins had to be lifted a little and the bladder manipulated to free it from the cork.

When stretching the first bladder onto a frame, a border of 2 mm was left around the pins and the pins were stretched in a clockwise manner so that pins were placed next to adjacently placed pins. This resulted in the bladder being unevenly stretched. The edge of the bladder between the first several pins was very straight, but the tissue between pins stretched towards the end of the stretching sequence was heavily scalloped. During the procedure, one of the pins ripped out of the bladder

A border of approximately 5 mm was left around of the pins of the second bladder, and the bladder was stretched by placing the pins into the frame evenly and in opposing pairs. This resulted in the bladder being stretched evenly, with the scalloping around the tissue being of a similar amplitude. No pins ripped from the bladder tissue, however a slight amount of tearing was observed around a small number of the pins.

### 6.3.3 Decellularisation

To test the hypothesis that bladders are able to be decellularised when configured into flat sheets of tissue, two batches (one fresh, one twice-frozen) of three bladders were stretched onto a bespoke frame which applied strains of 2.00 and 1.40 to bladder tissue in the longitudinal ($x$) and circumferential ($y$) directions.

Bladders were dissected, cut into flat sheets of appropriate sizes and stretched onto these frames. Stretching was performed in order to deform the bladder as evenly and symmetrically as possible, and care was taken to stretch the tissue slowly to allow time for the material to creep in order to minimise the risk of tearing. Bladders were placed into containers filled with a series of decellularisation solutions, which resulted in the entire tissue being fully submerged in the solutions.

After decellularisation, samples were taken from the tissues for histological analysis and a DNA extraction and quantification assay to asses whether the tissues had been successfully decellularised Tissue biocompatibility was investigated with a contact cytotoxicity test, and the collagen denaturation temperature of the tissues were found using DSC. The collagen denaturation temperatures of these samples were compared with the bladders decellularised in the previous chapters in this thesis.

#### 6.3.3.1 Histology

Samples were taken from fresh bladders, and fresh and twice-frozen bladders which were decellularised when stretched on a frame. Sections were stained with either

| | DNA content per dry weight ($ng \cdot mg^{-1}$) | | | |
|---|---|---|---|---|
| | Samples | | | Mean ± 95 % CI |
| Fresh controls | 2570 | 3020 | 2140 | $2580 \pm 1090$ |
| Decellularised, from fresh | 0.0* | 50.9 | 1.5 | $17.5 \pm 71.9$ |
| Decellularised, twice-frozen | 1.6 | 25.2 | 60.7 | $29.2 \pm 73.9$ |

*Not detectable.

**Table 6.2: The DNA content of samples taken from bladders decellularised using the flat-bed method.** Means and confidence intervals were calculated from $n = 3$ bladder samples. The DNA content of one decellularised sample was too low to be detected.

H&E or DAPI.

Fresh sections stained with H&E showed an intact urothelium and cells present throughout all the layers of the tissue (Figures 6.12a and 6.12b). All decellularised sections were devoid of urothelium but had a remaining histoarchitecture comparable to that of native bladder, but with no evidence of cell nuclei or cell fragments (Figures 6.12c to 6.12f).

Native bladder sections stained with DAPI showed a high concentration of cell nuclei in the tissue, particularly in the urothelial layer (Figures 6.13a and 6.13b). No cell nuclei were observed in sections taken from decellularised bladders (Figures 6.13c to 6.13f).

#### 6.3.3.2 Total DNA quantification

A spectrophotometer was used to quantify the DNA extracted from samples of fresh and decellularised bladders. Samples decellularised using the flat-bed method had a mean DNA content per dry weight of $17.5\,ng \cdot mg^{-1}$ and $29.2\,ng \cdot mg^{-1}$ for the samples decellularised from fresh and from twice-frozen respectively. These figures represented a mean reduction in DNA content of 99.3 % and 98.9 % relative to the native controls. The data are shown in Table 6.2.

#### 6.3.3.3 Contact cytotoxicity

Tissue samples from bladders decellularised using the flat-bed method incubated with either BHK cells (Figure 6.14) or L929 cells (Figure 6.15) for 48 h to determine whether they would be cytotoxic to cells. There was a high density of cells in the cell-only control wells. These cells had a normal morphology. Cells in the wells

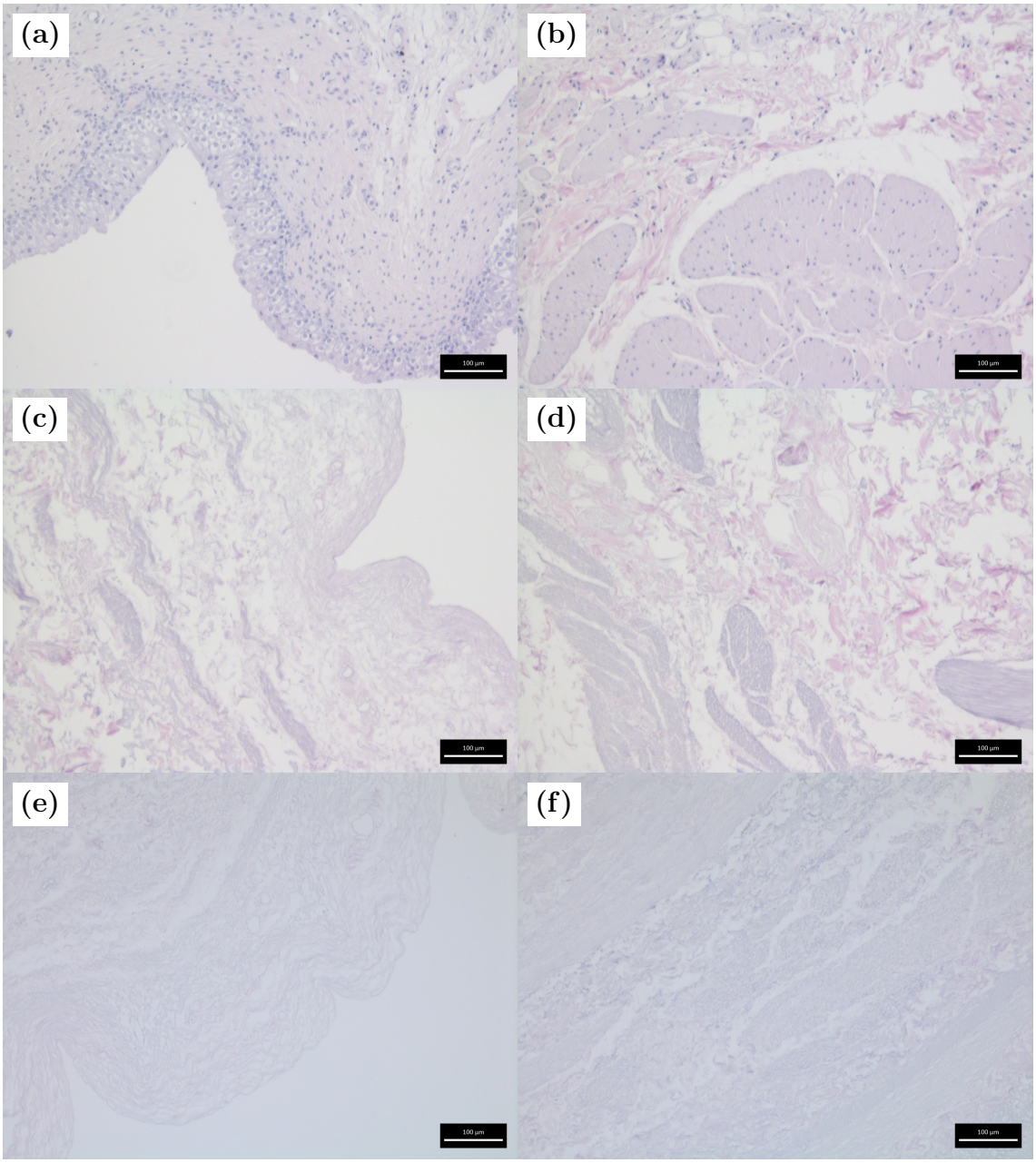


**Figure 6.12: Images of H&E stained sections from bladders decellularised using the flat-bed method.** (a) and (b) are fresh controls; (c) and (d) are from bladders decellularised from frozen; (e) and (f) are from bladders decellularised from fresh. (a), (c) and (e) are images of the luminal surface and (b), (d) and (f) are images of the muscular layer. All images were captured at 10× magnification. Scale bars are 100 µm.

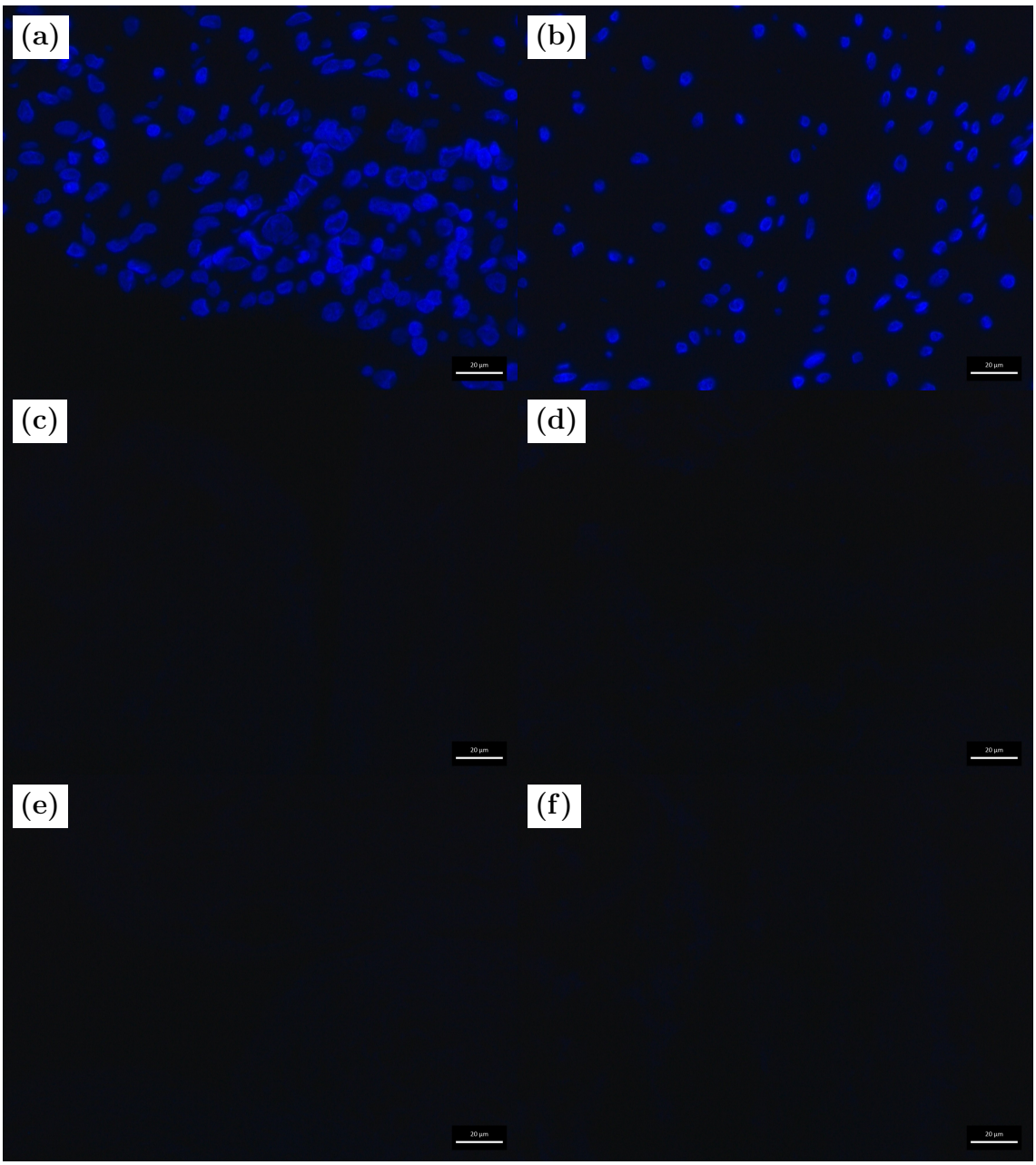


**Figure 6.13: Images of DAPI stained sections of bladders decellularised using the flat-bed method.** (a) and (b) are fresh controls; (c) and (d) are from bladders decellularised from frozen; (e) and (f) are from bladders decellularised from fresh. (a), (c) and (e) are images of the luminal surface and (b), (d) and (f) are images of the muscular layer. All images were captured at 40× magnification. Scale bars are 20 µm.

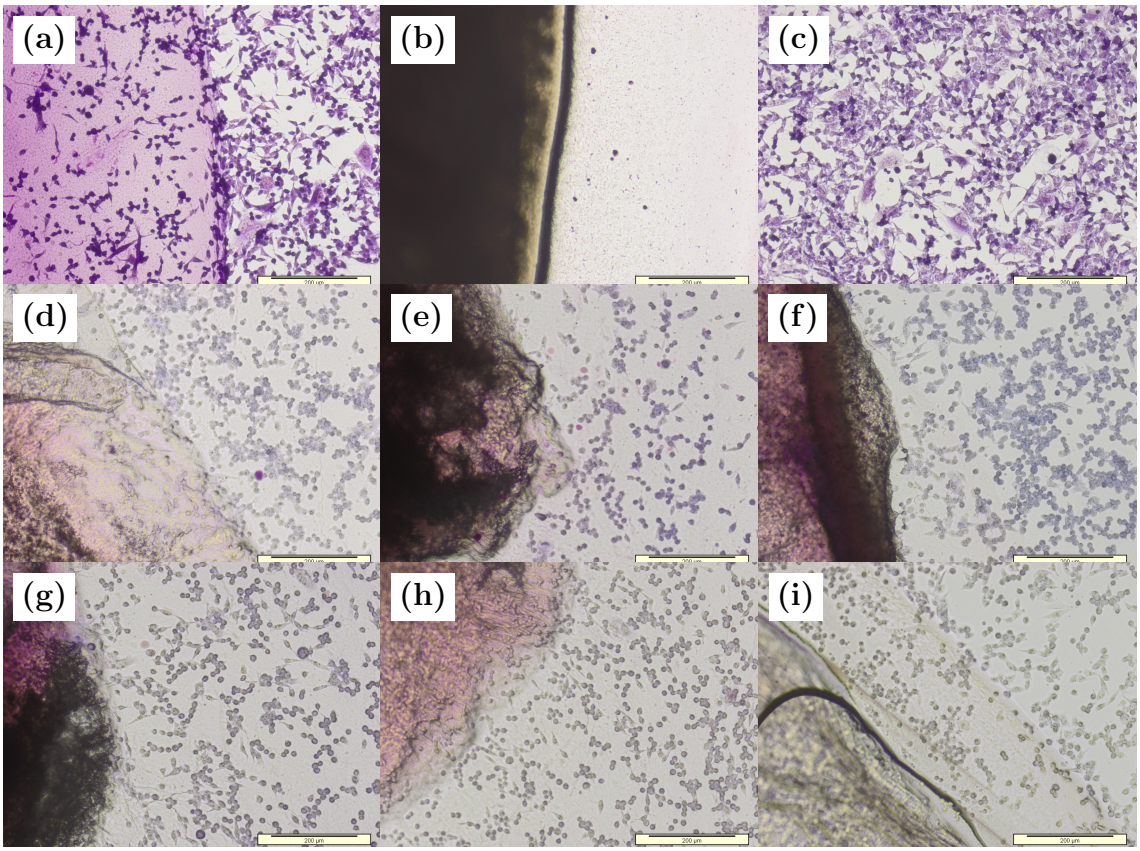


**Figure 6.14: Contact cytotoxicity assay using BHK cells of bladder tissue decellularised using the flat-bed method.** Control samples are (a) collagen gel, (b) cyanoacrylate glue and (c) cells only. Samples decellularised on the frame from frozen are shown in (d), (e) and (f). Samples decellularised on the frame from fresh are shown in (g), (h) and (i). All images were captured using a 10× magnification. Scale bars are 200 µm.

containing collagen gel were slightly less confluent than the cell-only controls, and were more rounded with fewer projections. There was a very low density of cells in the regions next to the drops of cyanoacrylate contact adhesive. Cells observed here were rounded and shrunken in morphology. Cell growth did not appear to be inhibited when cells were cultured with decellularised tissue samples. Cells were able to grow up to all pieces of tissue with a density comparable to the collagen gel control samples. Most cells had a normal morphology with cytoplasmic projections. Cell behaviour was similar to the collagen gel only control group.

#### 6.3.3.4 Differential scanning calorimetry

DSC was used to determine the collagen denaturation temperature of bladders decellularised using the calculated filling method (Chapter 3) and bladders decellularised using the flat-bed method (this chapter). For each of these methods, samples were

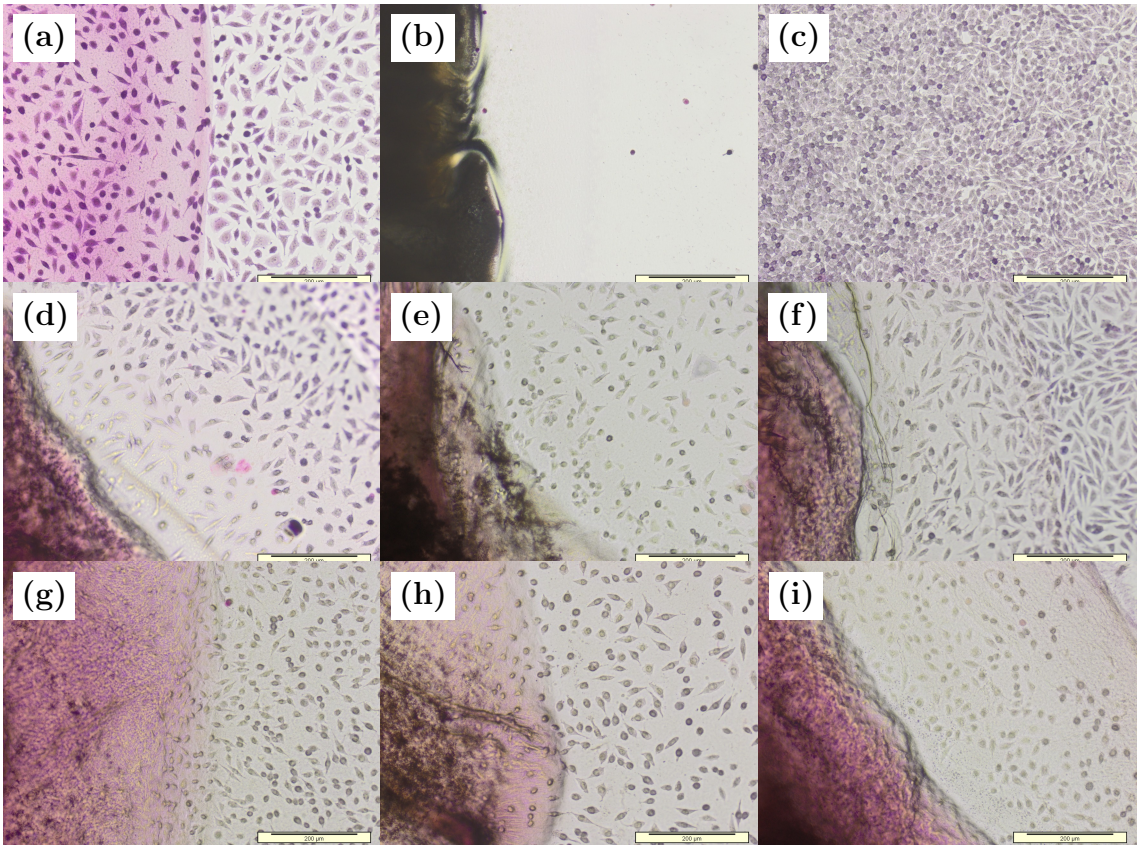


**Figure 6.15: Contact cytotoxicity assay using L929 cells of bladder tissue decellularised using the flat-bed method.** Control samples are (a) collagen gel, (b) cyanoacrylage glue and (c) cells only. Samples decellularised on the frame from frozen are shown in (d), (e) and (f). Samples decellularised on the frame from fresh are shown in (g), (h) and (i). All images were captured using a 10× magnification. Scale bars are 200 µm.

tested from bladders which were decellularised from both fresh and twice-frozen. Samples for testing were taken from three different regions: the centre of the dorsal surface (region A), the centre of the right lateral side (region C), and the midpoint of these two points (region B). Fresh, twice-frozen, heated and NBF-fixed native bladder samples were used as controls. A two-way ANOVA was used to determine whether the decellularisation processes or the region of sampling had a significant affect on the collagen denaturation temperature of the tissue. A Tukey HSD test was used to compare the differences between means for factors with significantly differing group means.

All samples tested using DSC exhibited a peak in the resulting heat flow curve except the control samples which were fixed with NBF. A value for the collagen denaturation temperature was consequently found for all other samples. Heated samples had a denaturation temperature much lower than all the other types of samples which were tested, and were therefore excluded from the ANOVA. The means of the collagen denaturation temperature for the different types of bladder tissue which were tested are shown in Figure 6.16. These values represent the means of all samples (all regions) for each tissue type. There were only small variations between the collagen denaturation temperatures of the different regions for each of the different methods of decellularisation (Figure 6.17).

The ANOVA showed that the region the samples were taken from did not significantly affect the transition temperature ($p = 0.909$), however the bladder condition did significantly affect the temperature ($p < 0.001$). The Tukey HSD test revealed that the mean of the denaturation temperature of the bladders decellularised from fresh using the calculated filling method was significantly higher than the means of all the other groups. The mean denaturation temperature of the bladders decellularised from frozen using the calculated filling method differed significantly from the mean of the fresh bladder control group only. The means of the bladders decellularised using the flat-bed method did not significantly differ from the collagen denaturation temperature means of the control groups. The mean denaturation temperature of the twice-frozen native control group was slightly higher than the fresh control group, but this was not significant.

## 6.4 Discussion

Application of biaxial strain to bladder tissue resulted in a reduction in thickness of the tissue which is necessary for decellularisation of full-thickness porcine bladders (Bolland *et al.*, 2007). Previously, biaxial strain was applied by distending bladders

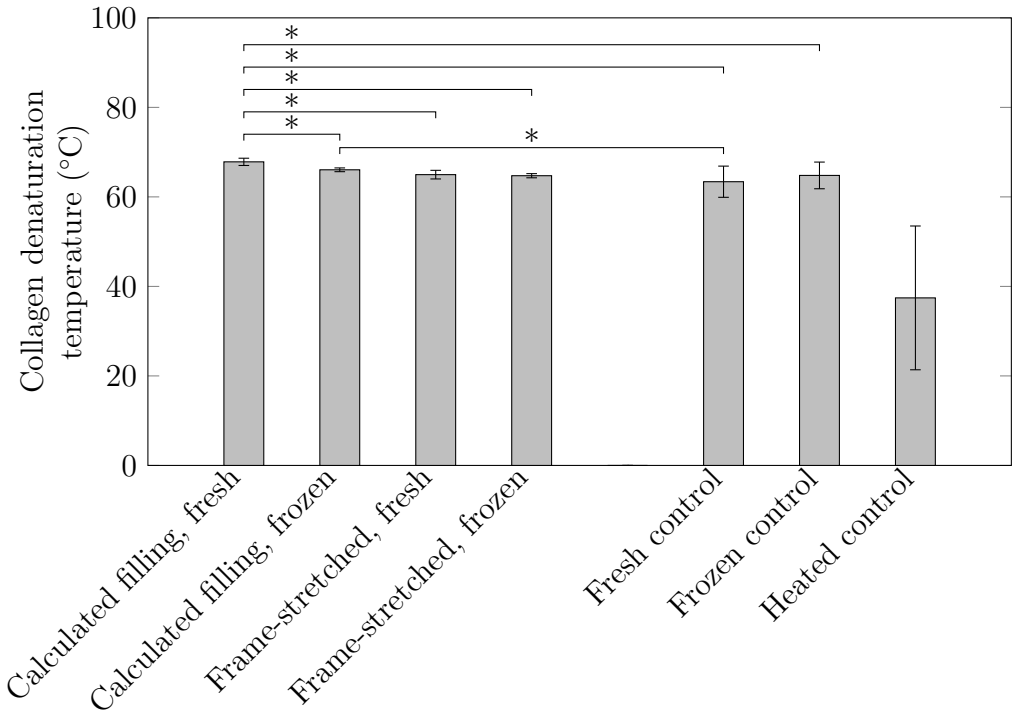


**Figure 6.16: The collagen denaturation temperatures of decellularised and control bladder tissues.** Samples were tested using differential scanning calorimetry. All frozen samples were frozen and thawed twice. Bars show the mean for all samples in each group, and the error bars show the 95 % confidence intervals. The significance bars indicate the group means which significantly differed according to the Tukey HSD test ($*$ indicates $p < 0.05$). The heated fresh control group was excluded from the Tukey test.

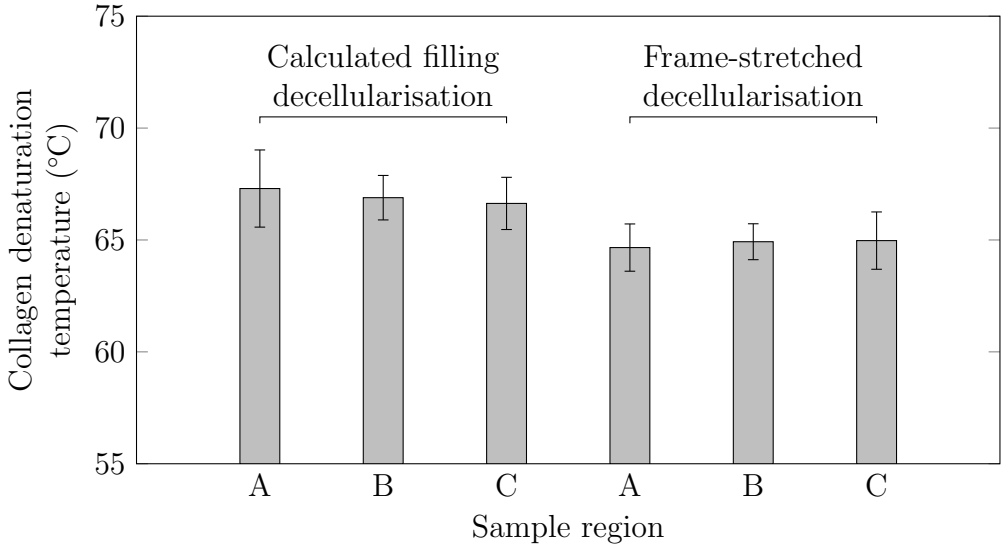


**Figure 6.17: The collagen denaturation temperatures of the different regions of decellularised and control bladder tissues.** Samples were tested using differential scanning calorimetry. Region A was the centre of the dorsal surface, region C was the centre of the right lateral side, and region B was the midpoint of points A and C. Bars represent the mean of each decellularisation method (fresh and frozen) for each region, and the error bars show the 95 % confidence intervals.

with decellularisation solutions, however this process was not suitable to perform as part of a manufacturing process. It was thought that decellularising flat sheets of bladder would overcome the manufacturing-related problems associated with distending bladders, therefore making it viable to manufacture decellularised bladder. In order to test the hypotheses that bladder tissue could be decellularised when stretched into a flat sheet configuration, a piece of equipment was designed which was capable of stretching flat sheets of bladder tissue.

In Chapter 4, a biaxial strain state was found which, when applied to whole bladders, resulted in tissue decellularisation. The state was achieved by applying strains of 2.00 and 1.40 to bladder tissue in the circumferential and longitudinal directions. Due to the incompressibility of soft tissue, these strains corresponded to a specific $z$ strain of -0.861. In Chapter 5, an FEM model was used to find an optimal method for applying biaxial strain to rectangular sheets of bladder tissue. The optimal stretching method ensured that the required region of tissue was subjected to a $z$ strain which was within 10 % of the required $z$ strain (-0.861). It was hypothesised that this would be adequate for decellularisation.

A frame was designed so that bladder tissue would be stretched according to the optimal stretching regime, found in Chapter 5 using the finite element method. The final design of the frame is shown in Figures 6.6 and 6.11. It enabled a piece of

bladder tissue to be stretched to the specific size defined by the size of the frame and was able to sufficiently support bladder tissue in the deformed state. This passive and specific design of the frame therefore proved to be sufficient for the purposes of this proof-of-principle test. The frame was manufactured using the 3D printing method of SLS. All the features of the frame (e.g. pin levers) were adequately reproduced and functioned as required. The frames were also able to be autoclaved several times, with no apparent change to the material. The material also did not appear to be affected by the chemicals used during the decellularisation process. The choice of material (Duraform PA) and manufacturing method were therefore suitable for the frame.

An active/dynamic frame design was considered during the design process. Such a frame would be of benefit to a manufacturing process by increasing the speed and minimising the manipulation with which bladder tissue could be stretched for decellularisation. However, the technology which would be incorporated into the body of the frame, such as mechanical mechanisms or actuators, would add significant complexity to the device. This would not only result in each frame being more costly to produce, but they would take up more space in the processing environment, all the components of the device would have to be compatible with the environmental requirements of the decellularisation process (e.g. temperature resistance, water resistance), and the longevity and maintenance of these components would have to be considered. Additionally, the frame is only used to stretch the tissue at one point during the process, and for the majority of the process the frame is required to hold the bladder statically, suggesting that it would be sub-optimal to design a dynamic frame which would remain static for the significant majority of its working life. Therefore a passive frame design was adopted. This allowed a simple frame to be made from a single material. Consequently there were few design limitations imposed by choice of material, such as chemical resistance and mechanical strength, which more complex mechanical designs may have been limited by. The bladder was stretched onto the frame by hand, however this was a one-off procedure at the start of the process, and the minimal frame design helped improve the ease with which solutions were changed throughout the process. To improve the speed and accuracy of stretching the tissue onto the passive frames, a dedicated piece of equipment could be designed to perform that specific function.

Pins (modified dissecting needles) were used to pierce and then stretch the bladder tissue. These were able to be suitably manipulated by hand so that the tissue could be mounted onto the frame. However, the plastic handles were not as robust and easy to grip as was desired. The handles of the pins were hollow, which sometimes allowed the needles of the pins to slip relative to the handles. Filling these cavities

with a filler material may have make them more stable and suited for use. Sturdier dissecting needles with textured metal handles may have been more appropriate for applying the required forces to the tissue, and would have been more easily sterilised. The dissecting needles which were used were of a varying sharpness, likely due to variability in the manufacturing process of the needles. Blunter pins did not pierce tissue as cleanly, and therefore resulted in more damage being caused to the tissue, which may have reduced the ability of that region of the tissue to support the stretching of the tissue. Consistently sharp pins would therefore have resulted in less damage being caused to the tissue by the pins.

The geometries of the pin cavities and pin retaining levers allowed pins to be easily inserted into the frame. Pins did not freely come out of the frame unless they were intentionally removed. These geometries were therefore suitable for the designed purposes. Details of the geometries are shown in Figures 6.3 and 6.8. No damage was caused to any of the frames during use. The thickness of the material, particularly in the levers (2 mm), was therefore sufficient to ensure the frame was strong enough to be subjected to its intended use. Some levers did appear to hold some lasting deformation after being displaced. It was likely that this was a result of material viscoelasticity rather than plastic deformation, because these effects did not appear to be long-lasting. However, this effect was minimal, and it was therefore likely that the levers would continue to function properly after multiple uses.

The supporting structure of the frame did not excessively deform when the tissue was stretched onto it. Beam bending theory estimated that the magnitude of this would result in the bladder being under-stretched by less than 0.2 mm. This was negligible compared to the dimensions of the stretched tissue, and was therefore within acceptable limits.

Other decellularisation protocols have used volumes of solutions at each stage of the process which were proportional to the amount of tissue being decellularised, such as those found in the literature (Hogg *et al.*, 2013; Montoya & McFetridge, 2009), and those used in our laboratory for tissues such as arteries (1 ml solution per 1 mm length of tissue); human amnion (5 ml solution per 1 $cm^2$ area of tissue); and porcine pericardium (2 ml solution per 1 $cm^2$ area of tissue). The original decellularisation protocol used 1 L of solution per bladder at each stage of the process (Bolland *et al.*, 2007). This volume was used so that the bladders could be sufficiently distended for the tissue to be stretched enough for the solutions to diffuse into the tissue walls. If the tissue had been stretched by a different method, it is likely that lower volumes of solution would have been adequate to decellularise the tissue. It is likely therefore that there exists a minimum volume of solution per amount of tissue which is required to decellularise porcine bladder. In order to minimise the number of

variables which were changed between the flat-bed decellularisation method and the other bladder decellularisation methods which were used in this thesis, the same volumes of decellularisation solutions were used; 2 L at each stage of the process. However, due to the flat nature of the frame-stretched bladder tissue, lower volumes of solutions could have been used whilst still keeping the tissue fully stretched and completely submerged in solution. Therefore, unlike the original method of distending bladders, the minimum volume of decellularisation solutions required for the flat-bed method is not limited by the geometry of the tissue. Consequently, the use of lower volumes of solutions in the flat-bed method may be investigated. Volumes of solutions may be found which are proportional to the amount of tissue which is being decellularised, similarly to other tissue decellularisation protocols. This would minimise the volumes required for the decellularisation process.

Designed features incorporated into the frame allowed them to be vertically stacked. Frames were not stacked during decellularisation because it was not necessary during the proof-of-principle study. However, the stacking which was possible indicated that stacking may be feasible to incorporate into future frame designs, provided it was beneficial to the decellularisation process. Stacking frames may allow pieces of bladder tissue to be densely packed. This would allow a greater number of tissue pieces to fit into an incubator, and may therefore increase the maximum batch size. Densely packed tissue pieces would also take up less space in a manufacturing facility.

The frames were not completely square, and so care had to be taken so that the tissue was mounted in the correct orientation on each frame. The orientation of each frame was discerned by observing the location of the levers on the frames. However, this was not overly obvious, and the frames would have benefited from more obvious spacial features to discern their orientation to decrease the possibility of mounting the tissue in the incorrect orientation.

Bladders were mounted onto the frames by first laying the tissue onto a cork board, then using a guide plate to push pins through the tissue. The mounting procedure is shown in Figure 6.5. This proved to be a successful method of inserting pins into the required points in the tissue. However, the action of pushing pins into the tissue and cork caused some of the tissue to get dragged down and become pinched between the pin and the cork. To ensure the tissue was fully placed on each pin, the tissue on each pin had to be re-adjusted to free the pinched tissue. This was an awkward step which risked pins being accidentally removed from the tissue. This unnecessary step could be avoided with the use of an alternative piece of equipment in place of the cork board. Additionally, it was difficult to remove the guide plate once the pins were in place, and therefore an alternative guide plate design may

simplify the process.

Before the tissue was mounted on the frame, it had to be transferred from the cork board to the frame. This step was difficult to perform because the bladder could not be supported by anything rigid, and so it had to be transferred by hand. Care had to be taken when handling this limp material because there was a risk of the pins falling out of the tissue when it was being transferred to the frame. Replacing dislodged pins back into the tissue was not an easy or accurate process. Although this method of transferring the pins to the frame was effective, an alternative method which enables delivery of the tissue to the frame in a rigid fashion and which does not require the tissue to be manipulated by hand would be preferred.

Before the frames were used for bladder decellularisation, two bladders were preliminarily stretched onto frames to ensure that the stretching procedure was feasible. The first bladder was stretched by placing adjacent pins into the frame in a clockwise fashion. This resulted in the tissue not being stretched symmetrically, and inserting the final pin into the frame caused this pin to rip out of the tissue. The second bladder was stretched in a symmetrical fashion, and the resulting tissue was uniformly deformed. Despite the small number of samples ($n = 2$), it was evident that the difference in stretching regime contributed to the variation in the uniformity of the tissue deformation. The effect that the stretching regime had on the resulting tissue deformation was a result of the elastic hysteresis which soft tissue exhibits (Safadi & Rubin, 2014). When the bladder tissue was stretched asymmetrically, there were regions of the tissue which were subjected to strains greater than if all the pin displacements had been applied at the same time. The hysteresis of the elasticity of the tissue meant that the strain in these regions failed to recover, and these regions of tissue retained their over-stretched state when the other pins were placed into the frame. Stretching the tissue symmetrically resulted in a minimal amount of over-stretching of the tissue, and the over-stretching which occurred was symmetrical. Consequently, this led to the tissue being stretched uniformly. Therefore, materials exhibiting elastic hysteresis such as porcine bladder must be loaded in a fashion which minimises over-stretching of the material during the stretching process. Because of this finding, bladders mounted onto frames for decellularisation were stretched in a symmetrical manner.

When pieces of bladder tissue were stretched onto the decellularisation frames, small amounts of tearing of the tissue was sometimes observed, resulting in an enlargement of the hole the particular pin had been pushed through. This sometimes occurred when the tissue was stretched too quickly. To prevent this, care had to be taken in order to stretch the tissue slowly, to allow the viscoelastic material to creep so that it could be stretched without tearing. Some bladders were susceptible to tearing even

when stretched at a slow rate. This tearing typically occurred during the procedure when bladders were stretched in a symmetrical fashion: when the second pair of corner pins were stretched. In order to minimise the tearing when these pins were stretched, the pins adjacent to the ones being stretched were sometimes displaced. This shared the force required to stretch the tissue over three pins instead of one, decreasing the tissue stress and reducing the risk of tearing. This mode of tearing would have been minimised if all the pins could have been displaced simultaneously. Bladder tissue with a larger outside border was able to be stretched more quickly without the tissue showing signs of tearing. A larger border around the tissue decreased the stress around the pins because the same amount of force was being shared by a greater thickness of border material. Border widths of approximately 5 mm were much more robust than the 2 mm border width specified in the previous chapter. Therefore, a wider border outside the pins would be preferable in order to decrease the risk of this mode tearing. In addition to this, it was noticed that bladder tissue often became unevenly stretched when the border around the tissue was not cut to a uniform width. This made it more difficult to stretch the tissue, and increased the risk of tearing. This was because wider borders resulted in a greater tensile stress to nearby tissue regions, and less wide borders resulted in a lesser tensile stress being applied to adjacent tissue regions. In order to balance these forces, the tissue was therefore pulled towards the edges of the tissue with the wider borders. Therefore, in order to minimise the chance of tearing and to maximise deformation uniformity, it is desirable for pieces of bladder tissue to have a border of a uniform width.

There was a noticeable tactile difference between stretching fresh bladder tissue and stretching twice-frozen bladder tissue onto the frame for decellularisation. The fresh bladders felt more compliant and easy to stretch, whereas the twice-frozen bladders felt stiffer, as though a greater amount of force was required to stretch it in comparison. This observation was supported by the findings in Chapter 4, where the transition strain of twice-frozen bladder tissue was calculated to be significantly less ($p = 0.001$) than that of fresh bladder tissue (2.04 and 1.91 as compared to 2.88 and 2.61, in the $x$ and $y$ directions respectively). This increase in transition strain is likely to have caused the observed differences between the tissue types, because stretching both materials beyond the transition stress of the twice-frozen tissue would result in greater stresses, and therefore a greater stretching force, in the twice-frozen tissue. Theses differences did not affect how the material was stretched onto the frames.

The original decellularisation process required each bladder to be emptied of solution and refilled with a different solution at each stage of the process. During the process,

bladders were decellularised in containers which also had to be emptied and refilled with a different solution. This was a very time-consuming and labour-intensive process. Bladders which were stretched onto frames did not have to be individually filled, and therefore each stage of the process involved changing the solution in the container only. This procedure was far easier to perform, and required considerably less time to complete (approximately 15 min compared to 1 h for $n = 3$).

All bladders ($n = 3$) were stacked on a single IKA KS 130 orbital shaker during decellularisation. Originally, the intention was to place each bladder on a Grant PSU 10i orbital shaker. A preliminary test using the Grant shaker demonstrated that it was not suitable for the container (270 mm × 270 mm × 125 mm) which was selected to contain the bladder frames. The Grant shaker had a larger rotational radius, and therefore was run at a lower rotational speed than was required for the IKA shaker. This lower rotational speed was similar to the natural frequency of the oscillation of solution in the bladder container, and the shaker failed to maintain a constant speed. This demonstrated that the shaking regime which the bladder tissue is subjected to is not only affected by the shaker it is placed on, but the container it is placed in.

Histology and DNA quantification were used to assess the tissue which was decellularised using the flat-bed method. The DNA content of the bladders was decreased by more than 99 % relative to the native control tissue, and the mean DNA content was less than the mean amount reported in the original decellularisation process (Bolland *et al.*, 2007). The mean DNA content of both the fresh and twice-frozen flat-bed decellularised bladders were less than the maximum level of dsDNA suggested by Crapo *et al.*, 2011 for decellularised tissue (less than 50 ng · mg$^{-1}$). Two out of six of the bladders had tissue DNA concentrations which were above this suggested level (50.9 ng · mg$^{-1}$ and 60.7 ng · mg$^{-1}$), however the DNA quantification technique used in this study measured the content of both dsDNA, ssDNA and ssRNA; whereas the criterion suggested by Crapo *et al.* was only for dsDNA. Samples for histology were taken from different regions of the tissue in order to determine whether it was likely that the entire region region of interest of the tissue had been decellularised. Histological samples were taken from locations within a central 8 cm × 8 cm region of the final piece of bladder tissue. This area was equal to the size required for an acellular bladder patch material which could be used in surgery. All histological sections taken from the sampled regions demonstrated a removal of cellular material (Figures 6.12 and 6.13). This suggested that all cellular material had been removed from the central 8 cm × 8 cm regions of the decellularised tissue. This supported the hypotheses that bladders were able to be decellularised when biaxial strain is applied in a flat sheet configuration, and that it was adequate

for bladders to be stretched to within 10 % of the target $z$ strain for this to occur. Therefore, it was demonstrated that a region of decellularised bladder could be produced using the flat-bed method which was of a clinically relevant size.

Collagen is the the most abundant structural protein in bladder tissue (Aitken & Bägli, 2009), and changes to the degree of collagen crosslinking is associated with abnormal tissue function (Skrzyński *et al.*, 2010). When tissue containing collagen is heated, there is a point known as the collagen denaturation temperature whereby the collagen molecules change from an ordered to a random structure (Bigi *et al.*, 1987). A change in the degree of collagen crosslinking results in a change in the collagen denaturation temperature of the tissue (Sionkowska & Kamińska, 1999), and therefore this transition temperature can be used to assess the level of crosslinking is biological tissue.

All samples which were tested using DSC produced heat flow curves which exhibited a point of transition. The exceptions to this were the control samples which were fixed using NBF. These samples were very highly crosslinked by the fixing process, and therefore were unlikely to denature in the tested temperature range. The control samples which were heated were done so in order to break some—but not all—of the hydrogen bonds within the tissue and to disrupt the collagen structure. The bonds in the structure which remained were consequently able to be broken at a lower temperature, which therefore resulted in the reduction of denaturation temperatures which were observed. There was no significant difference between the fresh and twice-frozen native bladder tissue samples. This indicated that freezing and thawing did not affect the integrity of the collagen structure of the tissue. This was contrary to findings in the literature, which demonstrated that freezing causes tissue dehydration, resulting in a change in denaturation temperature (Venkatasubramanian *et al.*, 2010). However, frozen tissue samples were stored in PBS prior to testing, and the effects of tissue hydration on thermal stability have been known to be reversible (Venkatasubramanian *et al.*, 2010). Therefore it is likely that the denaturation temperature of bladder tissue was affected by the freezing process, but that these effects were reversed prior to DSC testing. There were no significant differences between the collagen denaturation temperatures of the bladder tissues which were decellularised using the flat-bed method and the native bladder tissues, which suggested that the decellularisation process also resulted in a negligible change to the structure of the collagen.

The mean denaturation temperatures of the tissue decellularised from fresh using the calculated filling method and the tissue decellularised from twice-frozen using the calculated filling method were significantly higher (ANOVA and post Tukey HSD test) than the means of the other tissue types. The fresh calculated filling samples

had a significantly higher mean than all the other group means, and the twice-frozen calculated filling samples had a significantly higher mean than the fresh native group mean. This was surprising because these samples were subjected to the same decellularisation conditions as the bladders which were frame-stretched. However, the twice-frozen calculated filling bladder samples were stored for longer than the flat-bed tissue samples before being tested, and the fresh calculated filling bladder samples were stored for much longer than the other samples. These samples were not stored in UV-resistant containers, and so may have been subjected to low dosages of UV irradiation. UV radiation is known to cause crosslinking of collagen (Weadock *et al.*, 1995), which would account for the observed increases in collagen denaturation temperature. No significant differences in collagen denaturation temperature were found between the different regions of the decellularised tissues. This suggests that the negligible impact of the decellularisation process on the collagen was consistent across all regions of these tissues.

## 6.5 Conclusions

Specifications were defined for a porcine bladder tissue decellularisation process which would not require whole bladders to be distended, and therefore would be compatible with a scalable manufacturing process. A frame design was developed which would be able to support a stretched piece of bladder tissue in the required biaxial strain state which was determined in Chapter 5. A procedure was developed to mount bladder tissue onto the frame as part of the decellularisation process. Possible improvements for the frame design and tissue mounting procedure were identified.

Decellularising bladder tissue in a flat sheet configuration was easier to perform and less time-consuming than the previous method of distending bladders. Histological sections taken from samples of bladders decellularised using this flat-bed method showed no signs of cellular material. DNA quantification demonstrated that the DNA content of the decellularised bladders was reduced by more than 99 % relative to native tissue. Cells cultured with samples taken from decellularised bladders did not exhibit any cytotoxic effects. The collagen denaturation temperatures of frame-stretched decellularised bladders were not significantly different from those of native bladder tissue. There appeared to be no differences between the bladder tissue which was decellularised from twice-frozen, and tissue decellularised from fresh. The decellularised regions of bladder tissue which were produced were of a clinically relevant size.

# Chapter 7

# Discussion and future work

## 7.1 General discussion

The overall aim of this study was to develop a procedure for decellularising full-thickness porcine bladder tissue which would be suitable for translation to a scalable manufacturing process. A technique was developed to stretch flat sheets of bladder tissue onto bespoke equipment, which allowed the tissue to be processed using a previously established decellularisation protocol. The strains applied to flat bladder sheets during decellularisation were demonstrated to result in tissue decellularisation when applied to whole distended bladders. Applying strain was necessary in order to reduce the thickness of the bladder wall tissue, which had previously been demonstrated to be necessary for the decellularisation solutions to diffuse into the biomaterial in sufficient concentrations to remove immunogenic material. Finite element modelling was used to demonstrate that suitable strains were applied to all regions of the flat tissue sheets when the biaxial strains were applied. Tissue decellularised using the new technique exhibited no evidence of cellular material and its ECM histoarchitecture was preserved. These findings were verified using histology and DNA extraction and quantification.

There is a current clinical need for a material to be used to augment the bladders of patients with end-stage bladder disease. The current gold standard surgical intervention is augmentation enterocystoplasty, which involves augmenting the bladder with tissue taken from the patient's gastrointestinal tract (Greenwell *et al.*, 2001). However, there are numerous problems associated with the use of this tissue, such as mucus secretion, stone formation, metabolic disturbances, and increased risk of malignancy (Gough, 2001). An alternative augmentation material may provide a similar or improved performance compared to gastrointestinal tissue, but without the limitations of the use of the mucus-secreting and absorptive epithelium. It may

be possible to produce a material which is able to form functional bladder tissue upon implantation using tissue engineering principles.

Natural biological scaffolds are a potential source of scaffold material for regenerating and repairing tissues of the body. This is because they can mimic the structure and function of the native ECM and retain many of the proteins which are present (Badylak *et al.*, 2012). Several protocols have been developed to decellularise tissues in order to make them suitable for use as decellularised allografts or xenografts. These protocols make use of a variety of techniques to remove immunogenic material from tissues, including physical (e.g. manual disruption, agitation and thermal shock), chemical (e.g. solvents, detergents and ionic solutions) and enzymatic (e.g. trypsin, DNase) methods (Gilbert, 2012). Previously, a process was developed to decellularise full-thickness porcine bladders (Bolland *et al.*, 2007). The process was based on a protocol by which was developed in order to decellularise cardiac valves (Booth *et al.*, 2002). Unlike cardiac valves, porcine bladder tissue was too thick to allow effective penetration of the decellularisation solutions into the tissue. It was consequently necessary to apply hydrostatic pressure to the whole bladders in order to distend them with the required solutions, thereby stretching the tissue and reducing its thickness. This state of deformation was hypothesised to be fundamental to the decellularisation of porcine bladders.

Several requirements need to be met for a novel surgical material to be used clinically. These include demonstrating the material is of benefit to the target patient population, acquiring appropriate regulatory approval for the material, ensuring the material can be manufactured in a way which assures the quality of each piece of material, and economic viability. The original bladder decellularisation process was not feasible or economically viable to be produced as part of a manufacturing process because the method of distending each bladder at each stage of the process was time-consuming, difficult to perform, and required volumes of solution to be used based on the filling requirements of the organs rather than the chemical action of the solutions. Therefore, an alternative method of decellularising porcine bladder was required which would reduce the thickness of the tissue in order to demonstrate the proof of technical principle that decellularised bladder could be produced using a method that was compatible with a manufacturing process.

The original decellularisation process involved distending bladders with volumes of 500 ml (Bolland *et al.*, 2007). Preliminary tests demonstrated that this did not always result in a complete removal of cellular components from the tissues (Figure 3.1). It was subsequently hypothesised that this single volume was not sufficient to decellularised bladders of differing sizes, particularly larger bladders which may need to be filled by amounts greater than 500 ml in order to sufficiently stretch the

tissue. It is possible that the bladders which were used by Bolland *et al.* were of a more consistent size than the ones used in this study, and therefore 500 ml was a sufficient volume to fill the bladders in the previous study. However, the patent which was filed alongside the original study reported that bladders may need to be filled with a range of volumes during decellularisation (from 250 ml to 750 ml) depending on the initial size of the organ (Bolland *et al.*, 2008). This filling criterion was non-specific, and therefore inadequate for determining how much stretch should be applied to bladder tissue during decellularisation.

In order to determine the specific volumes which bladders should be filled with during decellularisation, an experiment was carried out to identify a relationship between the pre-distended dimensions and filled capacity of fresh bladders. The initial dimensions of twelve bladders were recorded. The bladders were suspended from a rig and filled until their capacity was reached. Several relationships were found predicting bladder capacity from bladder length, width, area, thickness and tissue volume (Figures 3.2 and 3.3). Of these relationships, the one which predicted capacity from width × apex-to-ureter length was subsequently used to predict bladder capacity from initial bladder dimensions because of its high correlation ($R^2 = 0.924$) and simplicity to compute under laboratory conditions. The relationship for bladder capacity were used to calculate the filling volumes of six bladders during decellularisation. The six bladders which were distended with these volumes showed no evidence of cellular material when examined histologically (Figures 3.5 and 3.6) and a mean reduction in DNA content of 99.2 %. The mean volume the bladders were filled with during decellularisation was 726 ml, which suggested that 500 ml may not have been suitable for applying the stretch required for decellularising these bladders.

In order to determine the state of mechanical deformation of bladder tissue during decellularisation, studies were conducted in which twelve bladders were immersed in a tank in order to simulate decellularisation conditions and filled with PBS quasi-statically until failure. The capacities of these bladders were calculated using the previously found relationship between capacity and width × length. Measurements taken during the experiment were later used to calculate the stress, strain and thickness of the bladders when they were filled with volumes equal to their calculated capacities (Figure 4.8). The strains of bladders filled to their calculated capacities were found to be invariant with bladder capacity, demonstrated by the gradients of the relationships, which were found to be statistically indifferent compared to zero ($p_x = 0.331$, $p_y = 0.667$). The means of the strains were equal to 2.00 in the circumferential ($x$) direction and 1.40 in the longitudinal ($y$) direction. These strains were subsequently applied to bladders which were distended and subject to

the decellularisation process. Sutures placed on the surface of the bladders were used to monitor the strains applied to the tissue during filling. Samples taken from these bladders for histological analysis indicated that the tissues were acellular (Figures 3.5 and 3.6), and DNA quantification was used to determine a mean DNA reduction of 99.6 % relative to native tissue. It was therefore concluded that application of these strains to bladder tissue provided adequate thinning of the tissue to result in decellularisation.

The immersed distension experiment was used to calculate how much strain should be applied to bladder tissue so that it would be fully decellularised by the diffusion of solutions into the tissue. Bladder capacity was the criterion which was used to determine the point at which bladders were sufficiently stretched. A relationship to calculate bladder capacity from initial bladder size was found in Chapter 3. Permeability studies could also have been used to find the point at which solutions would have adequately diffused into the tissue for decellularisation. However, due to the complex nature of the decellularisation process—which involves numerous solutions at different temperatures, each designed to perform a specific action on the tissue—it is likely that numerous studies would have had to be performed in order to determine the thickness of tissue required for each step of the process. These studies would have acquired a more in-depth knowledge of the basic science regarding the mechanics of the diffusion of solutions into bladder tissue, and would likely have found a more accurate solution for the critical decellularisation thickness of bladder tissue. However, the main aim of this project was to develop a new process for decellularising bladder tissue, and therefore a complete understanding of the effect of tissue stretching on the diffusion of solutions into the tissue was not necessary to achieve this objective. Instead, an approach was taken whereby a state of bladder stretching—which would result in decellularisation—was hypothesised (bladder capacity), and then the tissue was processed when held in this state in order to determine whether the state deformed the tissue sufficiently for decellularisation to occur. Whilst this method resulted in less background knowledge being uncovered, it was still able to determine a stretching criterion for bladder tissue to allow decellularisation to occur, and enabled the project to progress onto developing a manufacturing-compatible process; the main aim of this project.

When bladders were immersed and distended to determine the mechanical deformation state of the tissue during decellularisation, the gradient of the relationship between bladder capacity and tissue thickness did not significantly differ from zero ($p = 0.632$, Figure 4.8b), and the thickness of the tissues were found to be $0.61 \pm 0.09$ mm (mean $\pm$ 95 % CI). It was therefore concluded that the thicknesses of the bladders were invariant with bladder capacity. However, serial application of

the Grubbs' test for outliters identified two outliers of tissue thickness which were significantly greater than the thicknesses of the other bladders. These wall thicknesses of these bladders were calculated to be 1.08 mm and 1.32 mm. It is possible that these thicknesses may not have been sufficiently small enough for the tissue to be decellularised, and therefore these bladders should be excluded from the decellularisation process. Due to bladder tissue being incompressible (Wells & Liang, 2011), tissue which was atypically thick when subject to the same decellularisation strains would have been atypically thick before stretching occurred. Therefore, an initial inspection of bladders could be undertaken to exclude overly thick bladders—with thicknesses above a critical thickness—from a manufacturing process. The critical thickness could be found by decellularising bladders of varying thicknesses, and observing which bladders exhibited signs of cellular material after processing. It may be necessary to vary the strain applied to the tissue in order to test a specific range of bladder thicknesses. Due to the consistent density of bladder tissue (Chapter 4), the initial thicknesses of bladder tissue could be accurately calculated from the size and mass of the bladder tissue. Determination of bladder thicknesses using this method is likely to be quicker and easier than measuring thickness directly, and therefore more suited to a manufacturing process.

In order for a decellularised bladder biomaterial to be used in surgery, it must be of a clinically useful size. Information was gathered from surgeons that a minimum useful size for such a material would be 8 cm × 8 cm. So that a patch of this size could be produced, it was necessary to understand how the size of the bladder tissue changed throughout the decellularisation process. It was noted in Chapter 4 that filling bladders during decellularisation by suspending them from the neck resulted in tissue which was overly stretched in the longitudinal direction compared to bladders which were immersed during filling. The tissue remained overly stretched in the longitudinal direction during and after decellularisation. This demonstrated that the size which bladders were stretched to during filling affected the final size of the tissues following decellularisation. It was hypothesised that there existed a relationship between the strain applied to bladders during decellularisation and the final strain of the tissue at the end of the process. To investigate this, the distances between markers placed on bladders were measured before, during and following decellularisation. Bladders ($n = 3$) were decellularised by the immersed controlled strain method, and strain measurements were taken in both the longitudinal and circumferential directions. A strong positive relationship ($R^2 = 0.963$, Figure 4.14) was found between decellularisation strain and final strain, which supported the hypothesis. The relationship was therefore used to calculate that applying strains of 2.00 and 1.40 during decellularisation would result in final tissue strains of 0.926 and

0.488 in the circumferential ($x$) and longitudinal ($y$) directions respectively. Therefore, in order to produce a decellularised bladder patch which is 80 mm × 80 mm in size, an initial tissue size of 41.4 cm × 53.8 cm would be required. By using the relationship to predict the required initial size of the tissue, a region of tissue which is no bigger than required can be produced, minimising waste in the decellularisation process.

The strong positive relationship which was found between decellularisation strain and final strain indicated that decellularising bladder tissue resulted in permanent tissue deformation; deformation which was proportional to the strain applied to the tissue during the process. The permanent deformation was likely to have been a result of applying strain to the tissue during decellularisation, the decellularisation process itself, or a combination of both processes. Therefore, the deformation to a new relaxed state was likely to have been mediated by changes to collagen alignment and coiling, and a loss of smooth muscle cells. Both of these have been shown to contribute to a change in soft tissue length (Chang *et al.*, 1998; Venkatasubramanian *et al.*, 2010). Furthermore, the relationship demonstrated that a greater strain applied to tissue during decellularisation resulted in a greater loss of collagen coiling. Due to the important role that collagen coiling contributes to the deformation of the tissue, a loss of coiling is associated with a decrease in both transition strain and tissue extensibility (Fratzl *et al.*, 1998), and therefore it is highly likely that the degree to which bladder is stretched during decellularisation will determine the degree to which a decrease in transition strain and tissue extensibility is observed, provided the tissue has been sufficiently stretched for decellularisation to occur.

It was thought that stretching bladder tissue in a flat sheet configuration would overcome the problems associated with distending bladders during decellularisation, and therefore be compatible with a manufacturing process. To apply the required biaxial strains to the tissue, it was decided to apply the stretch using discrete points (e.g. hooks or pins). Cruciform-shaped specimens have also been used to apply biaxial strain to tissue (Zhao *et al.*, 2014), however these require much larger pieces of tissue to be used which would not have been possible given the size of porcine bladders. The method of applying biaxial strain using discrete points is one which has been commonly adopted in the literature (Cooney *et al.*, 2016; Shahmansouri *et al.*, 2016; Khoiy & Amini, 2016; Macrae *et al.*, 2016). Deforming tissue in this manner is also conducive to producing patches of the square 8 cm × 8 cm shape required clinically. However, this method of stretching does not result in application of a completely uniform strain field to the tissue, and therefore a mode of stretching was sought which would provide adequate strain to a piece of tissue of the required size.

Finite element modelling (FEM) was used to determine an optimal mode of stretching bladder tissue. The $z$ strain of the tissue was used as the measure of tissue stretching efficacy. Specifically, the fraction of elements which were stretched to within 10 % of the target $z$ strain was calculated for each computed model, and used as the measure of comparison between different models. Increasing the number of points the tissue was stretched with and the border width of the tissue both increased the fraction of elements which were stretched to within the target strain range, (Figures 5.7 and 5.8) however variation in the number of points had a greater impact on strain uniformity than border width. Stretching a piece of tissue using greater than five discrete points along each side of the rectangular material resulted in a negligible increase in the area of the tissue which was stretched to within the required specifications. Eilaghi *et al.*, 2009 also reported five to be an optimal number of discrete points to use along each side of biaxially stretched specimens. When stretching bladder tissue using five discrete points, it was found that a mean of 84.8 % (for various widths of border) of the bladder area was stretched to within 10 % of the target strain. (Nielsen *et al.*, 1991), who stretched tissue using four discrete points along each edge, reported that the strain of a biaxially tested specimen was uniform to within 3 % of the applied strain for a region equal to 25 % of the overall dimensions.

It was noticed that when stretched using discrete points, the central region of the tissue tended to be sufficiently stretched, whereas the regions of the tissue proximal to the pins were typically under-stretched. This is visualised in Figure 5.11. It was consequently hypothesised that there existed a stretching scenario whereby a central region of the tissue would be stretched to within 10 % of the target $z$ strain, and that this central region could be dissected from the other tissue to form the final tissue patch. A model was generated which resulted in over 99 % of the elements within the central 80 % of the tissue being stretched to within 10 % of the target $z$ strain, which used five pins along each edge of the tissue to apply the required strains, when using a border width of 2 mm or greater. Eilaghi *et al.*, 2009 found that the shape of the border region had little effect on the strain state of the tissue. When modelling the stretching of a central region of bladder tissue, the width of the border was affected by the uniformity of the strain field, however this affect was minimal above border widths of 2 mm (Figure 5.8). However, Eilaghi *et al.*, 2009 used a border width which was 10 % of the width of the main area of the material, whereas a 2 mm border of bladder material represented 2.8 % of the main area width. It is therefore likely that above a certain border width, the shape of the material makes little difference to the uniformity of the tissue. This suggests that when stretching bladder tissue as part of a manufacturing process, the border of the tissue will not

need to be cut with a high level of precision provided that a minimum border width of 2 mm is achieved.

A problem with the stretching regime which was used to apply strain to the bladder was that tissue had to be wasted during the decellularisation process. The dimensions of the region of the tissue which would make up the final patch material were 41.6 mm × 53.8 mm. In addition to this, an inside border of 2.5 mm × 3.1 mm and an outside border of at least 2 mm were required, resulting in a total tissue size of 50.5 mm × 64.0 mm. These border regions were not likely to become decellularised, however they were still in contact with the decellularisation solutions, and therefore may result in larger volumes of decellularisation solutions being required to ensure the decellularisation of the patch region of the tissue. More importantly, a larger size of tissue would require a bladder of a larger size from which this piece of tissue could be isolated. Consequently, a larger tissue size would effectively exclude a greater number of (smaller-sized) bladders from the decellularisation process, since they would not be sufficiently large to produce a region of the required size. Using data collected from bladders tested using the immersed distension experiment, 54 % (13/24) of bladders would be of a suitable size for decellularisation and 46 % (11/24) of bladders would not be suitable for the decellularisation process. However, the number of bladders rejected from the process could be decreased by decreasing the initial size of the tissue. This could be achieved by increasing the acceptable range of $z$ strain which would be considered to be acceptable for tissue stretching. The acceptable strain range which was used in this study was that the tissue had to be within 10 % of the target $z$ strain of $-0.861$. This resulted in a minimum of 82.8 % of the main area of the stretched tissue being stretched to within this range. A larger range may be used provided that evidence is gathered regarding the acceptable tolerance for this strain to ensure complete tissue decellularisation. The percentage of the main area of the tissue which is stretched to within the required specifications could also be increased by increasing the number of discrete points used to stretch the tissue, although this would make the tissue stretching process increasingly more complex.

In order to investigate whether flat sheets of bladder could be decellularised, it was necessary for flat sheets of bladder tissue to be held in a stretched state during decellularisation. A piece of equipment was designed which was able to hold pieces of bladder tissue in the way which was modelled in Chapter 5. The equipment consisted of a rigid frame which was manufactured using the 3D printing method of selective laser sintering (SLS). The frame was made from the autoclavable and chemical-resistant polymer Duraform PA (polyamide/nylon). The frame was designed so that customised dissecting needles were able to integrate with the frame in a manner

which supported the tissue in the required state of deformation.

A process for manufacturing decellularised bladder would benefit from using lower volumes of decellularisation solutions. Bladders decellularised using the flat-bed method were immersed in containers filled with 2 L of decellularisation solution. These volumes were used in order to maintain consistency with the other protocols developed in this thesis. However, unlike the method of distending bladders, the minimum volumes of solutions required to decellularise flat sheets of tissue are not limited by the geometry of the tissue. Other decellularisation protocols, including those found in the literature and those developed in our laboratory, have used volumes of solutions which were proportional to the amount of tissue which was being decellularised. For example, (Hogg *et al.*, 2013) used 1 L solution per 2500 $cm^2$ human dermis, (Montoya & McFetridge, 2009) used 100 ml solution per 85 mm length of human umbilical vein, and in our laboratory arteries have required (1 ml solution per 1 mm length of tissue); human amnion has required(5 ml solution per 1 $cm^2$ area of tissue); and porcine pericardium has required (2 ml solution per 1 $cm^2$ area of tissue) It is therefore highly likely that there exists a ratio of solution volume to amount of bladder tissue which would result in the tissue being reliably decellularised whilst not using an excess of solution. Finding this ratio would make the process more economical and require bladders to take up less space in a manufacturing facility.

A procedure was developed to mount bladder tissue onto the decellularisation frames (Figure 6.5). The procedure involved firstly dissecting a region of tissue from the dorsal surface of a bladder of the required size for decellularisation, using the pin guide plate as a guide. The pin guide plate was then used to guide pins through the bladder tissue and into the cork board below at the required locations. The guide plate was removed, the pins were extracted from the cork board but not the tissue, and the tissue was transferred by hand to the frame. Pins were slowly placed into the required locations in the frame in opposing pairs, using a sequence which ensured that the tissue was evenly stretched. The procedure adequately stretched the tissue in the required manner, and was sufficient for this proof-of-principle study.

Several problems were identified with the bladder mounting procedure. Placing the pins through the tissue and into the cork board resulted in the tissue being pinched between the needle of the pin and the cork board, and care was required to free the material, which posed the risk of pins coming free from the tissue. Additionally, cork changed its appearance when autoclaved. It became more brittle, and it is likely that a piece of cork would only be able to be used a limited number of times. Bladders were transferred to the frames by hand. The loose nature of the tissue made this procedure difficult: during the transfer the pins were at risk from being

displaced from the material This also made it difficult to identify the corner pins to begin the stretching process. The process therefore required care and time to be taken due to the risk of human error, as stretching the bladder using the wrong pins may have resulted in damage to the tissue.

Bladder tissue was stretched onto the frames by hand. This was carried out by moving the pins into the required locations on the frame. Preliminary tests indicated that the sequence which the pins were placed into the frame affected the final deformation of the stretched tissue. It was thought that this was due to the elastic hysteresis which soft tissue exhibits (Safadi & Rubin, 2014). It was important to stretch the tissue uniformly in order to prevent some regions of the tissue from being under-stretched, and to minimise the risk of damage to the tissue caused by the pins. Furthermore, it was shown in Chapter 4 that the strain applied during decellularisation affected the amount of permanent deformation which occurs during the decellularisation process. Therefore, it is likely that tissue which is not stretched uniformly during decellularisation will not be homogeneous at the end of the process. It is desirable for surgical patches to be homogeneous, because the localised variations in mechanical properties (due to a differing amounts of collagen coiling) are likely to result in varied cell behaviour in the implanted scaffold (Farhat & Yeger, 2008). In order to ensure that the decellularised tissue would be homogeneous, the tissue was stretched uniformly onto the frames. Uniformity was maximised by stretching the pins in opposing pairs, in a sequence which kept the material as symmetrical as possible during the procedure. Although this method did result in evenly stretched tissue, the stretching process resulted in regions of the tissue which were temporarily over-stretched, which risked damage being caused to the tissue. A method of stretching the bladders which displaced all the pins simultaneously would stretch the tissue uniformly, not over-stretch any regions of the tissue, and would minimise the risk of tissue damage.

It was discussed in Chapter 6 that stretching the tissue onto frames occasionally resulted in rips into the tissue, caused by the pins. As mentioned above, the mounting process of placing two pins at a time into the frame contributed to this. Supporting the tissue by moving adjacent pins helped minimise this effect. It was also noticed that stretching the tissue too quickly increased the risk of tearing; a consequence of the viscoelastic nature of the tissue. Stretching the tissue slowly minimised tearing by allowing the material to undergo viscoelastic creep. However, this was difficult to judge by eye, and therefore a technique which limited or controlled the rate at which strain could be applied to the tissue would eliminate this source of the problem. Initially, the pin guide plate was used to cut pieces of bladder tissue with border widths of 2 mm. It was noticed that tearing was less prevalent in tissue with larger border

widths. This was because the force required to stretch the tissue was spread over a larger cross section of material, resulting in a reduction in tissue stress. Consequently, border widths of up to 5 mm were used where possible in order to minimise tearing. However, using larger border widths required a larger amount of tissue to be used, and therefore it would be desirable to find an optimal border width capable of stretching the tissue to minimise the size of tissue required for decellularisation. An FEM model could be used to find the optimal width of border which minimises the required tissue size whilst not resulting in excessive tissue stresses.

In order to test the hypothesis that bladder tissue could be decellularised in a flat sheet configuration, both fresh ($n = 3$) and twice-frozen ($n = 3$) bladders were stretched onto frames and were subject to the decellularisation process. The quantity of DNA in the tissue was reduced by a mean of 99.1 % relative to native bladder tissue, and the DNA content of each batch of decellularised bladders ($17.5 \pm 71.9\,\mathrm{ng \cdot mg^{-1}}$ for once-frozen, $29.2 \pm 73.9\,\mathrm{ng \cdot mg^{-1}}$ for twice-frozen; mean $\pm$ 95 % CI) was less than the DNA content reported in the original decellularisation process ($100 \pm 100\,\mathrm{ng \cdot mg^{-1}}$, Bolland *et al.*, 2007). The mean DNA content of each batch of bladders also satisfied the criterion suggested by Crapo *et al.* of $50\,\mathrm{ng \cdot mg^{-1}}$ for the upper limit of DNA content in decellularised tissues. There was also a lack of visible dsDNA in decellularised tissue sections which were stained with DAPI. Tissue sections stained with H&E also demonstrated an absence of cellular material and conservation of the tissue histoarchitecture. Furthermore, there were no differences, either through gross observation of when sections of these tissues were observed histologically, between the tissue decellularised from fresh and the tissue decellularised from twice-frozen (Figures 6.12 and 6.13). These findings therefore supported the hypothesis that bladder tissue is able to be decellularised when stretching in a flat sheet configuration. The method which was used to stretch tissue onto frames during decellularisation resulted in some regions of the tissue being under-stretched, but within 10 % of the target $z$ strain (see Chapter 5). These findings therefore also demonstrated that the regions of the tissue which were less stretched were still stretched adequately for decellularisation.

Bladder urothelium deteriorates rapidly if it is left in contact with urine (Southgate *et al.*, 2002). Prolonged exposure could cause damage to the underlying layers of the tissue and subsequently affect the structure and composition of the ECM. To prevent this from occurring, the original decellularisation process used bladders which were transported fresh from the abattoir in transport medium. Decellularisation of these bladders began within 4 h of animal slaughter to minimise tissue degradation (Bolland *et al.*, 2007). However, it is not feasible for bladders to be collected from an abattoir and immediately processed as part of a manufacturing

process. For flexibility with transportation and storage, it would be ideal for the tissue to be frozen and thawed twice before processing. Bladders transported for the original process were also preserved by transporting in transport medium. This solution was designed to maintain viable urothelial cells (Southgate *et al.*, 2002), and therefore may have been unnecessary for transporting bladder tissue destined for decellularisation.

Freezing and thawing is known to cause disruption to the ECM of biological tissue due to the formation of ice crystals (Huang *et al.*, 2013). It is therefore likely that subjecting bladder tissue to two freeze-thaw cycles may have some lasting effects on the structure and mechanical properties of the tissue. Additionally, transporting bladders without the use of transport medium may result in degradation of the urothelium, thereby exposing the underlying layers of bladder tissue to urine and the degradation products of the urothelium. This may result in alterations to the biochemical composition of the tissue caused by autolysis. To assess the impact of freezing and transportation without transport medium on bladder tissue, the mechanical properties of fresh (transported with transport medium), once-frozen and twice-frozen (both transported without transport medium) bladders were compared. Bladders were mechanically tested using the immersed distension experimental method in order to collect biaxial stress–strain data for these three tissue types. The stress–strain curves were used to calculate the toe region modulus, linear region modulus, transition stress and transition strain of the tissues in the circumferential ($x$) and longitudinal ($y$) directions. The intrinsic link between the biaxial stress–strain responses of these materials in each of their directions meant that, these parameters could not be calculated directly from the stress–strain curves. To do this, a new variable was derived which was named uniaxial equivalent strain (UE strain) (see Appendix C). When stress was plotted against UE strain, the gradients of these curves were equal to the modulus of the material in each direction. This meant that the required material parameters could be found directly from these graphs. There was no significant difference between the toe region moduli ($p = 0.234$) of the different tissue types, indicating that the tissues were similarly stiff in the toe region of the curves. However there was a significant reduction in the linear region modulus ($p < 0.001$) of the frozen tissue types, which suggested that the transition point occurred at a lower strain, followed by a reduced tissue modulus between transition and failure as indicated by the decrease in linear region modulus for the frozen tissue types ($p = 0.001$). These freezing-induced changes have also been reported in the literature (Grassl *et al.*, 2004; Venkatasubramanian *et al.*, 2006), and have been reported to be caused by an increase in collagen fibre alignment and a lack of smooth muscle function Venkatasubramanian *et al.*, 2010.

The increased collagen fibre alignment meant that the fibres began to bear load at lower strains, causing the observed decrease in transition strain. However, the study did not postulate why there would be a decrease in linear region modulus of the tissue. It is likely that during the alignment of the collagen fibres, some fibres become more aligned than others, therefore causing the fibres to bear load over a wider strain range.

The observed differences between fresh and frozen tissue were significant but not large, and therefore there would be little difference between the mechanical performance of these tissues if implanted *in vivo*. However, changes in the ECM stiffness are known to affect cell behaviour through differences in biomechanical signalling (Korossis *et al.*, 2006), which could affect how the scaffold would regenerate, and therefore further experimentation would be required to determine whether these changes in mechanical properties would significantly affect the performance of the biomaterial when used surgically. A decrease in tissue extensibility was also observed during the bladder tissue decellularisation process (Bolland *et al.*, 2007). It would therefore be valuable to investigate the mechanical properties of bladder tissue which has been decellularised following a freezing regime to determine the interaction of these two processes.

Bladders transported without transport medium were dissected and rinsed with PBS before being frozen. This was performed to displace the urine in order to prevent degeneration of the urothelium, and therefore minimise damage to the underlying layers of tissue. During a manufacturing process it may not be possible to carefully dissect and wash large numbers of bladder before they are frozen because it is likely that freezing would take place before transportation, at the abattoir. However, it would be necessary to evacuate urine from the organs before freezing in order to ensure the tissue was not damaged before decellularisation. Therefore, a suitable method of rinsing the inside of bladders quickly and simply before freezing may be required. For example, it may be feasible to make a cut in the bladder tissue from the urethra down the ventral surface (to prevent damage to parts of the tissue which would be used in decellularisation), and to shake them against an absorbent material (in order to remove excess liquid and prevent ice crystal formation).

It was thought that a change to the transportation and storage regime of bladder tissue may have resulted in changes to the efficacy of the decellularisation process as freezing has been shown to decrease the effectiveness of decellularisation (Tuan-Mu *et al.*, 2014). To assess whether transporting bladders without transport medium and subjecting them to two freeze-thaw cycles had an effect on the outcome of the process, both fresh (transported with transport medium) and twice-frozen bladders (transported without transport medium) were decellularised using

both the calculated filling decellularisation method and the flat-bed decellularisation method. Freezing the tissue did not appear to impair the ability of the tissue to be distended with solution or stretched onto the frames, which corroborates with the previous findings that frozen tissue is stiffer than fresh tissue. Assessment of the decellularised tissue using histology (Figures 3.5, 3.6, 6.12 and 6.13) and DNA extraction and quantification demonstrated that both the fresh tissue and the twice-frozen tissue were acellular. There were no significant differences between the DNA content of fresh and twice-frozen decellularised tissue ($31.6 \pm 31.2\,\mathrm{ng \cdot mg^{-1}}$ and $21.1 \pm 21.9\,\mathrm{ng \cdot mg^{-1}}$ respectively, mean $\pm$ 95 % CI). This indicated that bladders may be transported without transport medium and put through two freeze-thaw cycles before being decellularised with no detrimental effect on the process. Freezing and thawing tissue is a technique which has previously been used to aid the decellularisation of biological tissue (Fermor *et al.*, 2015), therefore it was likely that freezing and thawing the tissue aided the removal of cellular material from the tissue rather than hindered it. However, the compounding effect of freezing, thawing and decellularising tissue may have resulted in a difference in the mechanical properties of the decellularised tissue.

The procedure developed to stretch flat sheets of bladder proved to be suitable for this proof-of-concept study. However, several problems were identified with the process which may be circumvented with a change to the design of the equipment which was used. There were problems associated with the use of a cork board to aid the placement of the pins into the tissue. An alternative pin placement block could therefore be developed, which could the take the form of a flat piece of material, with cavities placed in the required locations in order for the pins to pass through the entire thickness of the tissue. It is likely that this block would have to be developed alongside a revised guide plate which would be compatible with the block. Difficulties were also found when the tissue was transferred from the cork board to the frame. It would be desirable for a piece of equipment to be designed which would be able to carry the tissue to the frame, rather than performing the transfer by hand. The pin placement block could be developed so that it is also suitable for performing this transfer. It may have to remain in place on the frame until the tissue was mounted, and it is possible that the block may have to dock with the frame during decellularisation. The current stretching procedure of systematically placing pairs of pins into their final positions resulted in regions of the tissue becoming over-stretched and risked the tissue being torn. These problems could be minimised by placing additional pin cavities into the design of the frame so that the tissue could be incrementally stretched. Applying the strain in several increments would also be less demanding on the user, and would slow down the user to allow the material to

undergo viscoelastic creep.

Minimising human error and human input in the developed protocol is likely to improve process efficiency and improve the quality of the decellularised tissue. A pin guide plate was used to ensure pins were placed into the correct locations in the tissue. Placing the guide plate into the required location and removing it again took up time, and the use of the plate required it to be sterilised. Replacing the guide plate with a non-contact method of guiding the pins in place would therefore decrease the complexity of the procedure. This could be achieved by projecting the locations onto the tissue (e.g. using lasers). Alternatively, a piece of equipment could be developed to place pins into the tissue at the correct locations. Such a piece of equipment may place pins more quickly and accurately than if performed manually.

It was previously discussed that it would be ideal to stretch the tissue by moving all the pins simultaneously. This would minimise the chances of tearing the tissue and result in tissue which is uniformly deformed. A bespoke piece of equipment could be designed to perform this task of deforming the tissue linearly from an unstretched state to a fully stretched state. Such a piece of equipment should displace the pins adequately slowly to allow the tissue to undergo the required viscoelastic creep, and allow the tissue to be easily transferred to the frames for decellularisation. The frames themselves could be designed to stretch the tissue, however it is likely that this would add complexity to and increase the size of the frames, which ideally should be as compact as possible in order to minimise solution volumes in the decellularisation process.

Translation of the developed protocol to a commercial manufacturing process may be further adapted to more easily accommodate larger batch sizes. Features were designed into the frame which allowed them to be vertically stacked. These demonstrated that it may be possible to connect frames together in a way which would save space and reduce the volumes of decellularisation solutions required during decellularisation. It is foreseeable that a container could be designed which would allow several frames to be stacked alongside each other, allowing large batches of tissue to be processed whilst occupying a minimal space. This is particularly important for the current lab-based protocol, in which the tissues must be placed into incubators of a limited size. However, the flow of fluid in a container which houses several bladders may be very different from the current process of agitating the bladders on shakers. The orientation of the flat tissue sheets and their position in the tank is likely to also affect the fluid flow around the tissue, and these containers may be too large to be placed onto orbital shakers. It may therefore be more practicable to design a container in which flow is provided to the decellularisation solutions by

means of a pump. A pump system may add complexity to the system and be difficult to implement. However, it may make the changing of solutions easier, reduce the risk of contamination, and may allow solutions to be changed without having to move the bladders into an aseptic environment.

## 7.2 Conclusions

Decellularisation protocols developed in the literature have used the application of hydrostatic pressure to tissues and organs in order to decellularise the tissue (Price *et al.*, 2010; Ott *et al.*, 2008; Montoya & McFetridge, 2009). However, none of these protocols employed the use of hydrostatic pressure in order to apply large mechanical deformations to the tissues. The exception to this is the original full-thickness bladder decellularisation process, which used a novel method of applying hydrostatic pressure in order to distend bladder tissue (Bolland *et al.*, 2007). It was thought that diffusion of the decellularisation solutions into the tissue was facilitated by the reduction in thickness caused by distending the organs. However, the method of distending the organs was not considered to be compatible with a manufacturing process. The main aim of this study was to develop a new method of deforming bladder tissue which would be compatible with a manufacturing process. To do this, an experiment was performed in order find a relationship which was able to determine the specific volumes bladders should be filled with during decellularisation in order to ensure complete cell removal. The filling volumes were then used to determine the state of deformation of bladders during decellularisation. It was found that the biaxial strain of the tissue was constant across all bladders filled to these volumes. Decellularising bladder tissue in a flat sheet configuration was chosen as a configuration which would be most suited to a manufacturing process. A suitable mode of stretching flat sheets of bladder tissue was determined by modelling the deformation of the tissue when the previously found strains were applied. Equipment was designed in order to stretch bladder tissue according to this mode of stretching. Bladders stretched onto the equipment and subject to the decellularisation protocol exhibited a complete removal of cellular material. The proof-of-principle that bladder tissue could be decellularised in a flat-sheet configuration was therefore demonstrated. This represented the first time large deformations have been mechanically applied to a tissue as part of a decellularisation process. A decellularisation method was developed which could be applied to the commercial manufacture of acellular full-thickness porcine bladder tissue.

## 7.3 Future work

- Decellularise various thicknesses of bladder tissue in order to determine the maximum thickness of tissue which is decellularised by the process. Use this to determine an upper limit on the initial thickness of bladders which are able to be successfully decellularised, so that excessively thick bladders may be excluded from the process.

- Investigate whether applying different strains to bladder tissue during decellularisation results in decellularised tissue with varying mechanical properties.

- Determine the minimum volumes of solutions required to decellularised flat sheets of bladder tissue. This could be done by decellularising bladder tissue using varying volumes of decellularisation solutions and assessing the tissue for signs of cellular material. When implementing the minimum solution volume as part of the decellularisation protocol, a factor of safety for the volume should be used.

- Minimise the size of bladder material required for the flat-bed decellularisation method, so that fewer bladders will be excluded from the process due to inadequate size. Approaches for this may involve stretching the tissue with a greater number of discrete points, determination of a wider tolerance for the $z$ strain of the stretched tissue, and modelling the deformation of the bladder tissue around the pins to determine a minimum safe width for the thickness of the outside border of the tissue.

- Make improvements to the design of the equipment used for decellularising bladders using the flat-bed method. Improvements have already been identified for the design of a pin placement block (to replace the cork board), and for changes to the frame so that tissue can be stretched incrementally.

- Design equipment to further optimise the decellularisation process for commercial manufacture. A piece of equipment capable of applying even and slow biaxial strain to bladder tissue would improve the quality of and remove the human error involved in stretching the tissue. A tank capable of containing several bladders during decellularisation is likely to increase batch sizes, reduce solution changing times and optimise the use of space.

# Bibliography


Abrams, P., Cardozo, L., Fall, M., Griffiths, D., Rosier, P., Ulmsten, U., Kerrebroeck, P. van, Victor, A. & Wein, A. (2002). The standardisation of terminology of lower urinary tract function: Report from the standardisation sub-committee of the International Continence Society. *Neurourology and Urodynamics* 21(2), 167–178.

Aitken, K. J. & Bägli, D. J. (2009). The bladder extracellular matrix. Part I: Architecture, development and disease. *Nature Reviews Urology* 6(11), 596–611.

Atala, A. (2011). Tissue engineering of human bladder. *British Medical Bulletin* 97(1), 81–104.

Atala, A., Bauer, S. B., Soker, S., Yoo, J. J. & Retik, A. B. (2006). Tissue-engineered autologous bladders for patients needing cystoplasty. *The Lancet* 367(9518), 1241–1246.

Avanzini, A. & Battini, D. (2016). Integrated experimental and numerical comparison of different approaches for planar biaxial testing of a hyperelastic material. *Advances in Materials Science and Engineering* 2016.

Bader, A., Schilling, T., Teebken, O., Brandes, G., Herden, T., Steinhoff, G. & Haverich, A. (1998). Tissue engineering of heart valves - Human endothelial cell seeding of detergent acellularized porcine valves. *European Journal of Cardiothoracic Surgery* 14(3), 279–284.

Badylak, S. F., Kropp, B., McPherson, T., Liang, H. & Snyder, P. W. (1998). Small intestinal submucosa: A rapidly resorbed bioscaffold for augmentation cystoplasty in a dog model. *Tissue Engineering* 4(4), 379–387.

Badylak, S. F., Lantz, G. C., Coffey, A. & Geddes, L. A. (1989). Small intestinal submucosa as a large diameter vascular graft in the dog. *Journal of Surgical Research* 47(1), 74–80.

Badylak, S. F., Tullius, R., Kokini, K., Shelbourne, K. D., Klootwyk, T., Voytik, S. L., Kraine, M. R. & Simmons, C. (1995). The use of xenogeneic small intestinal submucosa as a biomaterial for Achille's tendon repair in a dog model. *Journal of Biomedical Materials Research* 29(8), 977–985.

Badylak, S. F., Taylor, D. & Uygun, K. (2011). Whole-Organ Tissue Engineering: Decellularization and Recellularization of Three-Dimensional Matrix Scaffolds. *Annual Review of Biomedical Engineering* 13(1), 27–53.

Badylak, S. F., Weiss, D. J., Caplan, A. & Macchiarini, P. (2012). Engineered whole organs and complex tissues. *The Lancet* 379(9819), 943–952.

Biers, S. M., Venn, S. N. & Greenwell, T. J. (2012). The past, present and future of augmentation cystoplasty. *BJU International* 109(9), 1280–1293.

Bigi, A., Cojazzi, G., Roveri, N. & Koch, M. (1987). Differential scanning calorimetry and X-ray diffraction study of tendon collagen thermal denaturation. *International Journal of Biological Macromolecules* 9(6), 363 –367.

Bolland, F., Korossis, S., Wilshaw, S.-P., Ingham, E., Fisher, J., Kearney, J. N. & Southgate, J. (2007). Development and characterisation of a full-thickness acellular porcine bladder matrix for tissue engineering. *Biomaterials* 28(6), 1061–1070.

Bolland, F., Southgate, J., Korossis, S. & Ingham, E. (2008). Decellularised bladder tissue. Pat. 2440054 A.

Booth, C., Korossis, S. A., Wilcox, H. E., Watterson, K. G., Kearney, J. N., Fisher, J. & Ingham, E. (2002). Tissue engineering of cardiac valve protheses I: Development and histological characterization of an acellular porcine scaffold. *Journal of Heart Valve Disease* 11(4), 457–462.

Brown, A. L., Farhat, W., Merguerian, P. A., Wilson, G. J., Khoury, A. E. & Woodhouse, K. A. (2002). 22 week assessment of bladder acellular matrix as a bladder augmentation material in a porcine model. *Biomaterials* 23(10), 2179–2190.

Bullock, N., Sibley, G. & Whitaker, R. H. (1994). *Essential urology*. 2nd ed. Churchill Livingstone.

Capolicchio, G., Aitken, K. J., Gu, J. X., Reddy, P. & Bägli, D. J. (2001). Extracellular matrix gene responses in a novel ex vivo model of bladder stretch injury. *The Journal of Urology* 165(6, Supplement), 2235–2240.

Cartmell, J. & Dunn, M. (2000). Effect of chemical treatments on tendon cellularity and mechanical properties. *Journal of Biomedical Materials Research* 49(1), 134–140.

Ceonzo, K., Gaynor, A., Shaffer, L., Kojima, K., Vacanti, C. & Stahl, G. (2006). Polyglycolic acid-induced inflammation: Role of hydrolysis and resulting complement activation. *Tissue Engineering* 12(2), 301–308.

Chang, S. L., Howard, P. S., Koo, H. P. & Macarak, E. J. (1998). Role of type III collagen in bladder filling. *Neurourology and Urodynamics* 17(2), 135–145.

Chen, G., Ushida, T. & Tateishi, T. (2000). A hybrid network of synthetic polymer mesh and collagen sponge. *Chemical Communications* n/a(16), 1505–1506.

Chen, G., Ushida, T. & Tateishi, T. (2001). Development of biodegradable porous scaffolds for tissue engineering. *Materials Science and Engineering: C* 17(1-2), 63–69.

Clayton, D. B., Brock, J. W. & Joseph, D. B. (2010). Urologic management of spina bifida. *Developmental Disabilities Research Reviews* 16(1), 88–95.

Cooney, G. M., Moerman, K. M., Takaza, M., Winter, D. C. & Simms, C. K. (2015). Uniaxial and biaxial mechanical properties of porcine linea alba. *Journal of the Mechanical Behavior of Biomedical Materials* 41, 68 –82.

Cooney, G. M., Lake, S. P., Thompson, D. M., Castile, R. M., Winter, D. C. & Simms, C. K. (2016). Uniaxial and biaxial tensile stress–stretch response of human linea alba. *Journal of the Mechanical Behavior of Biomedical Materials* 63, 134 –140.

Crapo, P. M., Gilbert, T. W. & Badylak, S. F. (2011). An overview of tissue and whole organ decellularization processes. *Biomaterials* 32(12), 3233–3243.

Daly, K., Stewart-Akers, A., Hara, H., Ezzelarab, M., Long, C., Cordero, K., Johnson, S., Ayares, D., Cooper, D. & Badylak, S. (2009). Effect of the $\alpha$gal epitope on the response to small intestinal submucosa extracellular matrix in a nonhuman primate model. *Tissue Engineering - Part A* 15(12), 3877–3888.

Davis, N. F., Callanan, A., McGuire, B. B., Mooney, R., Flood, H. D. & McGloughlin, T. M. (2011). Porcine extracellular matrix scaffolds in reconstructive urology: An ex vivo comparative study of their biomechanical properties. *Journal of the Mechanical Behavior of Biomedical Materials* 4(3), 375–382.

Dewan, P., Stefanek, W., Lorenz, C. & Byard, R. (1994). Autoaugmentation omentocystoplasty in a sheep model. *Urology* 43(6), 888 –891.

Egusa, S. (1968). Experimental study on vascular graft. II. Replacement of inferior vena cava and abdoninal aorta with the autogenous segment of small intestine submucosa. *Acta Medica Okayama* 22(4), 153–165.

Eilaghi, A., Flanagan, J. c., Brodland, G. & Ethier, C. f. g. (2009). Strain uniformity in biaxial specimens is highly sensitive to attachment details. *Journal of Biomechanical Engineering* 131(9).

Farhat, W. A. & Yeger, H. (2008). Does mechanical stimulation have any role in urinary bladder tissue engineering? *World Journal of Urology* 26(4), 301–305.

Fauza, D. O., Fishman, S. J., Mehegan, K. & Atala, A. (1998). Videofetoscopically assisted fetal tissue engineering: Bladder augmentation. *Journal of Pediatric Surgery* 33(1), 7–12.

*FEBio 2.2 User's Manual*. https://febio.org/.

Feil, G., Christ-Adler, M., Maurer, S., Corvin, S., Rennekampff, H.-O., Krug, J., Hennenlotter, J., Kuehs, U., Stenzl, A. & Sievert, K.-D. (2006). Investigations of

Urothelial Cells Seeded on Commercially Available Small Intestine Submucosa. *European Urology* 50(6), 1330–1337.

Fermor, H., Russell, S., Williams, S., Fisher, J. & Ingham, E. (2015). Development and characterisation of a decellularised bovine osteochondral biomaterial for cartilage repair. *Journal of Materials Science: Materials in Medicine* 26(5), 186.

Flood, H. D., Malhotra, S. J., O'Connell, H. E., Ritchey, M. J., Bloom, D. A. & McGuire, E. J. (1995). Long-term results and complications using augmentation cystoplasty in reconstructive urology. *Neurourology and Urodynamics* 14(4), 297–309.

Fratzl, P., Misof, K., Zizak, I., Rapp, G., Amenitsch, H. & Bernstorff, S. (1998). Fibrillar Structure and Mechanical Properties of Collagen. *Journal of Structural Biology* 122(1), 119 –122.

Freytes, D. O., Badylak, S. F., Webster, T. J., Geddes, L. A. & Rundell, A. E. (2004). Biaxial strength of multilaminated extracellular matrix scaffolds. *Biomaterials* 25(12), 2353 –2361.

Gilbert, T. W. (2012). Strategies for tissue and organ decellularization. *Journal of Cellular Biochemistry* 113(7), 2217–2222.

Gilbert, T. W., Sellaro, T. L. & Badylak, S. F. (2006). Decellularization of tissues and organs. *Biomaterials* 27(19), 3675–3683.

Gonzalez, R., Buson, H., Reid, C. & Reinberg, Y. (1995). Seromuscular colocystoplasty lined with urothelium: Experience with 16 patients. *Urology* 45(1), 124 –129.

Gough, D. C. S. (2001). Enterocystoplasty. *BJU International* 88(7), 739–743.

Grassl, E., Barocas, V. & Bischof, J. (2004). Effects of freezing on the mechanical properties of blood vessels. *American Society of Mechanical Engineers, Heat Transfer Division, (Publication) HTD* 375(1), 699–703.

Greenwell, T. J., Venn, S. N. & Mundy, A. R. (2001). Augmentation cystoplasty. *BJU International* 88(6), 511–525.

Hearn, E. J. (1997). *Mechanics of Materials: An Introduction to the Mechanics of Elastic and Plastic Deformation of Solids and Structural Materials*. 3rd ed. Burlington: Butterworth-Heinemann.

Herbert, A, Jones, G. L., Ingham, E & Fisher, J (2015). A biomechanical characterisation of acellular porcine super flexor tendons for use in anterior cruciate ligament replacement: Investigation into the effects of fat reduction and bioburden reduction bioprocesses. *Journal of Biomechanics* 48(1), 22–29.

Hogg, P., Rooney, P., Ingham, E. & Kearney, J. (2013). Development of a decellularised dermis. *Cell and Tissue Banking* 14(3), 465–474.

Huang, Q., Ingham, E., Rooney, P. & Kearney, J. (2013). Production of a sterilised decellularised tendon allograft for clinical use. *Cell and Tissue Banking* 14(4), 645–654.

Kheir, E., Stapleton, T., Shaw, D., Jin, Z., Fisher, J. & Ingham, E. (2011). Development and characterization of an acellular porcine cartilage bone matrix for use in tissue engineering. *Journal of biomedical materials research Part A* 99(2), 283–294.

Khoiy, K. & Amini, R. (2016). On the biaxial mechanical response of porcine tricuspid valve leaflets. *Journal of Biomechanical Engineering* 138(10).

Khoury, J. M., Timmons, S. L., Corbel, L. & Webster, G. D. (1992). Complications of enterocystoplasty. *Urology* 40(1), 9 –14.

Knight, R. & Ingham, E. (2006). Allogeneic Cells and Tissues. *Wiley Encyclopedia of Biomedical Engineering*. John Wiley & Sons, Inc.

Korossis, S., Bolland, F., Ingham, E., Fisher, J., Kearney, J. & Southgate, J. (2006). Tissue engineering of the urinary bladder: Considering structure-function relationships and the role of mechanotransduction. *Tissue Engineering* 12(4), 635–644.

Korossis, S. A., Booth, C., Wilcox, H. E., Watterson, K. G., Kearney, J. N., Fisher, J. & Ingham, E. (2002). Tissue engineering of cardiac valve prostheses II: Biomechanical characterization of decellularized porcine aortic heart valves. *Journal of Heart Valve Disease* 11(4), 463–471.

Korossis, S. A., Wilcox, H. E., Watterson, K. G., Kearney, J. N., Ingham, E. & Fisher, J. (2005). In-vitro assessment of the functional performance of the decellularized intact porcine aortic root. *Journal of Heart Valve Disease* 14(3), 408–421.

Korossis, S., Bolland, F., Southgate, J., Ingham, E. & Fisher, J. (2009). Regional biomechanical and histological characterisation of the passive porcine urinary bladder: Implications for augmentation and tissue engineering strategies. *Biomaterials* 30(2), 266–275.

LamVanBa, O., Aharony, S., Loutochin, O. & Corcos, J. (2015). Bladder tissue engineering: A literature review. *Advanced Drug Delivery Reviews* 82-83, 31 –37.

Langer, R. & Vacanti, J. P. (1993). Tissue Engineering. *Science*. New Series 260(5110), 920–926.

Lantz, G., Badylak, S., Coffey, A., Geddes, L. & Blevins, W. (1990). Small intestinal submucosa as a small-diameter arterial graft in the dog. *Journal of Investigative Surgery* 3(3), 217–227.

Lapides, J. & Nesbit, R. M. (1976). *Fundamentals of urology*. Saunders.

Lawler, M. R., Foster, J. H. & Scott, H. (1971). Evaluation of canine intestinal submucosa as a vascular substitute. *The American Journal of Surgery* 122(4), 517–519.

Li, C., Xu, Y.-M., Liu, Z.-S. & Li, H.-B. (2013). Urethral Reconstruction With Tissue Engineering and RNA Interference Techniques in Rabbits. *Urology* 81(0), 1075–1080.

Li, K., Zhao, H., Liu, W. & Yin, Z. (2015). Material properties and constitutive modeling of infant porcine cerebellum tissue in tension at high strain rate. *PLoS ONE* 10(4).

Lun, S. *et al.* (2010). A functional extracellular matrix biomaterial derived from ovine forestomach. *Biomaterials* 31(16), 4517–4529.

Lyons, M., Winter, D. & Simms, C. (2014). Mechanical characterisation of porcine rectus sheath under uniaxial and biaxial tension. *Journal of Biomechanics* 47(8), 1876–1884.

Maas, S. A., Ellis, B. J., Ateshian, G. A. & Weiss, J. A. (2012). FEBio: finite elements for biomechanics. *Journal of biomechanical engineering* 134(1), 011005.

Macrae, R., Miller, K. & Doyle, B. (2016). Methods in Mechanical Testing of Arterial Tissue: A Review. *Strain* 52(5), 380–399.

Magnan, M., Berthod, F., Champigny, M.-F., Soucy, F. & Bolduc, S. (2006). In vitro reconstruction of a tissue-engineered endothelialized bladder from a single porcine biopsy. *Journal of Pediatric Urology* 2(4), 261–270.

Matsumoto, T., Holmes, R., Burdick, C., Metzger, J., Heisterkamp 3rd., C. & O'Connell Jr., T. (1966a). A study of inverted intestinal graft in the major veins. *Angiology* 17(11), 842–850.

Matsumoto, T., Holmes, R., Burdick, C., Heisterkamp 3rd., C. & O'Connell Jr., T. (1966b). Replacement of large veins with free inverted segments of small bowel: autografts of submucosal membrane in dogs and clinical use. *Annals of Surgery* 164(5), 845–848.

Mauney, J. R., Cannon, G. M., Lovett, M. L., Gong, E. M., Vizio, D. D., Gomez III, P., Kaplan, D. L., Adam, R. M. & Estrada Jr., C. R. (2011). Evaluation of gel spun silk-based biomaterials in a murine model of bladder augmentation. *Biomaterials* 32(3), 808–818.

Meinel, L., Hofmann, S., Karageorgiou, V., Kirker-Head, C., McCool, J., Gronowicz, G., Zichner, L., Langer, R., Vunjak-Novakovic, G. & Kaplan, D. L. (2005). The inflammatory responses to silk films in vitro and in vivo. *Biomaterials* 26(2), 147 –155.

Montoya, C. V. & McFetridge, P. S. (2009). Preparation of ex vivo–based biomaterials using convective flow decellularization. *Tissue Engineering Part C: Methods* 15(2), 191–200.

Mundy, A. J., Fitzpatrick, J. M., Neal, D. E., George, N. J. R. & Mundy, A. R. (2004). *The Scientific Basis of Urology, Second Edition*. 2nd ed. Informa Healthcare, 265–326.

Nakanishi, Y., Chen, G., Komuro, H., Ushida, T., Kaneko, S., Tateishi, T. & Kaneko, M. (2003). Tissue-engineered urinary bladder wall sing {PLGA} mesh-collagen hybrid scaffolds: a omparison study of collagen sponge and gel as a scaffold. *Journal of Pediatric Surgery* 38(12), 1781–1784.

Nerem, R. M. (1995). Tissue engineering: from biology to biological substitutes. *Biorheology* 32(2), 193–194.

Nielsen, P., Hunter, P. & Smaill, B. (1991). Biaxial testing of membrane biomaterials: Testing equipment and procedures. *Journal of Biomechanical Engineering* 113(3), 295–300.

Novick, A. C., Straffon, R. A., Koshino, I., Banowsky, L. H., Levin, H., Kambic, H. & Nosé, Y. (1978). Experimental bladder substitution using a biodegradable graft of natural tissue. *Journal of Biomedical Materials Research* 12(2), 125–147.

Oberpenning, F., Meng, J., Yoo, J. J. & Atala, A. (1999). De novo reconstitution of a functional mammalian urinary bladder by tissue engineering. *Nature Biotechnology* 17(2), 149–155.

Ogden, R. W. (1972). Large deformation isotropic elasticity - on the correlation of theory and experiment for incompressible rubberlike solids. *Rubber Chemistry and Technology* 46(2), 398–416.

Ogden, R., Saccomandi, G. & Sgura, I. (2004). Fitting hyperelastic models to experimental data. *Computational Mechanics* 34(6), 484–502.

Ott, H. C., Matthiesen, T. S., Goh, S.-K., Black, L. D., Kren, S. M., Netoff, T. I. & Taylor, D. A. (2008). Perfusion–decellularized matrix: using nature's platform to engineer a bioartificial heart. *Nature medicine* 14(2), 213–221.

Pattison, M., Webster, T. J., Leslie, J., Kaefer, M. & Haberstroh, K. M. (2007). Evaluating the In Vitro and In Vivo Efficacy of Nano-Structured Polymers for Bladder Tissue Replacement Applications. *Macromolecular Bioscience* 7(5), 690–700.

Pattison, M. A., Wurster, S., Webster, T. J. & Haberstroh, K. M. (2005). Three-dimensional, nano-structured {PLGA} scaffolds for bladder tissue replacement applications. *Biomaterials* 26(15), 2491 –2500.

Prevel, C., Eppley, B., Summerlin, D.-J., Jackson, J., McCarty, M. & Badylak, S. (1995). Small intestinal submucosa: Utilization for repair of rodent abdominal wall defects. *Annals of Plastic Surgery* 35(4), 374–380.

Price, A. P., England, K. A., Matson, A. M., Blazar, B. R. & Panoskaltsis-Mortari, A. (2010). Development of a decellularized lung bioreactor system for bioengineering the lung: the matrix reloaded. *Tissue engineering Part A* 16(8), 2581–2591.

Probst, M., Dahiya, R., Carrier, S. & Tanagho, E. A. (1997). Reproduction of functional smooth muscle tissue and partial bladder replacement. *British Journal of Urology* 79(4), 505–515.

Rashid, B., Destrade, M. & Gilchrist, M. D. (2013). Mechanical characterization of brain tissue in simple shear at dynamic strain rates. *Journal of the Mechanical Behavior of Biomedical Materials* 28, 71 –85.

Reynard, J., Brewster, S. & Biers, S. (2009). *Oxford Handbook of Urology*. 2nd ed. Oxford Handbooks Series. OUP Oxford.

Ricard-Blum, S. & Ville, G. (1989). Collagen cross-linking. *International Journal of Biochemistry* 21(11), 1185 –1189.

Rieder, E., Kasimir, M.-T., Silberhumer, G., Seebacher, G., Wolner, E., Simon, P. & Weigel, G. b. (2004). Decellularization protocols of porcine heart valves differ importantly in efficiency of cell removal and susceptibility of the matrix to recellularization with human vascular cells. *Journal of Thoracic and Cardiovascular Surgery* 127(2), 399–405.

Rohrmann, D., Albrecht, D., Hannappel, J., Gerlach, R., Schwarzkopp, G. & Lutzeyer, W. (1996). Alloplastic Replacement of the Urinary Bladder. *The Journal of Urology* 156(6), 2094–2097.

Safadi, M. & Rubin, M. (2014). Modeling rate-independent hysteresis in large deformations of preconditioned soft tissues. *International Journal of Solids and Structures* 51(18), 3265 –3272.

Scott, R., Deane, R. F. & Callander, R. (1982). *Urology illustrated*. 2nd ed. Churchill Livingstone.

Shahmansouri, N., Alreshidan, M., Emmott, A., Lachapelle, K., Cartier, R., Leask, R. L. & Mongrain, R. (2016). Evaluating ascending aortic aneurysm tissue toughness: Dependence on collagen and elastin contents. *Journal of the Mechanical Behavior of Biomedical Materials* 64, 262 –271.

Sharma, A. K. *et al.* (2013). Cotransplantation with specific populations of spina bifida bone marrow stem/progenitor cells enhances urinary bladder regeneration. *Proceedings of the National Academy of Sciences of the United States of America* 110(10), 4003–4008.

Sionkowska, A. & Kamińska, A. (1999). Thermal helix-coil transition in {UV} irradiated collagen from rat tail tendon. *International Journal of Biological Macromolecules* 24(4), 337 –340.

Skandalakis, J. E. & Colborn, G. L. (2004). *Skandalakis' Surgical anatomy: the embryologic and anatomic basis of modern surgery*. Skandalakis' Surgical Anatomy: The Embryologic and Anatomic Basis of Modern Surgery v. 2. PMP.

Skrzyński, S, Sionkowska, A & Marciniak, A (2010). DSC study of collagen in disc disease. *Journal of Biophysics* 2009.

Southgate, J., Masters, J. R. & Trejdosiewicz, L. K. (2002). Culture of Human Urothelium. *Culture of Epithelial Cells*. Ed. by R. I. Freshney & M. G. Freshney. John Wiley & Sons, Inc. Chap. 12, 381–399.

Stenzl, A., Strasser, H., Klima, G., Eder, I., Frauscher, F., Klocker, H., Bartsch, G. & Ninkovic, M. (2000). Reconstruction of the lower urinary tract using autologous muscle transfer and cell seeding: Current status and future perspectives. *World Journal of Urology* 18(1), 44–50.

Stoker, J. (2009). Anorectal and pelvic floor anatomy. *Best Practice & Research Clinical Gastroenterology* 23(4), 463–475.

Subramaniam, R., Hinley, J., Stahlschmidt, J. & Southgate, J. (2011). Tissue Engineering Potential of Urothelial Cells From Diseased Bladders. *The Journal of Urology* 186(5), 2014–2020.

Tanagho, E. A. & McAninch, J. W. (2004). *Smith's General Urology*. 16th ed. Smith's General Urology. McGraw-Hill.

Tu, D. D. *et al.* (2013). Bladder tissue regeneration using acellular bi-layer silk scaffolds in alarge animal model of augmentation cystoplasty. *Biomaterials* 34(34), 8681 –8689.

Tuan-Mu, H.-Y., Yu, C.-H. & Hu, J.-J. (2014). On the Decellularization of Fresh or Frozen Human Umbilical Arteries: Implications for Small-Diameter Tissue Engineered Vascular Grafts. *Annals of Biomedical Engineering* 42(6), 1305–1318.

Twizell, E. H. & Ogden, R. W. (1983). Non-linear optimization of the material constants in Ogden's stress-deformation function for incompressinle isotropic elastic materials. *The ANZIAM Journal* 24 (04), 424–434.

Venkatasubramanian, R. T., Wolkers, W. F., Shenoi, M. M., Barocas, V. H., Lafontaine, D., Soule, C. L., Iaizzo, P. A. & Bischof, J. C. (2010). Freeze–Thaw Induced Biomechanical Changes in Arteries: Role of Collagen Matrix and Smooth Muscle Cells. *Annals of Biomedical Engineering* 38(3), 694–706.

Venkatasubramanian, R., Grassl, E., Barocas, V., Lafontaine, D. & Bischof, J. (2006). Effects of freezing and cryopreservation on the mechanical properties of arteries. *Annals of Biomedical Engineering* 34(5), 823–832.

Veronda, D. & Westmann, R. (1970). Mechanical characterization of skin—Finite deformations. *Journal of Biomechanics* 3(1), 111 –124.

Wahl, E. F., Lerman, S. E., Lahdes-Vasama, T. T. & Churchill, B. M. (2004). Measurement of bladder compliance can be standardized by a dimensionless number: theoretical perspective. *BJU International* 94(6), 895–897.

Weadock, K. S., Miller, E. J., Bellincampi, L. D., Zawadsky, J. P. & Dunn, M. G. (1995). Physical crosslinking of collagen fibers: Comparison of ultraviolet irradiation and dehydrothermal treatment. *Journal of Biomedical Materials Research* 29(11), 1373–1379.

Wells, P. N. T. & Liang, H.-D. (2011). Medical ultrasound: imaging of soft tissue strain and elasticity. *Journal of The Royal Society Interface* 8(64), 1521–1549.

Wezel, F., Southgate, J. & Thomas, D. F. M. (2011). Regenerative medicine in urology. *BJU International* 108(7), 1046–1065.

Wilcox, H. E., Korossis, S. A., Booth, C., Watterson, K. G., Kearney, J. N., Fisher, J. & Ingham, E. (2005). Biocompatibility and recellularization potential of an acellular porcine heart valve matrix. *Journal of Heart Valve Disease* 14(2), 228–236.

Wilshaw, S.-P., Kearney, J., Fisher, J. & Ingham, E. (2006). Production of an acellular amniotic membrane matrix for use in tissue engineering. *Tissue Engineering* 12(8), 2117–2129.

Wyndaele, J. J., Gammie, A., Bruschini, H., De Wachter, S., Fry, C. H., Jabr, R. I., Kirschner-Hermanns, R. & Madersbacher, H. (2011). Bladder compliance what does it represent: Can we measure it, and is it clinically relevant? *Neurourology and Urodynamics* 30(5), 714–722.

Zhang, Y., Kropp, B. P., Lin, H.-K., Cowan, R. & Cheng, E. Y. (2004). Bladder Regeneration with Cell-Seeded Small Intestinal Submucosa. *Tissue Engineering* 10(1-2), 181–187.

Zhao, X., Berwick, Z., Krieger, J., Chen, H., Chambers, S. & Kassab, G. c. d. (2014). Novel Design of Cruciform Specimens for Planar Biaxial Testing of Soft Materials. *Experimental Mechanics* 54(3), 343–356.

Zheng, M. H., Chen, J., Kirilak, Y., Willers, C., Xu, J. & Wood, D. (2005). Porcine small intestine submucosa (SIS) is not an acellular collagenous matrix and contains porcine DNA: Possible implications in human implantation. *Journal of Biomedical Materials Research Part B: Applied Biomaterials* 73B(1), 61–67.

Zuo, K., Pham, T., Li, K., Martin, C., He, Z. & Sun, W. (2016). Characterization of biomechanical properties of aged human and ovine mitral valve chordae tendineae. *Journal of the Mechanical Behavior of Biomedical Materials* 62, 607 –618.

# Appendix A

# Materials and Equipment

## A.1 Sources of chemicals and reagents

| Chemical/Reagent | Company |
|---|---|
| Acetic Acid, glacial (17.4 mM) | Thermo Fisher Scientific Ltd. |
| Aprotinin (50 ml; 10,000 KIU.ml$^{-1}$) | Mayfair house |
| Bovine Serum Albumin | - |
| Benzonase nuclease hc, purity >99 % (250 U.$\mu$ l$^{-1}$) | Merck |
| Calcium acetate 97+ % (Dried) | Thermo Fisher Scientific Ltd. |
| Cyanoacrylate contact adhesive: Scotch® Super Glue Liquid | 3M UK PLC |
| Dako fluorescence mounting medium | - |
| DAPI (4',6-diamidino-2-phenylindole dihydrochloride) | Sigma-Aldrich |
| DMSO | - |
| DNAse I (10,000 U/ml) | - |
| DNeasy kit | Qiagen |
| Dulbecco's minimal essential medium | Sigma |
| DPBS (without Ca/Mg, suitable for cell culture) | Sigma |
| EDTA (disodium ethylenediaminetetraacetic acid) | Thermo Fisher Scientific Ltd. |
| Eosin Y | Merck Millipore |
| Eppendorf thermomixer | Eppendorf |
| Ethanol 190 % proof | Sigma-Aldrich |

| Chemical/Reagent | Company |
|---|---|
| Foetal bovine serum | Sera Lab |
| Food colouring, black | Morrisons |
| Giemsa stain | - |
| Glasgow's minimla essential media | Sigma |
| Haematoxylin (Mayer's) | Atom Scientific |
| HBSS (Hank's Balanced Salt Solution) with $Ca^{2+}/Mg^{2+}$, $NaHCO_3$, phenol red | Sigma-Aldrich |
| HEPES (1 M) | Sigma-Aldrich |
| Hydrochloric acid (6 M) | Fisher Scientific |
| Isopropanol | - |
| L-glutamine (200 mM) | Sigma |
| Litmus paper | - |
| LancerClean disinfectant | Lancer UK Ltd |
| Magnesium chloride hexahydrate | Thermo Fisher Scientific Ltd. |
| Methylated spirits | Biostains Ready Reagents |
| Molecular grade water | Sigma-Aldrich |
| Neutral Buffered Formalin (10 % v/v) | Biostains Ready Reagents |
| Paraffin wax | Raymond A Lamb Ltd |
| PBS tablets (Dulbecco's 'A' PBS tablets, without Ca/Mg) | Oxoid |
| Penicillin (5000 U/ml)/streptomycin (5 mg/ml) | Sigma |
| Peracetic Acid, 32 % (v/v) | Sigma-Aldrich |
| RNAse A (100 U/ml) | - |
| RNase A (17,000 U) | Qiagen |
| Scott's tap water | Probably some dude called Scott |
| SDS (sodium dodecyl sulphate) | Thermo Fisher Scientific Ltd. |
| SLS pH Buffer Coloured Red pH4 | Scientific Laboratory Supplies |
| SLS pH Buffer Coloured Yellow pH7 | Scientific Laboratory Supplies |
| SLS pH Buffer Coloured Blue pH10 | Scientific Laboratory Supplies |
| Sodium chloride (NaCl) | Thermo Fisher Scientific Ltd. |
| Sodium hydroxide (NaOH) | Scientific Laboratory Supplies |
| Tris (trizma base) | Sigma-Aldrich |
| Trypan blue solution, 0.4 % (v/v) | Sigma |
| Trypsin-EDTA solution | Sigma |
| Tryptone phosphate broth | Sigma |
| Virkon® Rely+On™ | DuPont |

| Chemical/Reagent | Company |
|---|---|
| Water, nuclease-free (R0582) | Fermentas |
| Xylene | Biostains Ready Reagents |
| Zinc acetate 99.9 % | Sigma-Aldrich |
| Zinc chloride | Fluka |

## A.2 Sources of equipment

| Equipment | Company |
|---|---|
| Accumax Pipette Controller | Fine Care Biosystems |
| Airone 1800R Fume hood | Safelab Systems Ltd |
| Bench vice | - |
| Bunsen burner | - |
| Camera, Olympus 450D | Olympus |
| Camera stand | Manfrotto |
| Cell$^{B}$ Microscope Software, v3.2 | Olympus |
| Centrifuge, Harrier 15/80 | Sanyo |
| Centrifuge, Evolution RC | Sorvall |
| Clamp for retort stand | - |
| Dissection kit | Thackray Instruments |
| Dissecting needles | - |
| DSC Q2000 | TA Instruments |
| FastPette$^{TM}$ V2 Pipette Controller | Labnet International, Inc. |
| Finnpipette Pipettes (0.2–2 $\mu$l, 2–20 $\mu$l, 20–200 $\mu$l & 200–1000 $\mu$l) | Scientific Laboratory Supplies |
| Forceps, blue plastic Spencer Wells | Fisher Scientific Ltd |
| Freezer, cell culture | - |
| Glass tank (12 in × 12 in × 8 in) | Pet & Garden World, Leeds |
| Glass troughs E105 | Raymond A Lamb |
| Haemacytometer, Neubauer Improved | - |
| Heat sealer | - |
| Heraeus Hera Safe Class II biosafety cabinet | Thermo Electron Corporation, USA |
| Heraeus Incubator | Jencons PLC |
| Histology cassettes CMB-160-030R | Thermo Fisher Scientific Ltd. |
| Histology moulds E10.8/4161 | Raymond A Lamb |

| Equipment | Company |
|---|---|
| Histology water bath MH8515 | Barnstead Electrothermal |
| HM 3550 Hand Sack Sealer | Hulme Martin Heat Sealers Ltd |
| Hot Air Steriliser | Genlab Limited |
| Hotplate Stirrer heat-stir CB162 | Stuart Scientific |
| Hotplate E18/1 | R.A. Lamb |
| Hot wax oven E18/31 | Raymond A Lamb |
| Incubator, cell culture | - |
| Instron 3365 | Instron |
| Jenway 3510 pH Meter | Jenway Ltd |
| Lamp, magnifying: Daylight™ D20251 | The Daylight Company |
| Lancer 810 LX undercounter glassware washer | Lancer UK Ltd |
| Magnetic flea | - |
| Microcentaur centrifuge | MSE |
| Microscope, inverted: Olympus CK40 | Olympus |
| Microtome, Leica RM2255 | Leica |
| Modulyo Freeze Drier | Thermo Savant |
| Mr Frosty | - |
| Nanodrop ND-1000 spectrophotometer | Labtech |
| Olympus BX51 Microscope | Olympus |
| Pipe fittings | - |
| PIPETMAN® Pipettes (0.2–2 $\mu$l, 2–20 $\mu$l, 20–200 $\mu$l & 200–1000 $\mu$l) | Gilson, Inc. |
| Peristaltic Pump | - |
| Precision Balance GR-200 | A&D Instruments Ltd |
| Purelab Option Water Purification System | ELGA |
| Refrigerator, cell culture | - |
| Retort stand | - |
| Retort stand clamp | - |
| Ruler, 150 mm, stainless steel | Fisher Scientific Ltd |
| Ruler, 300 mm, stainless steel | Fisher Scientific Ltd |
| Slide holder E102 | Raymond A Lamb |
| Spatulas | - |
| Table shaker KS 130 | IKA |
| Table shaker PSU 10i | Grant |

| Equipment | Company |
|---|---|
| Table shaker POS 300 | Grant |
| Tissue Processor TP1020 | Leica |
| Tubing | - |
| Tubing connector, 3-way | - |
| Pipe fittings | - |
| Water bath | - |
| Triplered SG Series Compact | Triple Red |
| Wax dispenser E66 | Raymond A Lamb |
| Whiteley Fume hood | Whiteley |
| Whrli mixer CM-1 vortexer | Thermo Fisher Scientific |
| Zeiss AX10 Microscope | Carl Zeiss |
| Zeiss HXP 100 | Carl Zeiss |

## A.3 Sources of glassware and plasticware

| Glassware/Plasticware | Company |
|---|---|
| Beaker, 3 L | Scientific Laboratory Supplies |
| Duran bottles (0.25 l, 0.5 l, 1 l and 2 l) | Scientific Laboratory Supplies |
| Funnel, small with long neck | Scientific Laboratory Supplies |
| Funnel, medium with short neck | Scientific Laboratory Supplies |
| Jar, polypropylene, wide neck with lid, 1 l | Thermo Scientific Nalgene |
| Measuring cylinders (50 mm, 100 mm, 250 mm and 1000 mm) | Scientific Laboratory Supplies |
| Mr Frosty | - |
| Petri Dish, glass, large (200 mm) | Smith Scientific Ltd |

## A.4 Sources of consumables

| Consumable | Company |
|---|---|
| Autoclave plain closure bags | Westfield Medical Limited |
| Autoclave tape SLS1612 | Scientific Laboratory Supplies |
| Bijous (sterile, 5 ml) | - |

| Consumable | Company |
|---|---|
| Cable ties (100 mm × 2.5 mm) | ARCO Limited |
| Coverslips, glass, E105 | Scientific Laboratory Supplies |
| Cryovials, 1 ml | - |
| Eppendorf for DNA assay | - |
| Flat Sterilisation Pouches | Westfield Medical Limited |
| Foil | - |
| Histology cassettes | - |
| Measuring dishes | Scientific Laboratory Supplies |
| Micro tube I, 1.5 ml, loop cap, Simport | VWR International |
| Minisart syringe filters, 0.2 µm pore size | Sartorius Stedim UK Ltd. |
| Needles, Neolus Hypodermic Terumo-Thin 25G 16mm (NN-2516R) | Terumo UK Ltd. |
| Parafilm | - |
| Pipettes, Pasteur | - |
| Pipette Tips, TipOne® (10 µl, 20 µl, 200 µl and 1000 µl) | STARLAB |
| Serological Pipettes, sterile (5 ml, 10 ml and 25 ml) | Starstedt AG & Co. |
| Scalpel blades, No. 22, non-sterile | Swann-Morton Limited |
| Scalpel blades, No. 22, sterile | Swann-Morton Limited |
| Sterilin pots (150 ml and 250 ml) | - |
| Superfrost slides | Scientific Laboratory Supplies |
| Superfrost plus slides MIC3040 | Scientific Laboratory Supplies |
| Syringes (1 ml, 2.5 ml, 5 ml, 10 ml, 20 ml and 50 ml) | Terumo UK Ltd. |
| Tissue culture flasks (T75, T175) | Thermo fisher scientific |
| Tissue culture 6-well plates | Thermo fisher scientific |
| Universal containers (20 ml) | - |

# Appendix B

# Dimensions of bladder tissue to model

The bladder was modelled as a cube with dimensions in the $x$ (height), $y$ (width) and $z$ (depth) directions. These dimensions correspond to the transverse length, longitudinal length and thickness respectively of the bladder tissue. It was assumed that the final size of the material was equal to the size of the material during decellularisation, i.e. contraction of the material after decellularisation was not yet taken into account.

## B.1 Total size of bladder patch

### B.1.1 Width and height—$x$ and $y$ dimensions

The final size of the patch must be $80\,\text{mm} \times 80\,\text{mm}$, as defined in the product specification.

To fully decellularise the bladder, strains of 2.0 and 1.4 must be applied to the material in the $x$ and $y$ directions respectively. Therefore these strains correspond to stretches of 3.0 and 2.4 in the $x$ and $y$ directions (Equation B.1).

$$\lambda = \varepsilon + 1 \tag{B.1}$$

The final length, $l$, of a material is related to the initial length, $L$, when a stretch of $\lambda$ is applied to it by the following relationship (Equation B.2):

$$\lambda = \frac{l}{L} \tag{B.2}$$

| Dimension | $x$ | $y$ | Expression |
|---|---|---|---|
| Final dimension, $l$ (mm) | 80 | 80 | $l$ |
| Strain, $\varepsilon$ | 2.0 | 1.4 | $\varepsilon$ |
| Stretch, $\lambda$ | 3.0 | 2.4 | $\lambda = \varepsilon + 1$ |
| Initial dimension, $L$ (mm) | 26.67 | 33.33 | $L = l/\lambda$ |
| Extension, $e$ (mm) | 53.33 | 46.67 | $e = l - L$ |

**Table B.1:** Dimensions of bladder to be modelled

The final dimensions of the patch must be 80 mm × 80 mm. From this, the initial dimensions of the bladders can be calculated to be 26.67 mm and 33.33 mm in the $x$ and $y$ directions. Extensions of 53.33 mm and 46.67 mm must therefore be applied. This data is summarised in Table B.1.

### B.1.2 Depth—$z$ dimension

The initial thickness to be used will be the mean starting thickness of the bladders used in the immersed distension experiment. The mean initial thickness was equal to 5.0 mm.

## B.2 Size of modelled area

Due to symmetry of the model, half of the material will be modelled in each of the three dimensions. The initial dimensions are therefore half of those stated above, and are equal to 13.33 mm and 16.67 mm in the $x$ and $y$ directions respectively. The extensions are also halved, and are equal to 26.67 mm and 23.33 mm in the $x$ and $y$ directions. The initial thickness of the tissue model was therefore 2.50 mm. These dimensions are summarised in Table B.2.

| | Dimensions (mm) | |
|---|---|---|
| | Total patch | Modelled area |
| Initial height ($x$ length) | 26.67 | 13.33 |
| Initial width ($y$ length) | 33.33 | 16.67 |
| Initial depth ($z$ length) | 5.00 | 2.50 |
| Extension, $x$ direction | 53.33 | 26.67 |
| Extension, $y$ direction | 46.67 | 23.33 |
| Final height ($x$ length) | 80.00 | 80.00 |
| Final width ($y$ length) | 80.00 | 80.00 |

**Table B.2:** Dimensions of bladder area to be modelled

# Appendix C

# Uniaxial equivalent strains

## C.1 Uniaxial deformation

The stress, $\sigma$ of a material in uniaxial tension can be given as a function of its modulus, $E$, and applied strain, $\varepsilon$:

$$\sigma = E\varepsilon \tag{C.1}$$

Thus, when stress is plotted against strain, the gradient of the curve is the modulus of the material at that point.

## C.2 Plane stress deformation, isotropic

For an isotropic material in plane stress, the strains can be expressed as follows:

$$\varepsilon_x = \frac{1}{E}(\sigma_x - \nu\sigma_y) \qquad \varepsilon_y = \frac{1}{E}(\sigma_y - \nu\sigma_x) \tag{C.2}$$

Rearranging these gives:

$$\sigma_x - \nu\sigma_y = E\varepsilon_x \qquad \sigma_y - \nu\sigma_x = E\varepsilon_y \tag{C.3}$$

And again, the modulus can be found if the expressions for the stresses ($\sigma_x - \nu\sigma_y$, $\sigma_y - \nu\sigma_x$) are plotted against the strains ($\varepsilon_x$, $\varepsilon_y$).

## C.3 Plane stress deformation, orthotropic

For an orthotropic material in plane stress, the strains can be expressed as follows:

$$\varepsilon_x = \frac{1}{E_x}\sigma_x - \frac{\nu}{E_y}\sigma_y \qquad \varepsilon_y = \frac{1}{E_y}\sigma_y - \frac{\nu}{E_x}\sigma_x \tag{C.4}$$

Where $E_x$ and $E_y$ are the modulii in the $x$ and $y$ directions respectively. Rearranging these so they are given explicitly in terms of $E_y$, Equation C.4 now becomes:

$$E_y = \frac{\nu\sigma_y}{\frac{\sigma_x}{E_x} - \varepsilon_x} \qquad\qquad E_y = \frac{\sigma_y}{\varepsilon_y + \frac{\nu}{E_x}\sigma_x} \tag{C.5}$$

Equating these gives:

$$\frac{\sigma_y}{\varepsilon_y + \frac{\nu}{E_x}\sigma_x} = \frac{\nu\sigma_y}{\frac{\sigma_x}{E_x} - \varepsilon_x} \tag{C.6}$$

Which can be rearranged to be explicit with respect to $\sigma_x$:

$$\frac{\sigma_x}{E_x} - \varepsilon_x = \nu\varepsilon_y + \frac{\nu^2}{E_x}\sigma_x \tag{C.7}$$

$$\sigma_x - E_x\varepsilon_x = \nu E_x\varepsilon_y + \nu^2\sigma_x \tag{C.8}$$

$$E_x(\varepsilon_x + \nu\varepsilon_y) = \sigma_x(1 + \nu^2) \tag{C.9}$$

$$\sigma_x = E_x\frac{\varepsilon_x + \nu\varepsilon_y}{1 + \nu^2} \tag{C.10}$$

Therefore, similarly:

$$\sigma_y = E_y\frac{\varepsilon_y + \nu\varepsilon_x}{1 + \nu^2} \tag{C.11}$$

Let us now define the following expressions

$$\varepsilon_{x,equiv} = \frac{\varepsilon_x + \nu\varepsilon_y}{1 + \nu^2} \qquad\qquad \varepsilon_{y,equiv} = \frac{\varepsilon_y + \nu\varepsilon_x}{1 + \nu^2} \tag{C.12}$$

as the 'uniaxial equivalent strains' in the $x$ and $y$ directions. Plotting a graph of $\sigma_x$ and $\sigma_y$ against $\varepsilon_{x,equiv}$ and $\varepsilon_{y,equiv}$ respectively results in curves where $E_x$ and $E_y$ are the gradients.

# Appendix D

# Stress-stretch relationships derived from the Ogden model strain-energy function

In order to fit the Ogden model to experimental stress-strain data, a stress-stretch relationship must be derived from the strain-energy function of the model for the given mode of deformation. The strain-energy function of the hyperelastic Ogden model is shown in Equation D.1 (*FEBio 2.2 User's Manual*)

$$W = \sum_{i=1}^{N} \frac{c_i}{m_i^2} \left(\lambda_1^{m_i} + \lambda_2^{m_i} + \lambda_3^{m_i} - 3\right) + U(J) \tag{D.1}$$

where $W$ is the stored strain energy per unit volume of the material, $(c_i, m_i)$ are the material parameters for the Ogden model, $(\lambda_1, \lambda_2, \lambda_3)$ are the principal stretches of deformation, and $U(J)$ determines the volumetric behaviour of the material.

Assuming incompressible means the product of the principal stetches must equal one (Equation D.2).

$$\lambda_1 \lambda_2 \lambda_3 = 1 \tag{D.2}$$

The principal Cauchy stresses, $\sigma_i$ $(i = \{1, 2, 3\})$, are defined in Equation D.3, where $p$ is the hydrostatic pressure term introduced because material incompressibility is assumed.

$$\sigma_i = \lambda_i \frac{\partial W}{\partial \lambda_i} - p \tag{D.3}$$

Differentiating the strain-energy equation (Equation D.1) with respect to the three

principal stretches produces Equations D.4 to D.6.

$$\frac{\partial W}{\partial \lambda_1} = \sum_{i=1}^{N} \frac{c_i}{m_i} \lambda_1^{m_i - 1} \tag{D.4}$$

$$\frac{\partial W}{\partial \lambda_2} = \sum_{i=1}^{N} \frac{c_i}{m_i} \lambda_2^{m_i - 1} \tag{D.5}$$

$$\frac{\partial W}{\partial \lambda_3} = \sum_{i=1}^{N} \frac{c_i}{m_i} \lambda_3^{m_i - 1} \tag{D.6}$$

Substituting Equation D.3 into Equations D.4 to D.6, in order to eliminate $W$ and replace it with $\sigma$, results in Equations D.7 to D.9.

$$\sigma_1 = \sum_{i=1}^{N} \frac{c_i}{m_i} \lambda_1^{m_i} - p \tag{D.7}$$

$$\sigma_2 = \sum_{i=1}^{N} \frac{c_i}{m_i} \lambda_2^{m_i} - p \tag{D.8}$$

$$\sigma_3 = \sum_{i=1}^{N} \frac{c_i}{m_i} \lambda_3^{m_i} - p \tag{D.9}$$

The following sections derive the equations expressing stress in terms of stretch and the Ogden model material parameters. These equations are found for three mode of deformation: uniaxial, biaxial and equibiaxial tension.

## D.1 Uniaxial Tension

For a material in uniaxial tension $\sigma_2 = \sigma_3 = 0$. Because of incompressibility, $\lambda_2 = \lambda_3 = \lambda^{-\frac{1}{2}}$ (from Equation D.2). Subtracting Equation D.8 from Equation D.7 gives Equation D.10.

$$\sigma_1 = \sum_{i=1}^{N} \frac{c_i}{m_i} \left( \lambda_1^{m_i} - \lambda_1^{-\frac{1}{2} m_i} \right) \tag{D.10}$$

## D.2 Biaxial Tension

For a material in biaxial tension $\sigma_3 = 0$, and incrompressibility (Equation D.2) means that $\lambda_3 = (\lambda_1 \lambda_2)^{-\frac{1}{2}}$. Subtracting Equation D.9 from Equation D.7 and Equation D.9 from Equation D.8 we now find:

$$\sigma_1 = \sum_{i=1}^{N} \frac{c_i}{m_i} \left( \lambda_1^{m_i} - (\lambda_1 \lambda_2)^{-m_i} \right) \tag{D.11}$$

$$\sigma_2 = \sum_{i=1}^{N} \frac{c_i}{m_i} \left( \lambda_2^{m_i} - (\lambda_1 \lambda_2)^{-m_i} \right) \tag{D.12}$$

## D.3 Equibiaxial Tension

If the stresses and strains in the $x$ and $y$ directions are the same, $\sigma_1 = \sigma_2$ and $\lambda_1 = \lambda_2$. Equation D.11 and Equation D.12 now become Equation D.13.

$$\sigma_1 = \sigma_2 = \sum_{i=1}^{N} \frac{c_i}{m_i} \left(\lambda_1^{m_i} - \lambda_1^{-2m_i}\right) \tag{D.13}$$

# Appendix E

# A relationship for $z$ stretch in terms of $z$ Lagrange strain

### Deformation tensor and stretch

The deformation tensor, $F$, is defined as below.

$$F_{iJ} = \frac{\partial x_i}{\partial X_J} \tag{E.1}$$

Considering the deformation in the $z$ direction, the deformation tensor was expressed in terms of the stretch in the $z$ direction.

$$F_{zz} = \frac{\partial x_z}{\partial X_z} = \lambda_z \tag{E.2}$$

The right Cauchy-Green deformation tensor could then be expressed as:

$$\mathbf{C} = \mathbf{F}^T\mathbf{F} = \lambda_z^2 \tag{E.3}$$

### Lagrange strain and stretch

The Lagrange strain tensor is defined as below.

$$\mathbf{E} = \frac{1}{2}(\mathbf{C} - \mathbf{I}) \tag{E.4}$$

And therefore the Lagrange strain in the $z$ direction, $\varepsilon_{Lz}$, can be expressed in terms of the $z$ direction stretch and $z$ direction strain:

$$\varepsilon_{Lz} = \frac{1}{2}(\lambda_z^2 - 1) \tag{E.5}$$

$$\varepsilon_{Lz} = \frac{1}{2}[(\varepsilon_z + 1)^2 - 1] \tag{E.6}$$

The $z$ direction stretch and strain can of course then be defined in terms of the $z$ direction Lagrange strain:

$$\lambda_z = \sqrt{2\varepsilon_{Lz} + 1} \tag{E.7}$$

$$\varepsilon_z = \sqrt{2\varepsilon_{Lz} + 1} - 1 \tag{E.8}$$

# Appendix F

# Finding the thickness from a ratio of areas

We need to find the thickness between two area, where the size of the inside area is known and the ratio of the two areas is known. A diagram of the scenario is shown in Figure F.1.

Let $f_A$ and $f_B$ be the fraction of the areas $A$ and $B$ relative to the total area $T$, such that $A = f_A T$ and $B = f_B T$. The sum of the fractions must sum to 1, which means that $f_A + f_B = 1$, and therefore $f_B = 1 - f_A$. The two areas can now be equated:

$$\begin{aligned} A = f_A T, \quad B = f_B T \\ \therefore \quad T = \frac{A}{f_A} = \frac{B}{f_B} \\ \therefore \quad B = \frac{f_B}{f_A} A \\ \therefore \quad 0 = B - \frac{1 - f_A}{f_A} A \end{aligned} \tag{F.1}$$

The main area, $A$, is equal to the product of the length of its sides:

$$A = xy \tag{F.2}$$

The inside border area can be separated into 8 rectangles, summed, and expressed as follows:

$$\begin{aligned} B &= 4t^2 + 2xt + 2yt \\ &= 4t^2 + (2x + 2y)t \end{aligned} \tag{F.3}$$

$$\tag{F.4}$$

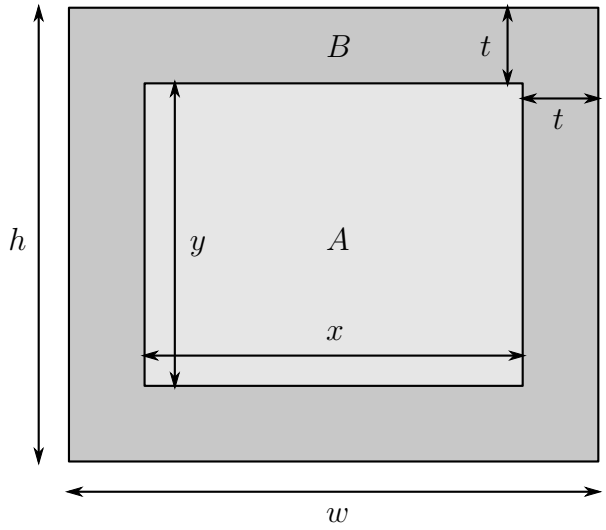


**Figure F.1: Schematic of how the inside border thickness is calculated.** $A$ is the area of the main area. $B$ is the area of the inside border. $x$ and $y$ are the dimensions of the main area. $t$ is the border thickness.

These areas (Equation F.2, Equation F.4) can now be substituted into Equation F.1 to give:

$$0 = 4t^2 + (2x + 2y)t - \frac{1 - f_A}{f_A}xy \tag{F.5}$$

For this problem, the main area needs to take up 80% of the total area, therefore $f_A = 0.8$. From previous calculations: $x = 124.6$mm, $y = 129.1$mm. Now this quadratic can be solved to find the values of $t$.

Solving this quadratic gives $t = 7.5$mm.

# Appendix G

# Design specification of a scalable manufactruing process for decellularising bladders

## G.1 Requirements

1. Involves a standard method of dissecting bladders before decellularisation, from bladders which are provided whole and intact, covered in some connective tissue and with a length of urethra of at least 2 cm still attached.
2. Applies a sufficient amount of biaxial strain to the walls of bladders for the duration of the process:
   a) Strain in apex-to-base direction: 1.4
   b) Strain in transverse direction: 2.0
3. Keeps the bladder tissue completely immersed in decell solution.
4. Can be used in the temperature range 1–45 °C
5. Can be placed in an incubator and a cold room.
6. Does not allow solution to evaporate, leak or spill.
7. To prevent microbial growth, it must:
   a) Be compatible with aseptic technique.
   b) Involve a bioburden step at the start of the process (not yet tested).
8. Can be autoclaved.
9. Allows decell solutions to be easily changed at each stage (e.g. pouring out or draining the vessel).
10. Can be placed on a piece of agitation equipment (e.g. orbital shaker, bottle roller).
11. Is made from a minimal number of parts.

12. Can decellularise 3 – 6 bladders at once, but is also infinitely scalable.
13. Lower volumes of solution are used compared to the 1 L used in the original process.
14. Produces patches that are 8 cm × 8 cm in size at the end of the process. Dissection could be involved.
15. Must be made of materials suitable to exposure to the environmental conditions.
16. The equipment must be re-useable, or have very cheap disposable parts.
17. Can be used by a single operator.
18. Can be lifted when full of water.
    a) Total maximum weight should be $< 3$ kg for above shoulder lifting as per the HSE Manual Handling Operations Regulations 1992.

## G.2 Desirables

1. The volume of solution should be limited by the mass or area of the bladder tissue, and not by the geometric requirement of the solution to fully immerse the bladders; use a certain calculated ratio of bladder area or weight to solution volume ratio.
2. Ideal target time for changing solutions: 10–30 s (compared to 5 – 10 min via the previous method).
3. Produces patches that are 10 cm × 10 cm in size at the end of the process.
4. The bladder tissue can be seen during decellularisation i.e. the walls of the container are transparent.

## G.3 Concept process

1. Is a self-contained machine that requires no human input throughout the duration of the process.
2. Can control the temperature of the environment to within the range of 1–45 °C.
3. Can provide agitation to the decell solutions during incubation.

# Appendix H

# Beam bending of frame

## H.1 Beam bending of pin retainers

We need to know what the maximum stress will be at the bottom of the pin retaining lever. Using beam bending theory, we can find a relationship between stress and end beam deflection. We will do this so we can choose the correct geometry so that the plastic will not undergo plastic deformation.

The model of the beam is shown in Figure H.1.

### Beam displacement

Using the following equation for beam bending (Hearn, 1997):

$$\frac{d^2y}{dx^2} = \frac{M(x)}{EI} \tag{H.1}$$

Also using the coordinate system shown in Figure H.1, the bending moment, $M$, is

$$M = -FL + Fx \tag{H.2}$$

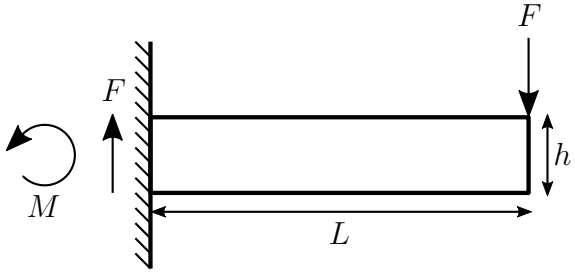


**Figure H.1: The pin retaining beam modelled with beam bending theory.**

Which can be written as

$$EI\frac{d^2y}{dx^2} = Fx - FL \tag{H.3}$$

Integrating with respect to $x$:

$$EI\frac{dy}{dx} = \frac{1}{2}Fx^2 - FLx + c_1 \tag{H.4}$$

At the wall ($x = 0$), the slope of the beam is zero $\frac{dy}{dx} = 0$. Therefore, $c_1 = 0$. Integrating again with respect to x:

$$EIy = \frac{1}{6}Fx^3 - \frac{1}{2}FLx^2 + c_2 \tag{H.5}$$

Again, the slopt of the wall is zero at the wall, thus $x = 0$, $\frac{dy}{dx} = 0$ and therefore, $c_2 = 0$. To find the deflection of the beam at the end of it, we let $x = L$:

$$EIy = \frac{1}{6}FL^3 - \frac{1}{2}FL^3 = -\frac{1}{3}FL^3 \tag{H.6}$$

Rearranging to be explicit with respect to the applied force:

$$F = -\frac{3EIy}{L^3} \tag{H.7}$$

**Stress at the tethered end of the beam**

As before, the bending moment in the beam is:

$$M = -FL + Fx \tag{H.8}$$

The stress is greatest at the tethered end of the beam ($x = 0$). The bending moment now becomes:

$$M = -FL \tag{H.9}$$

The simple theory of elastic bending states:

$$\sigma = \frac{My}{I} \tag{H.10}$$

Putting Equation H.9 into Equation H.10 gives us:

$$\sigma = -\frac{FLy}{I} \tag{H.11}$$

The magnitude of the stress is at a maximum when $y = \frac{h}{2}$. This now gives us:

$$\sigma = -\frac{FLh}{2I} \tag{H.12}$$

Rearranging in terms of the force gives us:

$$F = -\frac{2I\sigma}{Lh} \tag{H.13}$$

**Stress and displacement**

Equating Equation H.7 and Equation H.13 gives us:

$$\frac{3EIy}{L^3} = \frac{2I\sigma}{Lh} \tag{H.14}$$

Simplifying:

$$\frac{3Ey}{L^2} = \frac{2\sigma}{Lh} \tag{H.15}$$

For a given length, height, displacement and modulus $(L, h, y, E)$, the maximum stress in the beam can be found with the following equation:

$$\sigma = \frac{3Ehy}{2L^2} \tag{H.16}$$

This will be used to ensure the material does not become plastically deformed when used, and so can be re-used without impairing function.

## H.2 Beam bending of frame when supporting the bladder

The maximum deflection of the frame was calculated by modelling the frame using Euler-Bernoulli beam bending theory. The frame was modelled as a beam of length $L$, and with a square cross-section of width $w$ and height $h$. The stretched bladder exerted a force on the frame with magnitude $F$ at a perpendicular distance $d$ away from the neutral axis of the beam. Therefore the bending moment applied to each end of the beam is equal to $M = Fd$. The beam is modelled as shown in Figure H.2.

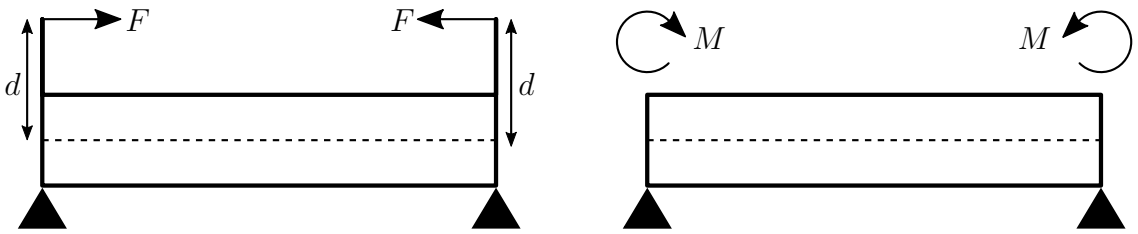


**(a)** Forces **(b)** Moments

**Figure H.2: Modelling frame bending using beam bending theory.** The bladder tissue exerts a force $F$ a perpendicular distance of $d$ away from the neutral axis of the beam. This is equivalent to a moment of magnitude $M$ being applied to each end of the beam.

Using Equation H.1 an expression was found for the deflection of the beam (Equation H.17).

$$\begin{aligned} EI\frac{d^2y}{dx^2} &= M \\ EI\frac{dy}{dx} &= Mx + c_1 \\ \text{at } x = \frac{L}{2}, \frac{dy}{dx} = 0 \quad &\therefore c_1 = -\frac{ML}{2} \\ EI\frac{dy}{dx} &= Mx - \frac{ML}{2} \\ EIy &= \frac{1}{2}Mx^2 - \frac{1}{2}MLx + c_2 \\ \text{at } x = 0, y = 0 \quad &\therefore c_2 = 0 \\ EIy &= \frac{1}{2}Mx(x - L) \\ y &= \frac{Fdx(x - L)}{2EI} \end{aligned} \tag{H.17}$$

For a beam with a square cross-section, the second moment of area, $I$, can be expressed in terms of the width $w$ and height $h$ (Equation H.18).

$$I = \frac{wh^3}{12} \tag{H.18}$$

Substituting Equation H.18 into Equation H.17 gives an expression for beam displacement in terms of the dimensions and material properties of the beam (Equation H.19).

$$y = \frac{6Fdx(x - L)}{Ewh^3} \tag{H.19}$$

Displacement is at a maximum in the centre of the beam, when $x = \frac{L}{2}$. Substituting this into Equation H.19 gives an expression for the maximum displacement of the frame when loaded with bladder tissue, shown in Equation H.20.

$$y = \frac{3FL^2d}{2Ewh^3} \tag{H.20}$$